DISSERTATION

METABOLIC SUPPORT OF PREIMPLANTATION EMBRYO GROWTH AND VIABILITY

Submitted by

Kyle Joseph Fresa

Department of Biomedical Sciences

In partial fulfillment of the requirements

For the Degree of Doctor of Philosophy

Colorado State University

Fort Collins, Colorado

Summer 2024

Doctoral Committee:

Advisor: Elaine Carnevale
Co-Advisor: Adam Chicco

Dawit Tesfaye
Rebecca Krisher
Christopher Gentile

ABSTRACT

METABOLIC SUPPORT OF PREIMPLANTATION EMBRYO GROWTH AND VIABILITY

Early embryo metabolism involves essential and dynamic biological reactions that support viability, growth, and pregnancy establishment. Embryo metabolism not only serves to provide energy through ATP synthesis, but also facilitates the production of macromolecules such as proteins, nucleotides, and lipids. The ways in which embryos balance catabolic and anabolic activity during the preimplantation stage are not well understood; however, understanding these processes may lead to improved fertility treatments, embryo culture, and pregnancy outcomes. The studies described in this dissertation utilize innovative methods, such as stable isotope tracer analysis to track carbon and nitrogen flux through various pathways, oxygen microsensors to determine individual embryo respiration under various conditions, and proteomic analysis to determine the impacts of metabolic disturbances on embryo viability. The overarching hypothesis of this dissertation is that embryo viability is dependent on efficient and tightly regulated metabolic activity, and disturbances to metabolic function ultimately lead to reduced developmental potential. To test this hypothesis, a series of projects were conducted to 1) evaluate the importance of phosphoenolpyruvate carboxykinase (PEPCK) during early development, 2) uncover the function of PEPCK to support catabolic and anabolic activity in early embryos, and 3) determine the impacts of delayed embryo development on embryo metabolism and pathway regulation.

These projects revealed important insights into the impact of embryo metabolism on development, including the discovery of a novel, PEPCK-mediated pathway that embryos utilize

to balance energy production and biosynthesis. Furthermore, the impact of delayed embryo development was demonstrated to alter embryo metabolic activity and pathway regulation, including increased aerobic activity and altered protein expression. These findings improve our understanding of metabolic activity and regulation during preimplantation development, highlighting the impact of metabolic activity to promote ATP production, biosynthesis, developmental kinetics, and ultimately survival. The experimental outcomes presented in this dissertation provide a foundation for targeted approaches to improve embryo development and reproductive success.

ACKNOWLEDGEMENTS

I would like to thank my advisors, Dr. Elaine Carnevale and Dr. Adam Chicco, for their support throughout the entirety of my PhD. Their brilliance and leadership skills changed the way I approach new challenges, both in my professional and personal life. They challenged me to take part in many different types of studies, which has allowed me to grow as a researcher and investigate a wide range of topics. I was encouraged to pursue my own research goals, and it allowed me to develop as a scientist, acquire a predoctoral fellowship, and establish myself within research. Their mentorship has taught me about what it means to be a scientist, from approaching problems to solving them with precision and purpose. Additionally, the influence of my committee has been integral to my success as a PhD student. Dr. Rebecca Krisher was a major inspiration for my embryo metabolism projects, Dr. Chris Gentile helped facilitate my progress as a student, and Dr. Dawit Tesfaye was always there for me during times in which I needed his expertise. My success at CSU would not have been possible without my advisors and committee.

I would also like to acknowledge the impact of my team at the Jones Institute for Reproductive Medicine, prior to starting my PhD. Dr. Gerry Celia introduced me to the field of reproduction, personally trained me in many skills that have used in my studies, and selflessly encouraged me to pursue my goal of becoming a PhD. My team of physicians, embryologists, nurses, and many others allowed me to learn about infertility and form scientific questions that would eventually lead to projects during my PhD. I will never forget the impact of this time on my life.

DEDICATION

I dedicate this dissertation to my family: Jillian, Eva, Gregg, and Olivia Fresa. My wife, Jillian, has been a major source of inspiration over the past several years. She has been with me through the highs and lows of my PhD, and I cannot thank her enough for her support. Jillian is a brilliant and fun person to be around, and it has made my experience a very positive one. She is my world, and I cannot imagine doing this without her by my side. My mother, Eva, has always found ways to inspire me during challenging times. Her confidence in me to pursue my goals has kept me on track during my entire career. She has always seen the best in me, and that has meant so much over the years. My father, Gregg, is someone I have always admired for his goal-driven mindset and approach to solving problems. He has always encouraged me to take risks to find success, and he made my decision to leave my job, move across the country, and pursue a doctoral degree much easier. Finally, my sister, Olivia, is an amazing person with the patience and dedication to achieve anything. Her adaptable approach to teaching has opened my mind to the power of education to improve peoples' lives. She inspires me to invest in others and find ways to help them achieve their own goals. Of course, there are many others who have supported me through this program, so I want to thank all friends, family, colleagues, and fellow scientists.

TABLE OF CONTENTS

LIST OF TABLES

LIST OF FIGURES

APPENDIX II

CHAPTER I: HYPOTHESES AND EXPERIMENTAL AIMS

Overarching Hypothesis

The regulation of metabolism during early embryo development is critical for survival, growth, and pregnancy establishment; however, the mechanisms which embryos utilize to meet energy and biosynthetic demands are not well understood. Age, stress, diet, and many other factors are associated with lower fertility and are often accompanied with impaired embryo development. Regulatory mechanisms that facilitate ATP production, redox control, and biosynthesis in embryos are still largely undiscovered, although evidence suggests that embryos display metabolic adaptations similar to other proliferative cell types. It is critical to understand how embryo metabolism promotes growth in order to develop targeted approaches to combat infertility and improve culture systems. Historically, efforts to characterize embryo metabolism have been limited to assessment of spent media, low-resolution isotope tracer analysis, or the use of simple media formulations that are now outdated. Modern approaches such as single-cell mass spectrometry and electrochemical microsensors are now available to evaluate embryo metabolism with much greater detail.

The experiments within this dissertation explore the metabolic mechanisms and characteristics that promote embryo development to the blastocyst stage. A variety of modern methods were used to 1) evaluate a novel mechanism mediated by PEPCK that facilitates the balance of cytosolic and mitochondrial metabolism, and 2) demonstrate metabolic dysfunction in slow-growing embryos. Techniques such as immunofluorescence, siRNA gene silencing, enzyme inhibition, stable isotope metabolic tracer analysis, and electrochemical sensor readings were used to investigate these topics. Through use of various methodologies, these studies

further demonstrate the importance of embryo metabolism to support pathways critical for cell proliferation. I hypothesized that similar to other proliferative cell types, the balance of energy production and biosynthesis of macromolecules is connected through the organized shuttling of metabolic intermediates, and dysregulation of these pathways are detrimental to the developing embryo. To test this hypothesis, three experiments were conducted to determine the regulation of metabolic intermediate shuttling and investigate the impact of metabolic dysfunction on embryo viability.

Projects

1. Evaluate the expression and importance of phosphoenolpyruvate carboxykinase (PEPCK) activity during early embryo development

Regulation of cell proliferation is essential for proper embryo growth and survival. Timely development of cleavage-stage embryos into blastocysts is associated with embryo viability, and studies in bovine embryos have shown that rate of development after the blastocyst stage is critical for maintenance of pregnancy. In general, proliferating cells tend to display altered metabolic processes to increase biosynthesis and energy production. Recent work in cancer cells has identified phosphoenolpyruvate carboxykinase (PEPCK), an enzyme known primarily for its role in gluconeogenesis, as a major regulatory enzyme influencing nutrient uptake, biosynthesis, and cell proliferation. Prior to this study, the role of PEPCK to support embryo development had not been investigated, although the cytoplasmic isoform of PEPCK was known to be expressed during preimplantation development. Aimed to determine whether PEPCK played a role in the regulation of embryo metabolism, similar to cancer cells, this project investigated the expression and importance of PEPCK from the zygote to blastocyst stage.

Hypothesis: PEPCK activity is important for the metabolic regulation of cell proliferation during preimplantation embryo development

Specific Aim 1: Confirm expression of PEPCK isoforms during various stages of early embryo development

Specific Aim 2: Determine the importance of PEPCK activity to promote embryo growth and survival

Specific Aim 3: Investigate a role of PEPCK to sustain embryo viability in nutrient-poor conditions

This project utilized in vitro produced bovine embryos to determine the function of PEPCK to support growth and metabolism. Embryos were cultured under standard conditions before assessing PEPCK isoform expression, treated with a PEPCK inhibitor or isoform-specific siRNA to determine the effect on development, and cultured in carbohydrate-free media with a PEPCK inhibitor to investigate the effect on metabolic flexibility. The results supported the conclusions that PEPCK is expressed throughout early embryo development and is important for viability. The findings supported the hypothesis that PEPCK is important for the metabolic regulation of cell proliferation in embryos. This led to more targeted approaches to understand the function of PEPCK in a second experiment.

2. Determine the function of PEPCK to regulate carbon flux and anabolic activity in early embryos

Although not demonstrated in embryos, PEPCK promotes growth and survival by increasing availability of anabolic intermediates in other prolific cells. The findings from Project 1 suggested that an important role of PEPCK during development was to improve the metabolism of non-glycolytic energy sources to support growth, although the exact mechanism

was unclear. Thus, we wanted to investigate a potential role of PEPCK to regulate monocarboxylate (pyruvate) and amino acid (glutamine) metabolism to support embryo growth. Pyruvate and glutamine are known to be important metabolic substrates during preimplantation development, although the mechanisms involved in shuttling these substrates into various metabolic pathways are not well understood. PEPCK is a cataplerotic enzyme and has been shown to improve biosynthetic activity by removing oxaloacetate, a TCA cycle intermediate, increasing the availability of metabolic intermediates available for biosynthetic pathways. Dysfunction of PEPCK can lead to reduced TCA cycle activity, impairing overall nutrient flux and cell growth. In this project, the impact of PEPCK activity on pyruvate and glutamine metabolism during cleavage-stage embryo development was assessed using a PEPCK inhibitor and stable isotope metabolic tracer analyses. Relative amounts of metabolites, including the peak area of heavy isotope-labeled products found in pathways such as the TCA cycle, gluconeogenesis, nucleotide synthesis, and amino acid synthesis were compared to determine the role of PEPCK to regulate metabolic activity. In a follow-up study, electrochemical sensors were used to determine the effect of PEPCK activity to regulate mitochondrial and cytoplasmic metabolism. Use of these techniques helped support a specific role of PEPCK to support the balance of catabolic and anabolic activity necessary for survival in embryos.

Hypothesis: PEPCK facilitates the coordination of cytosolic and mitochondrial metabolism of carbon derived from pyruvate and amino acids to meet energy and anabolic demands.

Specific Aim 1: Determine whether PEPCK stimulates pyruvate metabolism to meet energy and biosynthetic demands in preimplantation embryos.

Specific Aim 2: Evaluate a role of PEPCK to increase glutamine metabolism to meet energy and biosynthetic demands in preimplantation embryos.

Specific Aim 3: Determine the impact of PEPCK activity on mitochondrial oxygen consumption and redox control in early embryos.

In this project, bovine in vitro-produced embryos were obtained using methods from the previous study. Inhibition of PEPCK was used to evaluate the impact of PEPCK on pyruvate and glutamine metabolism using stable isotope metabolic tracers. Integration of heavy isotope labeled carbons sourced from pyruvate and glutamine into metabolites and products found in specific metabolic pathways indicated the metabolic role of these two substrates to support catabolic and anabolic activity. In addition, the effects of PEPCK were evaluated by comparing the amounts of heavy-isotope carbons found in specific metabolites. Thus, we were able to elucidate the impact of PEPCK to shuttle carbons from pyruvate and glutamine to support growth. After this experiment, cleavage-stage embryos were evaluated for oxygen consumption rate (OCR) and extracellular acidification rate (ECAR) prior to and after addition of a PEPCK inhibitor. Data generated from these experiments revealed a major impact of PEPCK to support mitochondrial and cytoplasmic metabolic activity. PEPCK activity was determined to be critical for the production of glycolytic intermediates in preimplantation embryos, marking the first demonstration of gluconeogenesis in bovine embryos. PEPCK activity was also shown to increase carbon flux through the TCA cycle. Evaluation of OCR and ECAR further supported the hypothesis, as OCR was impaired and ECAR increased following PEPCK inhibition. In addition, these projects revealed differences in the shuttling of pyruvate and glutamine into biosynthetic pathways such as amino acid synthesis, gluconeogenesis, and nucleotide production. These studies have contributed to a greater understanding of mammalian embryo metabolism and provide useful methods for future studies of nutrient shuttling and metabolic pathway regulation during the preimplantation stage.

3. Investigate the metabolic characteristics associated with delayed blastocyst formation

Embryos that grow slowly tend to have reduced implantation and live birth outcomes. Despite this, the reasons behind delayed development are not clear. Metabolism during the early stages of embryo development is critical for producing energy and biosynthetic material needed for normal growth. Any disruptions to these processes can reduce the viability of an embryo, leading to embryonic arrest and death. It has been previously hypothesized that elevated catabolic activity is detrimental to embryo survival, as it limits the embryo's ability to shuttle metabolites into anabolic pathways. However, we have also demonstrated that in certain cases, such as in aging horses, oocyte metabolism is decreased, potentially contributing to reduced energy availability to support essential processes. Therefore, the rate of metabolism likely has an ideal zone, where there is the correct balance between ATP production and generation of biosynthetic material. Regardless, the influence of metabolism to support rapid growth of the embryo is not fully understood, and it is unknown whether metabolic disturbances are responsible for the reduced pregnancy outcomes following transfer of slow-growing embryos. In addition, the genetic sex of the embryo may differentially contribute to causes of delayed development. Therefore, assessment of the metabolic activity and protein expression of slow growing embryos may explain why certain embryos take longer to develop. To test this hypothesis, a set of experimental aims were produced to determine the impacts of metabolic activity on embryo growth rate.

Hypothesis: Delayed embryo development is associated with an imbalance of energy production and biosynthetic activity.

Specific Aim 1: Determine the effects of delayed embryo growth on oxygen consumption rate, extracellular acidification rate, and reactive oxygen species production.

Specific Aim 2: Determine the effects of delayed embryo growth on the expression of proteins involved in cell metabolism

Specific Aim 3: Determine potential sex differences in male and female embryos that may contribute to delayed embryo development.

Normal and slow-growing expanded male and female blastocysts were collected on day 7 (normal) and day 8.5-9 (delayed) and evaluated for oxygen consumption rate, extracellular acidification rate, and proteomic expression of metabolic enzymes. This study demonstrated that embryos that take longer to form blastocysts consume excessive amounts of oxygen, indicative of elevated oxidative metabolism, and have increased electron transport system complex proteins. Delayed embryos had downregulated biosynthetic proteins, indicating that catabolism and anabolism was not properly regulated in slow-growing embryos. In addition, male and female embryos had similar respiratory activity, although unique metabolic differences could have occurred in substrate utilization and biosynthetic activity. The results obtained from the study support the hypothesis and indicate that metabolic regulation of embryo development is critical to the timing of embryo development and overall viability.

The three projects described in this dissertation highlight the importance of metabolic mechanisms to promote early embryo growth. These studies utilize targeted methods to determine the role of nutrient shuttling, mitochondrial function, and biosynthetic activity necessary for survival. These studies contribute to a greater understanding of embryo metabolism and present novel methods to further investigate mechanisms that exist in embryos of many species, including humans. The projects described in this dissertation will hopefully contribute to advancements in embryo selection, culture techniques, and future studies of embryo metabolism to improve pregnancy outcomes.

CHAPTER II: PEPCK IS ESSENTIAL DURING PREIMPLANTATION EMBRYO DEVELOPMENT

Summary

The regulation of metabolic mechanisms within embryos to meet energy and biosynthetic demands is not well understood, although studies in other prolific cells have identified a role of PEPCK, a gluconeogenic enzyme, to promote growth and survival by increasing availability of anabolic intermediates. To investigate the importance of PEPCK activity in developing embryos, the present study evaluated expression of PEPCK isoforms during multiple stages of preimplantation development, the effects of reduced activity of PEPCK during early embryo culture, a function of PEPCK to support embryo development in suboptimal conditions, and its role to regulate pyruvate and glutamine metabolism. In vitro produced bovine embryos were obtained following fertilization of cumulus-oocyte complexes harvested from slaughterhouse-derived ovaries and cultured to the blastocyst stage. Mitochondrial and cytoplasmic PEPCK isoforms were compared in oocytes, cleavage embryos, morulae, and blastocysts using immunofluorescence. Zygotes cultured in hydrazine sulfate, a PEPCK inhibitor, for 8 days resulted in reduced blastomere numbers in cleavage stage embryos and impaired blastocyst formation. Microinjection of mitochondrial and cytoplasmic isoform-specific siRNA at the zygote stage reduced blastomere cell numbers after 56 h. Deprivation of carbohydrates during

---

[1]Chapters II and III have been prepared for submission to *Nature Metabolism*. Authors: Kyle J. Fresa, Shaun Bevers, Ming-Hao Cheng, Thomas W Chen, Travis Nemkov, Elaine M. Carnevale, Adam J. Chicco. Funding through USDA NIFA Predoctoral Fellowship Award No. 2023-67011-40510, CRC Bovine Foundation grant, and ARBL Translational Reproductive Biotechnology grant.

culture further augmented embryo sensitivity to PEPCK inhibition, revealing a potential function of PEPCK to support energy and anabolic demands using alternative metabolic substrates. Our results suggest that PEPCK is a pro-survival metabolic enzyme essential for bovine preimplantation embryo development.

Introduction

Bovine embryos produced through in vitro fertilization (IVF) and embryo culture have become the primary source of commercial embryos, although only 20-40% of fertilized embryos develop to the blastocyst stage for transfer.[1] Pregnancy retention following transfer of in vitro produced (IVP) embryos is approximately 24% lower than in vivo produced embryos, and only 27% of transferred IVP embryos result in a live calf.[2] Ideal in vitro culture systems need to tailor to the specific demands of the embryo to improve IVF outcomes; however, the metabolic mechanisms that bovine embryos use to promote rapid cell division are poorly understood. Bovine embryos primarily metabolize pyruvate and lactate during cleavage stages and glucose at the blastocyst stage; however, benefits of non-carbohydrate metabolites, including lipids and amino acids, are important for blastocyst development in vitro.[3,4,5,6] Bovine blastocysts produced in glucose-free media appear to exhibit a range of metabolic adaptations to support development in considerably altered environments.[7] The ability of embryos to survive in a wide range of metabolic environments likely indicates that metabolic mechanisms exist to shuttle a variety of substrates into various metabolic pathways to promote survival. An understanding of these adaptations could lead to improvements in embryo culture and targeted selection of metabolically superior embryos to improve the efficiency of producing cattle embryos in vitro.

Phosphoenolpyruvate carboxykinase (PEPCK), a cataplerotic enzyme recognized as a rate-limiting enzyme for gluconeogenesis, has recently been shown to participate in the metabolic regulation of cell proliferation.[8] PEPCK's two isoforms, cytoplasmic PEPCK-C (*PCK1*) and mitochondrial PEPCK-M (*PCK2*), catalyze the conversion of oxaloacetate to phosphoenolpyruvate (PEP), which can then undergo a series of reactions to produce glucose via gluconeogenesis or be oxidized to pyruvate and enter the TCA cycle.[9,10] Knockdown of PEPCK in cancer cells has been demonstrated to impair tumor growth, limit glucose and glutamine metabolism, and reduce biosynthetic activity.[8,11,12] These studies highlight PEPCK's cataplerotic activity to be pro-survival, pulling metabolic intermediates from the TCA cycle to use for anabolic processes. As intermediates leave the TCA cycle, new substrates enter via anaplerosis, increasing TCA cycle flux and metabolism of alternative substrates such as glutamine.[13] While it is clear that embryos require significant anabolic and catabolic activity to promote rapid growth, the role of PEPCK and gluconeogenic activity to support development has not been previously investigated.

The specific role and expression of PEPCK isoforms during bovine embryo development is poorly understood; however, cytoplasmic PCK1 is expressed in bovine oocytes, cleavage stage embryos, and blastocysts.[14] PCK1 gene expression increases in blastocysts following peroxisome proliferator-activated receptor-delta (PPAR-δ) activation[14] and higher gene expression of PCK1 in cumulus cells has been proposed as a biomarker to predict embryo development and pregnancy outcomes in humans.[15,16] The activity of both isoforms of PEPCK increase in mosquito embryos after feeding, although PCK1 upregulation occurs more rapidly.[17] Although previous studies do not adequately define the exact function of PEPCK during embryogenesis,

they suggest that PEPCK is likely regulated by nutrient availability and promotes development through metabolic alterations.

In the present study, we examined the function of PEPCK to promote metabolic flexibility and increase anabolic activity necessary during preimplantation embryo development. PEPCK inhibition and gene silencing was used to reduce PEPCK activity during preimplantation development and examine a role of PEPCK to support growth in suboptimal environments.

Methods

Study design

The present study utilized in vitro produced bovine embryos to determine the function of PEPCK to support growth and metabolism. First, embryos cultured in standard conditions were collected at various stages to determine the presence of PEPCK isoforms. Embryos were then cultured with a PEPCK inhibitor or injected with isoform-specific siRNA constructs to evaluate the importance of PEPCK function to support growth. A third experiment determined a role of PEPCK to support embryo growth in the absence of carbohydrates.

Embryo culture

Cumulus-oocyte complexes (COCs) were harvested from slaughterhouse-derived ovaries that were held for <3 h at approximately 25°C prior to COC aspirations. Only COCs having a compact, cumulus mass of ≥3 layers of cells and homogenous ooplasm were selected for the study. Chemically defined media for oocyte maturation, holding, fertilization, and two-stage embryo culture was formulated and made at The Animal Reproduction and Biotechnology Laboratory at Colorado State University according to standard protocols unless otherwise noted,

and included metabolic substrate concentrations are listed in Supplemental Tables 1-8.[18] COCs were washed and matured in chemically defined bovine oocyte culture medium (Supplemental Table 1) containing 20 mM HEPES-buffered TCM-199, 0.5% fatty acid-free bovine serum albumin, 25ug gentamicin sulfate, 0.1 mM cysteamine, 1 μg/μL estradiol 17β, 1 μg/μL LH (USDA-LH-B-5, United States Department of Agriculture), 15 ng/μL FSH (ovine FSH-20, National Institute of Diabetes and Digestive and Kidney Disease, Torrance, CA), and 50 ng/μL epidermal growth factor for 23±1 h at 38.5°C in 5% CO_2 and air. Expanded cumulus-oocyte complexes were transferred into chemically defined media for fertilization (Supplemental Table 2) with frozen-thawed, female sexed sperm from a single ejaculate (ST Genetics, Navasota, TX) for 18 h. Following fertilization, presumptive zygotes were vortexed for 90 s to remove cumulus cells and transferred into equilibrated embryo culture medium 1 (CDM-1) at 38.5°C in 5% CO_2, 5% O_2 and 90% N_2.[18] Following approximately 56 h of culture in CDM-1, embryos were removed and assessed for observance of cleavage and cell number. Cell numbers at 56 h were categorized into three groups to represent timing of embryo development: normal (6-10 cells), delayed (4-5 cells), and very delayed (2-3 cells).[19] Embryos were transferred into equilibrated embryo culture medium 2 (CDM-2) for the remainder of the experiment.[18] Blastocysts were removed and counted after approximately 114 h in CDM-2.

Immunohistochemistry

Bovine ovaries were obtained from a local slaughterhouse, fixed in a 10% buffered formalin solution, and cut into 5 μm tissue sections for subsequent immunohistochemical staining. Slides were immersed in Citrisolv™ (Thermo Fisher) three times for a total of 15 min, followed by rinsing in decreasing concentrations of ethanol (100% to 50%). Antigen retrieval

was accomplished by microwaving the slides submerged in an antigen unmasking solution (Vector Labs) for 15 min. Afterward, the slides were taken out, washed in phosphate-buffered saline (PBS) before being blocked in PBS containing 10% natural goat serum (blocking buffer) for 1 h. Following another wash in PBS, a fresh blocking buffer with a 1:100 dilution of primary antibodies PEPCK-C (501731159, Proteintech, Rosemont, IL) or PEPCK-M (MBS9611438, MyBioSource, San Diego, CA) was applied to the slides for overnight incubation at 4°C. The slides were then washed, and blocking buffer containing a biotinylated secondary antibody was added for 1 h. Subsequently, the slides were washed and incubated in VECTASTAIN ABC Reagent for 30 min. After another wash in PBS, 200 μL of DAB stain was added to the tissue for 10 min. The slides were washed in deionized water and mounted using VECTASHIELD Vibrance Antifade Mountain Medium. Negative control slides were not treated with the primary antibody. Hematoxylin and eosin (H&E) stain (Vector, Newark, CA) was used in place of a primary antibody to detect nuclei, cytoplasm, and extracellular matrices in tissue sections. Images were captured using an inverted microscope and CellSens software (Olympus, Tokyo, Japan).

Immunofluorescence

Stripped oocytes and embryos at the cleavage, morula/early blastocyst, and blastocyst stage (n=3-4 per stage for each PEPCK isoform) were incubated in fixation buffer (Dulbecco's phosphate-buffered solution [DPBS], 0.1% polyvinylpyrrolidone [PVP]) for 20 min, followed by three washes in washing buffer (DPBS, 0.1% PVP, 0.1% Tween). Embryos were placed in permeabilization buffer (DPBS, 0.3% Triton) for 30 min, washed, and transferred to blocking buffer (DPBS, 0.1% Tween, 1% BSA, 0.1M glycine, 10% horse serum) for 2 h. Embryos were

then washed and placed in antibody buffer containing a 1:50 dilution of PEPCK-C (501731159, Proteintech, Rosemont, IL) or PEPCK-M antibodies (MBS9611438, MyBioSource, San Diego, CA) diluted in antibody buffer (DPBS, 0.1% Tween, 1% BSA) overnight. Embryos were washed and placed in antibody buffer containing 1:200 dilution of secondary antibody (T-2767, Invitrogen, Waltham, MA) for 1 h, washed, and imaged using an inverted fluorescence microscope (Olympus, Tokyo, Japan). Non-specific binding was assessed by the addition of secondary antibody without primary antibody after blocking. Semiquantitative analysis of immunofluorescence intensity was performed using ImageJ (National Institutes of Health) across developmental stages for PEPCK-C and PEPCK-M using identical settings and subtracting the background signal from the mean fluorescence of the oocyte or embryo.

PEPCK inhibition: dose response and effect of carbohydrate-free media

Zygotes were cultured up to the blastocyst stage with hydrazine sulfate (HS; Sigma cat#455865) to inhibit PEPCK.[20] Two experiments were performed using HS to: 1) determine the effects of increasing concentration of HS on developmental outcomes, and 2) evaluate the function of PEPCK to support embryo development in nutrient-deprived conditions. For experiment 1, embryos were exposed to increasing doses of HS (0 mM [control], 0.05mM, 0.1 mM, 0.25 mM, 0.5 mM, and 1 mM) added directly to culture media (CDM-1 and CDM-2) after fertilization until the end of culture. Embryos were compared using developmental assessments of embryo viability including cleavage, cell number at approximately 56 h, and blastocyst formation after 114 h to determine the effects of PEPCK inhibition of embryo development.

For experiment 2, 0.25 mM HS, a dose demonstrated during experiment 1 to not affect cell numbers at 56 h of CDM-1 culture, was used to compare the effects of PEPCK inhibition

during the length of embryo culture in standard control media (CDM-1 and CDM-2) when compared to the same media without fructose (MCDM-1 and MCDM-2), the only carbohydrate used in CDM-1 and CDM-2 embryo culture media (Supplemental Tables 7-8). Embryos were divided into four groups for culture: 1) CDM-1/CDM-2 (control), 2) CDM-1/CDM-2 with 0.25 mM HS, 3) Modified, carbohydrate-free MCDM-1/MCDM-2, and 4) MCDM-1/MCDM-2 with 0.25 mM HS. Embryos were similarly compared using developmental assessment of embryo viability including cleavage, cell number at approximately 56 h, and blastocyst formation after 114 h.

Gene silencing of PEPCK isoforms

To determine the individual isoform of PEPCK that is most important for early embryo development, we used custom Silencer® Select siRNA constructs (Invitrogen, Waltham, MA) specific to bovine *PCK1* and *PCK2* to knock down expression of of PEPCK isoforms during the first three days of development. Three siRNA constructs per isoform were tested in bovine granulosa cells for specificity and knockdown potential using qPCR. Granulosa cells were harvested from the follicular fluid obtained during follicular aspiration of slaughterhouse-derived bovine ovaries, treated with red blood cell lysis buffer, and plated into 96-well plates containing equilibrated Ham's F12 medium (Thermo) supplemented with 10% fetal calf serum.[21] Individual siRNA constructs were added to Opti-MEM (Thermo) media containing Lipofectamine™ RNAiMAX (Thermo) and left for 20 mins prior to transfection. Lipofectamine-siRNA complexes were added to wells for a total concentration of 10 nM for 48 h. Cells were removed, washed with PBS, and pelleted prior to addition of 1mL Trizol® (Thermo) reagent. RNA isolation was conducted using the supplier's protocol and resuspended in RNase-free water.

Quantitative real-time PCR was used to compare expression of *PCK1* and *PCK2* in PCK1KD, PCK2KD, negative control, and culture control cells. Using the iScript™ cDNA Synthesis Kit (Bio-Rad, Hercules, CA), cDNA was produced from RNA samples and amplified using a LightCycler® 480 Real-time PCR system and Sybr Green (Roche, Indianapolis, IN). *PCK1* and *PCK2* expression was normalized to a housekeeping gene (*GAPDH*) for each sample and compared to culture and negative controls. Constructs used to knock down *PCK1* or *PCK2* in embryos were selected based on reduction in mRNA of the gene of interest when compared to cells transfected with non-targeted siRNA (Thermo) and no cross-reactivity among isoforms (Supplemental Figure S1).

Two hours after completion of in vitro fertilization, approximately 5-10 pL of 20 μM *PCK1*, *PCK2*, or non-targeted siRNA was injected into the cytoplasm of zygotes using an Eppendorf Femtojet® microinjector system. Following injection, zygotes were assessed for viability and added to equilibrated embryo culture medium 1 (CDM1) at 38.5°C in 5% CO_2, 5% O_2 and 90% N2 for 56 h prior to developmental assessment of cleavage and blastomere cell count.

Statistical analysis

Data including cleavage, rate of day-3 development, and blastocyst formation was analyzed using logistic regression and Dunnett's multiple comparisons test. One-way ANOVA, followed by Tukey's multiple comparisons test was used to compare fluorescence signal between embryo stages. Significance was defined at $p \leq 0.05$.

Results

PEPCK isoform expression in ovarian tissue and preimplantation embryos

Immunohistochemistry and immunofluorescence was used to determine expression of PEPCK-C and PEPCK-M in bovine ovarian tissue (Figure 1) and during stages of embryo development (Figure 2), respectively. Both isoforms had similar distribution within the ovary, concentrated in cumulus, granulosa, theca, and luteal cells (Figure 1A-F). Immunofluorescence of PEPCK-C and PEPCK-M demonstrated expression of both isoforms in mature oocytes, cleavage-stage embryos, morulae, and blastocysts (Figure 2A-H). Quantification of fluorescence signal revealed that PEPCK-M expression does not differ between stages from the oocyte to the blastocyst, although PEPCK-C was highest at the cleavage and morula stage when compared to oocytes ($p<0.0001$) and blastocysts ($p\leq0.0001$, Figure 2J-K). Expression of PEPCK-C was higher ($p=0.004$) in blastocysts than oocytes. Residual cumulus cell material located on the zona pellucida also appeared to express both PEPCK-C and PEPCK-M (Figure 1, Figure 2C,F).

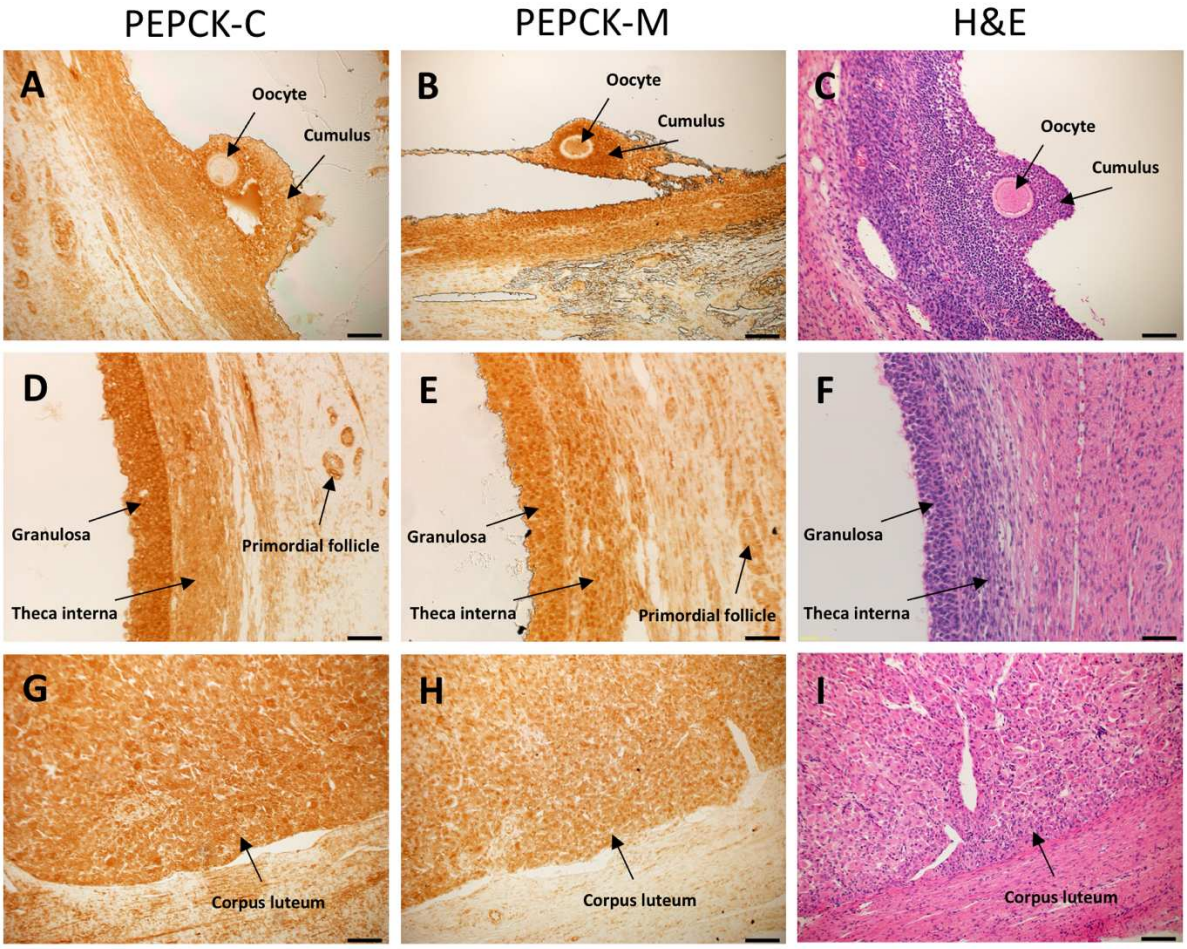

Figure 1: PEPCK expression within cross-sections of bovine ovarian tissue determined by immunohistochemistry. Cytoplasmic PEPCK-C, mitochondrial PEPCK-M, and hematoxylin-eosin (H&E) stain in (A-C) cumulus-oocyte complexes, (D-F) follicular cells, and (G-I) corpus luteum, respectively. Scale bar represents 100 µm (A-C, G-I) or 1 mm (D-F).

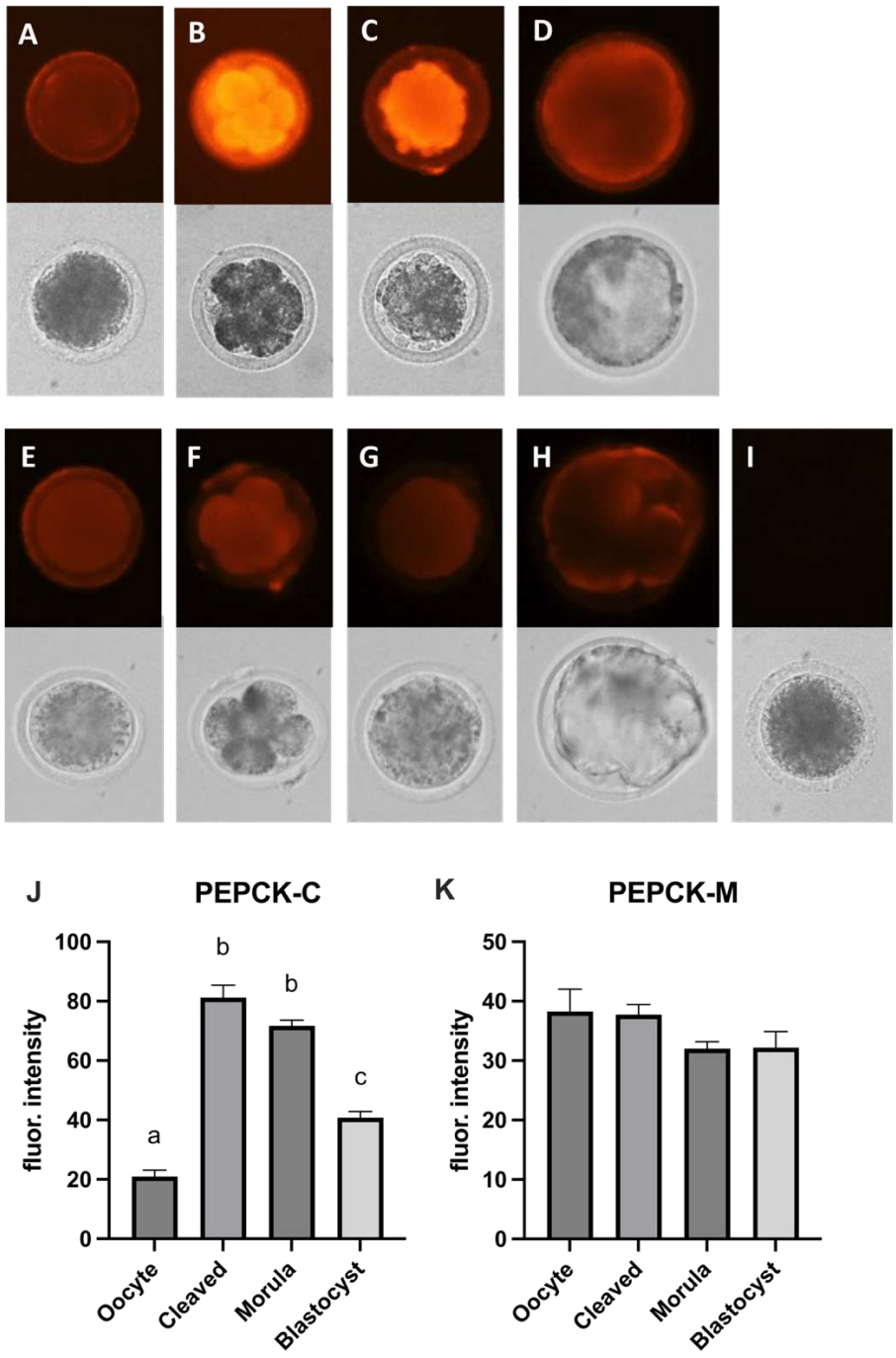

Figure 2: PEPCK expression during early bovine embryo development using immunofluorescence; (**A-D**) cytoplasmic PEPCK-C and (**E-H**) mitochondrial PEPCK in (**A,E**) mature oocytes, (**B,F**) cleavage-stage embryos, (**C,G**) morulae/early blast, and (**D,H**) blastocysts. (**I**) Negative control using a mature oocyte treated with secondary antibody without primary antibody. Fluorescence intensity of (**J**) PEPCK-C and (**K**) PEPCK-M in oocytes, cleavage-stage embryos, morulae/early blastocysts, and blastocysts (n=3-4 per stage, per isoform). A-c superscripts indicate differences between groups using one-way ANOVA with Tukey's multiple comparisons test at $p<0.05$.

PEPCK activity is essential for embryo development.

In vitro produced embryos were exposed to hydrazine sulfate (HS), a PEPCK inhibitor, from the zygote to blastocyst stage in vitro to determine the importance of PEPCK function during preimplantation development. HS only impaired ($p<0.0001$) cleavage at doses greater than 0.5 mM (Figure 3A). HS completely inhibited blastocyst development, reduced the percentage of normally developing (6-10 cell) embryos ($p<.0001$), and increased the percentage of very delayed (2-3 cell) embryos ($p<0.0001$) on day 3 when compared to controls at a dose of 0.5 mM (Figure 3B-C). Exposure to 0.25 mM HS reduced ($p<.0001$) blastocyst development by 88% when compared to controls, although it had no observable effect on day 3 embryos (Figure 3C).

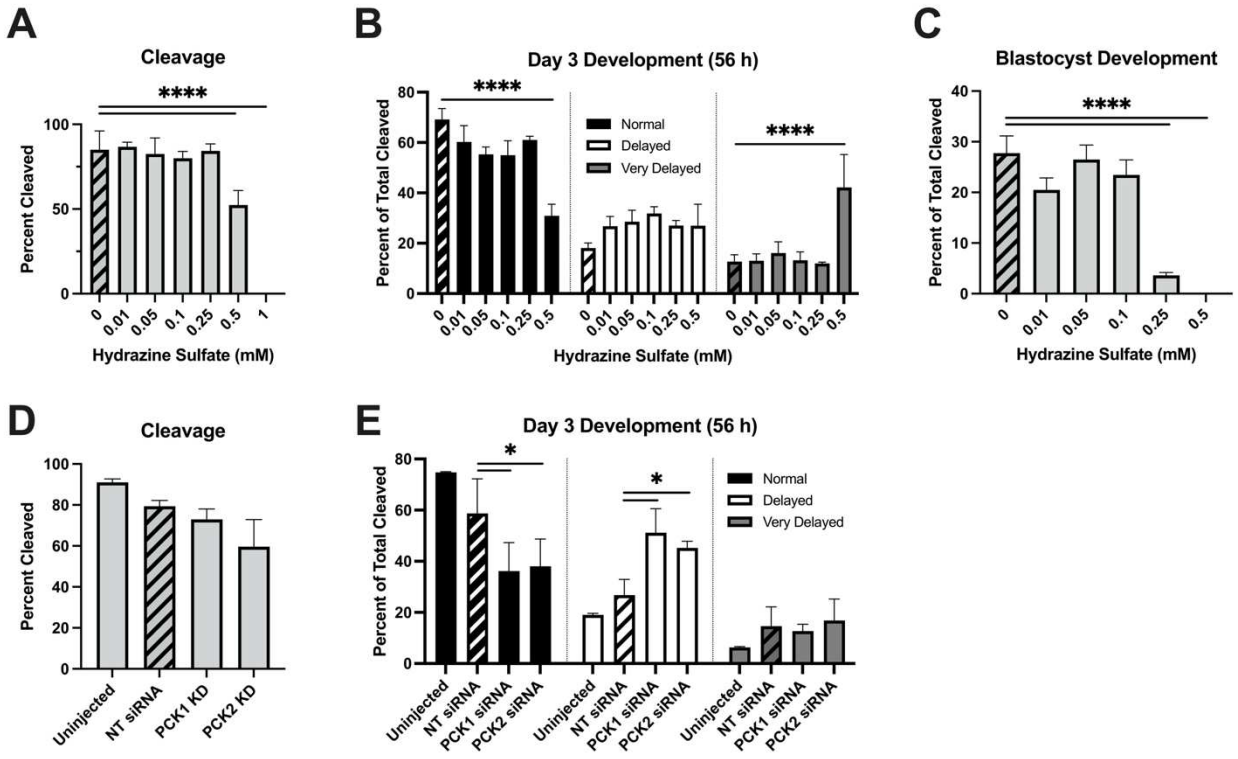

Figure 3: Morphometric and developmental assessment of in vitro produced embryos cultured with variable concentrations of hydrazine sulfate (**A-C**), a PEPCK inhibitor, or following injection of PCK1 or PCK2 specific siRNA (**D-E**). Outcomes included percent cleaved of total fertilized oocytes (**A,D**), developmental status of cleaved embryos following 56 h of culture

(**B,E**), and percent blastocyst development of total cleaved embryos (**C**). Asterisks indicate differences at $p<0.05$ * or $p<0.0001$ ****, obtained using logarithmic regression and Dunnett's test to compare each group to their respective controls (lined bars) of 0mM HS or NTsiRNA. Uninjected oocytes did not differ ($p>0.05$) per endpoint to confirm siRNA did not affect embryo development. Bars represent mean ± SEM.

Injection of PEPCK-specific siRNA impairs early embryo development

To determine the individual isoform of PEPCK that is most important for early embryo cleavage, we used custom siRNA constructs (Invitrogen) specific to bovine *PCK1* and *PCK2* to reduce expression of PEPCK isoforms during the first days of development. Injection of *PCK2* specific RNA reduced cleavage when compared to non-targeted (NT) siRNA ($p<0.02$), although no differences were observed following injection of *PCK1* siRNA (Figure 3D). Injection of *PCK1* and *PCK2* specific siRNA impaired early development when compared to non-targeted siRNA constructs, resulting in a 25% and 22% reduction ($p\leq0.0001$) in normally developing (6-10 cell) embryos on day 3, respectively (Figure 3E). No differences were observed between isoforms.

Greater reliance on PEPCK activity in nutrient-deprived conditions.

We next assessed the viability of embryos cultured in control (CDM1/CDM2) or carbohydrate-free media with and without a PEPCK inhibitor to determine if PEPCK supports development during suboptimal nutrient conditions. Presumptive zygotes were cultured to the blastocyst stage while exposed to 0.25 mM HS while in control medium (CDM1 and CDM2 containing 0.5 and 2 mM fructose, respectively) or in carbohydrate-free medium without fructose. Cleavage was similar in all groups regardless of exposure to HS (Figure 4A). However, there was a reduction ($p<0.0001$) in normal developing (6- to 10-cell) embryos at 56 h when

cultured in carbohydrate-free media with HS (FF+HS) when compared to control media (C) (Figure 4B). No other group, including C+HS differed from controls. A significant increase ($p<0.0001$) in delayed (4- to 5-cell) and very delayed (2- to 3-cell) embryos was observed in only the group cultured in carbohydrate-free medium with HS (FF+HS) when compared to media with carbohydrates or without carbohydrates and no HS after 56 h (Figure 4B). PEPCK inhibition completely inhibited blastocyst development in the FF+HS groups, and only 2% of embryos developed to blastocysts in the C+HS group (Figure 4C). Blastocyst development in carbohydrate-free media was similar to control media.

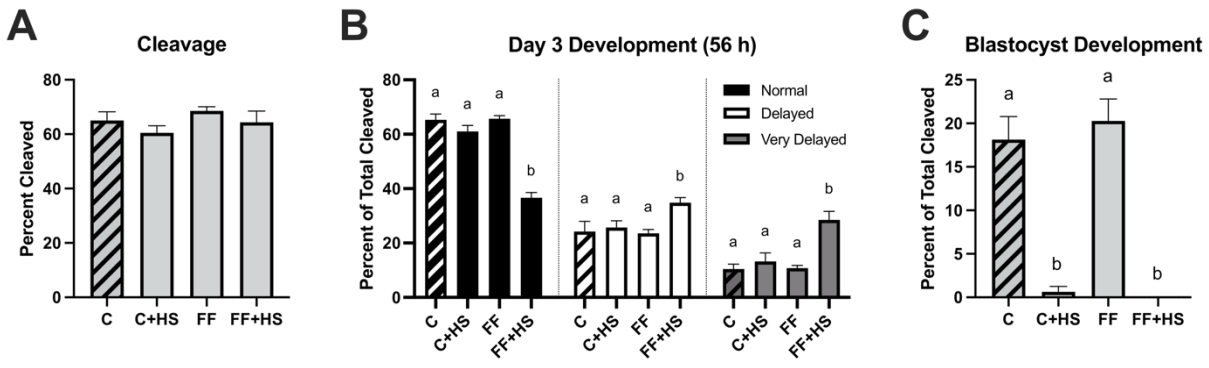

Figure 4: Morphometric and developmental assessment of in-vitro produced embryos cultured in standard (C) or carbohydrate-free (FF) media with or without the addition of 0.25 mM hydrazine sulfate (HS). Outcomes included (**A**) percent cleaved of total fertilized oocytes, (**B**) developmental status of cleaved embryos following 56 h of culture, and (**C**) percent blastocyst development of total cleaved embryos. [ab] Superscripts indicate differences at $p<0.05$ obtained using logarithmic regression and Dunnett's test to compare to compare each group to controls (lined bars). Bars represent mean ± SEM.

Discussion

The present study is the first to demonstrate the importance of phosphoenolpyruvate carboxykinase (PEPCK) function during preimplantation bovine embryo development. This study utilized a series of experiments to determine expression of cytoplasmic and mitochondrial isoforms of PEPCK during embryo development, and the importance of PEPCK function at

various stages of early development. We showed that PEPCK is expressed throughout the entirety of early development and supports cleavage cell divisions and blastocyst formation. Additionally, PEPCK activity appears to be most critical in suboptimal environments, likely due to its role to stimulate pyruvate and glutamine metabolism.

Prior to implantation, embryos are limited to intracellular energy stores and the surrounding oviductal, uterine, or in vitro environment to meet cellular demands. Compared to serum concentrations, bovine oviductal and uterine fluid is low in glucose and high in lactate during estrus.[22] Nutrient concentrations within the uterine lumen are dynamic during estrus, and are affected by repeat breeding, metritis, and systemic progesterone concentrations.[23–26] Within the uterus, a bovine blastocyst/conceptus undergoes rapid proliferation, growing from 2 mm on day 12 to 20 cm by day 19, doubling in length every day between days 9 and 16.[27,28] Implantation of the conceptus does not typically occur until day 22,[29] indicating a major role of the uterine environment to supply adequate metabolic fuels to sustain rapid proliferation and maintain pregnancy. An inability of the conceptus to adapt to its environment will result in ceased embryo development and termination of pregnancy.[30] Thus, cellular mechanisms that modify metabolic activity in response to increased energy demand or a lack of specific substrates are likely critical factors to early embryo survival, proliferation, and pregnancy establishment. Recent studies in cancer cells have highlighted PEPCK as a pro-survival metabolic enzyme capable of improving the use of various metabolic substrates to meet energy and anabolic demands. Thus, we hypothesized that embryos may utilize similar machinery to promote survival in varying conditions.

In the present study, cytoplasmic and mitochondrial isoforms of PEPCK were present throughout bovine preimplantation embryo development. Both PEPCK isoforms convert

oxaloacetate to phosphoenolpyruvate (PEP^{2-}), either in the mitochondria (PEPCK-M, *PCK2*) or in the cytoplasm (PEPCK-C, *PCK1*).[31] Oxaloacetate, a product of the tricarboxylic acid (TCA) cycle, is converted to PEP^{2-} by PEPCK, which can exit the mitochondria and enter the cytoplasm via anion transporters.[32] PEP^{2-} may then reenter the TCA cycle as pyruvate or enter gluconeogenesis, a series of reactions that produce glucose and several important anabolic intermediates including glucose-6-phosphate (pentose phosphate pathway [PPP], glycogen production), fructose-6-phosphate (PPP), 3-phosphoglycerate (one-carbon metabolism), and dihydroxyacetone phosphate (glyceroneogenesis).[31] These pathways are active during bovine preimplantation embryo development and play important roles in biosynthesis and redox control in proliferating cells.[33,34] While it is expected that the required intermediates used in these pathways typically result from glycolysis, the ability of bovine embryos to reach the blastocyst stage in the absence of glucose and fructose[7] suggests that alternative sources of these intermediates can be produced via PEPCK-mediated gluconeogenic activity.

As embryos approached the blastocyst stage, they become more sensitive to PEPCK inhibition, associating with rapid cell division and increased need for biosynthesis, ATP, and redox control.[35–37] Although PEPCK is primarily recognized for its role in gluconeogenesis, several studies have highlighted specific mechanisms in which PEPCK promotes cell proliferation and anabolism in highly prolific cells, such as cancer cells.[8,11,38] In general, the demand for glucose increases as cells proliferate rapidly, promoting ATP production, biosynthesis, and redox control.[39] Similar to studies in cancer cells, our study demonstrated that PEPCK activity promotes the metabolism of non-glycolytic substrates, such as pyruvate and glutamine in the TCA cycle, providing a secondary supply of energy and carbon sources for biosynthesis during preimplantation development.[8,12] These metabolic changes likely contribute

to embryo survival in suboptimal conditions in which utilization of non-carbohydrate carbon sources, such as glutamine, pyruvate, or lactate, are required to support high metabolic demands.[40] Therefore, PEPCK's function in embryos is likely an adaptive mechanism to increase energy production and anabolic activity from various metabolic substrates to support growth. No prior studies have evaluated a role of gluconeogenesis in mammalian preimplantation embryos, likely due to the typical availability of glucose in vivo and in culture systems. However, gluconeogenesis and glucose recycling (Cori cycle) has been observed in chick embryos.[41] While gluconeogenesis was not evaluated directly, PEPCK inhibition had the strongest effect on embryos cultured in media lacking glucose and fructose. NADPH generation, required for redox balance and biosynthesis of lipids and nucleotides, relies on glycolytic intermediates through the pentose phosphate pathway.[33,40] Embryos rely on tight control of redox balance to mitigate oxidative stress associated with high metabolic activity,[42] so PEPCK may provide an additional source of the required metabolic intermediates in times of high stress or low nutrient supply.

Based on findings from the present study, we suspect that PEPCK's role during embryo development is to increase the metabolism of substrates such as pyruvate and amino acids to meet energy and anabolic demands. PEPCK function is essential for adequate early embryo development and appears to be most important for survival in suboptimal environments. A greater understanding of PEPCK function could lead to improved culture systems and targeted selection of metabolically superior embryos to improve bovine assisted reproductive technology.

CHAPTER III: PEPCK REGULATES BIOENERGETIC AND BIOSYNTHETIC FLUX DURING EARLY EMBRYOGENESIS

Summary

Embryogenesis is a metabolically challenging process that requires partitioning of limited nutrients for energy production and biosynthetic pathways. How early-stage embryos balance these competing metabolic demands to support rapid cell division and growth is poorly understood. Herein, we demonstrate an essential role of phosphoenolpyruvate carboxykinase (PEPCK), an enzyme known primarily for its role in hepatic gluconeogenesis, in pre-implantation embryo development. Metabolic tracer studies show that PEPCK coordinates a preferential biosynthesis of glycolytic intermediates from oxaloacetate following pyruvate carboxylation and facilitates glutaminolysis by enabling the malate-aspartate shuttle and tricarboxylic acid cycle flux. PEPCK inhibition reduces embryo ATP levels and oxygen consumption while increasing extracellular acidification rates, demonstrating its broader role in regulating cellular energy production and redox balance between mitochondrial and cytosolic compartments. These results align with accumulating evidence from the cancer literature supporting a pivotal role of PEPCK in coordinating cellular bioenergetic and biosynthetic flux, which is essential for early embryogenesis and likely other processes involving rapid cell division and growth.

---

[2]Chapters II and III have been prepared for submission to *Nature Metabolism*. Authors: Kyle J. Fresa, Shaun Bevers, Ming-Hao Cheng, Thomas W Chen, Travis Nemkov, Elaine M. Carnevale, Adam J. Chicco. Funding through USDA NIFA Predoctoral Fellowship Award No. 2023-67011-40510, CRC Bovine Foundation grant, and ARBL Translational Reproductive Biotechnology grant.

Introduction

Embryogenesis is among the most metabolically demanding processes in the vertebrate live cycle. A developing embryo must simultaneously balance nutrient catabolism to meet increasing energy demands with the generation and supply of biomolecules for anabolic pathways that support exponential cell proliferation and growth. Mitochondria play a key role in these efforts by coordinating central carbon metabolism to meet bioenergetic demands through the production of ATP and generation of metabolic intermediates for biosynthetic reactions in the cytosol. These processes are coupled to the utilization of glycolytic intermediates by mitochondrial oxidation of reducing equivalents that maintain cellular redox balance and potential. Accordingly, oxygen consumption rates increase dramatically in cleavage-stage embryos prior to blastocyst formation, when rapid cell divisions occur without significant volumetric growth.[43] However, the metabolic mechanisms that integrate compartmentalized flux of metabolites through catabolic and anabolic pathways in developing embryos is poorly understood.

Phosphoenolpyruvate carboxykinase (PEPCK) catalyzes the decarboxylation of oxaloacetate (OAA) to phosphoenolpyruvate (PEP), which is recognized primarily as a rate-limiting reaction in hepatic gluconeogenesis. Recently, PEPCK has gained increasing attention as a key cataplerotic enzyme that links mitochondrial oxidative metabolism to anabolic activity during cancer cell proliferation.[8] In particular, knockdown of PEPCK impairs tumor growth and tricarboxylic acid (TCA) cycle flux and limits utilization of glucose and glutamine for biosynthetic activities, particularly under nutrient-deprived conditions.[8,12,11] In addition to catalyzing removal of carbons from the TCA cycle for anabolic pathways in the cytosol, PEPCK activity also enables further entry of anaplerotic substrates to the TCA cycle such as glutamine[13],

thereby promoting metabolic flexibility. While it is clear that embryos must meet significant bioenergetic and anabolic demands to enable rapid cell proliferation and growth, the precise role of PEPCK in embryogenesis is unclear.

Two isoforms of PEPCK exist in vertebrates with distinct and complementary metabolic functions; cytoplasmic PEPCK-C (*PCK1*) and mitochondrial PEPCK-M (*PCK2*).[9,10] Upregulation of *PCK1* in cumulus cells has been proposed as a biomarker of subsequent embryo potential and successful pregnancy in humans,[15,16] but its metabolic role and expression during embryogenesis is unknown. *PCK1* is expressed in bovine oocytes, cleavage stage embryos and blastocysts, and is upregulated in blastocysts following activation of peroxisome proliferator-activated receptor-delta (PPAR-δ),[14] consistent with its links to carbohydrate and lipid metabolism. PEPCK activity is critical for development of mosquito embryos, and expression of both isoforms increase following feeding, suggesting regulation by maternal nutrient status.[17] Therefore, it seems likely that PEPCK activity plays an important role in embryogenesis across species through modulation of metabolism, but direct evidence for this in mammals is lacking.

In the present study, we examined the ability of PEPCK to promote metabolic flexibility and anabolic nutrient flux during preimplantation bovine embryo development. Utilizing pharmacological inhibition, metabolic tracer analysis, and embryo metabolic analysis, we demonstrate that PEPCK activity is critical for the regulation of central carbon metabolism in embryos by facilitating flux of pyruvate and glutamine through the TCA cycle and gluconeogenic pathways.

Methods

Embryo culture

Cumulus-oocyte complexes (COCs) were harvested from slaughterhouse-derived ovaries held at approximately 25°C for a maximum of 3 h prior to COC aspirations. COCs were selected for the study based on having a compact, cumulus mass of ≥3 layers of cells and homogenous ooplasm. In vitro maturation of obtained COC's was conducted in chemically defined bovine oocyte culture medium (IVM) containing 0.5% fatty acid-free bovine serum albumin, 0.1 mM cysteamine, 1 μg/μL estradiol 17β, 1 μg/μL LH (USDA-LH-B-5, United States Department of Agriculture), 15 ng/μL FSH (ovine FSH-20, National Institute of Diabetes and Digestive and Kidney Disease, Torrance, CA), and 50 ng/μL epidermal growth factor for 23±1 h at 38.5°C in 5% CO_2 and air. All chemically defined media used for oocyte maturation, holding, fertilization, and embryo culture were prepared at The Animal Reproduction and Biotechnology Laboratory at Colorado State University using standard protocols unless specified otherwise, and are described in detail in Supplemental Figures 1-6, 9-10.[18] Expanded cumulus-oocyte complexes were transferred into chemically defined media (F-CDM) for fertilization with frozen-thawed, female sexed sperm from a single ejaculate (ST Genetics, Navasota, TX) for 18 h. Following fertilization, presumptive zygotes were vortexed for 90 s to remove cumulus cells and transferred into equilibrated embryo culture medium 1 (CDM-1) at 38.5°C in 5% CO_2, 5% O_2 and 90% N_2 for the remainder of the experiment, up to 56 h.

Isotopolouge metabolic tracer analysis

Stable isotope tracer analysis was used to assess the impact of PEPCK activity on the uptake and metabolism of pyruvate and glutamine in cleaved embryos. Following the completion

of fertilization, day 1 presumptive zygotes were placed in equilibrated CDM-1 embryo culture media with and without 0.25 mM HS for 50 h. The dose of HS used was previously confirmed to not affect embryo development at the cleavage stage. Individual cleaved embryos (n=32 per condition) were then placed in separate 500 µL wells and incubated for an additional 6 h in CDM-1-based medium containing 0.5 mM $^{13}C_3$ sodium pyruvate (490717, Sigma) or 1 mM $^{13}C_5$,$^{15}N_2$ L-Glutamine (607983, Sigma) in the presence and absence of 0.25 mM HS (Supplemental Tables 9-10). Following isotopolouge incubation, embryos were collected, washed in phosphate-buffered saline (PBS), and snap frozen for mass spectrometry-based metabolic flux (UHPLC-MS) analysis.

Prior to LC-MS analysis, samples were placed on ice and re-suspended with methanol:acetonitrile:water (5:3:2, v:v). Suspensions were vortexed continuously for 30 min at 4°C. Insoluble material was removed by centrifugation at 10,000 g for 10 min at 4°C and supernatants were isolated for metabolomics analysis by UHPLC-MS. Analyses were performed as previously published.[44,45] Briefly, the analytical platform employs a Vanquish UHPLC system (Thermo Fisher Scientific, San Jose, CA, USA) coupled online to a Q Exactive mass spectrometer (Thermo Fisher Scientific, San Jose, CA, USA). Samples were resolved over a Kinetex C18 column, 2.1 x 150 mm, 1.7 µm particle size (Phenomenex, Torrance, CA, USA) equipped with a guard column (SecurityGuard™ Ultracartridge – UHPLC C18 for 2.1 mm ID Columns – AJO-8782 – Phenomenex, Torrance, CA, USA) using an aqueous phase (A) of water and 0.1% formic acid and a mobile phase (B) of acetonitrile and 0.1% formic acid for positive ion polarity mode, and an aqueous phase (A) of water:acetonitrile (95:5) with 1 mM ammonium acetate and a mobile phase (B) of acetonitrile:water (95:5) with 1 mM ammonium acetate for negative ion polarity mode. Samples were eluted from the column using either an isocratic

elution of 5% B flowed at 250 µl/min and 25ºC or a gradient from 5% to 95% B over 1 min, followed by an isocratic hold at 95% B for 2 min, flowed at 400 µl/min and 45ºC. The Q Exactive mass spectrometer (Thermo Fisher Scientific, San Jose, CA, USA) was operated independently in positive or negative ion mode, scanning in Full MS mode (2 µscans) from 60 to 900 m/z at 70,000 resolution, with 4 kV spray voltage, 45 shealth gas, 15 auxiliary gas. Calibration was performed prior to analysis using the Pierce™ Positive and Negative Ion Calibration Solutions (Thermo Fisher Scientific). Acquired data was then converted from raw to mzXML file format using Mass Matrix (Cleveland, OH, USA). Metabolite assignments, isotopologue distributions, and correction for expected natural abundances of deuterium, ^{13}C, and ^{15}N isotopes were performed using MAVEN (Princeton, NJ, USA).[46] Targeted metabolites of interest included labeled tricarboxylic acid cycle intermediates, glycolytic intermediates, nucleotides, amino acids, and products of various metabolic pathways. The peak area of unlabeled and heavy isotope-labeled products were compared among groups. Isotope-containing metabolites are denoted based on the number of heavy-isotope containing carbons and nitrogens (M+1, M+2, etc.).

Embryo metabolic assays: OCR, ECAR

Upon completion of fertilization, day 1 presumptive zygotes were cultured in equilibrated CDM-1 embryo culture media for 50 h. Cleavage stage embryos (n=13), selected based on normal development (approximately 8-cell) and morphological quality assessment, were collected at 50h and held in HCDM-1 holding media at 4-5°C for 1.5 to 2 h prior to metabolic assessment. A multichannel, three-electrode electrochemical multisensor platform was utilized to monitor the metabolic activities of cleavage-stage embryos including oxygen consumption and

extracellular acidification. The device used gold working and counter electrodes, along with a silver/silver chloride pseudo-reference electrode, all integrated into a multi-sensor chip. The oxygen sensor surface was functionalized with a solid electrolyte, Nafion™ (Chemours, Wilmington, DE), while ECAR was measured using an indium tin oxide pH electrode micropatterned using photolithography. Further details regarding the design and use of this platform is described in previous studies.[47,48]

Six cleavage-stage embryos were warmed to 38.5°C for 15 min prior to analysis, transferred to warmed GMOPS™ holding media (Vitrolife, Sweden) containing 0.04% essentially fatty acid-free BSA, and evaluated in parallel for approximately 1 h per measurement within individual sealed 250 μL microchambers maintained at 38.5°C. Oxygen consumption rate (OCR) and extracellular acidification rate (ECAR) were measured synonymously in individual embryos using amperometry and potentiometry, respectively. Baselines of each rate were established prior to sample injection, and the platform began recording basal rates from each embryo 10 min after injection to minimize disturbances. Once stable metabolic rates were obtained for all embryos, defined as a maximum deviation of less than 5% over a 3-minute period for each metabolic rate measurement, HS was added to each chamber to achieve a concentration of 0.25 mM. Stable metabolic rates were recorded for all embryos and compared to baseline to detect changes in OCR and ECAR following PEPCK inhibition.

Statistical analysis

Metabolic tracer data was compared using unpaired, two-tailed t-test. OCR and ECAR measurements were analyzed using paired, two-tailed t-test. Significance was defined at $p \leq 0.05$.

Results

PEPCK regulates gluconeogenesis and aspartate synthesis from exogenous pyruvate

Given the importance of exogenous pyruvate for optimal metabolic plasticity during early embryo development,[49] we investigated the impact of PEPCK activity on its contribution to central carbon metabolism by isotopolouge tracer analysis in day 3 cleaved embryos cultured with or without 0.25 mM HS. This concentration of HS was selected to partially inhibit PEPCK activity without significantly disrupting embryo cleavage as demonstrated in previous experiments. Figure 5A illustrates predicted $^{13}C_3$-pyruvate carbon incorporation into the major metabolic pathways represented by detected metabolites in the presence and absence of PEPCK inhibition, based on current understanding of carbon atom transitions and ^{13}C labeling patterns in mammalian cells.[50,51]

The metabolic fates of $^{13}C_3$-pyruvate carbons arise primarily from M+2 acetyl-CoA produced by pyruvate dehydrogenase (PDH) or M+3 oxaloacetate (OAA) produced by pyruvate carboxylase (PC). PEPCK inhibition did not significantly decrease (p=0.12) intracellular M+3 pyruvate (Fig. 5B). Robust M+3 labeling was detected in multiple glycolytic intermediates upstream of PEP that was largely abolished by PEPCK inhibition (Fig. 5C), including a reduction in M+3 D-fructose 1,6 bisphosphate (p=0.0002), M+3 1/2/3-bisphosphoglycerate (p=0.03), and no detectable M+3 2/3 phospho-D-glycerate in the HS group compared to controls. In glycolytic intermediates, M+2 labeling was nearly undetectable. PEPCK inhibition also decreased (p=0.02) labeling in uridine diphosphate (UDP)-glucose (Fig. 5D) but did not significantly decrease (p=0.17) M+3 UDP alone (Fig. 5E). PEPCK inhibition decreased (p=0.04) M+6 labeling of ascorbate/vitamin C (Fig. 1F), which derives all of its carbons from glucose.[52]

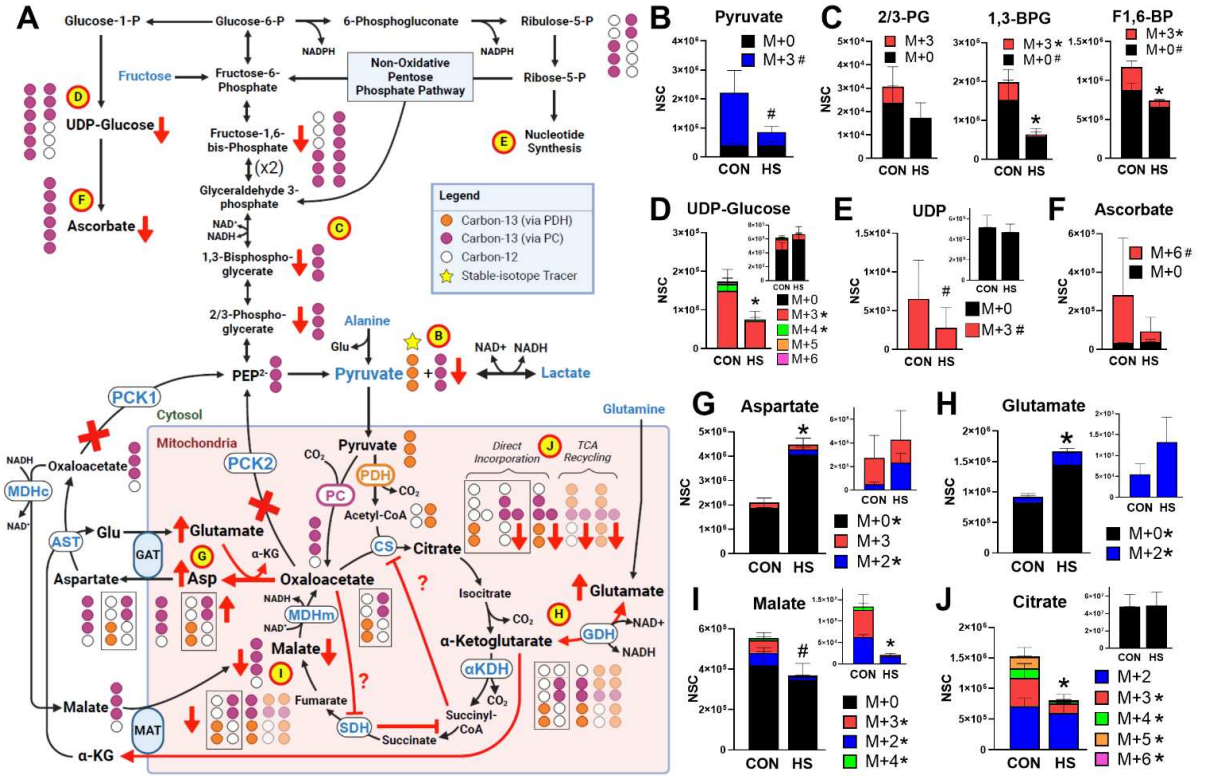

Figure 5: Impacts of PEPCK activity on pyruvate metabolism in cleavage-stage embryos. (**A**) Schematic representing predicted incorporation of carbons from $^{13}C_3$-pyruvate into the major metabolic pathways represented by detected metabolites in the presence and absence of PEPCK inhibition (HS; 0.25 mM hydrazine sulfate). Carbon atom positional transitions are indicated for major metabolites containing ^{13}C derived from pyruvate entering central carbon metabolism through pyruvate dehydrogenase (PDH; orange), pyruvate carboxylase (PC; purple) or unlabeled sources (white), with faded molecules indicating transitions produced by TCA recycling. Metabolites in blue text were provided in the culture medium. Red "X"s and arrows represent demonstrated or predicted effects of PEPCK inhibition. Circled letters correspond to the adjacent data panels in the figure and corresponding text. Data panels represent mean ± SEM of normalized spectral counts (NSC) for unlabeled (M+0; black) and ^{13}C-labeled isotopologues (M+2, +3, +4, etc. indicating number of carbons labeled) of pyruvate (**B**), glycolytic intermediates (**C**), uridine diphosphate (UDP)-glucose (**D**), UDP (**E**), ascorbate (**F**), aspartate (**G**), glutamate (**H**), malate (**I**), and citrate (**J**). Symbols indicate mean differences between (CON) and HS-treated E3 embryos ($N = 5$ replicates of 32 pooled embryos per sample, for a total of 160 embryos per group) by independent samples *t*-test at $^{*}P<0.05$ and $^{\#}P<0.10$.

Interestingly, PEPCK inhibition markedly increased levels of total (p=0.02) and M+2 labeled (p=0.06) aspartate, with no significant impact (p=0.8) on M+3 labeling (Fig. 5G).

Similarly marked increases in unlabeled (p=0.03) and M+2 (p=0.27) glutamate were seen with

PEPCK inhibition (Fig. 5H). However, total malate levels declined along with marked reductions in M+2 ($p=0.001$), M+3 ($p=0.006$), and M+4 ($p=0.08$) labeling following PEPCK inhibition (Fig. 5I). Total levels of citrate, another TCA cycle intermediate, was not affected by PEPCK inhibition; however, M+3, M+4, M+5 and M+6 citrate was reduced ($p<0.04$) compared to controls (Fig. 5J). These results indicate a major function of PEPCK to facilitate gluconeogenesis from pyruvate and increase anaplerotic/cataplerotic flux to/from the TCA cycle that may be important for coordinating cellular redox balance, bioenergetics and biosynthetic processes in developing embryos.

PEPCK facilitates glutaminolysis by enabling the MAS and TCA cycle flux

To further investigate the impact of PEPCK on early embryo metabolism supported by anaplerotic substrates, we traced the fate of carbons and nitrogens from $^{13}C_5{}^{15}N_2$ L-glutamine in the presence and absence of HS. Glutamine is deaminated by glutaminase (GS) in the mitochondrial matrix, thereby generating $^{13}C_5{}^{15}N_1$ (M+5/N+1) glutamate, which enters central carbon metabolism through the production of α-KG by glutamate dehydrogenase (GDH) or mitochondrial AST (Fig. 6A).[53]

Hydrazine sulfate treatment had no effect on embryo glutamine levels, indicating no impact of PEPCK activity on cellular glutamine uptake (Fig. 6B). However, levels of M+5/N+1 glutamate increased 2-fold following PEPCK inhibition, while both M+5 and N+1 labeling were nearly absent ($p<0.3$, Fig. 6C). Aspartate levels were higher following PEPCK inhibition, particularly with M+4/N+1 ($p=0.05$) and M+4 ($p=0.005$) labeling (Fig. 6D). However, a five-fold increase ($p=0.01$) in inosine was also seen following PEPCK inhibition, with only N+1 labeling that followed an identical pattern ($p=0.005$, Fig. 6E). Therefore, as seen in the ^{13}C-

pyruvate tracer studies, decreasing PEPCK resulted in an excessive production of aspartate from mitochondrial OAA.

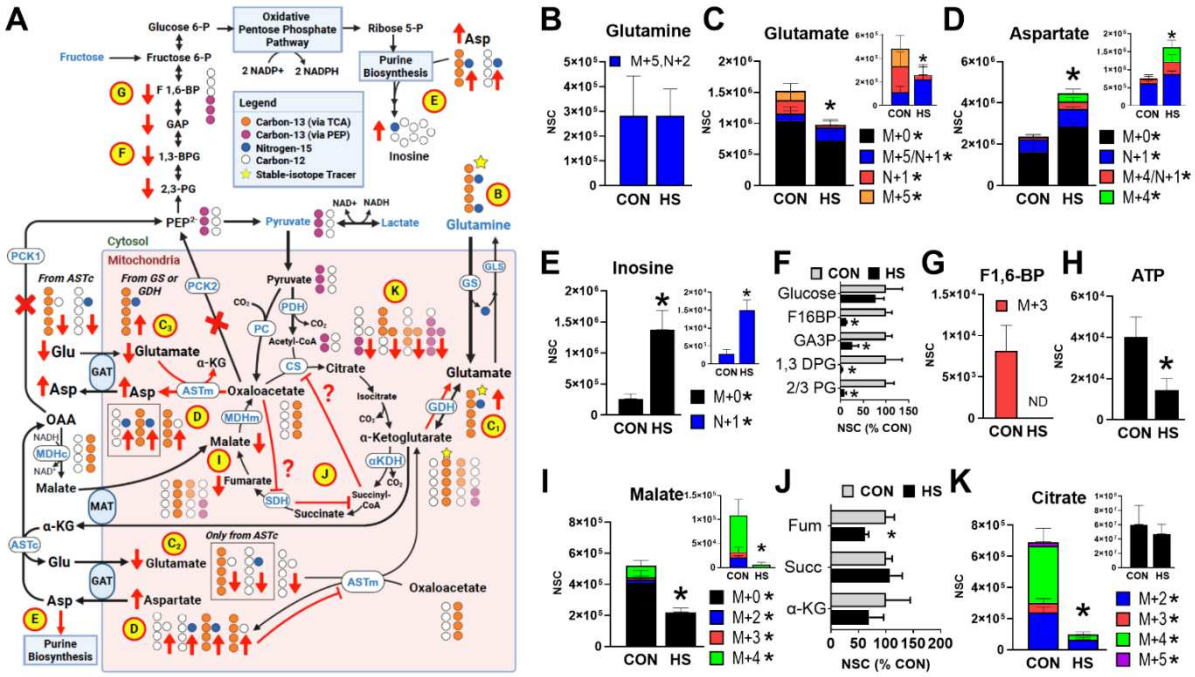

Figure 6: Impacts of PEPCK activity on glutamine metabolism in cleavage-stage embryos. (**A**) Schematic representing predicted incorporation of carbons and nitrogens from $^{13}C_5{}^{15}N_2$ L-glutamine into the major metabolic pathways represented by detected metabolites in the presence and absence of PEPCK inhibition (HS; 0.25 mM hydrazine sulfate). Carbon atom positional transitions are indicated for major metabolites containing ^{13}C derived from glutamine entering central carbon metabolism as α-ketoglutarate (α-KG; orange), following reentry at phosphoenolpyruvate (PEP; purple) or unlabeled sources (white), with faded molecules indicating transitions produced by TCA recycling, and labeled nitrogen in blue. Metabolites in blue text were provided in the culture medium. Red "X"s and arrows represent demonstrated or predicted effects of PEPCK inhibition. Circled letters correspond to the adjacent data panels in the figure and corresponding text. Data panels represent mean ± SEM of normalized spectral counts (NSC) for unlabeled (M+0; black) and ^{13}C-labeled isotopologues (M+2, +3, +4, etc. indicating number of carbons labeled) of glutamine (**B**), glutamate (**C**), aspartate (**D**), inosine (**E**), total glycolytic intermediates (**F**), M+3 labeled fructose 1,6-bisphosphate (**G**), adenosine triphosphate (ATP; **H**), malate (**I**), total fumarate (Fum), succinate (Succ) and α-KG (**J**), and citrate (**K**). *P<0.05 for mean differences between (CON) and HS-treated E3 embryos (N = 5 replicates of 32 pooled embryos per sample, for a total of 160 embryos per group) by independent samples t-tests.

Inhibition of PEPCK markedly decreased total levels of glycolytic intermediates in our glutamine tracer studies (Fig. 6F), similar to findings in the pyruvate tracer studies. However, isotopic labeling from glutamine was undetectable in 3-carbon metabolites, and only trace levels of M+3 labeling was seen in fructose 1,6-bisphosphate, which was absent following PEPCK inhibition (Fig. 6G).

In contrast to the marked increase in inosine (the precursor of all purine nucleotides), total ATP levels decreased 65% ($p=0.05$) following PEPCK inhibition (Fig. 6H). This was associated with a 58% decrease ($p=0.05$) in total malate levels, and almost absent M+4, M+3, and M+2 labeling ($p<0.03$, Fig. 6I). Total fumarate levels tended to be similarly decreased ($p=0.07$) by PEPCK inhibition, while total succinate and α-KG levels were unaffected (Fig. 6J). Moreover, robust M+4 and M+2 labeling of citrate derived from TCA cycle flux of glutamate-derived α-KG through OAA was nearly abolished ($p<0.002$) by PEPCK inhibition (Fig. 6K), similar to reductions in ^{13}C-labeling of citrate from OAA derived from the pyruvate isotoplouge (Fig. 5J).

PEPCK inhibition decreases OCR and increases ECAR in cleaved embryos

To further determine the impact of PEPCK function on embryo metabolism, we utilized a custom-built micro-metabolic sensor capable of simultaneously monitoring the oxygen consumption rate (OCR), used to evaluate mitochondrial oxidative metabolism, and extracellular acidification rate (ECAR), a measure of glycolytic flux, of individual day 3 embryos.[48] The addition of 0.25 mM HS reduced ($p=0.04$) basal OCR by 55% (Fig.7A). This was accompanied by a reciprocal 77% increase ($p=0.04$) in ECAR (Fig. 7B).

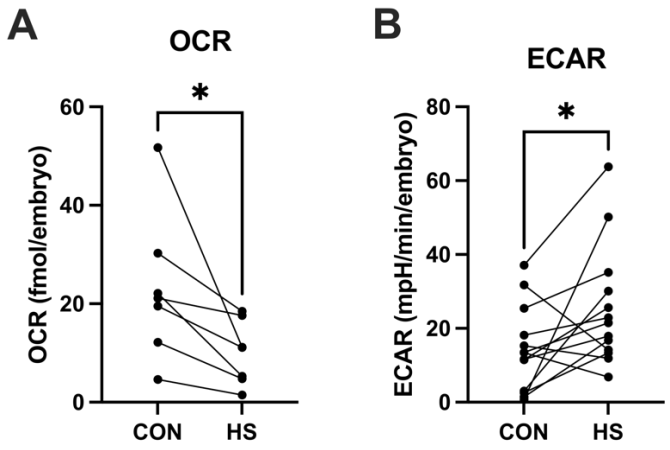

Figure 7: Embryo metabolic assays before (CON) and after addition of 0.25mM hydrazine sulfate (HS) in individual 8-cell embryos. A custom metabolic microsensor was used to measure (**A**) basal rates of oxygen consumption (OCR) as a measure of aerobic metabolism and (**B**) extracellular acidification rate (ECAR) as a measure of glycolytic activity. * Asterisks indicate differences between time points using paired t-test at $P < 0.05$.

Discussion

Pre-implantation embryogenesis is a critical developmental window that requires dynamic, spatial, and temporal coordination of metabolism by mechanisms that are incompletely understood.[49,54] Following oocyte fertilization, the zygote undergoes a series of mitotic cell cleavages without a significant change in embryo volume, which dramatically increases the nuclear:cytoplasmic area ratio and volume-specific metabolic rate. Studies in a wide range of species have found that for cleavage-stage embryos to develop beyond the morula stage to blastocyst formation, they are heavily reliant upon the metabolism of exogenous pyruvate, generation and partitioning of metabolic intermediates that support *de novo* nucleotide synthesis and cellular redox homeostasis, and an elevated rate of oxidative metabolism over glycolysis to meet energy demands.[43] Herein, we show that PEPCK activity plays a pivotal role in integrating all three of these processes in cleavage-stage embryos, linking mitochondrial and cytosolic metabolism to regulate bioenergetic and biosynthetic pathways necessary for development to the

blastocyst stage. Our data demonstrates that PEPCK facilitates pyruvate and glutamine metabolism in the TCA cycle and into various anabolic pathways, thereby supporting metabolic plasticity to ensure embryo survival under states of nutrient stress. These findings align with accumulating evidence for important roles of PEPCK in cancer and stem cell proliferation,[55,56] emphasizing a broader biological relevance of this enzyme beyond its canonical role in hepatic gluconeogenesis.

A common feature of early embryonic metabolism in species ranging from insects[57] to Xenopus[58] and mammals[7,49,59] is that conventional glycolysis is neither necessary nor sufficient for cleavage development prior to the blastocyst stage. This is thought to reflect a preferential shunting of glycolytic intermediates into biosynthetic pathways during the cleavage stage,[43] particularly the PPP, which generates NADPH and ribose needed for production of membrane fatty acids and nucleotides, respectively.[60] In contrast to glucose, exogenous pyruvate is indispensable for development beyond the 2-cell stage,[49] when it is thought to serve as a primary source of acetyl-CoA for the TCA cycle, which supports generation of ATP and essential metabolic intermediates.[49,61] While carbohydrates and monocarboxylates (pyruvate and lactate) are the most frequently discussed energy substrates for developing embryos in the existing literature, supplementation of alternative substrates in vitro, such as amino acids and fats, appear to improve embryo quality.[4–6] The extent of individual metabolic substrate contribution to embryo growth is largely unknown, although the present study demonstrates that while pyruvate and glutamine differentially incorporate into metabolic pathways in embryos, they also overlap considerably. In agreement with the findings of Sharpley et al.,[49] our study shows that an inherent metabolic flexibility exists during embryo development and is highly influenced by the balance and regulation of mitochondrial and cytoplasmic metabolism.

The present study highlights PEPCK as a pro-survival enzyme that supports the shuttling of metabolic substrates to maintain adequate flux throughout various metabolic pathways in embryos. Based on our data, the overall mechanism in which PEPCK facilitates survival involves gluconeogenic activity through pyruvate carboxylase (PC) and removal of oxaloacetate (OAA) from the TCA cycle to increase oxidative metabolism of pyruvate and glutamine. It is clear from our study that PEPCK regulates gluconeogenic activity in embryos, evidenced by reductions in labeled glycolytic intermediates from pyruvate and glutamine in addition to a reduced ability of embryos to survive in carbohydrate-free environments when PEPCK was inhibited. Based on our tracer data, gluconeogenic activity from pyruvate is pyruvate carboxylase (PC) dependent, instead of pyruvate dehydrogenase (PDH), as one labeled carbon is lost in the conversion of pyruvate to acetyl-CoA and all glycolytic intermediates contained three (M+3) labeled carbons.[62] This is consistent with the canonical role of PC as the rate-limiting enzyme in gluconeogenesis,[63] and demonstrates that a key contribution of PEPCK activity to cleavage-stage embryo metabolism may be to enable this "upstream" flux that favors both production of glycolytic intermediates and their shunting from hexose sugar catabolism into biosynthetic pathways such as the PPP. Interestingly, robust M+3 over M+2 labeling of aspartate from U^{13}C-pyruate indicates a similar channeling of PC-derived OAA toward aspartate synthesis, which is consistent with previous evidence for high affinity binding of mAST with PC over MDH.[64] Mitochondrial export of aspartate from this pathway could contribute to the observed M+3 labeling of glycolytic intermediates via a two-step conversion to OAA and phosphoenolpyruvate (PEP) by cytosolic AST and PEPCK, respectively, suggesting an interaction between PEPCK and MAS activities in addition to a role of both mitochondrial and cytosolic PEPCK isoforms to support gluconeogenic activity in embryos. This indicates that the majority of pyruvate used for

biosynthetic reactions is not utilized for ATP production, and instead leave the mitochondria as either PEP or aspartate. It is well described that excessive amounts of catabolic activity and aerobic respiration is detrimental to embryo viability,[65,66] so the ability to bypass the majority of the TCA cycle to favor more direct anabolic activity from pyruvate may be one of the reasons PEPCK is important for embryo growth.

Furthermore, PEPCK's function to remove oxaloacetate from the TCA cycle may prevent the buildup of oxaloacetate in the mitochondria, facilitating increased TCA cycle flux. In the present study, PEPCK inhibition resulted in reduced labeled TCA cycle intermediates, including citrate and malate, and reduced oxygen consumption rate by approximately 50%. As oxaloacetate has been demonstrated to inhibit succinate dehydrogenase (SDH),[67] we suspect that these observations may be a result of a similar mechanism. In addition to the importance of the TCA cycle for developing embryos, the malate-aspartate shuttle (MAS) plays a key role in cellular redox homoeostasis, proliferation, and embryo metabolism by coupling the transfer of reducing equivalents from the cytosol to mitochondria with malate oxidation and the generation of aspartate in mitochondria.[68–70] Cleavage-stage embryos are highly susceptible to reductive stress, indicating a need for NADH oxidation to maintain adequate levels of NAD+. While cytosolic NADH cannot directly traverse the mitochondrial membrane to be oxidized in the electron transport system, the production of malate from OAA oxidizes cytosolic NADH, enters the mitochondria in exchange for alpha-ketoglutarate (aKG), and is oxidized to reform mitochondrial OAA and NADH. This process facilitates the removal of OAA from the TCA cycle via its conversion to aspartate by mAST, and anaplerosis (addition) of aKG produced from glutamate in the same reaction, thus linking the two halves/phases of the TCA cycle/enabling continued flux through TCA cycle. The present data supports a major effect of PEPCK activity

on the MAS, evidenced by the excessive production of aspartate due to a buildup of mitochondrial OAA, leading to abnormal depletion of glutamate and reduced malate when PEPCK is inhibited. Further support of PEPCK function on mitigation of reductive stress can be inferred by increased extracellular acidification rate (ECAR) following PEPCK inhibition. ECAR is primarily a measurement of glycolytic activity and lactate efflux.[48] The production and removal of lactate from a cell is an essential mechanism to regenerate cytosolic NAD+, which is critical for several biosynthetic pathways in the cytosol.[71] While our data did not measure NADH levels directly, the present data supports that PEPCK is a primary regulator of redox control in developing embryos.

Based on findings from the present study, we suspect that PEPCK's role during embryo development is to regulate the metabolism of substrates such as pyruvate and amino acids to meet energy and anabolic demands. PEPCK function is essential for adequate early embryo development, promotes survival in suboptimal environments, and links mitochondrial and cytoplasmic metabolism. These data demonstrate the importance of metabolic flexibility and directed carbon flow to promote survival in a developing embryo. A greater understanding of the metabolic regulation of embryo growth could lead to improved culture systems and targeted selection of metabolically superior embryos to improve assisted reproductive technology.

CHAPTER IV: DELAYED BLASTOCYST EXPANSION AND GENETIC SEX ALTERS THE METABOLIC AND PROTEOMIC SIGNATURE OF BOVINE EMBRYOS

Summary

Slow growing embryos are associated with reduced implantation potential and live birth rates; however, inherent causes of delayed development are not well understood. Metabolism during preimplantation development is responsible for the production of energy and biosynthetic material to support growth, and disturbances to these pathways can reduce embryo viability. The present study utilized electrochemical microsensors to determine differences in oxygen consumption rate and extracellular acidification rate between normal and slow growing, male and female bovine blastocysts. In addition, pooled samples of embryos were subjected to proteomic analysis to determine differences in the abundance of proteins associated with metabolism between both sexes and developmental timing status. In comparison to blastocysts developing over a normal timespan, blastocysts forming 1 to 2 days later had a higher oxygen consumption rate, increased total electron transport complex proteins, and reduced abundance of biosynthetic enzymes when compared to blastocysts developing on a normal timeline. Embryo sex resulted in unique differences in metabolic enzyme abundance with potentially different contributions to delayed development. In addition, male and female embryos had differential protein abundances that may indicate differences in metabolic pathway activity at the blastocyst

---

[3]Chapter IV has been prepared for submission to *Biology of Reproduction*. Authors: Kyle J. Fresa, Ming-Hao Cheng, Alexandra Crook, Anthony Saviola, Thomas W Chen, Elaine M. Carnevale. Funding through USDA NIFA Predoctoral Fellowship Award No. 2023-67011-40510, CRC Bovine Foundation grant, and ARBL Translational Reproductive Biotechnology grant.

stage. Therefore, embryos that take longer to form blastocysts may have an imbalance in the regulation of energy production and biosynthetic activity, which may differentially impact male and female embryos.

Introduction

Preimplantation embryo development is characterized by rapid growth that is critical for pregnancy establishment in the cow.[27] Following fertilization, mammalian embryos must undergo cleavage, compaction into a morula, and formation of a blastocyst containing an inner cell mass, trophectoderm, and blastocoel in order to be considered viable.[72] Blastocysts, the most frequently used stage for embryo transfer and biopsy, usually form from 6 to 7 days in cows, 5 to 6 days in humans, and 4 to 5 days in mice; however, a percentage of embryos require additional time to develop to the blastocyst stage.[73–75] The causes of delayed embryo development are not well understood, although studies have correlated maternal and embryo intrinsic factors, such as maternal aging and aneuploidy to slower embryo growth.[73,76] Slower developing embryos are considered less viable in the bovine,[77] and transfer of in vitro produced, slow-growing embryos are associated with lower implantation, clinical pregnancy, and live birth rates in humans,[78,79] although the reasons behind this are not yet fully understood. Therefore, understanding the cause of delayed embryo development is essential to determine if culture methods or treatments can be developed to improve competence of embryos with delayed developmental timing.

During embryo development, metabolic pathways in the cytosol and mitochondria provide the necessary energy and biosynthetic material for ATP production, synthesis of macromolecules, and cell proliferation.[80] Bovine embryos are highly prolific from the blastocyst to the conceptus stage, doubling in length every day between days 9 and 16.[27,28] In order to

sustain the rapid cell proliferation required for embryo survival during this period, a balance of anabolic and catabolic activities are necessary.[81] The electron transport system, consisting of several protein complexes, forms a proton gradient in the mitochondria that drives the majority of ATP production in embryos.[82] In addition, adequate amounts of metabolic intermediates must be reserved for macromolecule biosynthesis to support growth.[43,80] Theories such as the quiet embryo hypothesis have historically suggested that a less mitochondrial activity is associated with improved developmental potential, allowing for more emphasis on anabolic activity.[65] In contrast, metabolic activity that is too low has also been shown to be detrimental for efficient embryo growth.[83] Environmental conditions, including culture conditions such as temperature and pH, can also affect the rate of embryo growth.[75,84,85] However, why certain embryos take longer to develop than others under the same culture conditions is not clear and is potentially associated with intrinsic embryo differences.

An optimal zone likely exists between low and high metabolic activity that promotes an ideal balance between catabolic and anabolic activity.[66] Few studies have accurately identified the extent of these margins and have been limited to indirect estimates of embryo metabolism, such as spent media metabolite concentrations. However, metabolic activity is dynamic during embryo development, including various changes in substrate metabolism and expression of metabolic enzymes at the blastocyst stage.[54] Our previous work has utilized novel electrochemical microsensors to quantify metabolic activities in oocytes and embryos derived from cows and horses associated with developmental stage and maternal conditions.[86–89] The use of these sensors offer a comprehensive assessment of the metabolic activities present in individual embryos, providing insight into mitochondrial function, glycolysis, and oxidative stress. Direct measurements of embryo metabolic parameters could provide a novel method to

identify alterations in individual embryo metabolic status, allowing new insight into why some embryos are delayed in development timing.

In the present study, we investigated metabolic activity associated with normal and delayed blastocyst formation for male and female embryos to better understand intrinsic embryo factors that affect development timing and associated viability. We postulated that blastocysts forming over a delayed timeline have intrinsic defects and compensatory mechanisms associated with altered metabolic function, which can affect anabolic versus catabolic activity and may differ by genetic sex. To test this hypothesis, we used novel microsensors to directly assess individual embryo metabolic parameters, including measurements of oxygen consumption, extracellular acidification, and reactive oxygen species (ROS) production. The proteome of male or female embryos, considered to be developing on a normal or delayed timeline, were assessed for differential catabolic, antioxidant, and biosynthetic proteins. The association of embryo metabolism and proteome were compared for normal- or delayed-developing embryos identified as male or female.

Methods

Embryo culture

Cumulus-oocyte complexes (COCs) were harvested from slaughterhouse-derived ovaries and selected based on having a compact cumulus mass of ≥3 layers. Chemically defined media formulated for bovine oocyte maturation (CDM-M), fertilization (CDM-F), two-stage embryo culture (CDM1 and CDM2), and HEPES-buffered holding media for room atmosphere (H-CDM) were made in-house at the Animal Reproduction and Biotechnology Laboratory at Colorado State University based on previously published and modified formulas, with

concentrations of metabolic substrates listed in Supplemental Tables 1-6.[18,90] Bovine serum albumin used in media formulations was fatty acid free (Sigma, St. Louis, MO). Oocyte maturation, fertilization, and embryo culture were performed in four-well dishes (NUNC, Thermo Fisher, Waltham, MA) with 0.5 ml of medium per well and 30 to 40 oocytes and 20 to 30 embryos per well. Approximately 300 COCs per replicate were matured in CDM-M, with additions of 0.1 mM cysteamine, 1 μg/μL estradiol 17β, 1 μg/μL LH (USDA-LH-B-5, United States Department of Agriculture), 15 ng/μL FSH (ovine FSH-20, National Institute of Diabetes and Digestive and Kidney Disease, Torrance, CA), and 50 ng/μL epidermal growth factor for 23±1 h at 38.5°C in an atmosphere of 5% CO_2 and air. After maturation, cumulus-oocyte complexes with expanded cumulus cells were fertilized with frozen-thawed, male- or female-sexed sperm, with ≥91% sex-specificity from a single ejaculate (ST Genetics, Navasota, TX) for 18±1 h in F-CDM. Start of sperm-oocyte coincubation was considered time 0 or Day 0. After fertilization, potential zygotes were transferred into holding medium (HCDM-1), vortexed for 90 sec to remove cumulus cells, washed, and transferred into equilibrated CDM-1 at 38.5°C in an atmosphere of 5% CO_2, 5% O_2 and 90% N_2. After approximately 56 h of culture in CDM-1, embryos were removed and assessed for cleavage into at least two blastomeres. Cleaved embryos were transferred into equilibrated CDM-2 at the same temperature and gas mix for the remainder of the experiment. All expanding blastocysts (including hatching and hatched blastocysts) were removed from CDM-2 on Day 7 after approximately 114 h and considered normal in development timing (Normal). The remaining developing embryos, at all developmental stages to early blastocyst, were left in the culture well until Day 8.5-9 or after approximately 144 to162 h of culture in CDM2 (Delayed), at which time expanding blastocysts were removed. Initial selection of embryos for further analysis included a real-time assessment of normal morphology

and an expansion score of ≥6; therefore, poor quality and poorly expanded blastocysts were excluded.[91] Blastocysts fertilized with sexed semen with a high probability of producing genetically female embryos (Female) or male embryos (Male) were maintained separately. Embryos from three replicates, including all groups (Normal or Delayed and Male or Female), were used for metabolic and proteomic analyses; an additional replicate was performed to obtain more embryos for metabolic assays. Images of individual embryos were obtained after culture and used for diameter measurements using CellSens software (Olympus, Tokyo, Japan). Blinded assessments of embryo quality scores (1, excellent to 4, degenerate) were performed using the images for statistical analyses.[91] Embryos for metabolic assays were maintained in holding medium (H-CDM) at 4 ºC for 1.5 to 2 h prior to metabolic sensor analyses. Embryos for proteomic analyses were obtained from three replicates, with each replicate providing between 5 and 10 pooled embryos per group, totaling 18 to 24 embryos for each of the four groups (Normal Male, Normal Female, Delayed Male, and Delayed Female). Pooled embryos were washed in and snap frozen in phosphate-buffered saline until proteomic analysis. The experimental design is depicted in Figure 8.

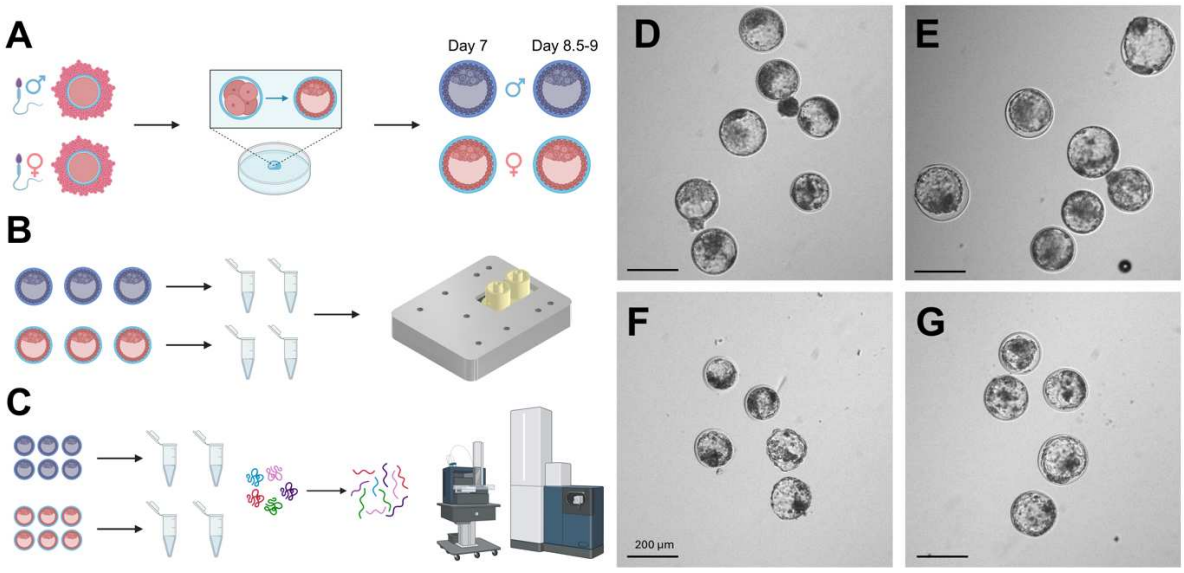

Figure 8: Experimental design and methodology. (**A**) In vitro matured cumulus oocyte complexes were fertilized with male- or female-sexed sperm. All embryos that reached an expanding blastocyst stage were removed from culture on day 7, with the embryo development timing considered normal (Normal); embryos at an earlier stage of development on Day 7, remained in culture until day 8.5 to 9, with embryo development timing considered delayed (Delayed). (**B**) Male and female embryos considered Normal or Delayed were placed in a microchamber for the analysis of oxygen consumption rate (OCR), extracellular acidification rate (ECAR), and hydrogen peroxide production rate, indicative of reactive oxygen species production (ROS). (**C**) Additional male and female blastocysts considered Normal or Delayed were pooled for proteomic analysis. Representative images blastocysts grouped in (**D**) Male Normal, (**E**) Female Normal, (**F**) Male Delayed, and (**G**) Female Delayed. Scale bar at 200 µm.

Microsensor analyses OCR, ECAR, and ROS

A multichannel, three-electrode configuration, electrochemical multisensor platform was used to assess the metabolic activity of individual embryos, including oxygen consumption rate (indicator of aerobic metabolism), extracellular acidification rate (indicator of anaerobic metabolism), and hydrogen peroxide production (indicator of ROS production). The platform consisted of gold working and counter electrodes, along with a silver/silver chloride pseudo-reference electrode, all deposited on a multi-sensor chip. The oxygen sensor surface was functionalized with Nafion, which served as a solid electrolyte; the hydrogen peroxide sensor employed a bare electrode; the indium tin oxide pH electrode was micropatterned using

photolithography. Additional details regarding sensor fabrication and calibration have been described in previous studies.[47,48]

Blastocysts were warmed to 38.5°C for 15 min prior to analysis. Embryos were transferred to a warmed MOPS-buffered holding medium (G-MOPS™; Vitrolife, Sweden) containing 0.04% fatty acid-free BSA; six embryos were individually evaluated in parallel for up to 1 h within a sealed 250-µL microchamber maintained at 38.5°C. Multiple metabolic rates were simultaneously monitored, including oxygen consumption rate (OCR), hydrogen peroxide rate (HPR), and extracellular acidification rate (ECAR). Amperometry was used for OCR and HPR measurements, while potentiometry was employed for ECAR assessment. Baselines of each rate were established prior to sample injection into the platform, and the platform started recording the basal rates from each embryo 10 min after the injection, allowing minimalization of disturbance from the injection process. Sensor readings were considered complete as soon as the platform detected stable metabolic rates from all six embryos; a stable measurement was defined as a maximum deviation of less than 5% over a 3-min window for each metabolic rate measurement.

Proteomics sample preparation and extraction

Preparation of proteomics samples from pooled embryos was performed at the University of Colorado School of Medicine Proteomics Core in Aurora, CO. Samples were reduced, alkylated, and digested using S-Trap™ micro filters (Protifi, Huntington, NY) according to the manufacturer's protocol. Digested peptides were cleaned using Pierce™ C18 Spin Tips (Thermo Scientific) according to the manufacturer's protocol, dried in a vacuum centrifuge, and resuspended in 0.1% formic acid (FA) in mass spectrometry-grade water. Peptides were loaded

into autosampler vials and analyzed directly using a NanoElute liquid chromatography system (Bruker, Germany) coupled with a timsTOF SCP mass spectrometer (Bruker, Germany). Peptides were separated on a 75 µm i.d. × 15 cm separation column packed with 1.9 µm C18 beads (Bruker, Germany) over a 90-min elution gradient. Buffer A was 0.1% FA in water and buffer B was 0.1% FA in acetonitrile. Instrument control and data acquisition were performed using Compass Hystar (version 6.0) with the timsTOF SCP operating in parallel accumulation-serial fragmentation (PASEF) mode under the following settings: mass range 100-1700 m/z, 1/k/0 Start 0.7 V s cm^{-2} End 1.3 V s cm^{-2}; ramp accumulation times were 166 ms; capillary voltage was 4500 V, dry gas 8.0 L min^{-1} and dry temp 200°C. The PASEF settings were: 5 MS/MS scans (total cycle time, 1.03 s); charge range 0–5; active exclusion for 0.2 min; scheduling target intensity 20,000; intensity threshold 500; collision-induced dissociation energy 10 eV.

Fragmentation spectra were searched against the UniProt bovine proteome database using the MSFragger-based FragPipe computational platform.[92] Contaminants and reverse decoys were added to the database automatically. The precursor-ion mass tolerance and fragment-ion mass tolerance were set to 15 and 20 ppm, respectively. Fixed modifications were set as carbamidomethyl (C), and variable modifications were set as oxidation (M), two missed tryptic cleavages were allowed, and the protein-level false discovery rate (FDR) was ≤ 1%.

Statistical analysis

For metabolic measurements, unpaired t-test was used to compare the effects of sex (Male and Female) or developmental timing status (Normal and Delayed). One-way ANOVA was used to compare all groups (Male Normal, Female Normal Male Delayed, and Female

Delayed) followed by Tukey's multiple comparisons post-hoc test to compare group means. For proteomic analysis, MetaboAnalyst was used to compare protein abundance between groups. Peak intensities were uploaded to MetaboAnalyst, normalized by median, log transformed (base 10), and autoscaled. Analyses included unpaired t-test to compare the effects of sex or developmental timing status, one-way ANOVA to compare all groups, and Fisher's LSD post-hoc test to compare group means. Differences in electron transport complex proteins between Normal and Delayed were evaluated by adding peak intensities in each sample and comparing with unpaired t-test. Significance was defined as $p<0.05$, and tendencies were reported for $p\leq0.1$.

Results

Oxygen consumption, extracellular acidification, and reactive oxygen species production

Differences in metabolism associated with embryo sex and developmental timing were assessed using an electrochemical, multichannel microsensor. Metabolic readings were obtained for 46 embryos grouped as Female Normal (n=11), Male Normal (n=13), Female Delayed (n=12), or Male Delayed (n=10). Embryo quality grade and diameter, respectively, did not differ by pooled sex (Male, 1.6±0.2 and 184.6±6.3 μm and Female, 2.3±0.1 and 182.1±5.9 μm, $p>0.1$) or pooled developmental timing (Normal, 1.9±0.1 and 189.1±4.9 μm and Delayed, 2.3±0.2 and 177.1±7.0 μm, $p>0.1$). Representative images of groups are included in Figure 8. Among all groups, OCR differed ($p=0.003$) and was greater ($p<0.04$) in Female Delayed than Male and Female Normal; Male Delayed was greater ($p=0.03$) than Male Normal and tended ($p=0.07$) to be greater than Female Normal (Figure 9A). Overall, OCR was greater ($p=0.0002$) in Delayed when compared to Normal (Figure 9B). When comparing Male and Female, OCR was similar ($p=0.9$) (Figure 9C). Extracellular acidification rate was not altered ($p=0.4$) among all groups,

regardless of developmental timing status and sex (Figure 9D-F). Hydrogen peroxide production rate (ROS) was similar among all groups (p=0.3); however, ROS tended to be higher in Delayed than Normal (p=0.1) and in Female than Male (p=0.07) (Figure 9G-I). Although metabolic differences were not significant for blastocysts of Female and Male, embryos capable of forming an expanding blastocyst, but delayed in development timing, had a metabolic profile suggestive of compensatory efforts to increase energy production.

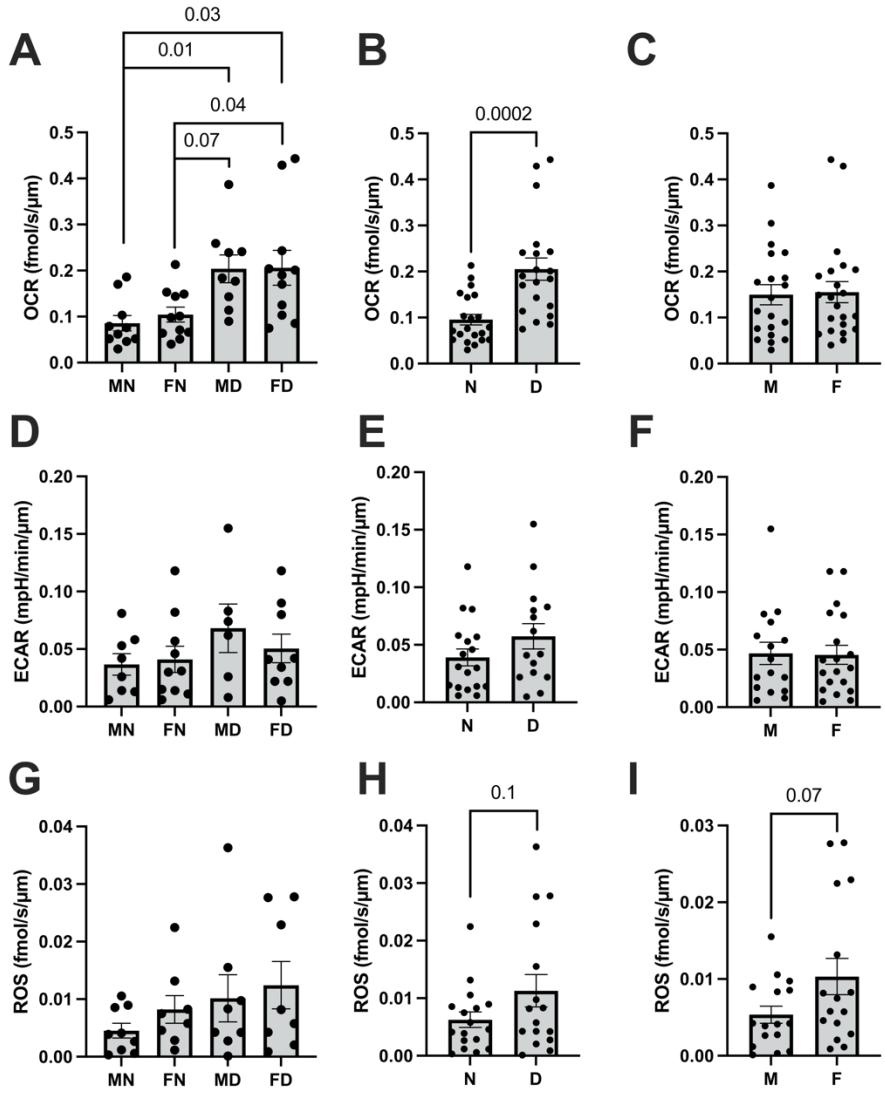

Figure 9: Embryo metabolic assays. Rates of (**A-C**) oxygen consumption (OCR), (**D-F**) extracellular acidification (ECAR), and (**G-I**) hydrogen peroxide production indicative of reactive oxygen species (ROS) in blastocysts forming on day 7 (normal development timing,

Normal, N, n=24) or day 8.5-9 (delayed development timing, Delayed, D, n=22) and produced using sperm sexed as female (F) or male (M). Three replicates with total embryos for MN (n=13), FN (n=11), MD (n=10) and FD (n=12). Data were compared using one way ANOVA and Tukey's test for multiple comparisons (A, D, G) or unpaired t-test (B-C, E-F, H-I). P-values ≤0.1 are presented above bars.

Protein differences associated with timing of embryo development

To further explore differences in metabolism associated with normal or delayed embryo development timing, Male (n=40 embryos) and Female (n=42 embryos) from three replicates were pooled to compare proteins associated with metabolism in Normal and Delayed. A total of 50 proteins were differentially abundant ($p<0.05$) between Normal and Delayed (Figure 10, Supplemental Table 11). Of those, 12 were higher, and 38 were lower (Figure 10A), with more component variability noted in Delayed versus Normal (Figure 10B). Pathway enrichment analysis revealed important functional clusters, with most affected in Delayed and including ribosomal activity, protein metabolism, biosynthetic processes, translation, and acetylation (Figure 10D). Proteins involved with biosynthesis were primarily lower in Delayed ($p<0.05$), including those associated with protein synthesis (ribosomal proteins RPS18, RPL26, RPL35A, RPS7, RPS21, RPL30; eukaryotic translation initiation factor 3 subunit J [EIF3J]; elongation factor 1-beta [EEF1B2]; eukaryotic translation initiation factor 5A-1 [EIF5A]), nucleotide production (adenylosuccinate lyase [ADSL], phosphoribosylpyrophosphate synthetase [PRPS1], transketolase [TKT]), lipogenesis (spermine synthase [SMS]), and ATP production (ATP synthase subunit D [ATP5PD]; ATP synthase F1 subunit delta [ATP5F1D]) (Table 1). Only two anabolic proteins were higher ($p<0.02$) in Delayed, involving biosynthesis of cholesterol (NAD(P)-dependent steroid dehydrogenase-like [NSDHL]) and ATP (ATP synthase membrane subunit f [ATP5MF]) (Table 1). In addition, two isoforms of peroxiredoxins (PRDX2 and PRDX3), antioxidant enzymes that reduce intracellular peroxides, were lower ($p<0.04$) in

Delayed (Table 1). The pro-apoptotic protein, scinderin [SCIN], was higher (p=0.02) in Delayed (Table 1). Proteins involved in the TCA cycle, such as citrate synthase (CS), were lower (p=0.04) in Delayed, while NADH dehydrogenase 1 beta subcomplex subunit 9 [NDUFB9], a component of complex I of the electron transport system, was higher in Delayed (p=0.03) (Table 1). Proteins were altered in embryos considered normal or delayed in development timing, consistent with reduced biosynthesis and more metabolic variability in Delayed.

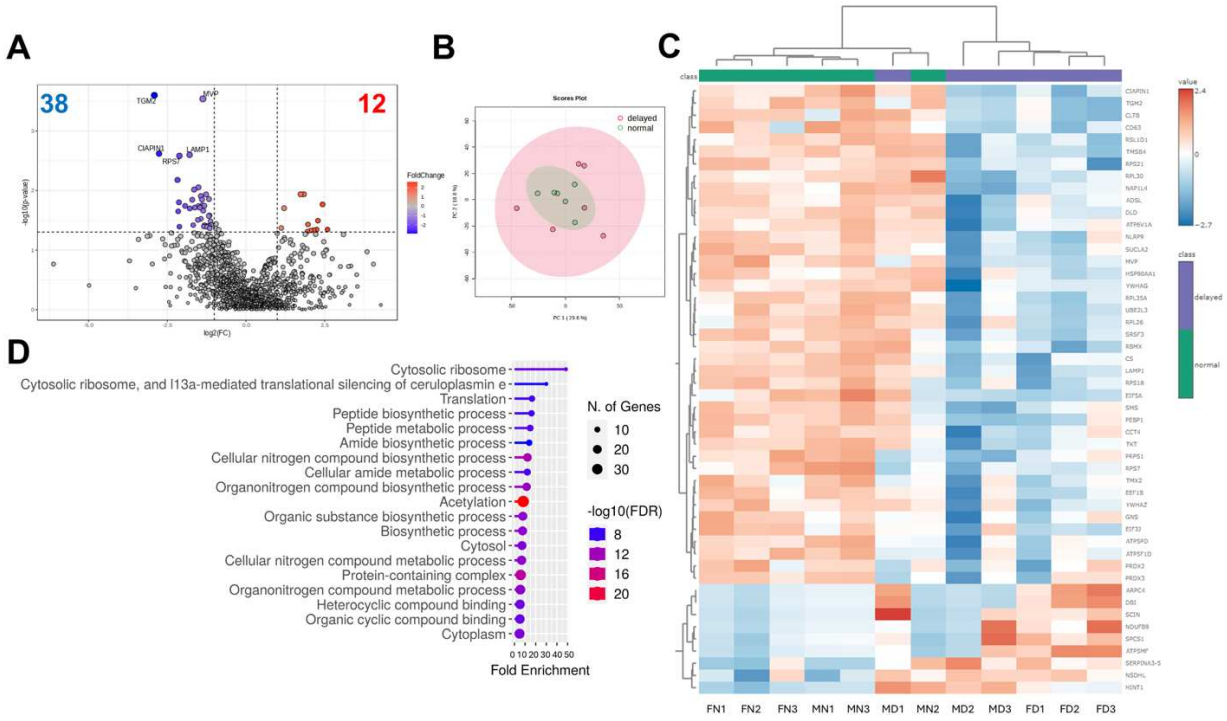

Figure 10: Protein abundance profile of pooled Male and Female embryos considered normal (Normal) or delayed (Delayed) in timing to reach the expanding blastocyst stage of development. (**A**) Volcano plot indicating fold differences, (**B**) Principal component analysis (PCA) plot with Normal (green) and Delayed (pink), (**C**) Heatmap and hierarchical clustering of 50 proteins with significant fold differences, (**D**) Enrichment analysis demonstrating similar pathway activity associated with protein differences. Three replicates with a total of 44 Normal and 38 Delayed blastocysts. Data were median normalized, log2 transformed, auto scaled, and compared using unpaired t-test with $p<0.05$. Horizontal line in volcano plot (A) at $p<0.05$.

Table 1. Pathway association, protein identification, fold difference (FD), and p-values associated with differentially abundant proteins for pooled Male and Female embryos considered normal (Normal) or delayed (Delayed) in timing to reach the expanding blastocyst stage of development. Three replicates with total embryos for Normal (n=44) and Delayed (n=38). Fold difference (FD) indicates Delayed relative to Normal.

Pathway	ID	Name	FD	P-value
Protein Synthesis	RPS18	Ribosomal protein S18	0.44	0.03
	RPL35A	Ribosomal protein L35a	0.46	0.03
	RPL26	Ribosomal protein L26	0.45	0.03
	RPS7	Ribosomal protein S7	0.23	0.003
	RPS21	Ribosomal protein S21	0.31	0.01
	RPL30	Ribosomal protein L30	0.29	0.02
	EIF3J	Eukaryotic translation initiation factor 3 subunit J	0.32	0.02
	EEF1B	Elongation factor 1-beta	0.38	0.01
	EIF5A	Eukaryotic translation initiation factor 5A-1	0.31	0.04
Nucleotide Production	ADSL	Adenylosuccinate lyase	0.45	0.04
	PRPS1	Phosphoribosylpyrophosphate synthetase 1	0.22	0.007
	TKT	Transketolase	0.35	0.02
Lipogenesis	SMS	Spermine synthase	0.35	0.03
TCA cycle/ATP Produciton	ATP5PD	ATP synthase subunit D	0.37	0.03
	ATP5F1D	ATP synthase F1 subunit delta	0.26	0.02
	ATP5MF	ATP synthase membrane subunit f	3.33	0.01
	CS	Citrate synthase	0.47	0.04
	NDUFB9	NADH dehydrogenase 1 beta subcomplex subunit 9	4.88	0.03
Stress Response	PRDX2	Peroxiredoxin 2	0.40	0.04
	PRDX3	Peroxiredoxin 3	0.22	0.02
Apoptosis	SCIN	Scinderin	2.44	0.02
Cholesterol Synthesis	NSDHL	NAD(P)-dependent steroid dehydrogenase-like	1.84	0.01

Electron transport system complex organization associated with developmental timing

To evaluate potential dysregulation of the electron transport system, as suggested by greater OCR in Delayed, sums of normalized protein intensities unique to individual electron transport system complexes were compared between Normal and Delayed. Complex II (succinate dehydrogenase) proteins were higher (p=0.02) in Delayed when compared to Normal (Figure 11B). Other complexes, including proteins for complex I (Type I NADH

dehydrogenase), complex III (CoQH2-cytochrome c reductase), and complex IV (cytochrome c oxidase) tended to be greater ($p \leq 0.8$) in Delayed when compared to Normal (Figure 11A, C-D). The sum of complex 5 (ATP synthase) proteins, all complexes, and total mitochondrial proteins did not differ ($p > 0.1$) by timing of blastocyst development (Figure 11E-G).

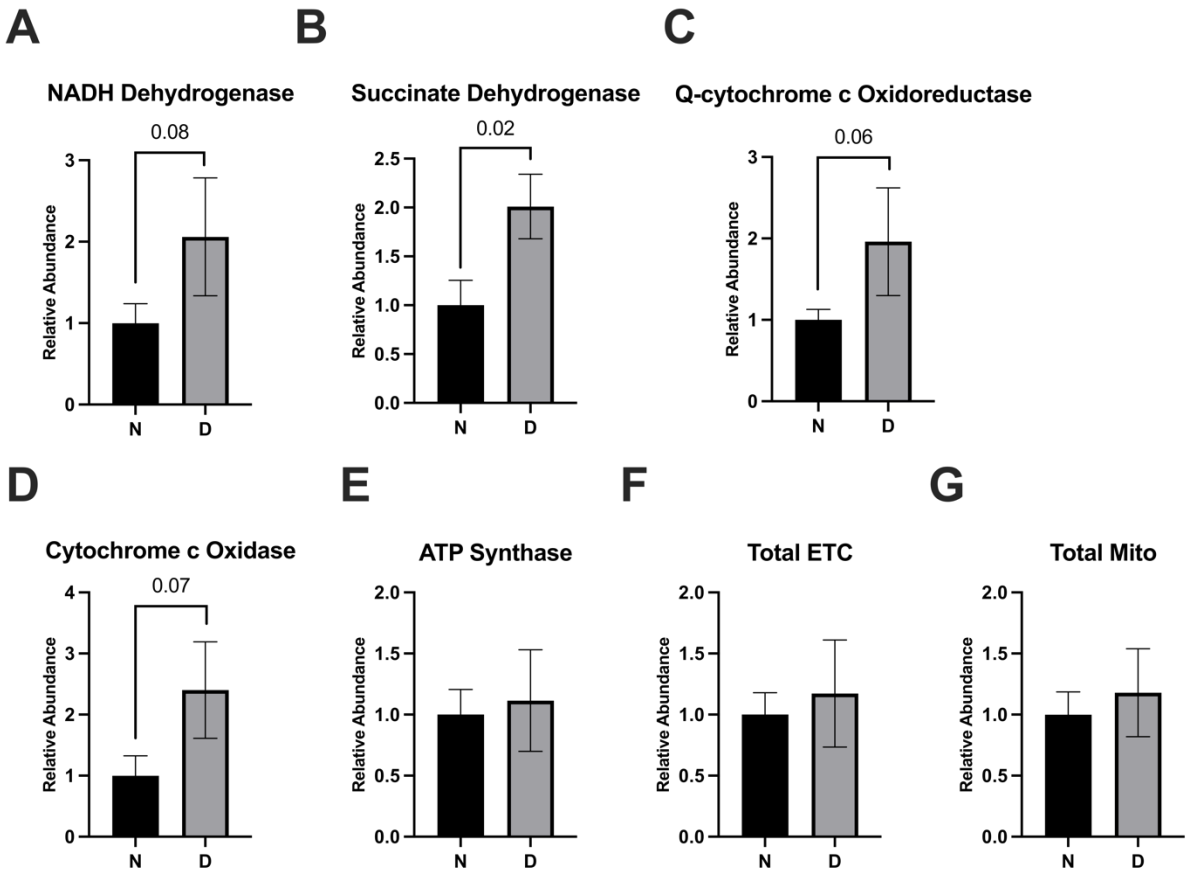

Figure 11: Means ± SEM for combined normalized intensity of proteins, from embryos considered normal (N) or delayed (D) in developmental timing, composing complexes I-V of the electron transport system: (A) Complex 1: NADH dehydrogenase, (B) Complex II: succinate dehydrogenase, (C) Complex III: Q-cytochrome c oxidoreductase, (D) Complex IV: cytochrome c oxidase, (E) Complex V: ATP synthase, (F) Combined intensity of all complexes, and (G) Total mitochondrial protein. Three replicates for a pooled total of embryos for Normal (n=44) and Delayed (n=38). Data were compared using unpaired t-test with p-values above bars for differences $p < 0.1$.

Protein differences associated with embryo sex

To evaluate overall differences in proteomes of Male and Female, embryos considered normal or delayed in developmental timing were pooled. A total of 48 proteins were greater ($p<0.05$) in Female when compared to Male, including pathways such as glucose metabolism (glucose transporter 1 [SLC2A1]; 6-phosphofructokinase [PFKL]); stress response (superoxide dismutase 2 [SOD2]; peroxiredoxin 4 [PRDX4]), mitochondrial function (isocitrate dehydrogenase [NAD] subunit beta [IDH3B]), and biosynthesis (D-dopachrome tautomerase [DDT]; vanin 1 [VNN1]) (Table 2, Supplemental Table 12). In comparison to Female, Male had greater ($p<0.05$) abundance of 23 proteins, involving pathways such as apoptosis (14-3-3 protein epsilon [YWHAE]) and biosynthesis (ribosomal protein S3A [RPS3A]; pyrroline-5-carboxylate reductase 3 [PYCR3]; HMG-CoA reductase [HMGCR]; ferrochelatase [FECH]) (Table 2). Therefore, protein differences were observed between Male and Female, suggesting that embryo sex could be associated with different proteomes, although sex differences were not observed in microsensor metabolic analyses.

To assess sex differences associated with embryos that developed at a normal (optimal) timing, the proteome of Male or Female embryos considered Normal were compared. Between the samples from the two groups obtained from three replicates, 27 proteins were greater in Female Normal (n=24 total embryos), and 38 proteins were greater in Male Normal (n=20 total embryos, $p<0.05$, Figure 13). Pathway enrichment analysis of embryos with normal development timing for Male and Female revealed possible differences in proteins involved with proteolysis (n=10) and cell cycle regulation (n=10); however, very few metabolic proteins were differentially abundant between Male and Female embryos with normal timing of development to the blastocyst stage (Figure 13). Cytochrome c oxidase subunit 6B1 (COX6B1), a component

of complex IV in the electron transport system, and mitochondrial 2-oxoglutarate/malate carrier protein (SLC25A11) were both higher in embryos with normal development timing for Male when compared to Female ($p<0.05$, Table 3). Although differences were observed in the proteome of Male and Female embryos with normal developmental timing, protein differences specifically associated with metabolism were minimal and supported microsensor metabolic analyses.

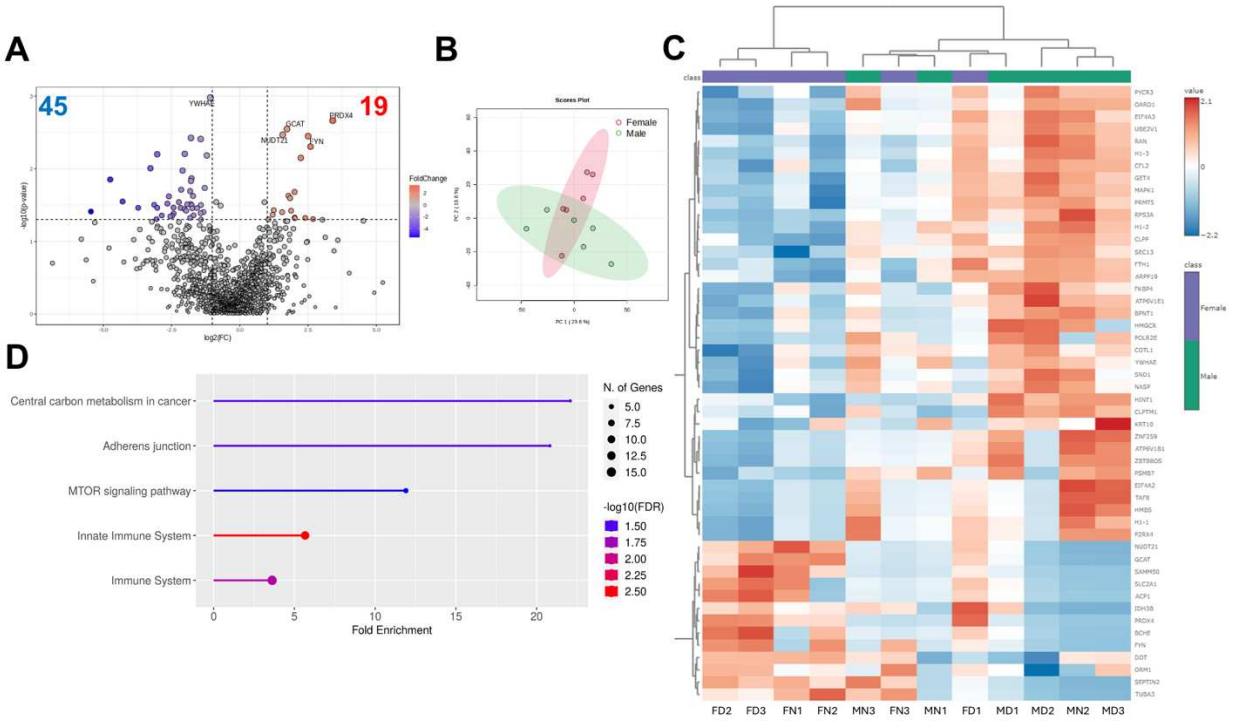

Figure 12. Protein abundance profile of pooled Male or Female blastocysts with normal and delayed development timing. (**A**) Volcano plot indicating fold differences, (**B**) Principal component analysis (PCA) plot with Male (green) and Female (pink), (**C**) Heatmap and hierarchical clustering of 50 proteins with significant fold differences, (**D**) Enrichment analysis demonstrating similar pathway activity associated with protein differences. Three replicates for a total of 40 Male and 42 Female embryos. Data were median normalized, log2 transformed, auto scaled, and compared using unpaired t-test with $p<0.05$. Horizontal line in volcano plot (A) at $p<0.05$.

Table 2. Pathway association, protein identification, fold difference (FD), and p-values associated with differentially abundant proteins for pooled Female or Male embryos considered normal (Normal) and delayed (Delayed) in timing to reach the expanding blastocyst stage of development. Three replicates with total embryos for Male (n=40) and Female (n=42). Fold difference indicates Female relative to Male.

Pathway	ID	Name	FD	P-value
Glucose Metabolism	SLC2A1	Glucose transporter protein type 1	1.55	0.04
	PFKL	Phosphofructokinase	2.02	0.05
Stress Response	SOD2	Superoxide dismutase 2	6.42	0.05
	PRDX4	Peroxiredoxin 4	10.57	0.002
TCA cycle/ATP Production	IDH3B	NAD-dependent isocitrate dehydrogenase	4.02	0.02
Biosynthesis	DDT	D-dopachrome tautomerase	2.37	0.04
	VNN1	Vanin 1	4.03	0.05
	RPS3A	Ribosomal protein S3A	0.41	0.02
	PYCR3	Pyrroline-5-carboxylate reductase 3	0.22	0.03
	HMGCR	HMG-CoA reductase	0.02	0.04
	FECH	Ferrochelatase	0.18	0.04

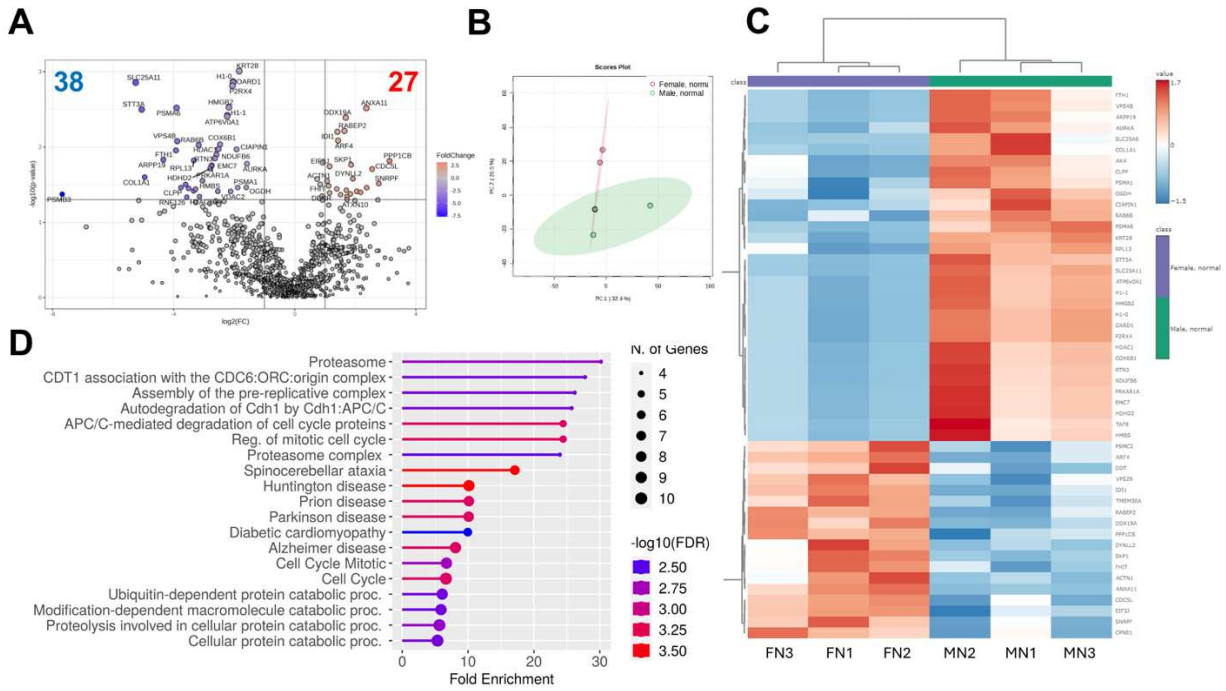

Figure 13: Protein abundance profile of embryos with normal timing of development for Male (MN) and Female (FN) blastocysts. (**A**) Volcano plot indicating fold differences, (**B**) Principal component analysis (PCA) plot with MN (green) and FN (pink), (**C**) Heatmap and hierarchical clustering of 50 proteins with significant fold differences, (**D**) Enrichment analysis

demonstrating similar pathway activity associated with protein differences. Three replicates with total embryos for MN (n=20) and FN (n=24). Data were median normalized, log2 transformed, auto scaled, and compared using unpaired t-test with $p<0.05$. Horizontal line in volcano plot (A) at $p<0.05$.

Table 3. Pathway association, protein identification, fold difference (FD), and p-values associated with differentially abundant proteins for Female or Male embryos considered normal (Normal) in timing to reach the expanding blastocyst stage of development. Three replicates with total embryos for Male (n=20) and Female (n=24). Fold difference (FD) indicates Female relative to Male.

Pathway	ID	Name	FD	P-value
Cell cycle regulation/protein degradation	PSMA6	Proteasome subunit alpha type-6	0.07	0.003
	HDAC1	Histone deacetylase 1	0.17	0.01
	ARPP19	cAMP-regulated phosphoprotein 19	0.05	0.01
	AURKA	Aurora kinase A	0.33	0.02
	SKP1	S-phase kinase-associated protein 1	3.63	0.02
	DYNLL2	Dynein light chain 2, cytoplasmic	3.78	0.03
	PSMC2	26S proteasome regulatory subunit 7	1.79	0.03
	PSMA1	Proteasome subunit alpha type-1	0.27	0.03
	SFN	14-3-3 protein sigma	1.86	0.04
	VPS4B	Vacuolar protein sorting-associated protein 4B	0.07	0.008
	FHIT	Bis(5'-adenosyl)-triphosphatase	2.17	0.03
	CLPP	ATP-dependent Clp protease proteolytic subunit, mitochondrial	0.07	0.03
	RNF126	E3 ubiquitin-protein ligase RNF126	0.08	0.05
TCA cycle/ATP Production	COX6B1	Cytochrome c oxidase subunit 6B1	0.18	0.009
	NDUFB6	NADH dehydrogenase [ubiquinone] 1 beta subcomplex subunit 6	0.17	0.01
	OGDH	2-oxoglutarate dehydrogenase complex component E1	0.33	0.03
Protein biosynthesis	RPL13	Large ribosomal subunit protein eL13	0.10	0.02
	EIF3J	Eukaryotic translation initiation factor 3 subunit J	2.22	0.02
	EIF3B	Eukaryotic translation initiation factor 3 subunit B	2.85	0.04

Sex-specific differences in slow-growing embryos

Proteomes of blastocysts considered to be Normal or Delayed from Male and Female were compared to determine if sex-specific differences were associated with slow-growing embryos. For Male Delayed relative to Male Normal, respectively, 16 and 2 proteins had greater

or less fold differences ($p<0.05$, Figure 14, Supplemental Table 14) primarily involving protein and nucleotide biosynthesis and including less phosphoribosylpyrophosphate synthetase 1 (PRPS1) and ribosomal proteins (RPS7, RPL35, RPL13A, RPL18, RPL10A) ($p<0.05$, Table 4). In contrast, substantially more differences were observed for Female, with 99 less and 83 greater fold differences in proteins for Female Delayed when compared to Female Normal ($p<0.05$, Figure 15, Supplemental Table 15). Pathway enrichment analysis of Normal and Delayed for Female revealed differences in pathways involved with mitochondrial function (n=39), cellular component biogenesis (n=40), and various macromolecule metabolic processes (n=63) (Figure 15D). In Female, Delayed when compared to Normal had higher stress response proteins including glutathione S-transferase 3 (MGST3), phospholipid hydroperoxide glutathione peroxidase (GPX4), and peroxiredoxin-4 (PRDX4) ($p<0.05$, Table 5). Proteins involved in protein synthesis also differed for Female Delayed versus Normal, with greater (elongation factor 1-alpha 1 [EEF1A1]; ribosomal proteins RPL7, RPS23, RPS25, RPL24) and less (ribosomal proteins RPL17, RPL3, RPL35A; eukaryotic translation initiation factor 3 subunit J [EIF3J], eukaryotic translation initiation factor 2 subunit 1 [EIF2S2]) ($p<0.05$, Table 5) fold differences. For Female with normal versus delayed timing development, enzymes involved with lipid metabolism were both higher (very-long-chain enoyl-CoA reductase [TECR]; ethanolamine-phosphate cytidylyltransferase [PCYT2]; diphosphomevalonate decarboxylase [MVD]) and lower (isopentenyl-diphosphate Delta-isomerase 1 [IDI1]; geranylgeranyl pyrophosphate synthase [GGPS1]) ($p<0.05$, Table 5). Similar to the trends observed with combined Male and Female, proteins involved in the electron transport system were generally greater in Female Delayed when compared to Normal, including ATP synthase subunit f (ATPMF), cytochrome b-c1 complex subunit 9 (UQCR10), NADH dehydrogenase [ubiquinone]

1 alpha subcomplex assembly factor 4 (NDUFAF4), NADH-ubiquinone oxidoreductase chain 5 (MT-ND5), and cytochrome c oxidase subunit 7A-related protein, mitochondrial (COX7A2L), although cytochrome b-c1 complex subunit 7 (UQCRB) was greater in Female Normal versus Delayed ($p<0.05$, Table 5). In addition, citrate synthase (CS) and succinate-CoA ligase (SUCLA2) were greater ($p\leq0.02$) in Female Normal when compared to Female Delayed (Table 5). Sex-associated differences in the proteomes of Male and Female blastocysts were observed, with substantially more variation noted for Female than Male.

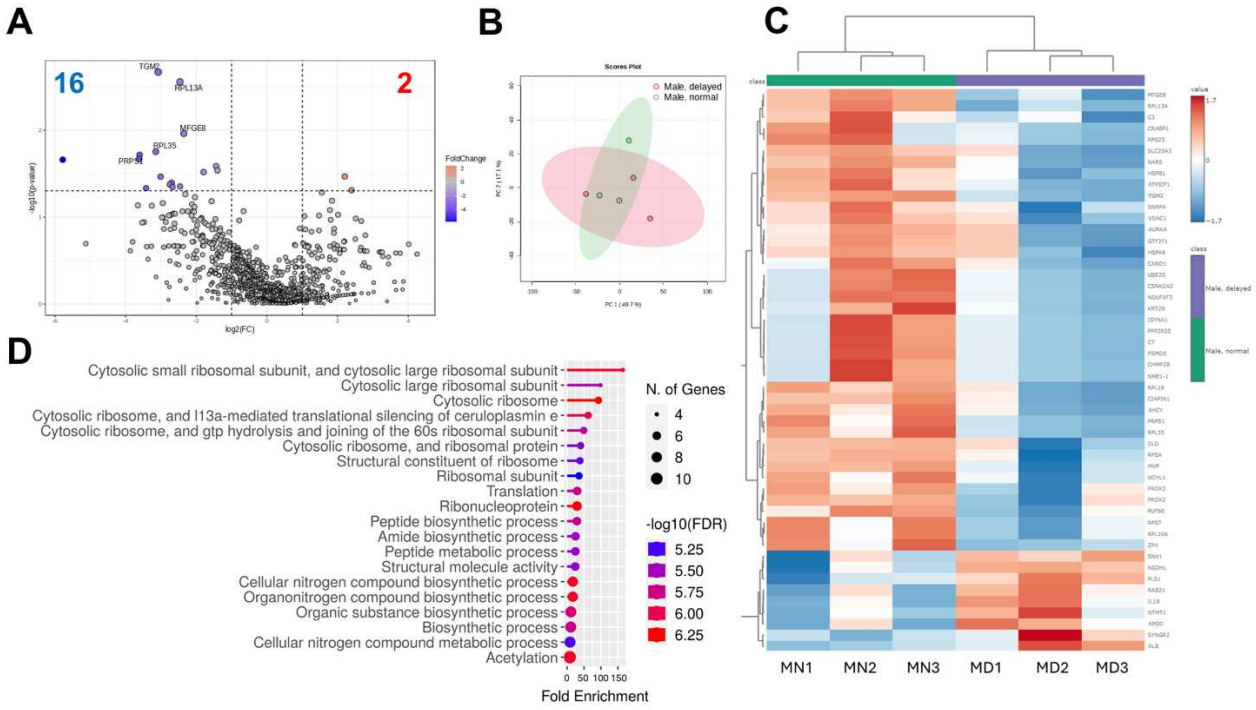

Figure 14. Protein abundance profile of Male embryos with normal (MN) and delayed (MD) timing of blastocyst development. (**A**) Volcano plot indicating fold differences, (**B**) Principal component analysis (PCA) plot with MN (green) and MD (pink), (**C**) Heatmap and hierarchical clustering of 50 proteins with significant fold differences, (**D**) Enrichment analysis demonstrating similar pathway activity associated with protein differences. Three replicates with total embryos for MN (n=20) and MD (n=20). Data were median normalized, log2 transformed, auto scaled, and compared using unpaired t-test with $p<0.05$. Horizontal line in volcano plot (A) at $p<0.05$.

Table 4: Pathway association, protein identification, fold difference (FD), and p-values associated with differentially abundant proteins for pooled Male embryos considered Normal and Delayed in developmental timing. Three replicates with total embryos for Normal (n=20) and Delayed (n=20). Fold difference indicates Male Delayed relative to Male Normal.

Pathway	ID	Name	FD	P-value
Protein Synthesis	RPL13A	Large ribosomal subunit protein uL13	0.18	0.003
	RPL35	Large ribosomal subunit protein uL29	0.11	0.02
	RPL10A	Large ribosomal subunit protein uL16z	0.15	0.04
	RPL18	Large ribosomal subunit protein eL18	0.14	0.04
	RPS7	Small ribosomal subunit protein eS7	0.16	0.05
Nucleotide Production	PRPS1	Ribose-phosphate pyrophosphokinase 1	0.08	0.02

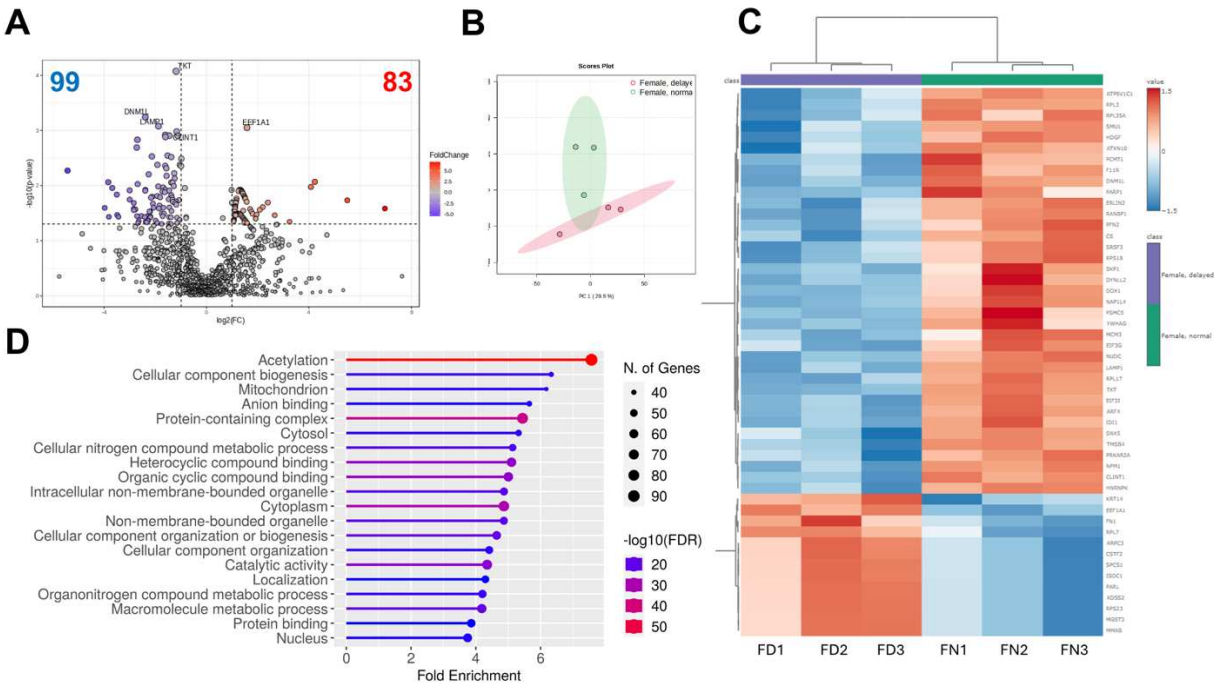

Figure 15. Protein abundance profile of Female embryos with normal (FN) and delayed (FD) timing of blastocyst development. (**A**) Volcano plot indicating fold differences, (**B**) Principal component analysis (PCA) plot with FN (green) and FD (pink), (**C**) Heatmap and hierarchical clustering of 50 proteins with significant fold differences, (**D**) Enrichment analysis demonstrating similar pathway activity associated with protein differences. Three replicates with total embryos for FN (n=24) and FD (n=18). Data were median normalized, log2 transformed, auto scaled, and compared using unpaired t-test with $p<0.05$. Horizontal line in volcano plot (A) at $p<0.05$.

Table 5. Pathway association, protein identification, fold difference (FD), and P-values associated with differentially abundant proteins for pooled Female embryos considered Normal and Delayed in timing to reach the expanding blastocyst stage of development. Three replicates with total embryos for Normal (n=24) and Delayed (n=18). Fold difference indicates Female Delayed relative to Female Normal.

Pathway	ID	Name	FD	P-value
Protein Synthesis	EEF1A1	Elongation factor 1-alpha 1	3.00	0.0009
	RPL17	Large ribosomal subunit protein uL22	0.46	0.001
	EIF3J	Eukaryotic translation initiation factor 3 subunit J	0.15	0.001
	RPL3	Large ribosomal subunit protein uL3	0.27	0.004
	RPS18	Small ribosomal subunit protein uS13	0.34	0.007
	RPL7	Large ribosomal subunit protein uL30	16.88	0.01
	RPL35A	RPL35A ribosomal protein L35a	0.19	0.01
	RPS23	Small ribosomal subunit protein uS12	2.52	0.01
	RPS25	Small ribosomal subunit protein eS25	2.26	0.02
	RPL24	Large ribosomal subunit protein eL24	45.10	0.02
	EIF2S2	Eukaryotic translation initiation factor 2 subunit 1	0.26	0.05
TCA cycle/ ATP Production	CS	Citrate synthase	0.51	0.003
	SUCLA2	Succinate--CoA ligase	0.26	0.02
	ATP5MF	ATP synthase subunit f, mitochondrial	2.21	0.02
	UQCR10	Cytochrome b-c1 complex subunit 9	2.12	0.03
	NDUFAF4	NADH dehydrogenase [ubiquinone] 1 alpha subcomplex assembly factor 4	2.22	0.03
	MT-ND5	NADH-ubiquinone oxidoreductase chain 5	2.53	0.03
	UQCRB	Cytochrome b-c1 complex subunit 7	0.31	0.04
	COX7A2L	Cytochrome c oxidase subunit 7A-related protein, mitochondrial	2.69	0.04
Lipid Metabolism	IDI1	Isopentenyl-diphosphate Delta-isomerase 1	0.15	0.002
	GGPS1	Geranylgeranyl pyrophosphate synthase	0.13	0.02
	TECR	Very-long-chain enoyl-CoA reductase	2.17	0.02
	PCYT2	Ethanolamine-phosphate cytidylyltransferase	2.40	0.03
	MVD	Diphosphomevalonate decarboxylase	2.20	0.03
Stress Response	MGST3	Glutathione S-transferase 3, mitochondrial	2.54	0.01
	HSP90AA1	Heat shock protein HSP 90-alpha	0.39	0.02
	GPX4	Phospholipid hydroperoxide glutathione peroxidase	2.77	0.02
	PRDX4	Peroxiredoxin-4	5.26	0.02

To better isolate possible sex differences associated with delayed embryo development, all groups (Normal, Delayed, Male and Female) were compared by ANOVA (Figure 16,

Supplemental Table 16). In Female, delayed embryo development timing was uniquely associated with higher ($p<0.05$) proteins involved with the stress response (peroxiredoxin-4 [PRDX4]; superoxide dismutase 2 [SOD2]; glutathione S-transferase 3 [MGST3]), anion transport (voltage-dependent anion-selective channel VDAC2, VDAC3), and protein biosynthesis (ribosomal protein S30 [FAU]; ribosomal protein S25 [RPS25]; eukaryotic translation elongation factor 1 alpha 1 [EEF1A1]) (Table 6). When compared to Female Delayed, Female Normal had higher ($p=0.04$) abundance of carnitine palmitoyltransferase II (CPT2), an enzyme important for fatty acid metabolism (Table 6). Only Male had proteins involved in nucleotide synthesis (phosphoribosyl pyrophosphate synthetase 1 [PRPS1]), protein biosynthesis (ribosomal proteins RPS7, RPSA), and anion transport (Voltage-dependent anion-selective channel 1 [VDAC1]) lower ($p<0.05$) in Delayed when compared to Normal (Table 6).

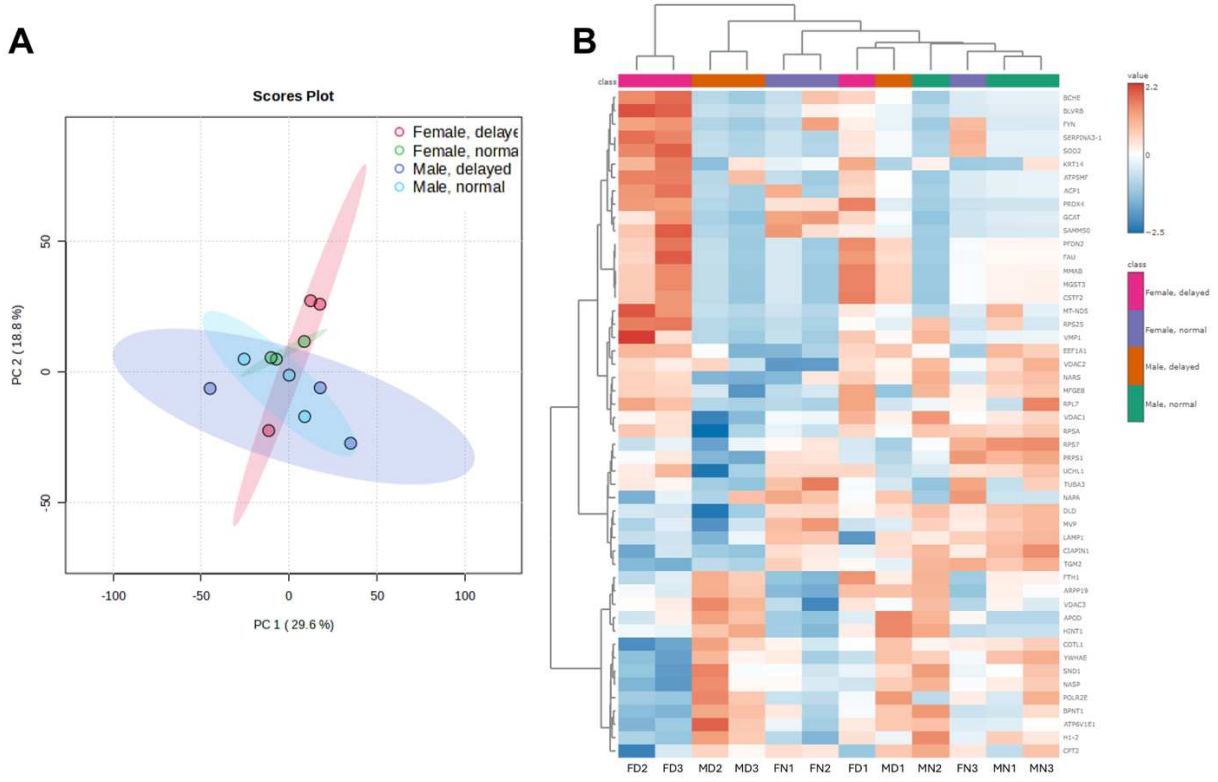

Figure 16. Effect of sex and developmental status on the protein abundance profile of pooled blastocysts from Female Normal (FN), Female Delayed (FD), Male Normal (MN), and Male Delayed (MD). (**A**) Principal component analysis (PCA) plot with FN (green), FD (pink), MN

(blue), and MD (purple). (**B**) Heatmap and hierarchical clustering of 50 proteins with significant fold differences. Three replicates with total embryos for MN (n=20), FN (n=24), MD (n=20) and FD (n=18). Data was median normalized, log2 transformed, auto scaled, and compared using one-way ANOVA and Fisher's LSD with $p<0.05$.

Table 6: Pathway association, protein identification, overall p-values, and significant group differences associated with differentially abundant proteins for Male Normal (MN), Female Normal (FN), Male Delayed (MD) and Female Delayed (FD). Three replicates with total embryos for MN (n=20), FN (n=24), MD (n=20) and FD (n=18). P-value was determined by one-way ANOVA, and Fisher's LSD indicates significant ($p<0.05$) comparisons among individual groups with higher protein abundance in first group relative to second group.

Pathway	ID	Name	P-value	Fisher's LSD
Stress Response	PRDX4	Peroxiredoxin 4	0.0004	FD-FN, FD-MD, FD-MN, FN-MD, FN-MN
	SOD2	Superoxide dismutase 2	0.04	FD-FN, FD-MD, FD-MN
	MGST3	Microsomal glutathione S-transferase 3	0.04	FD-FN, FD-MD, FD-MN
TCA cycle/ATP Production	MT-ND5	NADH dehydrogenase subunit 5	0.04	FD-FN, FD-MD, FD-MN
	ATP5MF	ATP synthase membrane subunit f	0.01	FD-FN, FD-MD, FD-MN
Anion Transport	VDAC1	Voltage-dependent anion-selective channel 1	0.05	FD-MD, MN-MD
	VDAC3	Voltage-dependent anion-selective channel 3	0.03	FD-FN, MD-FN, MN-FN
	VDAC2	Voltage-dependent anion-selective channel 2	0.02	FD-FN, MD-FN, MN-FN
Protein Synthesis	FAU	Ribosomal protein S30	0.03	FD-FN, FD-MD, FD-MN
	RPS25	Ribosomal protein S25	0.02	FD-FN, FD-MD
	EEF1A1	Eukaryotic translation elongation factor 1 alpha 1	0.02	FD-FN, MN-FN
	RPS7	Ribosomal protein S7	0.02	MN-FD, FN-MD, MN-MD
	RPSA	Ribosomal protein SA	0.04	FD-MD, MN-MD
Lipid Metabolism	CPT2	Carnitine palmitoyltransferase II	0.04	FN-FD, MD-FD, MN-FD
Nucleotide Synthesis	PRPS1	Phosphoribosyl pyrophosphate synthetase 1	0.007	FD-MD, FN-MD, MN-MD

Discussion

Intrinsic differences in embryo developmental potential are not yet fully understood. Not all embryos that develop to the blastocyst stage are viable, and faster developing embryos are typically associated with greater developmental potential.[77–79] In addition, sex of the bovine embryo has been postulated to be associated with speed of development and metabolism.[93] In the

present study, the metabolism and proteome of bovine blastocysts that developed during a normal or delayed timeline were compared to determine potential intrinsic causes of delayed preimplantation development, with a focus on imbalances of the catabolic and anabolic processes that are required in the rapidly growing embryo.

The metabolic regulation of cell proliferation is a hallmark of biological processes such as fetal development, cancer, and tissue repair. Metabolic pathways, such as glycolysis, oxidative phosphorylation, and amino acid metabolism, are dynamically modulated to support the energetic and biosynthetic demands of proliferating cells.[40] Dysregulation of these processes can lead to impaired growth, ultimately resulting in reduced viability.[80] Metabolic adaptations such as the Warburg effect have been hypothesized to play a role in embryos,[94] as studies of proliferative cell types indicate that redox balance and anabolic metabolism are of greater importance than ATP production during periods of rapid growth.[95] Respirometry and proteomic data from the present study provides evidence that blastocysts that are delayed in development deviate from these metabolic adaptations in comparison to blastocysts developing at a normal time interval, although the groups of blastocysts did not significantly differ in developmental stage, size, or morphology grades. Blastocysts delayed in development had a significantly increased oxygen consumption rate and a clear trend toward increased protein levels of electron transport system complexes than faster developing embryos, indicating that delayed blastocysts are exhibiting excessive catabolic activity, which may be limiting the quantity of metabolites able to enter anabolic pathways.

The quiet embryo hypothesis suggests that lower metabolic activity during the preimplantation stage is associated with greater implantation potential. This has been demonstrated in several studies, including reduced pyruvate metabolism and amino acid turnover

in early embryos as a predictor of viability and euploidy.[96–99] However, the original interpretation of the quiet embryo hypothesis has been modified to consider an upper and lower limit to account for embryos with markedly low metabolic activity, with studies correlating both low and high pyruvate consumption to be detrimental to blastocyst formation.[83,100] Delayed blastulation is a predictor of reduced implantation, euploidy, and pregnancy outcomes in humans.[79,101] Metabolic results of the present study provide novel support to the quiet embryo hypothesis, as blastocysts delayed in development had a greater oxygen consumption rate suggestive of more aerobic metabolism and energy production; in contrast, embryos with a "quieter" metabolism appeared to develop at a faster rate. The metabolic findings suggest an imbalance of anabolic and catabolic activity in blastocysts that develop on a delayed timeline.

Embryo proteomes supported metabolism results. Biosynthetic proteins involved in the production of nucleotides, proteins, and lipids were lower in blastocysts delayed versus normal in developmental timing. Protein biosynthesis and amino acid uptake is highly active at the blastocyst stage when compared to early-stage embryos.[102] Proteins that make up ribosomes and are involved in the recruitment of protein and mRNA components to ribosomes[103,104] were lower in delayed developing blastocysts, suggesting reduced translation. The rate of protein synthesis is highly correlated with cell proliferation, as protein synthesis is regulated by the cell cycle, although translation can also affect the progression of the cell cycle.[105] It is not clear whether the slow growth, and consequently altered cell cycle, was responsible for decreased abundance of protein synthesizing proteins, or whether lower protein biosynthetic enzymes induced slow growth. Regardless, the expression of ribosomal RNA and protein synthesizing genes increase dramatically at the blastocyst stage, and they are critical for the increased rate of ribosome biosynthesis in the later stages of preimplantation development.[106,107] Therefore, the observed

decrease in ribosomal activity could have influenced the rate of growth and contributed to delaying blastocyst formation.

Nucleotide synthesis is closely associated with embryo growth, as cells must replicate DNA and produce various RNAs to successfully divide and differentiate.[108,109] Phosphoribosepyrophosphate (PRPP), a major component of nucleotide molecules and a product of the pentose phosphate pathway, is derived primarily from carbohydrates, such as glucose and fructose.[110] Transketolase (TKT) is critical for the non-oxidative production of ribulose-5-phosphate, a precursor of PRPP.[111] Slower developing blastocysts had lower abundance of PRPS1 and TKT, thus indicating a potential reduction in PRPP synthesis and potentially impaired nucleotide synthesis. Dysfunction of the pentose phosphate pathway in embryos is associated with abnormal cell division and developmental arrest in embryos, due to reduced production of nucleotides.[112] However, the pentose phosphate pathway is also critical for redox control through generation of NADPH, which is essential for lipid, nucleotide, and amino acid synthesis.[33,40] In the present study, activity of the pentose phosphate pathway was not directly investigated, however, the finding suggest that further investigation into this area should be considered to more completely understand delayed embryo development.

The complete extent of sex-associated differences in embryo metabolism is not yet known, although individual embryo metabolism has not been thoroughly investigated. In the present study differences in OCR and ECAR between male and female blastocysts were not observed; however, proteomic data suggested that delayed development may have unique causes or responses depending on embryo sex. Certain differentially abundant proteins aligned with previous studies of embryo sex and metabolism, such as increased glycolytic activity in female mouse embryos,[113,114] consistent with elevated SLC2A1 and PFKL in Female when compared to

Male in the present study. Blastocysts produced using intracytoplasmic sperm injection can be disproportionately male and tend to grow faster, although they have higher rates of aneuploidy in humans.[115] Our study did not find many differentially abundant metabolic enzymes between male and female embryos, especially when comparing embryos of normal developmental timing status. This was expected and supports our sensor data indicating no differences in OCR or ECAR between the sexes. However, delayed development in female embryos seemed more consistently associated with mitochondrial dysfunction and stress, while male delayed embryos had more consistently lower biosynthetic proteins and had overall fewer differences between Normal and Delayed. Two peroxiredoxins were decreased in delayed embryos, indicating that these embryos may have reduced tolerance of oxidative stress. Interestingly, female delayed embryos had increased abundance of several antioxidant enzymes, although whether female embryos handle oxidative stress better than male embryos remains to be determined. Although currently impractical, sex-specific embryo culture techniques, especially regarding differential glucose uptake and tolerance to stress, may exist in the future to optimize metabolic demands of male and female embryos.

In the present study, it is unclear when the onset of metabolic differences occurred between normal and slow-growing embryos. The composition of the culture medium and incubation conditions for in vitro embryo culture can influence growth, epigenetics, and viability,[84,85] as will gamete quality.[116] To minimize these effects in the present study, embryos from IVF replicates were assigned to all metabolic and proteome groups, and sexed semen from the same ejaculate of a single bull was used with a proven high rate of sex specificity. Culture conditions were kept consistent, although embryos considered delayed remained in the same media well (500 µl) for up to 2 days. Therefore, the primary causes of delayed blastocyst

formation in the present study were probably due to intrinsic embryo differences, potentially associated with oocyte quality, fertilization, or genetic factors.

In conclusion, results of the present study demonstrated metabolic and proteomic differences between bovine blastocysts that developed on a normal or delayed timeline. Most notably, the balance of anabolic and catabolic embryo activity differed – with normal developing blastocysts having a "quieter" metabolism associated with greater biosynthesis, and delayed blastocysts having greater catabolism and oxidative stress. These data suggest that delayed blastocyst development is associated with an imbalance in the regulation of catabolic and anabolic metabolism, prioritizing energy production over biosynthetic needs. This can explain why some embryos do not undergo cell proliferation and differentiation as quickly as more viable embryos, and it highlights the importance of biosynthetic processes over catabolic activity in embryo development. Although differences in metabolism associated with embryo sex were limited in blastocysts developing over a normal timeline; more sex-associated variation was observed in embryos delayed in development, indicating potential differences in causative or compensatory mechanisms. Overall, metabolic activity associated with impaired cell proliferation in mammalian embryos was observed in the present study. Future investigations into the regulation of catabolic and anabolic activity in embryos and the causes of disturbances to these pathways may further identify causes of slow-embryo growth and provide a basis for culture systems to improve their viability.

CHAPTER V: CONCLUDING REMARKS AND FUTURE DIRECTIONS

In addition to meeting the energy demands required for survival, preimplantation embryos must produce adequate amounts of macromolecules, such as nucleotides, proteins, and lipids to sustain viability and achieve pregnancy. Compared to in vivo produced embryos, only a small percentage (20-40%) of in vitro produced embryos develop to the blastocyst stage in cows[1] and achieve pregnancy, indicating a need for greater understanding of embryo metabolism to ultimately improve culture techniques.[2] In addition, the timing of embryo development is highly associated with reproductive success, as the embryo will not survive if it cannot rapidly proliferate within its environment.[30] The studies conducted in this dissertation highlight specific metabolic mechanisms that influence the growth rate and viability of embryos during the preimplantation stage, involving the regulation of oxidative metabolism, nutrient shuttling, and biosynthetic activity. From the projects in this dissertation, we discovered a new mechanism involved with the regulation of catabolic and anabolic metabolism, and demonstrated how metabolic dysfunction may cause delayed embryo development.

The studies described in Chapter II-III were inspired by research in the cancer literature describing PEPCK as a pro-survival enzyme important for metabolic flexibility and TCA cycle flux.[8,11,38] Due to a similar need for increased biosynthetic activity required for survival in embryos, we hypothesized that PEPCK may provide a similar role to increase the availability of biosynthetic material, while also maintaining energy demands. Following the first experiments showing that development was compromised with inhibition and gene silencing of PEPCK, there was still a question as to whether the effects were due to an inhibition of gluconeogenic activity or whether PEPCK had a larger influence on the regulation of the TCA cycle and bioenergetics.

Through tracer analysis and embryo metabolic flux assays, it was clear that the role of PEPCK was much more than simply a gluconeogenic enzyme in embryos. PEPCK was not only critical for the production of anabolic intermediates from pyruvate and glutamine, but also promoted oxidative metabolism, influenced redox balance, and connected mitochondrial and cytosolic metabolism. Through PEPCK activity, embryos meet their metabolic demands with greater efficiency using a variety of metabolic substrates.

While embryos tend to grow according to consistent timelines, variation exists in the timing of developmental events, such as cleavage divisions and blastocyst formation. Slow-growing embryos are associated with maternal aging and aneuploidy,[73,76] and tend to result in decreased implantation, clinical pregnancy, and live birth rates in humans.[78,79] No prior studies have investigated metabolic dysfunction as a cause of delayed development; therefore, a combination of individual embryo metabolic assays and proteomics was used to determine differences between normal and delayed developing blastocysts. The results from this study suggest that delayed developing blastocysts are more catabolically active than normal, which aligns with other data that suggest low catabolic activity is beneficial for viability.[66] Proteomic assessment indicated that blastocysts forming on a delayed timeline tend to have reduced biosynthetic protein expression and an increase in electron transport system complexes, indicating a potential imbalance between energy production and anabolic activity. While embryo sex did not alter metabolism in normal embryos, the causes and effects of delayed development may be sex specific. In female blastocysts, mitochondrial and stress response proteins were associated with delayed development, while biosynthetic proteins were more consistently altered in males.

Embryo metabolism is flexible and dynamic, but the ways in which embryos achieve their metabolic needs are still being discovered. We found that PEPCK is a primary regulator of mitochondrial and cytoplasmic metabolic activity; however, the data that were generated from the study has much broader implications, including new ways of approaching embryo metabolic research, new pathways to study, and more metabolic substrates to investigate. Until recently, modern advancements in metabolic tracer flux analysis have not been utilized to study embryos.[49] Our study used bovine embryos to map out the metabolic products and intermediates sourced from pyruvate and glutamine; however, the metabolism of glucose, fructose, and lactate should be similarly investigated. The contributions of individual metabolic substrates to embryo growth should be better understood to improve in vitro embryo culture. In vivo- and in vitro-derived embryos are metabolically different;[42,117,118] therefore, the techniques described in this dissertation may be used to further elucidate these differences. Furthermore, while PEPCK was shown to be a major regulator of embryo metabolism, our studies highlight the influence of other metabolic enzymes such as pyruvate carboxylase and malate dehydrogenase that may be similarly critical to the balance of catabolic and anabolic activity in embryos. Finally, embryo metabolism is incredibly complex and dynamic, changing with the metabolic demands specific to different developmental stages. The present studies targeted the cleavage and blastocyst stage to investigate the function of PEPCK and the metabolic implications of delayed embryo development, respectively. Targeting later stages of embryo development, such as the elongation period in bovids, or even earlier during the first cell divisions, will likely differ from these studies and provide even more insight into the metabolic regulation of embryo growth. There is so much left to learn about embryo metabolism, and we are only getting started.

REFERENCES

1. Ferré, L. B. *et al.* Review: Recent advances in bovine in vitro embryo production: reproductive biotechnology history and methods. *Animal* **14**, 991–1004 (2020).
2. Ealy, A. D., Wooldridge, L. K. & McCoski, S. R. BOARD INVITED REVIEW: Post-transfer consequences of in vitro-produced embryos in cattle. *J. Anim. Sci.* **97**, 2555–2568 (2019).
3. Leese, H. J. & Barton, A. M. Pyruvate and glucose uptake by mouse ova and preimplantation embryos. *Reproduction* **72**, 9–13 (1984).
4. Rieger, D., Loskutoff, N. & Betteridge, K. Developmentally related changes in the uptake and metabolism of glucose, glutamine and pyruvate by cattle embryos produced in vitro. *Reprod. Fertil. Dev.* **4**, 547 (1992).
5. Ferguson, E. M. & Leese, H. J. A potential role for triglyceride as an energy source during bovine oocyte maturation and early embryo development. *Mol. Reprod. Dev.* **73**, 1195–1201 (2006).
6. Rieger, D., Loskutoff, N. M. & Betteridge, K. J. Developmentally related changes in the metabolism of glucose and glutamine by cattle embryos produced and co-cultured in vitro. *Reproduction* **95**, 585–595 (1992).
7. Takahashi, Y. In vitro development of bovine one-cell embryos: Influence of glucose, lactate, pyruvate, amino acids and vitamins. *Theriogenology* **37**, 963–978 (1992).
8. Montal, E. D. *et al.* PEPCK Coordinates the Regulation of Central Carbon Metabolism to Promote Cancer Cell Growth. *Mol. Cell* **60**, 571–583 (2015).
9. Méndez-Lucas, A. *et al.* PEPCK-M expression in mouse liver potentiates, not replaces, PEPCK-C mediated gluconeogenesis. *J. Hepatol.* **59**, 105–113 (2013).

10. Yu, S., Meng, S., Xiang, M. & Ma, H. Phosphoenolpyruvate carboxykinase in cell metabolism: Roles and mechanisms beyond gluconeogenesis. *Mol. Metab.* **53**, 101257 (2021).
11. Hyroššová, P. *et al.* PEPCK-M recoups tumor cell anabolic potential in a PKC-ζ-dependent manner. *Cancer Metab.* **9**, 1 (2021).
12. Montal, E. D. *et al.* Inhibition of phosphoenolpyruvate carboxykinase blocks lactate utilization and impairs tumor growth in colorectal cancer. *Cancer Metab.* **7**, 8 (2019).
13. Owen, O. E. The Key Role of Anaplerosis and Cataplerosis for Citric Acid Cycle Function*. 4.
14. Idrees, M. *et al.* The PPARδ Agonist GW501516 Improves Lipolytic/Lipogenic Balance through CPT1 and PEPCK during the Development of Pre-Implantation Bovine Embryos. *Int. J. Mol. Sci.* **20**, 6066 (2019).
15. Assou, S. *et al.* Dynamic changes in gene expression during human early embryo development: from fundamental aspects to clinical applications. *Hum. Reprod. Update* **17**, 272–290 (2011).
16. Assou, S. *et al.* A non-invasive test for assessing embryo potential by gene expression profiles of human cumulus cells: a proof of concept study. *Mol. Hum. Reprod.* **14**, 711–719 (2008).
17. da Silva, R. M. *et al.* Differential expression of PEPCK isoforms is correlated to Aedes aegypti oogenesis and embryogenesis. *Comp. Biochem. Physiol. B Biochem. Mol. Biol.* **256**, 110618 (2021).
18. De La Torre-Sanchez, J. F., Preis, K. & Seidel, G. E. Metabolic regulation of in-vitro-produced bovine embryos. I. Effects of metabolic regulators at different glucose

concentrations with embryos produced by semen from different bulls. *Reprod. Fertil. Dev.* **18**, 585 (2006).

19. Angel-Velez, D. *et al.* Embryo morphokinetics derived from fresh and vitrified bovine oocytes predict blastocyst development and nuclear abnormalities. *Sci. Rep.* **13**, 4765 (2023).
20. Siemens, A. E., Kitzes, M. C. & Berns, M. W. Hydrazine effects on vertebrate cells in vitro. *Toxicol. Appl. Pharmacol.* **55**, 378–392 (1980).
21. Gebremedhn, S. *et al.* MicroRNA-183-96-182 Cluster Regulates Bovine Granulosa Cell Proliferation and Cell Cycle Transition by Coordinately Targeting FOXO11. *Biol. Reprod.* **94**, 127, 1–11 (2016).
22. Hugentobler, S. A., Humpherson, P. G., Leese, H. J., Sreenan, J. M. & Morris, D. G. Energy substrates in bovine oviduct and uterine fluid and blood plasma during the oestrous cycle. *Mol. Reprod. Dev.* **75**, 496–503 (2008).
23. Funeshima, N. *et al.* Metabolomic profiles of plasma and uterine luminal fluids from healthy and repeat breeder Holstein cows. *BMC Vet. Res.* **17**, 54 (2021).
24. Tríbulo, P., Balzano-Nogueira, L., Conesa, A., Siqueira, L. G. & Hansen, P. J. Changes in the uterine metabolome of the cow during the first 7 days after estrus. *Mol. Reprod. Dev.* **86**, 75–87 (2019).
25. Caixeta, L. S. *et al.* Association of uterine fluid metabolites with the occurrence of metritis in dairy cows: A case-control study.
26. Simintiras, C. A., Sánchez, J. M., McDonald, M. & Lonergan, P. The influence of progesterone on bovine uterine fluid energy, nucleotide, vitamin, cofactor, peptide, and

xenobiotic composition during the conceptus elongation-initiation window. *Sci. Rep.* **9**, 7716 (2019).

27. Berg, D. K., van Leeuwen, J., Beaumont, S., Berg, M. & Pfeffer, P. L. Embryo loss in cattle between Days 7 and 16 of pregnancy. *Theriogenology* **73**, 250–260 (2010).
28. Betteridge, K. J., Eaglesome, M. D., Randall, G. C. B. & Mitchell, D. Collection, description and transfer of embryos from cattle 10–16 days after oestrus. *Reproduction* **59**, 205–216 (1980).
29. Pedersen, H. S. *et al.* Basic and practical aspects of pregnancy establishment in cattle. *Anim. Reprod.* **14**, 581–588 (2017).
30. Bilodeau-Goeseels, S. & Kastelic, J. P. Factors affecting embryo survival and strategies to reduce embryonic mortality in cattle. *Can. J. Anim. Sci.* **83**, 659–671 (2003).
31. Yang, J., Kalhan, S. C. & Hanson, R. W. What Is the Metabolic Role of Phosphoenolpyruvate Carboxykinase? *J. Biol. Chem.* **284**, 27025–27029 (2009).
32. Palmieri, F. The mitochondrial transporter family (SLC25): physiological and pathological implications. *Pfl□gers Arch. Eur. J. Physiol.* **447**, 689–709 (2004).
33. Javed, M. H. & Wright, R. W. Determination of pentose phosphate and Embden-Meyerhof pathway activities in bovine embryos. *Theriogenology* **35**, 1029–1037 (1991).
34. Ikeda, S., Koyama, H., Sugimoto, M. & Kume, S. Roles of One-carbon Metabolism in Preimplantation Period —Effects on Short-term Development and Long-term Programming—. 6.
35. Takahashi, M. Oxidative Stress and Redox Regulation on *In Vitro* Development of Mammalian Embryos. *J. Reprod. Dev.* **58**, 1–9 (2012).

36. Thompson, J. G., Sherman, A. N. M., Allen, N. W., McGowan, L. T. & Tervit, H. R. Total protein content and protein synthesis within pre-elongation stage bovine embryos. *Mol. Reprod. Dev.* **50**, 139–145 (1998).

37. Huppertz, B. & Herrler, A. Regulation of proliferation and apoptosis during development of the preimplantation embryo and the placenta. *Birth Defects Res. Part C Embryo Today Rev.* **75**, 249–261 (2005).

38. Méndez-Lucas, A., Hyrosˇsˇová, P., Novellasdemunt, L., Viñals, F. & Perales, J. C. Mitochondrial Phosphoenolpyruvate Carboxykinase (PEPCK-M) Is a Pro-survival, Endoplasmic Reticulum (ER) Stress Response Gene Involved in Tumor Cell Adaptation to Nutrient Availability*. **289**, 13 (2014).

39. Cairns, R. A., Harris, I. S. & Mak, T. W. Regulation of cancer cell metabolism. *Nat. Rev. Cancer* **11**, 85–95 (2011).

40. Zhu, J. & Thompson, C. B. Metabolic regulation of cell growth and proliferation. *Nat. Rev. Mol. Cell Biol.* **20**, 436–450 (2019).

41. Sunny, N. E. & Bequette, B. J. Gluconeogenesis differs in developing chick embryos derived from small compared with typical size broiler breeder eggs12. *J. Anim. Sci.* **88**, 912–921 (2010).

42. Hardy, M. L. M., Day, M. L. & Morris, M. B. Redox Regulation and Oxidative Stress in Mammalian Oocytes and Embryos Developed In Vivo and In Vitro. *Int. J. Environ. Res. Public. Health* **18**, 11374 (2021).

43. Ghosh, S., Körte, A., Serafini, G., Yadav, V. & Rodenfels, J. Developmental energetics: Energy expenditure, budgets and metabolism during animal embryogenesis. *Semin. Cell Dev. Biol.* **138**, 83–93 (2023).

44. Nemkov, T., Reisz, J. A., Gehrke, S., Hansen, K. C. & D'Alessandro, A. High-Throughput Metabolomics: Isocratic and Gradient Mass Spectrometry-Based Methods. in *High-Throughput Metabolomics: Methods and Protocols* (ed. D'Alessandro, A.) 13–26 (Springer New York, New York, NY, 2019). doi:10.1007/978-1-4939-9236-2_2.

45. Nemkov, T., Hansen, K. C. & D'Alessandro, A. A three-minute method for high-throughput quantitative metabolomics and quantitative tracing experiments of central carbon and nitrogen pathways. *Rapid Commun. Mass Spectrom.* **31**, 663–673 (2017).

46. Clasquin, M. F., Melamud, E. & Rabinowitz, J. D. LC-MS Data Processing with MAVEN: A Metabolomic Analysis and Visualization Engine. *Curr. Protoc. Bioinforma.* **37**, (2012).

47. Cheng, M.-H., Chicco, A. J., Ball, D. & Chen, T. W. Analysis of mitochondrial oxygen consumption and hydrogen peroxide release from cardiac mitochondria using electrochemical multi-sensors. *Sens. Actuators B Chem.* **360**, 131641 (2022).

48. Obeidat, Y. M. *et al.* Design of a multi-sensor platform for integrating extracellular acidification rate with multi-metabolite flux measurement for small biological samples. *Biosens. Bioelectron.* **133**, 39–47 (2019).

49. Sharpley, M. S., Chi, F., Hoeve, J. T. & Banerjee, U. Metabolic plasticity drives development during mammalian embryogenesis. *Dev. Cell* **56**, 2329-2347.e6 (2021).

50. Ahn, W. S. & Antoniewicz, M. R. Metabolic flux analysis of CHO cells at growth and non-growth phases using isotopic tracers and mass spectrometry. *Metab. Eng.* **13**, 598–609 (2011).

51. Buescher, J. M. *et al.* A roadmap for interpreting 13 C metabolite labeling patterns from cells. *Curr. Opin. Biotechnol.* **34**, 189–201 (2015).

52. Linster, C. L. & Van Schaftingen, E. Vitamin C: Biosynthesis, recycling and degradation in mammals. *FEBS J.* **274**, 1–22 (2007).

53. Yang, L., Venneti, S. & Nagrath, D. Glutaminolysis: A Hallmark of Cancer Metabolism. *Annu. Rev. Biomed. Eng.* **19**, 163–194 (2017).

54. Miyazawa, H. & Aulehla, A. Revisiting the role of metabolism during development. *Development* **145**, dev131110 (2018).

55. Abate, E. *et al.* Emerging roles of cytosolic phosphoenolpyruvate kinase 1 (PCK1) in cancer. *Biochem. Biophys. Rep.* **35**, 101528 (2023).

56. Wang, Z. & Dong, C. Gluconeogenesis in Cancer: Function and Regulation of PEPCK, FBPase, and G6Pase. *Trends Cancer* **5**, 30–45 (2019).

57. Yamada, T. *et al.* Role of glycogen in development and adult fitness in *Drosophila*. *Development* dev.176149 (2019) doi:10.1242/dev.176149.

58. Dworkin, M. B. & Dworkin-Rastl, E. Regulation of carbon flux from amino acids into sugar phosphates in Xenopus embryos. *Dev. Biol.* **138**, 177–187 (1990).

59. Chi, F., Sharpley, M. S., Nagaraj, R., Roy, S. S. & Banerjee, U. Glycolysis-Independent Glucose Metabolism Distinguishes TE from ICM Fate during Mammalian Embryogenesis. *Dev. Cell* **53**, 9-26.e4 (2020).

60. TeSlaa, T., Ralser, M., Fan, J. & Rabinowitz, J. D. The pentose phosphate pathway in health and disease. *Nat. Metab.* **5**, 1275–1289 (2023).

61. Butcher, L., Coates, A., Martin, K. L., Rutherford, A. J. & Leese, H. J. Metabolism of Pyruvate by the Early Human Embryo1. *Biol. Reprod.* **58**, 1054–1056 (1998).

62. MacDonald, M. J., Kaysen, J. H., Moran, S. M. & Pomije, C. E. Pyruvate dehydrogenase and pyruvate carboxylase. Sites of pretranslational regulation by glucose of glucose-induced insulin release in pancreatic islets. *J. Biol. Chem.* **266**, 22392–22397 (1991).

63. Groen, A. K. Control of gluconeogenesis in rat liver cells. **237**, (1986).

64. Fahien, L. A., Davis, J. W. & Laboy, J. Interactions between pyruvate carboxylase and other mitochondrial enzymes. *J. Biol. Chem.* **268**, 17935–17942 (1993).

65. Baumann, C. G., Morris, D. G., Sreenan, J. M. & Leese, H. J. The quiet embryo hypothesis: Molecular characteristics favoring viability. *Mol. Reprod. Dev.* **74**, 1345–1353 (2007).

66. Leese, H. J., Brison, D. R. & Sturmey, R. G. The Quiet Embryo Hypothesis: 20 years on. *Front. Physiol.* **13**, 899485 (2022).

67. Stepanova, A., Shurubor, Y., Valsecchi, F., Manfredi, G. & Galkin, A. Differential susceptibility of mitochondrial complex II to inhibition by oxaloacetate in brain and heart. *Biochim. Biophys. Acta BBA - Bioenerg.* **1857**, 1561–1568 (2016).

68. Sullivan, L. B. *et al.* Supporting Aspartate Biosynthesis Is an Essential Function of Respiration in Proliferating Cells. *Cell* **162**, 552–563 (2015).

69. Lane, M. & Gardner, D. K. Mitochondrial Malate-Aspartate Shuttle Regulates Mouse Embryo Nutrient Consumption *. *J. Biol. Chem.* **280**, 18361–18367 (2005).

70. Birsoy, K. *et al.* An Essential Role of the Mitochondrial Electron Transport Chain in Cell Proliferation Is to Enable Aspartate Synthesis. *Cell* **162**, 540–551 (2015).

71. Li, X. *et al.* Lactate metabolism in human health and disease. *Signal Transduct. Target. Ther.* **7**, 305 (2022).

72. Zhu, M. & Zernicka-Goetz, M. Principles of Self-Organization of the Mammalian Embryo. *Cell* **183**, 1467–1478 (2020).

73. Hernandez-Nieto, C. *et al.* Slow growing embryos biopsied on day 7: what are realistic expectations? *Fertil. Steril.* **110**, e72 (2018).

74. Isaac, E., Berg, D. K. & Pfeffer, P. L. Using extended growth of cattle embryos in culture to gain insights into bovine developmental events on embryonic days 8 to 10. *Theriogenology* **214**, 10–20 (2024).

75. Kelley, R. L. & Gardner, D. K. In vitro culture of individual mouse preimplantation embryos: the role of embryo density, microwells, oxygen, timing and conditioned media. *Reprod. Biomed. Online* **34**, 441–454 (2017).

76. Sainte-Rose, R., Petit, C., Dijols, L., Frapsauce, C. & Guerif, F. Extended embryo culture is effective for patients of an advanced maternal age. *Sci. Rep.* **11**, 13499 (2021).

77. Lonergan, P. Growth of Preimplatation Bovine Embryos. *Acta Vet. Scand.* **35**, 307–320 (1994).

78. Tubbing, A. *et al.* Increased live births after day 5 versus day 6 transfers of vitrified-warmed blastocysts. *J. Assist. Reprod. Genet.* **35**, 417–424 (2018).

79. Lane, S. L., Reed, L., Schoolcraft, W. B. & Katz-Jaffe, M. G. Euploid day 7 blastocysts of infertility patients with only slow embryo development have reduced implantation potential. *Reprod. Biomed. Online* **44**, 858–865 (2022).

80. Leese, H. J. Metabolism of the preimplantation embryo: 40 years on. *REPRODUCTION* **143**, 417–427 (2012).

81. Folmes, C. D. L. & Terzic, A. Metabolic determinants of embryonic development and stem cell fate. *Reprod. Fertil. Dev.* **27**, 82 (2015).

82. May-Panloup, P., Boguenet, M., El Hachem, H., Bouet, P.-E. & Reynier, P. Embryo and Its Mitochondria. *Antioxidants* **10**, 139 (2021).

83. Guerif, F., McKeegan, P., Leese, H. J. & Sturmey, R. G. A Simple Approach for COnsumption and RElease (CORE) Analysis of Metabolic Activity in Single Mammalian Embryos. *PLoS ONE* **8**, e67834 (2013).

84. Considerations Regarding Embryo Culture Conditions: From Media to Epigenetics. *In Vivo* **32**, (2018).

85. Castillo, C. M. *et al.* The impact of selected embryo culture conditions on ART treatment cycle outcomes: a UK national study. *Hum. Reprod. Open* **2020**, hoz031 (2020).

86. Catandi, G. D. *et al.* Equine maternal aging affects oocyte lipid content, metabolic function and developmental potential. *Reproduction* **161**, 399–409 (2021).

87. Catandi, G., Obeidat, Y., Chicco, A., Chen, T. & Carnevale, E. Basal and maximal oxygen consumption of oocytes from young and old mares. *Reprod. Fertil. Dev.* **31**, 208–208 (2019).

88. Catandi, G. D. *et al.* Follicular metabolic alterations are associated with obesity in mares and can be mitigated by dietary supplementation. *Sci. Rep.* **14**, 7571 (2024).

89. Obeidat, Y. *et al.* A multi-sensor system for measuring bovine embryo metabolism. *Biosens. Bioelectron.* **126**, 615–623 (2019).

90. Olson, S. E. & Seidel, G. E. Reduced oxygen tension and EDTA improve bovine zygote development in a chemically defined medium. *J. Anim. Sci.* **78**, 152 (2000).

91. Bo, G. & Mapletoft, R. Evaluation and classification of bovine embryos. *Anim. Reprod.* **10**, 344–348 (2013).

92. Kong, A. T., Leprevost, F. V., Avtonomov, D. M., Mellacheruvu, D. & Nesvizhskii, A. I. MSFragger: ultrafast and comprehensive peptide identification in mass spectrometry–based proteomics. *Nat. Methods* **14**, 513–520 (2017).

93. Gardner, D. K., Larman, M. G. & Thouas, G. A. Sex-related physiology of the preimplantation embryo. *Mol. Hum. Reprod.* **16**, 539–547 (2010).

94. Krisher, R. L. & Prather, R. S. A role for the Warburg effect in preimplantation embryo development: Metabolic modification to support rapid cell proliferation: T HE W ARBURG E FFECT IN E MBRYO D EVELOPMENT. *Mol. Reprod. Dev.* **79**, 311–320 (2012).

95. Liberti, M. V. & Locasale, J. W. The Warburg Effect: How Does it Benefit Cancer Cells? *Trends Biochem. Sci.* **41**, 211–218 (2016).

96. Conaghan, J., Hardy, K., Handyside, A. H., Winston, R. M. L. & Leese, H. J. Selection criteria for human embryo transfer: A comparison of pyruvate uptake and morphology. *J. Assist. Reprod. Genet.* **10**, 21–30 (1993).

97. Houghton, F. D. *et al.* Non-invasive amino acid turnover predicts human embryo developmental capacity. *Hum. Reprod.* **17**, 999–1005 (2002).

98. Sturmey, R. G. *et al.* Amino acid metabolism of bovine blastocysts: a biomarker of sex and viability. *Mol. Reprod. Dev.* **77**, 285–296 (2010).

99. Picton, H. M. *et al.* Association between amino acid turnover and chromosome aneuploidy during human preimplantation embryo development in vitro. *Mol. Hum. Reprod.* **16**, 557–569 (2010).

100. Leese, H. J. *et al.* Biological optimization, the Goldilocks principle, and how much is lagom in the preimplantation embryo. *Mol. Reprod. Dev.* **83**, 748–754 (2016).

101. Whitney, J. B., Balloch, K., Anderson, R. E., Nugent, N. & Schiewe, M. C. Day 7 blastocyst euploidy supports routine implementation for cycles using preimplantation genetic testing. *JBRA Assist. Reprod.* (2019) doi:10.5935/1518-0557.20180089.

102. Epstein, C. J. & Smith, S. A. Amino acid uptake and protein synthesis in preimplantation mouse embryos. *Dev. Biol.* **33**, 171–184 (1973).

103. Lee, A. S. Y., Kranzusch, P. J., Doudna, J. A. & Cate, J. H. D. eIF3d is an mRNA cap-binding protein that is required for specialized translation initiation. *Nature* **536**, 96–99 (2016).

104. Li Dongsheng, Wei Ting, Abbott Catherine M., & Harrich David. The Unexpected Roles of Eukaryotic Translation Elongation Factors in RNA Virus Replication and Pathogenesis. *Microbiol. Mol. Biol. Rev.* **77**, 253–266 (2013).

105. Department of Biochemistry and Biophysics, Texas A&M University, College Station, TX 77843, USA, Polymenis, M., Aramayo, R., & Department of Biology, Texas A&M University, College Station, TX 77843, USA. Translate to divide: control of the cell cycle by protein synthesis. *Microb. Cell* **2**, 94–104 (2015).

106. Taylor, K. D. & Pikó, L. Expression of ribosomal protein genes in mouse oocytes and early embryos. *Mol. Reprod. Dev.* **31**, 182–188 (1992).

107. LaMarca, M. J. & Wassarman, P. M. Relationship between rates of synthesis and intracellular distribution of ribosomal proteins during oogenesis in the mouse. *Dev. Biol.* **102**, 525–530 (1984).

108. Perry, A. C. F., Asami, M., Lam, B. Y. H. & Yeo, G. S. H. The initiation of mammalian embryonic transcription: to begin at the beginning. *Trends Cell Biol.* **33**, 365–373 (2023).

109. Kermi, C., Lo Furno, E. & Maiorano, D. Regulation of DNA Replication in Early Embryonic Cleavages. *Genes* **8**, 42 (2017).

110. Lane, A. N. & Fan, T. W.-M. Regulation of mammalian nucleotide metabolism and biosynthesis. *Nucleic Acids Res.* **43**, 2466–2485 (2015).

111. Hao, S. *et al.* The role of transketolase in human cancer progression and therapy. *Biomed. Pharmacother.* **154**, 113607 (2022).

112. Andriotis, V. M. E. & Smith, A. M. The plastidial pentose phosphate pathway is essential for postglobular embryo development in *Arabidopsis*. *Proc. Natl. Acad. Sci.* **116**, 15297–15306 (2019).

113. Gardner, D. K. & Leese, H. J. Assessment of embryo viability prior to transfer by the noninvasive measurement of glucose uptake. *J. Exp. Zool.* **242**, 103–105 (1987).

114. Lane, M. & Gardner, D. K. Fertilization and early embryology: Selection of viable mouse blastocysts prior to transfer using a metabolic criterion. *Hum. Reprod.* **11**, 1975–1978 (1996).

115. Dumoulin, J. C. M. *et al.* Growth rate of human preimplantation embryos is sex dependent after ICSI but not after IVF. *Hum. Reprod.* **20**, 484–491 (2005).

116. Lemseffer, Y., Terret, M.-E., Campillo, C. & Labrune, E. Methods for Assessing Oocyte Quality: A Review of Literature. *Biomedicines* **10**, 2184 (2022).

117. de Andrade Melo-Sterza, F. & Poehland, R. Lipid Metabolism in Bovine Oocytes and Early Embryos under In Vivo, In Vitro, and Stress Conditions. *Int. J. Mol. Sci.* **22**, 3421 (2021).

118. de Souza, D. K., Salles, L. P. & Rosa e Silva, A. A. M. Aspects of energetic substrate metabolism of in vitro and in vivo bovine embryos. *Braz. J. Med. Biol. Res.* **48**, 191–197 (2015).

APPENDIX I

Supplemental material for chapters II, III, and IV describing concentrations of metabolic substrates in media used for in vitro production of bovine embryos.

Supplemental Table 1: Concentrations of metabolic substrates in chemically defined medium for in vitro maturation of bovine oocytes (IVM)

Stock component	**Molarity (mM)**
Fructose	2.00
Glycine	4.90
Alanine-Glutamine	1.00
L-Lactate	10.00
Pyruvate	0.50
Myoinositol	2.77
Minimum Essential Media Non-essential Amino Acids (M-7145)	0.67
Taurine	0.10
Bovine Serum Albumin - Fatty Acid Free	0.01

Supplemental Table 2: Concentrations of metabolic substrates in chemically defined media for in vitro fertilization (F-CDM)

Stock component	**Molarity (mM)**
Glucose	0.88
Glycine	4.90
Alanine-Glutamine	1.00
L-Lactate	10.00
Pyruvate	0.50
Minimum Essential Media Non-essential Amino Acids (M-7145)	0.67
Bovine Serum Albumin - Fatty Acid Free	0.50

Supplemental Table 3: Concentrations of metabolic substrates in chemically defined media for handling of early embryos (HCDM-1)

Stock component	**Molarity (mM)**
Fructose	0.50
Glycine	4.90
Alanine-Glutamine	1.00
L-Lactate	10.00
Pyruvate	0.50
Minimum Essential Media Non-essential Amino Acids (M-7145)	0.67
Bovine Serum Albumin - Fatty Acid Free	0.25

Supplemental Table 4: Concentrations of metabolic substrates in chemically defined medium for in vitro culture of early embryos (CDM-1)

Stock component	**Molarity (mM)**
Fructose	0.50
Glycine	4.90
Alanine-Glutamine	1.00
L-Lactate	10.00
Pyruvate	0.50
Myoinositol	2.77
Minimum Essential Media Non-essential Amino Acids (M-7145)	0.67
Taurine	0.10
Bovine Serum Albumin - Fatty Acid Free	0.50

Supplemental Table 5: Concentrations of metabolic substrates in chemically defined medium for handling of late embryos (HCDM-2)

Stock component	**Molarity (mM)**
Fructose	2.00
Glycine	4.90
Alanine-Glutamine	1.00
L-Lactate	5.00
Pyruvate	0.20
Minimum Essential Media Non-essential Amino Acids (M-7145)	0.67
Basal Medium Eagle Essential Amino Acids (B-6766)	1.47
Bovine Serum Albumin - Fatty Acid Free	0.25

Supplemental Table 6: Concentrations of metabolic substrates in chemically defined medium for in vitro culture of late embryos (CDM-2)

Stock component	**Molarity (mM)**
Fructose	2.00
Glycine	4.90
Alanine-Glutamine	1.00
L-Lactate	5.00
Pyruvate	0.20
Myoinositol	2.77
Basal Medium Eagle Essential Amino Acids (B-6766)	1.47
Minimum Essential Media Non-essential Amino Acids (M-7145)	0.67
Bovine Serum Albumin - Fatty Acid Free	0.50

Supplemental Table 7: Concentrations of metabolic substrates in modified, carbohydrate-free chemically defined medium for in vitro culture of early embryos (MCDM-1)

Stock component	**Molarity (mM)**
Glycine	4.90
Alanine-Glutamine	1.00
L-Lactate	10.00
Pyruvate	0.50
MyoInositol	2.77
Minimum Essential Media Non-essential Amino Acids (M-7145)	0.67
Tuarine	0.10
Bovine Serum Albumin - Fatty Acid Free	0.50

Supplemental Table 8: Concentrations of metabolic substrates in modified, carbohydrate-free chemically defined medium for in vitro culture of late embryos (MCDM-2)

Stock component	**Molarity (mM)**
Glycine	4.90
Alanine-Glutamine	1.00
L-Lactate	5.00
Pyruvate	0.20
Myoinositol	2.77
Basal Medium Eagle Essential Amino Acids (B-6766)	1.47
Minimum Essential Media Non-essential Amino Acids (M-7145)	0.67
Bovine Serum Albumin - Fatty Acid Free	0.50

Supplemental Table 9: Concentrations of metabolic substrates in chemically defined medium for in vitro culture of early embryos (CDM-1) containing $^{13}C_3$ sodium pyruvate stable isotope tracer

Stock component	**Molarity (mM)**
Fructose	0.50
Glycine	4.90
Alanine-Glutamine	1.00
L-Lactate	10.00
$^{13}C_3$ sodium pyruvate	0.50
Myoinositol	2.77
Minimum Essential Media Non-essential Amino Acids (M-7145)	0.67
Taurine	0.10
Bovine Serum Albumin - Fatty Acid Free	0.50

Supplemental Table 10: Concentrations of metabolic substrates in chemically defined medium for in vitro culture of early embryos (CDM-1) containing $^{13}C_5$,$^{15}N_2$ L-Glutamine stable isotope tracer

Stock component	**Molarity (mM)**
Fructose	0.50
Glycine	4.90
$^{13}C_5$,$^{15}N_2$ L-Glutamine	1.00
L-Lactate	10.00
Pyruvate	0.50
Myoinositol	2.77
Minimum Essential Media Non-essential Amino Acids (M-7145)	0.67
Taurine	0.10
Bovine Serum Albumin - Fatty Acid Free	0.50

APPENDIX II

Supplemental material for Chapter II

Supplemental Figure 1: Validation of PCK1 (A) and PCK2 (B) knockdown in bovine granulosa cells following siRNA gene silencing relative to GAPDH. Bars represent mean ± SEM.

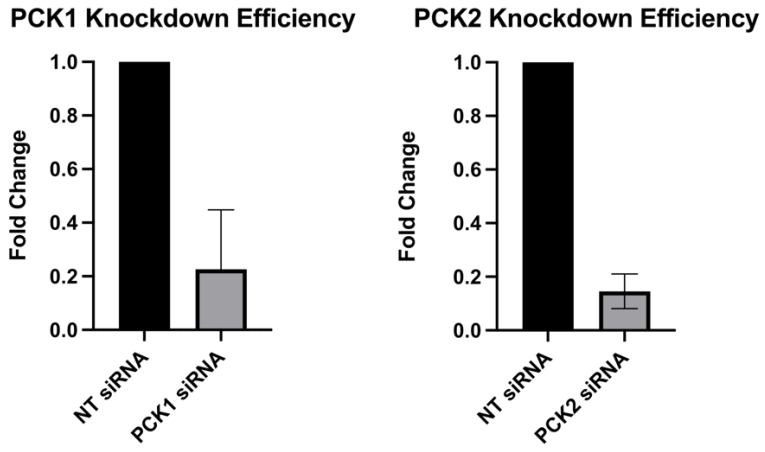

APPENDIX III

Supplemental Table 11: Protein identification, fold difference (FD), and p-values associated with differentially abundant proteins for pooled Male and Female embryos considered normal (Normal) or delayed (Delayed) in timing to reach the expanding blastocyst stage of development. Three replicates with total embryos for Normal (n=44) and Delayed (n=38). Fold difference (FD) indicates Delayed relative to Normal.

ID	Name	FD	P-value
TGM2	Protein-glutamine gamma-glutamyltransferase 2	0.13	0.0003
MVP	Major vault protein	0.39	0.0003
CIAPIN1	Anamorsin	0.15	0.0024
LAMP1	Lysosome-associated membrane glycoprotein 1	0.29	0.0025
RPS7	Small ribosomal subunit protein eS7	0.23	0.0026
PRPS1	Ribose-phosphate pyrophosphokinase 1	0.22	0.0066
SUCLA2	Succinate--CoA ligase [ADP-forming] subunit beta, mitochondrial	0.35	0.0089
DLD	Dihydrolipoyl dehydrogenase, mitochondrial	0.32	0.0097
NSDHL	Sterol-4-alpha-carboxylate 3-dehydrogenase, decarboxylating	3.58	0.0116
ATP5MF	ATP synthase subunit f, mitochondrial	3.33	0.0116
TMSB4	Thymosin beta-4	0.42	0.0116
NLRP9	NACHT, LRR and PYD domains-containing protein 9	0.37	0.0124
PEBP1	Phosphatidylethanolamine-binding protein 1	0.44	0.0139
EEF1B	Elongation factor 1-beta	0.38	0.0142
RPS21	Small ribosomal subunit protein eS21	0.31	0.0143
TMX2	Thioredoxin-related transmembrane protein 2	0.23	0.0158
SCIN	Scinderin	5.41	0.0171
RSL1D1	Ribosomal L1 domain-containing protein 1	0.38	0.0178
UBE2L3	Ubiquitin-conjugating enzyme E2 L3	0.40	0.0180
ATP5F1D	ATP synthase subunit delta, mitochondrial	0.26	0.0181
TKT	Transketolase	0.35	0.0183
EIF3J	Eukaryotic translation initiation factor 3 subunit J	0.32	0.0193
NAP1L4	Nucleosome assembly protein 1-like 4	0.36	0.0194
SPCS1	Signal peptidase complex subunit 1	2.32	0.0198
RPL30	Large ribosomal subunit protein eL30	0.29	0.0200
SRSF3	Serine/arginine-rich splicing factor 3	0.39	0.0218
PRDX3	Thioredoxin-dependent peroxide reductase, mitochondrial	0.22	0.0224
RPL26	Large ribosomal subunit protein uL24	0.45	0.0262
RPS18	Small ribosomal subunit protein uS13	0.44	0.0267
ATP5PD	ATP synthase subunit d, mitochondrial	0.37	0.0299
SMS	Spermine synthase	0.35	0.0311
NDUFB9	NADH dehydrogenase [ubiquinone] 1 beta subcomplex subunit 9	4.88	0.0321
RPL35A	Large ribosomal subunit protein eL33	0.46	0.0327
RBMX	RNA-binding motif protein, X chromosome	0.52	0.0363
SERPINA3-5	Serpin A3-5	3.92	0.0371
CS	Citrate synthase	0.47	0.0378

PRDX2	Peroxiredoxin-2	0.40	0.0380
EIF5A	Eukaryotic translation initiation factor 5A-1	0.31	0.0381
YWHAZ	14-3-3 protein zeta/delta	0.44	0.0393
CLTB	Clathrin light chain B	0.42	0.0395
ATP6V1A	V-type proton ATPase catalytic subunit A	0.41	0.0399
YWHAG	14-3-3 protein gamma	0.40	0.0402
CD63	CD63 antigen	0.23	0.0405
GNS	N-acetylglucosamine-6-sulfatase	0.42	0.0407
HINT1	Adenosine 5'-monophosphoramidase HINT1	2.18	0.0426
ADSL	Adenylosuccinate lyase	0.45	0.0431
CCT4	T-complex protein 1 subunit delta	0.51	0.0433
DBI	Acyl-CoA-binding protein	4.76	0.0450
ARPC4	Actin-related protein 2/3 complex subunit 4	6.03	0.0451
HSP90AA1	Heat shock protein HSP 90-alpha	0.55	0.0455
ARPC3	Actin-related protein 2/3 complex subunit 3	4.46	0.0461
DNAJA1	DnaJ homolog subfamily A member 1	4.18	0.0469
FUCA1	Tissue alpha-L-fucosidase	3.87	0.0487

Supplemental Table 12: Protein identification, fold difference (FD), and p-values associated with differentially abundant proteins for pooled Female or Male embryos considered normal (Normal) and delayed (Delayed) in timing to reach the expanding blastocyst stage of development. Three replicates with total embryos for Male (n=40) and Female (n=42). Fold difference indicates Female relative to Male.

ID	Name	FD	P-value
YWHAE	14-3-3 protein epsilon	0.47	0.001
PRDX4	Peroxiredoxin-4	10.57	0.002
GCAT	2-amino-3-ketobutyrate coenzyme A ligase, mitochondrial	3.31	0.003
NUDT21	Cleavage and polyadenylation specificity factor subunit 5	2.97	0.003
FYN	Tyrosine-protein kinase Fyn	5.66	0.004
H1-2	Histone H1.2	0.29	0.004
NASP	Nuclear autoantigenic sperm protein	0.37	0.004
SAMM50	Sorting and assembly machinery component 50 homolog	6.01	0.005
OARD1	ADP-ribose glycohydrolase OARD1	0.25	0.006
BPNT1	3'(2'),5'-bisphosphate nucleotidase 1	0.12	0.006
SND1	Staphylococcal nuclease domain-containing protein 1	0.43	0.007
TUBA3	Tubulin alpha-3 chain	4.71	0.007
PSMB7	Proteasome subunit beta type-7	0.10	0.010
ATP6V1E1	V-type proton ATPase subunit E 1	0.23	0.011
ARPP19	cAMP-regulated phosphoprotein 19	0.29	0.014
CLPTM1	Putative lipid scramblase CLPTM1	0.04	0.014
COTL1	Coactosin-like protein	0.29	0.015
RPS3A	Small ribosomal subunit protein eS1	0.41	0.018
MAPK1	Mitogen-activated protein kinase 1	0.23	0.019
SEC13	Protein SEC13 homolog	0.28	0.020
IDH3B	Isocitrate dehydrogenase [NAD] subunit beta, mitochondrial	4.02	0.021
BCHE	Cholinesterase	3.44	0.024
CLPP	ATP-dependent Clp protease proteolytic subunit, mitochondrial	0.31	0.024
UBE2V1	Ubiquitin-conjugating enzyme E2 variant 1	0.17	0.024
ORM1	Alpha-1-acid glycoprotein	3.58	0.025
POLR2E	DNA-directed RNA polymerases I, II, and III subunit RPABC1	0.05	0.028
FTH1	Ferritin heavy chain	0.55	0.029
GET4	Golgi to ER traffic protein 4 homolog	0.21	0.029
SEPTIN2	Septin-2	1.87	0.029
HMBS	Porphobilinogen deaminase	0.16	0.030
CFL2	Cofilin-2	0.29	0.031
H1-3	Histone H1.3	0.26	0.031

TAF8	Transcription initiation factor TFIID subunit 8	0.11	0.031
FKBP4	Peptidyl-prolyl cis-trans isomerase FKBP4	0.37	0.032
P2RX4	P2X purinoceptor 4	0.30	0.032
KRT10	Keratin, type I cytoskeletal 10	0.61	0.032
ATP6V1B1	V-type proton ATPase subunit B, kidney isoform	0.19	0.034
EIF4A2	Eukaryotic initiation factor 4A-II	0.08	0.034
ZNF259	Zinc finger protein ZPR1	0.12	0.035
PYCR3	Pyrroline-5-carboxylate reductase 3	0.22	0.035
HINT1	Adenosine 5'-monophosphoramidase HINT1	0.34	0.035
H1-1	Histone H1.1	0.30	0.035
ZBTB8OS	Protein archease	0.25	0.036
DDT	D-dopachrome decarboxylase	2.37	0.037
ACP1	Low molecular weight phosphotyrosine protein phosphatase	3.68	0.038
RAN	GTP-binding nuclear protein Ran	0.26	0.038
HMGCR	3-hydroxy-3-methylglutaryl-coenzyme A reductase	0.02	0.039
PRMT5	Protein arginine N-methyltransferase 5	0.40	0.039
SLC2A1	Solute carrier family 2, facilitated glucose transporter member 1	2.93	0.040
EIF4A3	Eukaryotic initiation factor 4A-III	0.37	0.041
PABPN1	Polyadenylate-binding protein 2	0.19	0.041
EHD1	EH domain-containing protein 1	2.30	0.043
PIK3R1	Phosphatidylinositol 3-kinase regulatory subunit alpha	0.31	0.044
MYG1	MYG1 exonuclease	0.14	0.044
FECH	Ferrochelatase, mitochondrial	0.18	0.044
FADD	FAS-associated death domain protein	0.17	0.045
VNN1	Pantetheinase	4.03	0.047
WASL	Actin nucleation-promoting factor WASL	0.28	0.047
SERPINA3-1	Serpin A3-1	5.26	0.047
PFKL	ATP-dependent 6-phosphofructokinase, liver type	4.05	0.048
SOD2	Superoxide dismutase [Mn], mitochondrial	6.42	0.049
NDUFB6	NADH dehydrogenase [ubiquinone] 1 beta subcomplex subunit 6	0.12	0.049
UCHL1	Ubiquitin carboxyl-terminal hydrolase isozyme L1	2.07	0.050
VAMP3	Vesicle-associated membrane protein 3	0.37	0.050

Supplemental Table 13: Protein identification, fold difference (FD), and p-values associated with differentially abundant proteins for Female or Male embryos considered normal (Normal) in timing to reach the expanding blastocyst stage of development. Three replicates with total embryos for Male (n=20) and Female (n=24). Fold difference (FD) indicates Female relative to Male.

ID	Name	FD	P-value
KRT28	Keratin, type I cytoskeletal 28	0.28	0.001
OARD1	ADP-ribose glycohydrolase OARD1	0.24	0.001
SLC25A11	Mitochondrial 2-oxoglutarate/malate carrier protein	0.03	0.001
H1-0	Histone H1.0	0.24	0.001
P2RX4	P2X purinoceptor 4	0.24	0.002
HMGB2	High mobility group protein B2	0.22	0.003
PSMA6	Proteasome subunit alpha type-6	0.07	0.003
ANXA11	Annexin A11	5.15	0.003
STT3A	Dolichyl-diphosphooligosaccharide--protein glycosyltransferase subunit STT3A	0.03	0.003
H1-1	Histone H1.1	0.21	0.004
ATP6V0A1	V-type proton ATPase subunit a	0.21	0.004
DDX19A	RNA helicase	3.22	0.004
RABEP2	Rab GTPase-binding effector protein 2	3.12	0.006
IDI1	Isopentenyl-diphosphate Delta-isomerase 1	2.65	0.006
ARF4	ADP-ribosylation factor 4	2.69	0.008
VPS4B	Vacuolar protein sorting-associated protein 4B	0.07	0.008
COX6B1	Cytochrome c oxidase subunit 6B1	0.18	0.009
RAB6B	Ras-related protein Rab-6B	0.11	0.009
HDAC1	Histone deacetylase 1	0.17	0.011
CIAPIN1	Anamorsin	0.26	0.011
FTH1	Ferritin heavy chain	0.07	0.011
NDUFB6	NADH dehydrogenase [ubiquinone] 1 beta subcomplex subunit 6	0.17	0.013
RTN3	Reticulon-3	0.16	0.014
ARPP19	cAMP-regulated phosphoprotein 19	0.05	0.015
RPL13	Large ribosomal subunit protein eL13	0.10	0.015
PPP1CB	Serine/threonine-protein phosphatase PP1-beta catalytic subunit	8.75	0.015
TMEM30A	Cell cycle control protein 50A	1.89	0.016
AURKA	Aurora kinase A	0.33	0.017
SKP1	S-phase kinase-associated protein 1	3.63	0.017
EMC7	Endoplasmic reticulum membrane protein complex subunit 7	0.15	0.018
PRKAR1A	cAMP-dependent protein kinase type I-alpha regulatory subunit	0.15	0.018
EIF3J	Eukaryotic translation initiation factor 3 subunit J	2.22	0.018

HDHD2	Haloacid dehalogenase-like hydrolase domain-containing protein 2	0.14	0.019
CDC5L	Cell division cycle 5-like protein	5.88	0.020
COL1A1	Collagen alpha-1(I) chain	0.03	0.025
DYNLL2	Dynein light chain 2, cytoplasmic	3.78	0.026
VPS29	Vacuolar protein sorting-associated protein 29	1.67	0.027
HMBS	Porphobilinogen deaminase	0.12	0.028
ACTN1	Alpha-actinin-1	2.10	0.028
SNRPF	Small nuclear ribonucleoprotein F	6.85	0.031
PSMC2	26S proteasome regulatory subunit 7	1.79	0.031
SLC25A6	ADP/ATP translocase 3	0.08	0.031
FHIT	Bis(5'-adenosyl)-triphosphatase	2.17	0.033
OGDH	2-oxoglutarate dehydrogenase complex component E1	0.33	0.034
CLPP	ATP-dependent Clp protease proteolytic subunit, mitochondrial	0.07	0.035
PSMA1	Proteasome subunit alpha type-1	0.27	0.035
CPNE1	Copine-1	5.19	0.035
AK4	Adenylate kinase 4, mitochondrial	0.09	0.035
DDT	D-dopachrome decarboxylase	2.62	0.036
TAF8	Transcription initiation factor TFIID subunit 8	0.10	0.036
ALB	Albumin	3.25	0.038
CHTOP	Chromatin target of PRMT1 protein	0.10	0.038
MARCKSL1	MARCKS-related protein	0.17	0.039
MESD	LRP chaperone MESD	4.12	0.039
VDAC2	Voltage-dependent anion-selective channel protein 2	0.23	0.039
ATP6V1C1	V-type proton ATPase subunit C 1	4.52	0.040
DENR	Density-regulated protein	2.22	0.041
NAPA	Alpha-soluble NSF attachment protein	3.58	0.042
PSMB3	Proteasome subunit beta type-3	0.00	0.042
EIF3B	Eukaryotic translation initiation factor 3 subunit B	2.85	0.043
SFN	14-3-3 protein sigma	1.86	0.045
SH3GL1	Endophilin-A2	3.30	0.045
H2AC20	Histone H2A type 2-C	0.11	0.045
RNF126	E3 ubiquitin-protein ligase RNF126	0.08	0.046
ATXN10	Ataxin-10	3.31	0.050

Supplemental Table 14: Protein identification, fold difference (FD), and p-values associated with differentially abundant proteins for pooled Male embryos considered Normal and Delayed in developmental timing. Three replicates with total embryos for Normal (n=20) and Delayed (n=20). Fold difference indicates Male Delayed relative to Male Normal.

ID	Name	FD	P-value
TGM2	Protein-glutamine gamma-glutamyltransferase 2	0.12	0.002
RPL13A	Large ribosomal subunit protein uL13	0.18	0.003
MFGE8	Lactadherin	0.20	0.011
RPL35	Large ribosomal subunit protein uL29	0.11	0.018
PRPS1	Ribose-phosphate pyrophosphokinase 1	0.08	0.019
NARS	Asparagine--tRNA ligase, cytoplasmic	0.08	0.021
ATP5IF1	ATPase inhibitor, mitochondrial	0.02	0.022
ZP4	Zona pellucida sperm-binding protein 4	0.37	0.026
MVP	Major vault protein	0.38	0.029
HSPB1	Heat shock protein beta-1	0.29	0.030
PLS1	Plastin-1	4.61	0.034
CIAPIN1	Anamorsin	0.12	0.034
RPL10A	Large ribosomal subunit protein uL1	0.15	0.040
RPL18	Large ribosomal subunit protein eL18	0.15	0.042
PUF60	Poly(U)-binding-splicing factor PUF60	0.18	0.044
RPS7	Small ribosomal subunit protein eS7	0.16	0.045
AHCY	Adenosylhomocysteinase	0.09	0.046
NSDHL	Sterol-4-alpha-carboxylate 3-dehydrogenase, decarboxylating	5.27	0.049

Supplemental Table 15: Protein identification, fold difference (FD), and P-values associated with differentially abundant proteins for pooled Female embryos considered Normal and Delayed in timing to reach the expanding blastocyst stage of development. Three replicates with total embryos for Normal (n=24) and Delayed (n=18). Fold difference indicates Female Delayed relative to Female Normal.

ID	Name	FD	P-value
TKT	Transketolase	0.44	0.0001
DNM1L	Dynamin-1-like protein	0.19	0.0006
LAMP1	Lysosomal membrane glycoprotein 1	0.27	0.0008
EEF1A1	Elongation factor 1-alpha 1	3.00	0.0009
CLINT1	Clathrin interactor 1	0.45	0.0010
NUDC	Nuclear migration protein	0.33	0.0012
NPM1	Nucleophosmin	0.37	0.0012
RPL17	Large ribosomal subunit protein uL22	0.46	0.0013
ARF4	ADP-ribosylation factor 4	0.33	0.0013
EIF3J	Eukaryotic translation initiation factor 3 subunit J	0.15	0.0015
IDI1	Isopentenyl-diphosphate Delta-isomerase 1	0.15	0.0020
NAP1L4	Nucleosome assembly protein 1-like 4	0.35	0.0029
TMSB4	Thymosin beta-4	0.23	0.0030
HNRNPK	Heterogeneous nuclear ribonucleoprotein K	0.39	0.0030
CS	Citrate synthase	0.51	0.0033
RPL3	Large ribosomal subunit protein uL3	0.27	0.0042
RANBP1	Ran-specific GTPase-activating protein	0.49	0.0042
F11R	Junctional adhesion molecule A	0.33	0.0044
ERLIN2	Erlin-2	0.50	0.0044
DDX1	ATP-dependent RNA helicase DDX1	0.34	0.0049
HDGF	Hepatoma-derived growth factor	0.02	0.0054
PCMT1	Protein-L-isoaspartate(D-aspartate) O-methyltransferase	0.42	0.0060
ATP6V1C1	V-type proton ATPase subunit C 1	0.21	0.0063
RPS18	Small ribosomal subunit protein uS13	0.34	0.0067
PFN2	Profilin-2	0.42	0.0074
KRT14	Keratin, type I cytoskeletal 14	18.77	0.0086
SMU1	WD40 repeat-containing protein SMU1	0.07	0.0087
YWHAG	14-3-3 protein gamma	0.39	0.0088
EIF3G	Eukaryotic translation initiation factor 3 subunit G	0.40	0.0089
SRSF3	Serine/arginine-rich splicing factor 3	0.16	0.0094
PSMC5	26S proteasome regulatory subunit 8	0.41	0.0103
SNX5	Sorting nexin-5	0.27	0.0104
RPL7	Large ribosomal subunit protein uL30	16.88	0.0106

PRKAR2A	cAMP-dependent protein kinase type II-alpha regulatory subunit	0.31	0.0108
ATXN10	Ataxin-10	0.08	0.0111
PARP1	Poly [ADP-ribose] polymerase 1	0.56	0.0111
ISOC1	Isochorismatase domain-containing protein 1	2.48	0.0120
MCM3	DNA replication licensing factor Mcm3	0.33	0.0120
SPCS1	Signal peptidase complex subunit 1	2.49	0.0120
CSTF2	Cleavage stimulation factor subunit 2	2.45	0.0120
RPL35A	RPL35A ribosomal protein L35a	0.19	0.0120
FN1	Fibronectin	1.98	0.0120
ARPC3	Actin-related protein 2/3 complex subunit 3	2.44	0.0121
ADSS2	Adenylosuccinate synthetase isozyme 2	2.52	0.0121
PARL	Presenilin-associated rhomboid-like protein, mitochondrial	2.52	0.0121
RPS23	Small ribosomal subunit protein uS12	2.52	0.0121
MMAB	Corrinoid adenosyltransferase MMAB	2.54	0.0122
MGST3	Glutathione S-transferase 3, mitochondrial	2.54	0.0122
DYNLL2	Dynein light chain 2, cytoplasmic	0.13	0.0122
SKP1	S-phase kinase-associated protein 1	0.19	0.0124
SSB	Single-stranded DNA-binding protein	0.36	0.0124
CTH	Cystathionine gamma-lyase	2.57	0.0124
ARPC4	Actin-related protein 2/3 complex subunit 4	2.57	0.0125
DBI	Acyl-CoA-binding protein	2.39	0.0126
STT3A	Dolichyl-diphosphooligosaccharide--protein glycosyltransferase subunit STT3A	2.59	0.0127
CDC37	Hsp90 co-chaperone Cdc37	0.30	0.0128
PSMB1	Proteasome subunit beta type-1	2.63	0.0131
PCNA	Proliferating cell nuclear antigen	0.32	0.0132
SCIN	Scinderin	2.65	0.0135
PFDN2	Prefoldin subunit 2	2.69	0.0140
RBMX	RNA-binding motif protein, X chromosome	0.09	0.0146
HSP90AA1	Heat shock protein HSP 90-alpha	0.39	0.0150
GPX4	Phospholipid hydroperoxide glutathione peroxidase	2.77	0.0154
SUCLA2	Succinate--CoA ligase	0.26	0.0155
SDHB	Succinate dehydrogenase [ubiquinone] iron-sulfur subunit, mitochondrial	0.23	0.0159
RAB3C	Ras-related protein Rab-3C	2.81	0.0162
TUBA3	Tubulin alpha-3 chain	0.29	0.0163
MVP	Major vault protein	0.39	0.0165
UBE2L3	Ubiquitin-conjugating enzyme E2 L3	0.22	0.0166
RAB18	RAB18	2.84	0.0168
RPS25	Small ribosomal subunit protein eS25	2.26	0.0171

TXNRD1	Thioredoxin reductase 1, cytoplasmic	2.87	0.0174
RENBP	N-acylglucosamine 2-epimerase	0.36	0.0178
GGPS1	Geranylgeranyl pyrophosphate synthase	0.13	0.0179
TMEM30A	Cell cycle control protein 50A	0.40	0.0181
MTHFD1L	Monofunctional C1-tetrahydrofolate synthase, mitochondrial	0.48	0.0183
RPL24	Large ribosomal subunit protein eL24	45.10	0.0185
FUCA1	Tissue alpha-L-fucosidase	2.24	0.0185
RPL30	Large ribosomal subunit protein eL30	0.44	0.0194
FAU	Small ribosomal subunit protein eS30	2.97	0.0197
GRPEL1	GrpE protein homolog 1, mitochondrial	0.40	0.0197
PPP1CA	Serine/threonine-protein phosphatase PP1-alpha catalytic subunit	2.22	0.0200
PRDX4	Peroxiredoxin-4	5.26	0.0203
MAL2	Protein MAL2	2.21	0.0203
LGALS1	Galectin-1	1.99	0.0205
ATP5MF	ATP synthase subunit f, mitochondrial	2.21	0.0206
PHPT1	14 kDa phosphohistidine phosphatase	0.14	0.0207
SMS	Somatostatin	0.43	0.0210
CLTA	Clathrin light chain A	0.23	0.0212
DLD	Dihydrolipoyl dehydrogenase, mitochondrial	0.44	0.0222
FKBP1A	Peptidyl-prolyl cis-trans isomerase FKBP1A	0.28	0.0229
STK25	Serine/threonine-protein kinase 25	2.18	0.0237
TPP1	Tripeptidyl-peptidase 1	2.18	0.0244
KRT78	Keratin, type II cytoskeletal 78	4.59	0.0245
MSN	Moesin	0.37	0.0249
TECR	Very-long-chain enoyl-CoA reductase	2.17	0.0250
RAD23B	UV excision repair protein RAD23 homolog B	0.24	0.0251
RPL26	E3 UFM1-protein ligase 1	0.31	0.0252
DAG1	Dystroglycan 1	0.06	0.0254
SEPTIN7	Septin-7	0.28	0.0260
HDDC2	5'-deoxynucleotidase HDDC2	125.05	0.0261
SNRPD2	Small nuclear ribonucleoprotein Sm D2	0.14	0.0263
HINT1	Adenosine 5'-monophosphoramidase HINT1	2.16	0.0265
DHFR	Dihydrofolate reductase	3.25	0.0267
NAPA	Alpha-soluble NSF attachment protein	0.15	0.0270
DLAT	Dihydrolipoyllysine-residue acetyltransferase component of pyruvate dehydrogenase complex	4.22	0.0276
PFDN4	Prefoldin subunit 4	0.14	0.0279
MFGE8	Lactadherin	2.70	0.0285
VPS35	Vacuolar protein sorting-associated protein 35	0.39	0.0289

HDAC1	Histone deacetylase 1	2.15	0.0295
RSL1D1	Ribosomal L1 domain-containing protein 1	0.22	0.0295
EIF5A	Eukaryotic translation initiation factor 5A-1	0.21	0.0295
LTF	Lactotransferrin	3.37	0.0297
EEF1B	Elongation factor 1-beta	0.30	0.0321
KRTCAP2	Keratinocyte-associated protein 2	2.35	0.0321
ATP6V1D	V-type proton ATPase subunit D	2.38	0.0322
ARPC1A	Actin-related protein 2/3 complex subunit 1A	2.38	0.0322
PSMA6	Proteasome subunit alpha type-6	2.39	0.0323
PCYT2	Ethanolamine-phosphate cytidylyltransferase	2.40	0.0323
PLD3	5'-3' exonuclease PLD3	3.48	0.0324
YARS1	Tyrosine--tRNA ligase, cytoplasmic	0.32	0.0324
NIFK	MKI67 FHA domain-interacting nucleolar phosphoprotein	2.13	0.0327
NDUFA11	NADH dehydrogenase [ubiquinone] 1 alpha subcomplex subunit 11	2.44	0.0328
PTRH2	Peptidyl-tRNA hydrolase 2, mitochondrial	2.26	0.0329
ASAH1	Acid ceramidase	2.45	0.0329
SNRPD1	Small nuclear ribonucleoprotein Sm D1	2.26	0.0330
VDAC3	Voltage-dependent anion-selective channel protein 3	3.89	0.0336
RTN3	Reticulon-3	2.23	0.0337
UQCR10	Cytochrome b-c1 complex subunit 9	2.12	0.0339
TRMT10C	tRNA methyltransferase 10 homolog C	0.09	0.0340
RABAC1	Prenylated Rab acceptor protein 1	2.22	0.0341
NDUFAF4	NADH dehydrogenase [ubiquinone] 1 alpha subcomplex assembly factor 4	2.22	0.0341
MT-ND5	NADH-ubiquinone oxidoreductase chain 5	2.53	0.0344
COL1A2	Collagen alpha-2(I) chain	2.53	0.0345
AK4	Adenylate kinase 4, mitochondrial	6.34	0.0345
MVD	Diphosphomevalonate decarboxylase	2.20	0.0347
TIMM21	Mitochondrial import inner membrane translocase subunit Tim21	0.17	0.0356
SPNS1	Protein spinster homolog 1	0.15	0.0357
UQCRB	Cytochrome b-c1 complex subunit 7	0.31	0.0360
CPT2	Carnitine O-palmitoyltransferase 2, mitochondrial	0.20	0.0360
ACTL6B	Actin-like protein 6B	2.62	0.0365
DDX19A	ATP-dependent RNA helicase DDX19A	0.22	0.0365
SNRPF	Small nuclear ribonucleoprotein F	0.09	0.0369
VPS28	Vacuolar protein sorting-associated protein 28 homolog	0.07	0.0369
CLTB	Clathrin light chain B	0.19	0.0372
ATP5PD	ATP synthase subunit d, mitochondrial	0.58	0.0372
RPS7	Small ribosomal subunit protein eS7	0.36	0.0374

STOML2	Stomatin-like protein 2, mitochondrial	0.38	0.0375
YWHAZ	14-3-3 protein zeta/delta	0.22	0.0380
GNS	N-acetylglucosamine-6-sulfatase	0.45	0.0380
COX7A2L	Cytochrome c oxidase subunit 7A-related protein, mitochondrial	2.69	0.0385
KGD4	Alpha-ketoglutarate dehydrogenase component 4	2.70	0.0386
DARS1	Aspartate--tRNA ligase, cytoplasmic	1.56	0.0388
HSP90AB1	Heat shock protein HSP 90-beta	0.58	0.0390
SLC25A11	Mitochondrial 2-oxoglutarate/malate carrier protein	3.78	0.0396
DSC2	Desmocollin-2	3.79	0.0399
SHMT2	Serine hydroxymethyltransferase, mitochondrial	2.76	0.0403
GBA1	Lysosomal acid glucosylceramidase	2.11	0.0411
CLIC1	Chloride intracellular channel protein 1	0.48	0.0418
PSMC6	26S proteasome regulatory subunit 10B	2.82	0.0422
MRPS25	Small ribosomal subunit protein mS25	2.09	0.0426
ACO1	Aconitate hydratase 1	2.10	0.0427
APMAP	Adipocyte plasma membrane-associated protein	2.85	0.0430
CPNE1	Copine-1	0.25	0.0431
MSH2	DNA mismatch repair protein Msh2	0.21	0.0431
NUP93	Nuclear pore complex protein Nup93	0.20	0.0432
DNAJA1	DnaJ homolog subfamily A member 1	2.09	0.0436
SH3GL1	Endophilin-A2	0.16	0.0438
ARHGAP29	Rho GTPase-activating protein 29	2.08	0.0446
AP2S1	AP complex subunit sigma	2.91	0.0450
RMDN1	Regulator of microtubule dynamics protein 1	0.19	0.0452
TMX1	Thioredoxin-related transmembrane protein 1	9.47	0.0453
SAE1	SUMO-activating enzyme subunit 1	0.20	0.0465
AHSG	Alpha-2-HS-glycoprotein	2.99	0.0474
VDAC2	Voltage-dependent anion-selective channel protein 2	2.77	0.0474
NASP	Nuclear autoantigenic sperm protein	0.45	0.0475
TGM2	Protein-glutamine gamma-glutamyltransferase 2	0.16	0.0476
MIF	Macrophage migration inhibitory factor	3.00	0.0477
EIF2S2	Eukaryotic translation initiation factor 2 subunit 1	0.26	0.0478
RER1	Protein RER1	0.36	0.0487
PEBP1	Phosphatidylethanolamine-binding protein 1	0.38	0.0495
BCS1L	Mitochondrial chaperone BCS1	0.30	0.0496

Supplemental Table 16: Protein identification, overall p-values, and significant group differences associated with differentially abundant proteins for Male Normal (MN), Female Normal (FN), Male Delayed (MD) and Female Delayed (FD). Three replicates with total embryos for MN (n=20), FN (n=24), MD (n=20) and FD (n=18). P-value was determined by one-way ANOVA, and Fisher's LSD indicates significant ($p<0.05$) comparisons among individual groups with higher protein abundance in first group relative to second group.

ID	Name	F-Stat	P-Value	Fisher's LSD
PRDX4	Peroxiredoxin-4	20.8	0.0004	Female, delayed - Female, normal; Female, delayed - Male, delayed; Female, delayed - Male, normal; Female, normal - Male, delayed; Female, normal - Male, normal
ARPP19	cAMP-regulated phosphoprotein 19	14.3	0.0014	Female, delayed - Female, normal; Male, delayed - Female, normal; Male, normal - Female, normal
MFGE8	Lactadherin	11.9	0.0025	Female, delayed - Female, normal; Female, delayed - Male, delayed; Male, normal - Female, normal; Male, normal - Male, delayed
YWHAE	14-3-3 protein epsilon	11.2	0.0031	Male, delayed - Female, delayed; Male, normal - Female, delayed; Male, delayed - Female, normal; Male, normal - Female, normal
TGM2	Protein-glutamine gamma-glutamyltransferase 2	9.3	0.0055	Female, normal - Female, delayed; Male, normal - Female, delayed; Female, normal - Male, delayed; Male, normal - Male, delayed
NASP	Nuclear autoantigenic sperm protein	9.2	0.0056	Female, normal - Female, delayed; Male, delayed - Female, delayed; Male, normal - Female, delayed
MVP	Major vault protein	8.6	0.0069	Female, normal - Female, delayed; Male, normal - Female, delayed; Female, normal - Male, delayed; Male, normal - Male, delayed
PRPS1	Ribose-phosphate pyrophosphokinase 1	8.5	0.0073	Female, delayed - Male, delayed; Female, normal - Male, delayed; Male, normal - Male, delayed
TUBA3	Tubulin alpha-3 chain	8.2	0.0081	Female, normal - Female, delayed; Female, normal - Male, delayed; Female, normal - Male, normal
HINT1	Adenosine 5'-monophosphoramidase HINT1	7.1	0.0122	Male, delayed - Female, delayed; Male, delayed - Female, normal; Male, delayed - Male, normal
ATP5MF	ATP synthase subunit f, mitochondrial	7.0	0.0124	Female, delayed - Female, normal; Female, delayed - Male, delayed; Female, delayed - Male, normal
UCHL1	Ubiquitin carboxyl-terminal hydrolase isozyme L1	6.9	0.0132	Female, delayed - Male, delayed; Female, normal - Male, delayed; Male, normal - Male, delayed
CIAPIN1	Anamorsin	6.7	0.0141	Female, normal - Female, delayed; Male, normal - Female, delayed; Male, normal - Male, delayed

VDAC2	Voltage-dependent anion-selective channel protein 2	6.5	0.0155	Female, delayed - Female, normal; Male, delayed - Female, normal; Male, normal - Female, normal
BLVRB	Flavin reductase (NADPH)	6.4	0.0164	Female, delayed - Female, normal; Female, delayed - Male, delayed; Female, delayed - Male, normal
COTL1	Coactosin-like protein	6.4	0.0164	Female, normal - Female, delayed; Male, delayed - Female, delayed; Male, normal - Female, delayed
RPS25	Small ribosomal subunit protein eS25	6.2	0.0174	Female, delayed - Female, normal; Female, delayed - Male, delayed
BCHE	Cholinesterase	6.1	0.0184	Female, delayed - Female, normal; Female, delayed - Male, delayed; Female, delayed - Male, normal
EEF1A1	Elongation factor 1-alpha 1	5.8	0.0214	Female, delayed - Female, normal; Male, normal - Female, normal
RPS7	Small ribosomal subunit protein eS7	5.7	0.0219	Male, normal - Female, delayed; Female, normal - Male, delayed; Male, normal - Male, delayed
LAMP1	Lysosome-associated membrane glycoprotein 1	5.5	0.0240	Female, normal - Female, delayed; Male, normal - Female, delayed
VDAC3	Voltage-dependent anion-selective channel protein 3	5.4	0.0253	Female, delayed - Female, normal; Male, delayed - Female, normal; Male, normal - Female, normal
NARS	Asparagine--tRNA ligase, cytoplasmic	5.4	0.0256	Female, delayed - Male, delayed; Male, normal - Female, normal; Male, normal - Male, delayed
KRT14	Keratin, type I cytoskeletal 14	5.2	0.0274	Female, delayed - Female, normal; Female, delayed - Male, delayed; Female, delayed - Male, normal
NAPA	Alpha-soluble NSF attachment protein	5.0	0.0300	Female, normal - Female, delayed; Female, normal - Male, normal
FTH1	Ferritin heavy chain	5.0	0.0301	Female, delayed - Female, normal; Male, delayed - Female, normal; Male, normal - Female, normal
POLR2E	DNA-directed RNA polymerases I, II, and III subunit RPABC1	5.0	0.0307	Male, delayed - Female, delayed; Male, delayed - Female, normal
FAU	Ubiquitin-like protein FUBI	4.9	0.0321	Female, delayed - Female, normal; Female, delayed - Male, delayed; Female, delayed - Male, normal
RPL7	Large ribosomal subunit protein uL30	4.8	0.0334	Female, delayed - Female, normal; Female, delayed - Male, delayed
PFDN2	Prefoldin subunit 2	4.7	0.0350	Female, delayed - Female, normal; Female, delayed - Male, delayed; Female, delayed - Male, normal
MT-ND5	NADH-ubiquinone oxidoreductase chain 5	4.7	0.0353	Female, delayed - Female, normal; Female, delayed - Male, delayed; Female, delayed - Male, normal
SND1	Staphylococcal nuclease domain-containing protein 1	4.7	0.0354	Male, delayed - Female, delayed; Male, normal - Female, delayed
ATP6V1E1	V-type proton ATPase subunit E 1	4.7	0.0358	Male, delayed - Female, delayed; Male, delayed - Female, normal

VMP1	Vacuole membrane protein 1	4.5	0.0385	Female, delayed - Female, normal; Female, delayed - Male, delayed
CPT2	Carnitine O-palmitoyltransferase 2, mitochondrial	4.5	0.0388	Female, normal - Female, delayed; Male, delayed - Female, delayed; Male, normal - Female, delayed
SOD2	Superoxide dismutase [Mn], mitochondrial	4.5	0.0392	Female, delayed - Female, normal; Female, delayed - Male, delayed; Female, delayed - Male, normal
MGST3	Glutathione S-transferase 3, mitochondrial	4.5	0.0402	Female, delayed - Female, normal; Female, delayed - Male, delayed; Female, delayed - Male, normal
MMAB	Corrinoid adenosyltransferase MMAB	4.5	0.0402	Female, delayed - Female, normal; Female, delayed - Male, delayed; Female, delayed - Male, normal
FYN	Tyrosine-protein kinase Fyn	4.4	0.0406	Female, delayed - Male, delayed; Female, delayed - Male, normal
BPNT1	3'(2'),5'-bisphosphate nucleotidase 1	4.4	0.0411	Male, delayed - Female, delayed; Male, normal - Female, delayed; Male, delayed - Female, normal
RPSA	Small ribosomal subunit protein uS2	4.4	0.0423	Female, delayed - Male, delayed; Male, normal - Male, delayed
APOD	Apolipoprotein D	4.3	0.0433	Male, delayed - Female, delayed; Male, delayed - Female, normal; Male, delayed - Male, normal
SERPINA3-1	Serpin A3-1	4.3	0.0445	Female, delayed - Female, normal; Female, delayed - Male, delayed; Female, delayed - Male, normal
CSTF2	Cleavage stimulation factor subunit 2	4.2	0.0456	Female, delayed - Female, normal; Female, delayed - Male, delayed; Female, delayed - Male, normal
ACP1	Low molecular weight phosphotyrosine protein phosphatase	4.2	0.0462	Female, delayed - Male, delayed; Female, delayed - Male, normal
SAMM50	Sorting and assembly machinery component 50 homolog	4.2	0.0464	Female, delayed - Male, delayed; Female, delayed - Male, normal
GCAT	2-amino-3-ketobutyrate coenzyme A ligase, mitochondrial	4.1	0.0478	Female, delayed - Male, delayed; Female, delayed - Male, normal; Female, normal - Male, delayed; Female, normal - Male, normal
VDAC1	Voltage-dependent anion-selective channel protein 1	4.1	0.0481	Female, delayed - Male, delayed; Male, normal - Male, delayed

APPENDIX IV

ADIPOSITY IN MARES INDUCES INSULIN DYSREGULATION AND MITOCHONDRIAL DYSFUNCTION WHICH CAN BE MITIGATED BY NUTRITIONAL INTERVENTION

Summary

Obesity is a complex disease associated with augmented risk of metabolic disorder development and cellular dysfunction in various species. The goal of the present study was to investigate the impacts of obesity on the metabolic health of old mares as well as test the ability of diet supplementation with either a complex blend of nutrients designed to improve equine metabolism and gastrointestinal health or L-carnitine alone to mitigate negative effects of obesity. Mares (n=19, 17.9±3.7 years) were placed into one of three group: normal-weight (NW, n=6), obese (OB, n=7) or obese fed a complex diet supplement for 12 weeks (OBD, n=6). After 12 weeks and completion of sample collections, OB mares received L-carnitine alone for an additional 6 weeks. Obesity in mares was significantly associated with insulin dysregulation, reduced muscle mitochondrial function, and decreased skeletal muscle oxidative capacity with greater ROS production when compared to NW. Obese mares fed the complex diet supplement had better insulin sensivity, greater cell lipid metabolism, and higher muscle oxidative capacity with reduced ROS production than OB. L-carnitine supplementation alone did not significantly

---

[4]Appendix IV was published in *Scientific Reports* in June 2024 (doi: 10.1038/s41598-024-64628-x). Authors: Kyle J. Fresa, Giovana Catandi, Luke Whitcomb, Raul A. Gonzalez-Castro, Adam J. Chicco, Elaine M. Carnevale. This study was funded by The Cecil and Irene Hylton Foundation, the Foundation for the Horse research grant, the USDA National Institute of Food and Agriculture Animal Health and Disease Grant No. COLV 2021-09/ Project Accession No. 1026913, and the Abney Foundation Scholarship.

alter insulin signaling, but improved lipid metabolism and muscle oxidative capacity with reduced ROS. In conclusion, obesity is associated with insulin dysregulation and altered skeletal muscle metabolism in older mares. However, dietary interventions are an effective strategy to improve metabolic status and skeletal muscle mitochondrial function in older mares.

Introduction

Obesity, or excess adiposity, is associated with health concerns in various species due to metabolic and cellular functional disorders. In horses, obesity affects up to 72% of certain populations in the United States and Europe, although percentages vary substantially among populations and breeds.[1,2] Horses are monogastric mammals that develop similar clinical pathologies as humans regarding metabolic disorders and insulin signaling.[3] Obesity in horses is commonly associated with insulin dysregulation (ID), increasing risks for hypertension, dyslipidemia, and vascular disease.[4] Horses with metabolic disorders rarely exhibit type-2 diabetes mellitus as observed in humans.[5] However, other severe pathologies can occur concurrent with ID, such as equine metabolic syndrome and endocrinopathic laminitis, which exhibit similar vascular disturbances as observed in cardiovascular diseases in humans.[6] The health risks of obesity are most notable in the human population, as the incidence of obesity has increased in the past 50 years, and now affects approximately 42% of adults in the United States.[7] Human obesity is associated with a variety of pathologies, such as insulin resistance, cardiovascular disease, and hypertension, although individual risk is highly variable based on factors such as age, sex, genetics, and exercise volume.[8,9,10] Health outcomes associated with metabolic disorders differ among mammalian species and present inherent difficulties to study treatments to improve insulin sensitivity.[11] However, the metabolic responses of horses and

humans to insulin dysfunction are potentially similar, especially when factors such as obesity, age, and sex are implicated.

Cellular metabolism is often altered with excess adiposity, displaying a shift toward fatty acid oxidation, impaired glucose metabolism, and/or reduced mitochondrial activity.[12,13] Potential underlying factors of disease associated with obesity involve disturbances in inflammatory and insulin signaling, which impair glucose homeostasis.[14–16] Skeletal muscle is rich in mitochondria for energy regulation, playing a crucial role in glucose homeostasis.[17,18,19] Skeletal muscle is the largest tissue in the body, representing approximately 40% of body mass in horses and humans, but the proportion of muscle is influenced by age, sex, fitness, genetics, and other factors.[19,20] Glucose uptake in mammalian skeletal muscle is regulated by insulin, which induces the translocation of glucose transporter type 4 (GLUT4) from intracellular compartments to the plasma membrane to support glucose influx.[21] Similar to humans, decreased insulin sensitivity in horses is associated with impaired GLUT4-mediated glucose uptake and increased reactive oxygen species (ROS) production in skeletal muscle, which can result in damage to DNA, proteins, and lipids.[22-23] An imbalance of ROS production and antioxidant response can drive oxidative stress, facilitating insulin dysregulation, mitochondrial dysfunction, and cell death.[24] The specific mechanisms that cause insulin dysregulation in horses are still an area of research. The availability of older animals with large muscle mass and similar metabolic dysfunction risks supports the use of older and obese horses as animal models to study systemic and cellular mechanisms associated with insulin sensitivity.

Reducing energy intake and exercising are often considered essential components for treating obesity and insulin dysregulation.[25,16,26] Dietary supplements with specific compounds are potentially valuable for improving metabolic status. However, dietary components often have

synergistic and complex interactions that are poorly understood in mammals. For instance, dietary chromium and L-carnitine supplementation appear to have positive effects on cell metabolism and mitochondrial function in obese mice and women.[27,28,29,30] L-carnitine facilitates the transport of long-chain fatty acids into mitochondria for energy production and is essential for fat metabolism in mammalian species.[31] L-carnitine also has antioxidant properties, as it scavenges free-radicals, reduces production of free-radicals in stressed mitochondria, and induces cellular production of antioxidant enzymes.[32] The impact of L-carnitine supplementation on metabolism and oxidative stress in skeletal muscle have not been described in the horse. In previous studies, we demonstrated positive effects on mitochondrial energy production and reduced oxidative stress in the ovarian follicular cells of older mares after supplementation with antioxidants, amino acids (including L-carnitine), omega-3-rich oils, probiotics, prebiotics, vitamins, and minerals.[33] These findings suggest that the impacts of other causes of metabolic stress, such as adiposity, could be mitigated using nutritional interventions.

We hypothesized that equine obesity would result in insulin dysregulation, altered lipid metabolism, and mitochondrial dysfunction, and that short-term supplementation of nutrients designed to improve equine metabolism and gastrointestinal health could mitigate these negative effects, independent of weight loss or exercise. We used a combination of morphometric and systemic assays, protein analysis, and high-resolution respirometry to evaluate mitochondrial and cellular function resulting from obesity and the potential of dietary supplementation of a complex dietary supplement or L-carnitine to improve insulin dysregulation and muscle mitochondrial function in mares.

Results

Mare morphometric measurements

Mean age was similar among groups for normal-weight (NW), obese (OB), and obese diet supplemented (OBD) mares (17.8±4.3, 18.1±3.9, 17.7±3.6 yr, respectively). Morphometric measurements were performed throughout the study to assess adiposity. Prior to sample collections, morphometric measurements of body condition score (BCS), percent body fat (BF), and neck score (NS) were higher ($p \leq 0.01$) in obese groups when compared to NW (Figure IV-1a-c). Body weight (BW) did not significantly differ ($p=0.1$) due to varying mare sizes (Figure IV-1d). Morphometric measurements were assessed every two weeks prior to sample collections to determine changes over time during feeding. No differences were observed between OB and OBD for morphometric measurements, and a BCS of ≥7, characterizing obesity, was confirmed for all mares in OB and OBD before sample collections.

Measurements of insulin dysregulation

The effect of adiposity and nutrient supplementation on insulin dysregulation and glucose response was assessed using multiple parameters. Systemic concentrations of insulin were measured at 12wk and were greater ($p<0.04$) in OB than NW and OBD after overnight fasting (Figure IV-2a). Fasting concentrations of glucose were greater ($p<0.03$) in NW than OB and OBD (Figure IV-2b). Circulating concentrations of leptin tended ($p=0.06$) to be elevated in OB when compared to NW, but not OBD ($p=0.5$, Figure IV-2c). The insulin response to glucose was determined using an oral sugar test, based on measurements of glucose and insulin at 0, 60, and 90 minutes after administration of corn syrup (Figure IV-2d,e).[34] Insulin concentration above 45 μU/ml after 60 and 90 minutes was used as a threshold for insulin dysregulation.[35] No NW mares, six of seven OB mares (86%), and two of seven OBD mares (28%) were positive for

insulin dysregulation (p=0.005, Figure IV-2e). Thus, OB were more frequently diagnosed with insulin dysregulation than NW mares, with a tendency (p=0.09) for more OBD than OB to have an insulin response within normal limits after sugar consumption. The reciprocal of the square root of insulin (RISQI) proxy identified a reduction in insulin sensitivity in OB when compared to NW (p=0.01) and a tendency (p=0.06) for increased insulin sensitivity in OBD when compared to OB (Figure IV-2g). Interestingly, the the modified insulin to glucose ratio (MIRG) proxy suggested increased pancreatic insulin release in both OB (p=0.0005) and OBD (p=0.01) when compared to NW (Figure IV-2f). In skeletal muscle, expression of serine-307 phosphorylated insulin receptor substrate-1 (IRS1) relative to total IRS1 protein was similar between NW and OBD, and both were reduced (p<0.002) when compared to OB (Figure IV-2h,i).

Systemic concentrations of fatty acids and carnitine species

Fasting concentrations of circulating non-esterified fatty acids (NEFA) were lower (p<0.004) in OB and OBD than NW (Figure IV-3a). Plasma concentrations of triglycerides were not different (p=0.2) among groups (Figure IV-3b). Proportion of saturated fatty acids related to total fatty acids measured in red blood cells (RBC) were not different among groups and did not change over time (Figure IV-3c). However, after 8 weeks of grain supplementation, the percentage of omega-3 polyunsaturated fatty acids (PUFA) was lower in OB and OBD when compared to the week 0 in RBC (p<0.0001, Figure IV-3d). In contrast, percentage of omega-6 PUFAs to total fatty acids increased in both OB (p=0.001) and OBD (p<0.0001) when compared to initial measurements in RBC (Figure IV-3e). Proportional composition of eicosapentaenoic acid (EPA)+ docosahexaenoic acid (DHA) in RBC tended (p=0.06) to decrease in OB and OBD groups when compared to previous measurements (Figure IV-3f). At 8 weeks, percentages of

omega-3 PUFAs were higher in OB ($p=0.005$) and OBD ($p=0.01$) than NW (Figure IV-3e) in RBC. However, no differences were observed among groups for percentage of omega-6 PUFAs. Percentage of EPA+DHA tended ($p=0.09$) to decrease in OB and OBD groups when compared to NW at 8 weeks of diet intervention (Figure IV-3f).

Circulating carnitine species were compared among groups to evaluate lipid metabolism at 12 weeks of dietary regime. Total carnitine species were increased ($p\leq0.005$) in OBD mares when compared to NW and OB (Figure IV-4a). Circulating L-carnitine was higher ($p<0.0005$) in OBD than NW and OB, demonstrating uptake from the dietary supplement (Figure IV-4b). This was accompanied by higher concentrations of acetyl-carnitine in OBD relative to OB ($p<0.0001$) and NW ($p=0.01$, Figure IV-4c). Differences in short chain acylcarnitine species were observed for OB and OBD ($p=0.02$), although medium and long chain species were not significantly different among the groups (Figures IV-4d-f). Plasma concentrations of individual acylcarnitine species for groups are shown in Table 1.

Ratios of key acylcarnitine species revealed differences in availability of L-carnitine and β-oxidation among groups. Ratios of C16:C3 were used to approximate completeness of β-oxidation, with lower values representing increased lipid metabolism efficiency due to higher amounts of oxidized C3 products. This ratio was lower ($p\leq0.04$) in OBD than OB and NW, suggesting that the diet supplement fed to OBD improved mitochondrial lipid metabolism (Figure IV-4g). Higher ($p<0.02$) free carnitine in relation to total carnitine was observed in OBD when compared to OB and NW (Figure IV-4h). The ratio of total acylcarnitine to free L-carnitine was lower ($p=0.004$) in OBD when compared to OB (Figure IV-4i), and tended ($p=0.06$) to be lower between OB and NW. Overall, the addition of targeted supplementation combining vitamins, trace minerals, amino acids (including L-carnitine), antioxidants, omega-3 fatty acids,

prebiotics and probiotics in OBD mares increased the availability of free L-carnitine and improved the efficiency of lipid metabolism.

Mitochondrial function in skeletal muscle

Analysis of skeletal muscle mitochondrial function was performed using the Oroboros high-resolution respirometer (Oroboros Instruments, Innsbruck, AT) to determine the effect of obesity and dietary nutritional supplementation on maximum mitochondrial oxygen consumption rate (OCR) and reactive oxygen species (ROS) production. The maximum OCR was lower ($p<0.01$) in skeletal muscle from OB than from NW or OBD (Figure IV-5a). ROS release rates tended to be higher ($p<0.1$) in OB compared to OBD, and were >2-fold higher ($P<0.003$) in OB than NW and OBD when expressed relative to OCR (Figure IV-5b,c). Despite these functional differences, protein abundance of superoxide dismutases 1 and 2, very long chain acyl-CoA dehydrogenase, electron transport chain complexes, and the phosphorylation state of pyruvate dehydrogenase (PDH) were similar among groups (Figure IV-5d-l).

Short-term L-carnitine supplementation on insulin sensitivity

To determine the specific effects of L-carnitine after the completion of the above experiment, mares previously in the OB group were maintained on the same feeding regime with the exception of inclusion of dietary L-carnitine (OBLC) for 6 weeks before additional sample collections. No significant differences were observed in morphometric measurements before and after L-carnitine supplementation (Figure IV-6a-d). Insulin regulation, as determined by an oral sugar test, was not affected (Figure IV-6e,f); six out of the seven mares were diagnosed with insulin dysfunction prior to (OB) and after L-carnitine (OBLC). However, insulin sensitivity determined by RISQI was reduced ($p=0.01$) after 6 weeks of L-carnitine consumption (Figure IV-6g). Insulin response determined by MIRG tended ($p=0.09$) to be higher for OBLC than OB,

and expression of serine-307 phosphorylated insulin receptor substrate-1 (IRS-1) to total IRS-1 in skeletal muscle tissue was not different before and after L-carnitine supplementation (Figure IV-6h-j).

Fatty acid metabolism after short-term L-carnitine

Plasma acylcarnitines were evaluated after 6 weeks of L-carnitine supplementation to obese mares. As expected, total carnitine concentration ($p=0.004$, Figure IV-7a) and L-carnitine concentration ($p=0.0007$, Figure IV-7b) were greater following supplementation, demonstrating an uptake of L-carnitine. Overall, total acylcarnitines were elevated ($p=0.005$) after supplementation (Figure IV-7c). Analysis of individual species demonstrated that short chain acylcarnitines were more consistently increased ($p=0.05$) than medium and long chain acylcarnitines (Figure IV-7d-f, Table 2). The C16:C3 fatty acid ratio was lower following L-carnitine supplementation ($p=0.0004$, Figure IV-7g), suggesting an improvement in complete β-oxidation of long-chain fatty acids. After supplementation of L-carnitine, free carnitine relative to total carnitine was higher ($p=0.02$, Figure IV-7h), while total acylcarnitines compared to free carnitines decreased ($p=0.01$, Figure IV-7i).

Mitochondrial function in skeletal muscle after L-carnitine supplementation

A skeletal muscle biopsy was taken after 6 weeks of L-carnitine supplementation to obese mares. After L-carnitine supplementation, maximum OCR tended to be greater ($p=0.09$, Figure IV-8a) and ROS production was lower ($p<0.005$, Figure IV-8b,c). Protein abundance of SOD1, SOD2, or electron transport chain complexes did not change after L-carnitine supplementation (Figure IV-8d-g,i-k), while phosphorylation of PDH was decreased ($p=0.02$; Figure IV-8h,l).

Discussion

In mares, limited research has been conducted to specifically assess insulin dysfunction and how dietary modifications can affect their metabolic and reproductive status. In the present study, we assessed the effects of adiposity on metabolic status, skeletal muscle mitochondrial function, insulin signaling, and lipid metabolism in mares and we examined the potential for dietary supplements to improve the metabolic function of skeletal muscle and systemic insulin dysregulation.

Cellular insulin sensitivity is not currently recognized as a defining characteristic in insulin-dysregulated horses; however, gastrointestinal factors such as incretin hormone release and overall gastrointestinal glucose uptake are known to be altered in insulin-dysregulated horses.[36] To date, the specific mechanisms that drive cellular insulin resistance in equine skeletal muscle are not understood. We have shown for the first time that serine-307 phosphorylation of insulin receptor substrate 1 (IRS1) is higher in skeletal muscle collected from obese mares with insulin dysregulation. This posttranslational modification is characteristic of insulin resistance in humans, which prevents the uptake of glucose into myocytes in response to insulin.[22] In addition, this signaling can be disrupted in humans by inflammation and/or oxidative stress, resulting in the phosphorylation of IRS1 and subsequent inhibition of GLUT-4 translocation, reducing cellular glucose uptake.[37] The IRS1 phosphorylation could serve as a cellular marker to identify insulin-dysregulated horses in inconclusive cases. However, the mechanisms responsible for IRS1 phosphorylation in horses require further investigation. The MIRG proxy suggested increased pancreatic insulin release in the obese groups, which is consistent with prediabetes in humans and insulin dysregulation in horses, as beta cells initially produce excessive insulin in order to reduce blood glucose.[36,38]

Skeletal muscle is the primary consumer of glucose in mammals, [39] affecting systemic glucose regulation.[16] We evaluated the effects of obesity on mitochondrial function, lipid metabolism, and oxidative stress in live skeletal muscle cells. Skeletal muscle from obese mares had lower mitochondrial oxidative capacity and greater ROS production compared to normal-weight mares, consistent with mitochondrial dysfunction.[40] ROS are capable of damaging lipids, proteins, and DNA unless removed by antioxidant enzymes or molecules.[41–43] In the present study, mitochondrial or cytoplasmic superoxide dismutase (SOD) protein expression was not altered in obese mares. Similar to our results, antioxidant parameters in equine skeletal muscle such as glutathione, activity of glutathione peroxidase (GPX), and expression of *GPX*, catalase, peroxiredoxin, glutathione synthetase, and glutathione reductase were not altered with adiposity. Only total superoxide dismutase activity was upregulated with increasing adiposity.[23] No oxidative damage was observed in skeletal muscle related to obesity alone or associated with hyperinsulinemia, suggesting that oxidative damage linked to obesity in skeletal muscle is not essential for the pathogenesis of hyperinsulinemia in obese horses.[23] However, ROS production in equine skeletal muscle is inversely associated with insulin sensitivity.[23] While we did not observe any decrease in mitochondrial protein expression to explain the lower OCR in obese mares, we did not evaluate changes in mitochondrial dynamics or individual enzyme activities that might have contributed to this effect.[44]

In mammals, including humans, lipid metabolism is closely coordinated with glucose homeostasis in response to insulin stimulation.[16] In humans, insulin resistance can also be induced by increased plasma concentrations of lipids.[16] Altered lipid metabolism is often characteristic of obesity, usually due to elevated circulating lipids and potentially impaired glucose uptake due to insulin resistance.[45] Metabolic dysregulation of plasmatic lipids promotes

mitochondrial dysfunction due to increased β-oxidation and subsequent peroxidation.[46] In our study, circulating triglycerides and lipid composition of red blood cells were similar among groups and over time. In obese mares, omega-6 polyunsaturated fatty acid (n-6 PUFA) were increased, while EPA+DHA, omega-3 polyunsaturated fatty acids (n-3 PUFA), and non-esterified (NEFA) were reduced when compared to normal-weight mares. Lower NEFA in obese groups may reflect a possible mitigation of adipose tissue lipolysis following grain feeding, as carbohydrate intake has been previously demonstrated to reduce NEFA concentrations in humans,[47] although a similar study has not been done in horses and the cause of altered NEFA concentrations was not determined in this study. The altered fatty acid distribution in obese mares was possibly caused by the adiposity associated with high caloric intake due to the inclusion of grain rather than dietary fatty acids. In humans, n-3 PUFAs have been demonstrated to reduce the production of inflammatory mediators, resulting in a positive effect on obesity, insulin resistance, and mitochondrial dysfunction.[48,49] There is a debate about whether n-6 PUFAs have pro- or anti-inflammatory effects.[48] In a mouse model, high levels of n-6 PUFAs promote the reduction of IRS1 phosphorylation in skeletal muscle,[50] which may exacerbate insulin resistance. Overall, insulin dysfunction is a complex syndrome that disrupts the close association between lipid metabolism and glucose homeostasis. Characterization of these mechanisms in obese horses can aid to identify new therapeutic approaches to reduce the negative effects of insulin dysfunction.

The most common treatments to improve obesity-related metabolic disorders in horses and people involve weight loss through dietary restrictions and exercise.[16,25,26] In horses, diet and exercise programs need to be adapted to the individual's demands for weight loss and improvement of insulin sensitivity, but such programs can have potential complications in

certain horses.[25,51] Specific dietary supplements have been shown to improve insulin sensitivity in humans and mice, and they have also been studied in horses. Supplementation with prebiotics such as short-chain fructo-oligosaccharides into the diet of obese horses has no effect on systemic glucose, triglycerides, or leptin, although they improve insulin sensitivity;[52] this beneficial effect is enhanced by the addition of vitamin and mineral nutraceutical supplements.[53] Similarly, the synergetic action of dietary leucine and resveratrol in insulin-dysregulated horses promotes an increase in insulin sensitivity and high molecular-weight adiponectin, an insulin-sensitizing adipokine.[54] In the present study, obese mares were fed a dietary supplement formatted to improve metabolism and gastrointestinal health in an attempt to restore insulin signaling and cellular function. When provided the targeted dietary intervention, obese mares had better glucose tolerance and insulin sensitivity, similar to normal-weight mares. In addition, skeletal muscle from diet supplemented obese mares (OBD) exhibited insulin signaling changes, as the abundance of serine-307 phosphorylated IRS1 was reduced to a similar level as in normal-weight mares. These findings support the concept that complex dietary supplementation can improve insulin dysregulation by targeting cellular mechanisms in the absence of exercise or weight loss in horses. The potential for dietary interventions to improve insulin resistance warrants further investigation.

Metabolic compounds such as L-carnitine have been used as dietary supplements alone or in combination to aid metabolic disorders. L-carnitine is the only molecule capable of transporting long-chain fatty acids across the inner mitochondrial membrane, where they are metabolized into short-chain fats, as β-oxidation cleaves two carbons per cycle to form a single acetyl-CoA molecule that can enter the citric acid cycle to produce ATP.[55,56] Acylcarnitines are the esters formed when fatty acids bind to L-carnitine to be carried into the mitochondria; thus,

analysis of acylcarnitine species are indicative of fat uptake and metabolism in the mitochondria.[55,56] Obese mares provided the complex diet supplement (OBD) resulted in increased circulating free L-carnitine and total acetylcarnitine species with a larger proportion of short-chain than medium- or long-chain acylcarnitines, implying completeness of β-oxidation due to improved mitochondrial function and fatty acid metabolism.[56] We subsequently examined the isolated effect of dietary L-carnitine on insulin dysregulation and lipid metabolism in obese mares (OBLC). Dietary L-carnitine did not result in changes in body condition of obese mares, suggesting it did not alter adiposity. However, proxies evaluating systemic insulin response tended to improve, and the ratio of phosphorylated IRS1 tended be less in skeletal muscle, suggesting a potential influence on insulin sensitivity. However, supplementation with L-carnitine alone lacked the significant impact observed with the complex diet supplementation, suggesting that synergistic interactions among the nutrients were important to optimize beneficial effects. As expected, dietary L-carnitine alone promoted higher systemic free L-carnitine and total acetylcarnitines, predominantly short-chain acylcarnitines. In humans, dietary L-carnitine increased plasmatic levels of free L-carnitine and acetylcarnitines and was associated with lower glucose and insulin in insulin-resistant individuals.[28] In overweight or obese women with polycystic ovary syndrome subjected to L-carnitine supplementation, insulin sensitivity was improved but lipid profiles were not altered.[57] Importantly, a meta-analysis of random trials demonstrates that dietary L-carnitine is effective in treating people with insulin resistance, and that the benefits increase with longer consumption.[58] Consistent with our study, dietary L-carnitine increased plasmatic free L-carnitine and short-chain acylcarnitines in 3-year old horses but did not improve insulin sensitivity,[59] possibly because L-carnitine effects are more evident in insulin-dysregulated horses as observed in insulin-sensitive humans.[28] Dietary supplementation

combining the synergistic effects of vitamins, trace minerals, amino acids (including L-carnitine), antioxidants, omega-3 fatty acids, prebiotics and probiotics appears promising to promote metabolic changes and improve mitochondrial function and lipid metabolism in obese patients.

Dietary strategies have been used in an attempt to modulate metabolic disorders; these include antioxidants compounds. Several antioxidants such as lipoic acid, resveratrol, coenzyme Q10 and epigallocatechin-3-gallate have anti-inflammatory properties and improve cellular glucose metabolism by reducing levels of oxidative stress.[60,61] In our study, obesity was associated with lower mitochondrial oxygen consumption in skeletal muscle and higher ROS production. Normal-weight and obese mares provided the diet supplement (OBD) had similar levels of skeletal muscle oxygen consumption and ROS production. Dietary L-carnitine alone promoted a reduction of ROS production in the skeletal muscle of obese mares. However, abundance of antioxidant enzymes such as SOD1 and SOD2, and electron transport chain complexes in skeletal muscle were not affected by obesity or dietary supplements. This finding may be explained by L-carnitine acting as an antioxidant to prevent lipid buildup and peroxidation in mitochondria.[62,63] Also, exogenous antioxidants contained in the dietary supplement may have either supplied the necessary antioxidant capacity or improved the endogenous potential to reduce oxidant production. For instance, lipoic acid is a potent antioxidant and a cofactor of mitochondrial dehydrogenase complexes, which can directly scavenge ROS or interact with other antioxidant molecules such as coenzyme Q10, vitamin C, and vitamin E to indirectly reduce oxidative stress.[61] Interestingly, we observed that dietary L-carnitine was associated with reduced phosphorylation of pyruvate dehydrogenase (PDH). Phosphorylation downregulates PDH activity to metabolize pyruvate into acetyl-CoA in

mitochondria.[64] Similar responses have been observed in mice and insulin-resistant patients subjected to dietary L-carnitine supplementation, showing increased PDH activity in skeletal muscle.[27,28] Overall, dietary antioxidants and L-carnitine appeared to reduce ROS production in the skeletal muscle independently of antioxidant mitochondrial enzymes and may have an impact on pyruvate metabolism for energy production in obese mares.

In summary, obesity was associated with insulin dysregulation, oxidative stress, and decreased mitochondrial function in mares. Results of the present study demonstrated that targeted dietary supplementation can reverse systemic and cellular negative effects associated with obesity, independent of weight loss or exercise, with the potential to improve systemic health. Additional research is needed to elucidate the mechanisms of insulin dysregulation and mitochondrial dysfunction in obese horses to create novel therapies and further improve well-being. In addition, specifically formulated dietary supplementation may provide support for the treatment of insulin resistance and diabetes in humans. Future studies are needed to address the role of inflammatory mechanisms in inducing cell stress and mitochondrial dysfunction to determine specific dietary components to restore cell function.

Methods

Study population and serum collection

Animal procedures were approved by Colorado State University's Institutional Animal Care and Use Committee and were carried out in accordance with relevant guidelines and regulations. All methods are reported in accordance with ARRIVE guidelines. Prior to start of the study, nonlactating, light-horse mares were evaluated for body condition scores (BCS, from 1, emaciated to 9, extreme obesity),[65] and divided into three groups based on age. All mares were

on a hay only diet prior to the start of the study, although they came from different locations. All mares had a BCS from 5 to 8 prior to assignment into groups. Mares with an initial BCS of 5 or 6 (moderate to moderately fleshy BCS) were assigned to the normal-weight group (NW, n=6, 17.8 ± 1.8 years, BCS 5.4 ± 0.2, mean ± SD). The remaining mares had BCS from 6 to 8 (moderately fleshy to fat), were paired by age, and then randomized into one of two overweight groups: obese (OB, n=7, 18.6 ± 1.5 years, BCS 7.2 ± 0.3) and obese dietary supplemented (OBD, n=7, mean age of 17.7 ± 1.4 years, BCS 6.9 ± 0.3). Mares were housed in large dry lots and each group was provided a unique dietary regime for the entirety of the study. Mares grouped as NW were fed grass/alfalfa mix hay at approximately 2% of body weight daily and 57 g daily of a commercial forage balancer (Free Balance 12:12®, Purina Animal Nutrition, Gray Summit, MO, USA). The base diet for OB and OBD was grass/alfalfa hay ad libitum and forage balancer. Twice daily, OB and OBD were also fed 0.75 kg of whole oats and 0.75 kg of cracked corn provided in a single lot from a local feed supplier. Mares in the OBD group received targeted supplementation designed to support equine metabolic and gastrointestinal health (187 g, divided into two feedings), of a combination of vitamins, trace minerals, amino acids (including L-carnitine), antioxidants, omega-3 fatty acids, prebiotics and probiotics formulated to support cellular metabolism (Platinum Performance Inc., Buellton, CA, USA). Mares were maintained on group-specific feeding regimens for approximately 12 weeks before blood and muscle collections.

In a follow-up study aimed to assess the isolated effects of L-carnitine supplementation , mares that were originally in the OB group were kept on the same diet (ad libitum hay, daily grain and forage balancer), but they were also fed 7.5 g of L-carnitine powder twice daily for 6 weeks, which was equivalent to the amount of L-carnitine included in the dietary supplement for

OBD. The L-carnitine supplemented obese mares (OBLC) were evaluated biweekly for markers of adiposity, as described below, for 6 weeks prior to blood and muscle collections. The effect of L-carnitine supplementation to the obsese mares was determined by comparing samples collected at 12 weeks for OB to samples collected from the same mares after an additional 6 weeks of L-carnitine supplementation, designated as OBLC.

Morphometric and insulin dysfunction assessments

Morphometric assessments were performed at 2-week intervals and included BCS (1-9)[65] and cresty neck score (0-5)[66]. An approximation of the percentage of body fat was calculated using a measurement of subcutaneous fat thickness obtained using a 10 MHz linear-array transducer that was placed approximately 7.6 cm cranial and 5 cm lateral from the tailhead and calculated using the following formula [(2.47 + 5.47 x tailhead fat (cm)].[67,68]

Insulin dysregulation was evaluated using an oral sugar test. Mares were fasted for at least 6 hours before being given an oral dose of Kroger® Lite Corn Syrup (The Kroger Co, Cincinnati, OH) at 0.15 mL/kg body weight.[34] Blood samples were collected into EDTA tubes by jugular venipuncture prior to and at 60 and 90 minutes after administration of corn syrup. Blood glucose was measured from whole blood directly after collection using a blood glucose monitor equilibrated for equine blood following the manufacturer's instructions (AlphaTRAK 2, Zoetis Inc., Kalamazoo, MI). For insulin measurements, blood was allowed to clot for 2 hours at 4°C, centrifuged at 1500g for 10 minutes, and plasma was stored at -20°C until radioimmunoassays for insulin quantification by a reference lab (Endocrinology Lab, Cornell University Animal Health Diagnostic Center, Ithaca, NY). Insulin concentrations at either 60- or 90-minute timepoints that were greater than 45 μU/mL were considered indicative of insulin dysregulation.[35] Insulin and glucose values collected prior to sugar administration were used to

calculate the reciprocal of the square root of insulin [RISQI; $(\text{fasted insulin})^{-0.5}$] and the modified insulin-to-glucose ratio [MIRG; $800 - 0.3\ (\text{fasted insulin} - 50)^2 / (\text{fasted glucose} - 30)$], with the proxies estimating insulin sensitivity and pancreatic response to glucose, respectively.[69]

Red blood cell lipid analysis

Before and at 4 and 8 weeks of dietary supplementation, 10 mL of whole blood was collected into EDTA tubes and centrifuged at 3000g for 10 minutes at room temperature. Pelleted red blood cells were transferred into cryovials, snap frozen in liquid nitrogen, and shipped on dry ice for membrane fatty acid composition (OmegaQuant Analytics LLC, Sioux Falls, South Dakota). Red blood cell membrane lipids were transesterified with boron trifluoride prior to gas chromatography to determine fatty acid composition, expressed as a weight percentage of total identified fatty acids.[70]

Determination of circulating non-esterified free fatty acids, triglycerides, and acylcarnitine species

Plasma samples were collected from all mares after 12 weeks of their respective (NW, OB, and OBD) diet, and again after 6 weeks of dietary L-carnitine for OBLC. Blood was collected by jugular venipuncture into EDTA tubes and centrifuged at 3000g prior to plasma collection. Plasma was snap frozen and stored at -20°C until analysis. Plasma concentrations of non-esterified free fatty acids were determined by a reference laboratory (Clinical Pathology Laboratory, Cornell University Animal Health Diagnostic Center). Plasma triglyceride concentrations were determined using a colorimetric assay kit (Cayman Chemical, Ann Harbor, MI, USA) using a single non treated 96-well microplate, read at 540-nm absorbance on a Synergy 2 microplate reader (Biotek, Agilent, Santa Clara, CA, USA). Plasma acylcarnitine profiles were assessed using liquid chromatography mass spectrometry at an external laboratory

(University of Colorado Anschutz Medical Campus School of Medicine Metabolomics Core, Aurora, CO).[71] Briefly, a standard solution (180 µL) containing known concentrations of acylcarnitine species in methanol were added to 20-µL aliquots of plasma. Samples were briefly vortexed and incubated at 20°C for 15 min, then centrifuged at 12700g. Approximately 100 µL of supernatant was transferred to a new tube, and 100 µL of 10 mM ammonium acetate was added to each sample. A 10-µL allotment of each sample was injected and analyzed using a Thermo Vanquisher Liquid Chromatography system coupled to a Q-Exactive™ Quadrupole-Orbitrap™ Mass Spectrometer as previously described in detail.[71]

Muscle sample collection

Punch biopsies of the semitendinosus muscle were obtained after mares were on their assigned diet for 12 weeks. Samples were immediately washed in BIOPS preservation solution containing 10 mM Ca-EGTA (0.1 M free calcium), 20 mM imidazole, 20 mM taurine, 50 mM K-MES, 0.5 mM DTT, 6.56 mM $MgCl_2$, 5.77 mM ATP, and 15 mM phosphocreatine at pH 7.1.[72] Half of the sample was snap frozen in liquid nitrogen and stored at -80°C for western blot analysis, while the other half was placed in fresh BIOPS buffer on ice for high-resolution respirometry.

High-resolution respirometry

Skeletal muscle samples were stored on ice overnight in BIOPS. Next day, samples were teased and treated with 50 µg/mL saponin on ice for 20 min with gentle rocking to permeabilize cell membranes while leaving mitochondrial membranes intact. Permeabilized fibers were then removed and rinsed in mitochondrial respiration medium (MIR05; 0.5mM EGTA, 3mM $MgCl_2$ hexahydrate, 60mM lactobionic acid, 20 mM taurine, 10 mM KH_2PO_4, 20 mM HEPES, 110 mM sucrose, and 0.1% BSA; pH 7.1). Fibers were gently blotted dry using Whatman® filter paper

(Cytiva, Marlborough, MA) and weighed immediately prior to adding approximately 5 mg to the oxygraph chamber containing 2 mL MIR05, horseradish peroxidase (1 U/mL), and Amplex UltraRed (5 μM) at 37°C. The chambers were saturated with >400 μM oxygen and stabilized before addition of metabolic substrates in order to maintain an assay oxygen concentration between 300-400 μM to avoid diffusion limitation on OCR and ROS release rates.[72] Maximum mitochondrial oxidative capacity (OCR) was evaluated following the addition of 1 mM malate, 0.05 mM palmitoylcarnitine, 5 mM pyruvate, 2.5 mM adenosine diphosphate, and 10 mM succinate. The net rate of mitochondrial H_2O_2 (ROS) release was measured simultaneously with OCR by monitoring the accumulation of chamber resorufin (Ex/Em 571/585 nm), the stable fluorescent product of 1:1 oxidation of Amplex UltraRed by H_2O_2 in the presence of horseradish peroxidase (HRP; 1 U/mL) following the addition of succinate using a custom-fitted fluorometer (O2k-Fluo LED2 module; Oroboros Instruments, Innsbruck, AT).[72,73,74]

Protein sample preparation and immunoblotting

Antibodies were purchased in Abcam (Waltham, MA), unless otherwise stated. Primary antibodies were phospho-IRS1 (Ser307), IRS1, OXPHOS, Cu/ZN SOD (SOD101; StressGen, Victoria, BC), Mn SOD (SOD111; StressGen), VLCAD (Santa Cruz Biotechnology, Dallas, TX), phospho-PDH, and PDH. Secondary antibodies included goat anti-rabbit IgG H&L-HRP and goat anti-mouse IgG H&L-HRP.

Frozen skeletal muscle tissue was thawed on ice, chipped to attain 30 mg of sample, and homogenized in M-PER™ Mammalian Protein Extraction Reagent lysis buffer (Thermo Fisher Scientific, Waltham, MA) containing Halt™ Protease and Phosphatase Inhibitor Single-Use Cocktail (Thermo Fisher Scientific) using a glass tissue homogenizer. Samples were sonicated and centrifuged at 10000g for 15 minutes. The supernatant was transferred into a new

microcentrifuge tube and stored at -80°C. Concentrations of protein were determined using the Pierce™ bicinchoninic acid assay (Thermo Fisher Scientific). Protein samples were prepared with Laemmli Buffer (Bio-Rad, Hercules, CA) and DTT Bolt™ (Thermo Fisher Scientific) to achieve concentrations of 30 µg/mL. Samples were denatured for 10 minutes at 90°C, cooled, and loaded into 12-well, 4-12% Bis-Tris polyacrylamide gels (Thermo Fisher Scientific) with a protein ladder to determine weight (Precision Plus Protein Standards Dual Color, Bio-Rad). Gels were run for 45 minutes at 150V, removed, and protein was transferred to a polyvinylidene difluoride (PVDF) membrane. The resulting membrane was washed in Tris-buffered saline (TBS) + Tween® (Sigma-Aldrich, St Louis, MO) and blocked with 5% non-fat dry milk in TBS for 1 hour. Following a wash, 1:1000 primary antibody in milk-TBS solution was added and rocked overnight at 4°C. After washing, 1:3000 secondary antibody was added and rocked for 1 hour. The membrane was washed and imaged with chemiluminescence. Band density representing the protein of interest's molecular weight were quantified via colorimetric analysis using ImageJ (NIH, Bethesda, MD) and standardized to total protein concentrations determined using Amido Black (Bio-Rad, Hercules, CA) protein stain.[75]

Statistical Analysis

Statistical analyses were conducted using GraphPad Prism 9.3.1 software. Continuous datasets were analyzed for normality and homogeneity of variances using the Shapiro-Wilk and Levene test. Repeated measures of morphometric data and glucose tolerance tests were compared within and between groups using two-way ANOVA with post-hoc Tukey's multiple comparison tests. Western blots, acylcarnitine profiles, oral sugar tests, and high resolution respirometry results were analyzed by one-way ANOVA with post-hoc Tukey's multiple comparison tests for normally distributed data sets. Kruskal-Wallis tests, followed by Dunn's

multiple comparison tests, were used for data that failed to be normally distributed. All pre-post analyses, before and after L-carnitine supplementation, were evaluated using two-tailed paired t-test. Values of $p<0.05$ were considered significant, while values $p\leq0.1$ were considered tendencies. Results are presented as mean ± SEM.

Tables

Table IV-1. Concentrations (nM, mean ± SEM) of individual acylcarnitine species in plasma of normal-weight (NW, n=6), obese (OB, n=7) and obese diet supplemented (OBD, n=6) mares after at least 6 weeks on the respective diets; [ab] Superscripts within the same row indicate difference at $p < 0.05$.

Short-chain acylcarnitines	NW	OB	OBD
Acetyl (C2)	17.66 ± 2.52[a]	12.13 ± 1.34[a]	26.56 ± 1.76[b]
Propionyl (C3)	1.07 ± 0.15[a]	0.76 ± 0.09[a]	1.93 ± 0.13[b]
Succinyl (C4-DC)	21.36 ± 3.06	18.99 ± 3.83	18.18 ± 2.03
Hydroxybutyryl (C4-OH)	0.50 ± 0.19	0.39 ± 0.15	0.85 ± 0.16
Butanoyl (C4)	0.88 ± 0.13[a]	1.38 ± 0.27[ab]	2.48 ± 0.41[b]
Hydroxyisovaleryl (C5-OH)	0.10 ± 0.05[ab]	0.08 ± 0.02[a]	0.25 ± 0.04[b]
Isovaleryl (C5)	0.36 ± 0.05[a]	0.24 ± 0.04[a]	0.66 ± 0.02[b]
Medium-chain acylcarnitines			
Adipyl (C6-DC)	0.53 ± 0.16	0.56 ± 0.09	0.61 ± 0.09
Hexanoyl (C6)	0.05 ± 0.01	0.04 ± 0.01	0.06 ± 0.004
Decanoyl (C10)	0.08 ± 0.01	0.05 ± 0.01	0.07 ± 0.01
Dodecanoyl (C12)	0.08 ± 0.01	0.05 ± 0.01	0.06 ± 0.005
Long-chain acylcarnitines			
Tetradecenoyl (C14:1)	0.26 ± 0.04[a]	0.10 ± 0.01[b]	0.13 ± 0.02[b]
Tetradecanoyl (C14)	0.09 ± 0.01	0.06 ± 0.01	0.07 ± 0.01
Hexadecenoyl (C16:1)	0.16 ± 0.03	0.14 ± 0.03	0.11 ± 0.02
Palmitoyl (C16)	0.45 ± 0.05	0.42 ± 0.09	0.47 ± 0.05
Linoleoyl (C18:2)	0.13 ± 0.03	0.11 ± 0.01	0.18 ± 0.04
Octadecenoyl (C18:1)	0.68 ± 0.08	0.67 ± 0.12	0.73 ± 0.11

Table IV-2. Concentrations (nM, mean ± SEM) of individual acylcarnitine species in plasma of obese mares (n=7) before (OB) and after 6 weeks of L-carnitine oral supplementation (OBLC); [ab] Superscripts within the same row indicate difference at $p < 0.05$. [cd] Superscripts within the same row indicate tendency at $p = 0.08$.

Short-chain acylcarnitines	OB	OBLC
Acetyl (C2)	12.13 ± 1.34[a]	27.46 ± 2.76[b]
Propionyl (C3)	0.76 ± 0.09[a]	2.54 ± 0.28[b]
Succinyl (C4-DC)	18.99 ± 3.83	12.68 ± 1.47
Hydroxybutyryl (C4-OH)	0.39 ± 0.15	0.90 ± 0.24
Butanoyl (C4)	1.38 ± 0.27	2.29 ± 0.46
Hydroxyisovaleryl (C5-OH)	0.08 ± 0.02	0.12 ± 0.01
Isovaleryl (C5)	0.24 ± 0.04[a]	0.59 ± 0.04[b]
Medium-chain acylcarnitines		
Adipyl (C6-DC)	0.56 ± 0.09[a]	0.42 ± 0.07[b]
Hexanoyl (C6)	0.04 ± 0.01	0.05 ± 0.01
Decanoyl (C10)	0.05 ± 0.01	0.04 ± 0.01
Dodecanoyl (C12)	0.05 ± 0.01	0.04 ± 0.003
Long-chain acylcarnitines		
Tetradecenoyl (C14:1)	0.10 ± 0.01	0.08 ± 0.01
Tetradecanoyl (C14)	0.06 ± 0.01	0.05 ± 0.01
Hexadecenoyl (C16:1)	0.14 ± 0.03[a]	0.08 ± 0.02[b]
Palmitoyl (C16)	0.42 ± 0.09	0.31 ± 0.02
Linoleoyl (C18:2)	0.11 ± 0.01[a]	0.07 ± 0.01[b]
Octadecenoyl (C18:1)	0.67 ± 0.12[c]	0.41 ± 0.03[d]

Figures

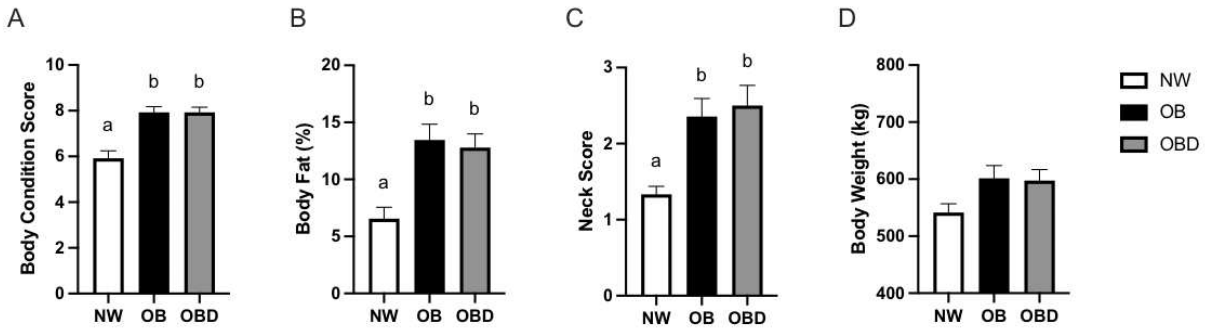

Figure IV-1. Morphometric and metabolic classification of mares. Morphometric measurements from normal-weight (NW), obese (OB) and obese diet supplemented (OBD) mares performed at week 12 of diet prior to sampling for (**a)** body condition score, (**b**) percentage of body fat calculated using a tailhead fat measurement (**c**), cresty neck score, (**d**) and body weight; [ab] superscripts indicate differences at $p < 0.05$. Bars represent mean ± SEM.

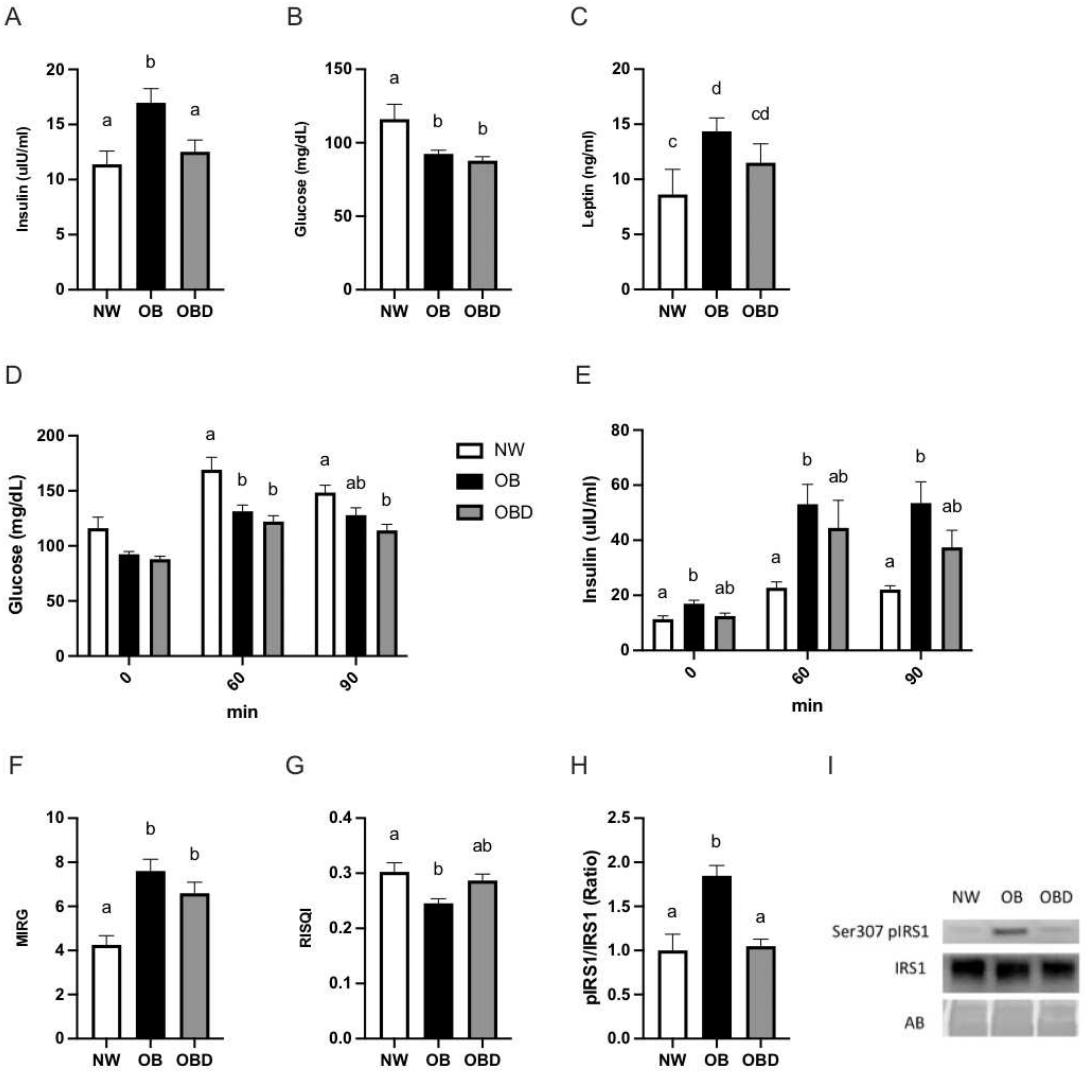

Figure IV-2: Metabolic hormone signaling and circulating metabolites. At 12 weeks of diet supplementation, normal-weight (NW), obese (OB) and obese diet supplemented (OBD) mares were fasted overnight before blood collection and analysis of basal concentrations of (**a**) insulin, (**b**) glucose, and (**c**) leptin; **(d-e)** glucose and insulin concentrations response within group after oral administration light corn syrup for an oral sugar test at 0 (basal), 60 and 90 min; Proxies, including (**f**) modified insulin to glucose ratio (MIRG) and (**g**) reciprocal of the square root of insulin (RISQI), used to quantify pancreatic response to glucose and insulin sensitivity, respectively; (**h**) ratio of phosphorylated IRS-1 to total IRS-1 in skeletal muscle; (**i**) Representative western blot for phosphorylation of IRS-1 to total IRS-1; ^{ab} Superscripts indicate differences at $p < 0.05$. ^{cd} Superscripts indicate differences at $p = 0.08$. Bars represent mean ± SEM.

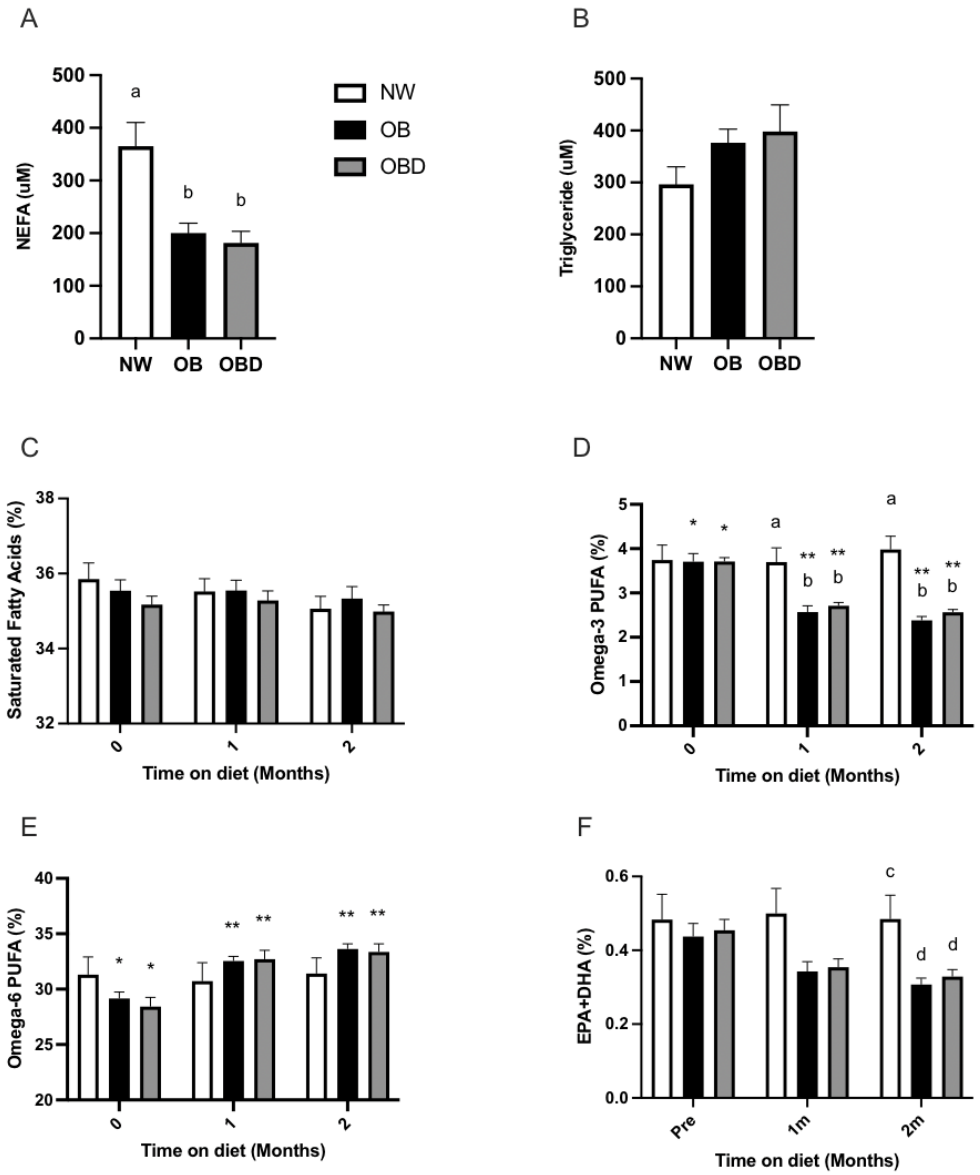

Figure IV-3: Fatty acid uptake and integration. Samples were collected after 12 weeks on diets for mares grouped into normal-weight (NW), obese (OB) and obese diet supplemented (OBD) after overnight fasting. Circulating (**a**) non-esterified fatty acids (NEFA) and (**b**) triglycerides were measured in plasma; Percentages of (**c**) saturated fatty acids, (**d**) omega-3 polyunsaturated fatty acids (PUFA), **(e)** omega-6 PUFA, and **(f)** EPA+DHA to total fatty acids were measured in red blood cell membranes. ^{ab} Superscripts indicate differences at $p < 0.05$ within time point. ^{cd} Superscripts indicate tendency at $p < 0.09$ within time points. *,** Asterisks indicate differences at $p < 0.05$ among months within individual groups. Bars represent mean ± SEM.

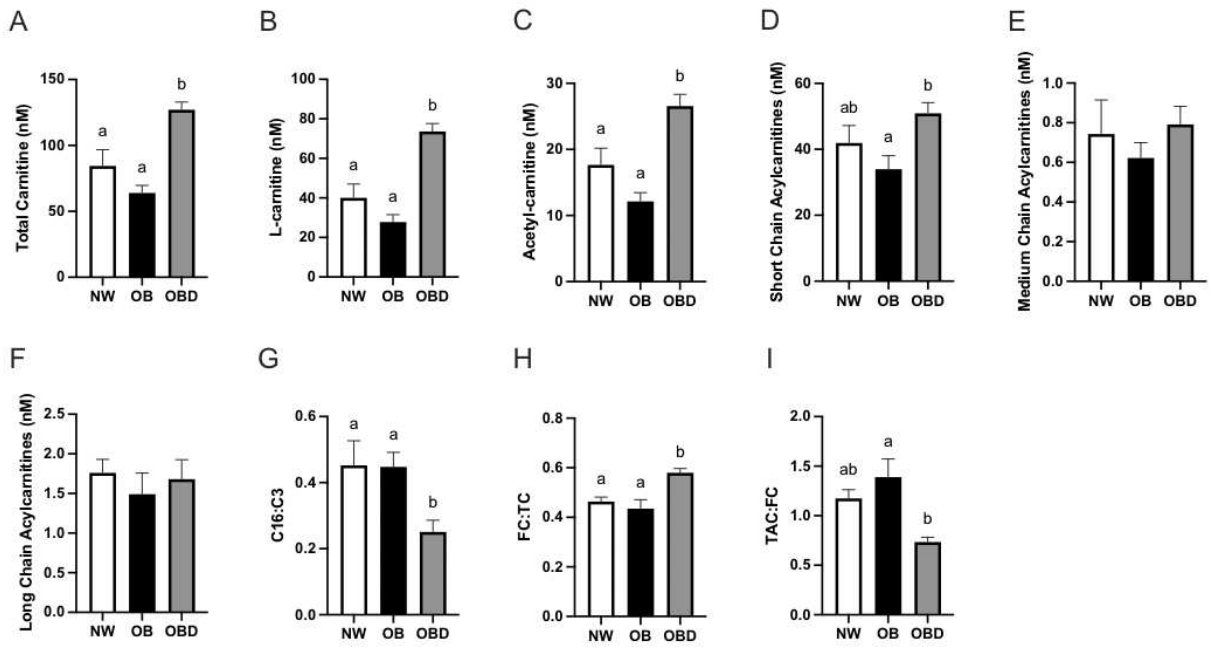

Figure IV-4: Acylcarnitine profiles. Serum acylcarnitine profiles were assessed 12 weeks after mares were placed on diets to maintain normal body weight (NW), obesity (OB) or obese diet supplemented (OBD). Serum samples were incubated and processed with an internal standard of known concentrations of acylcarnitines and analyzed using liquid chromatography mass spectrometry to determine concentrations of (**a**) total carnitine, (**b**) L-carnitine, (**c**) total acetyl carnitines, (**d**) short chain acylcarnitines, (**e**) medium chain acylcarnitines, and (**f**) long chain acylcarnitines; ratio of (**g**) C16:C3 which approximates completeness of β-oxidation, with lower values representing increased lipid metabolism efficiency; and ratios of (**h**) free carnitine to total carnitines (FC:TC) or (**i**) or total acetyl carnitines to free carnitine (TAC:FC) which represent carnitine availability. [ab] Superscripts indicate differences at $p < 0.05$. Bars represent mean ± SEM.

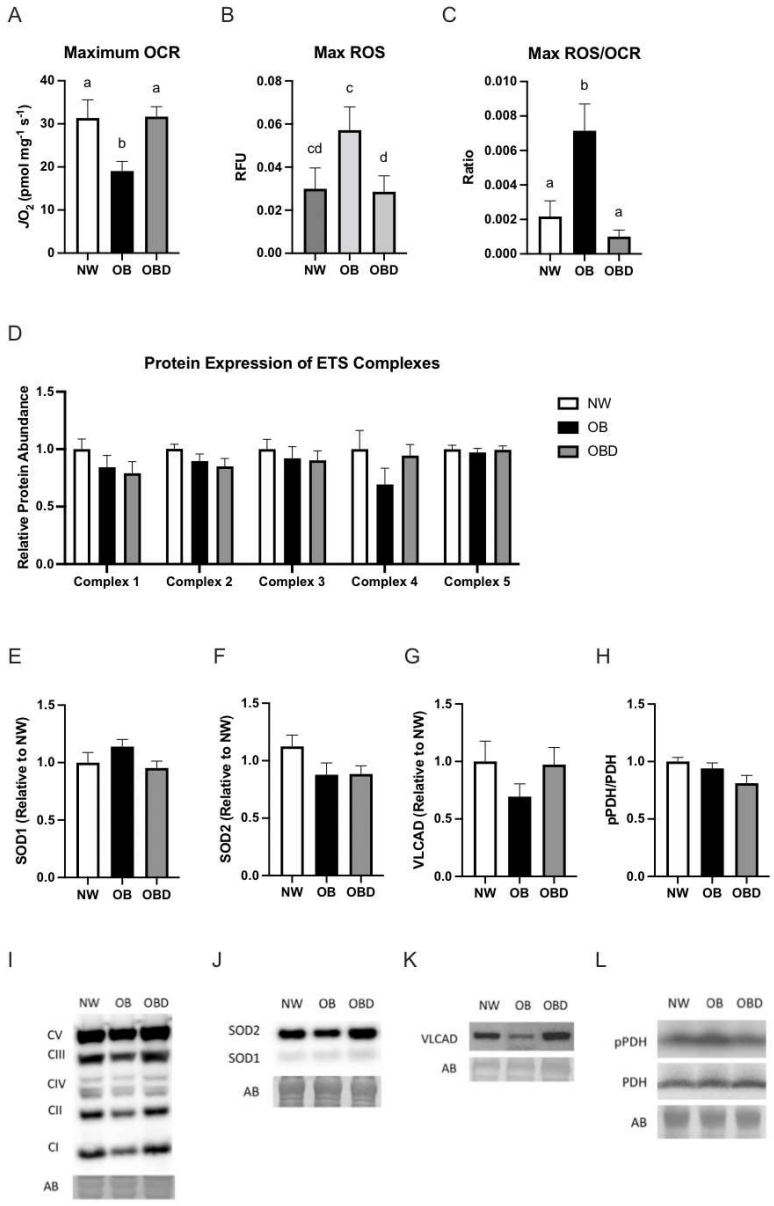

Figure IV-5: Skeletal muscle mitochondrial function. High-resolution respirometry and immunoblotting for selected protein expression was performed in skeletal muscle tissue collected 12 weeks after normal weight (NW), obese (OB) or obese diet supplemented (OBD). Skeletal muscle was obtained by biopsy of the semitendinosus muscle before being permeabilized and analyzed using an Oroboros O2K high-resolution respirometer for (**a**) mitochondrial oxidative capacity in the presence of metabolic substrates, (**b**) reactive oxygen species production, and (**c**) reactive oxygen species production relative to oxidative capacity. Muscle was used for immunoblotting of (**d**) electron transport system complexes I-V, (**e**, **f**) superoxide dismutase isoforms, (**g**) very long chain acyl-CoA dehydrogenase, and (**h**) phosphorylation of pyruvate dehydrogenase relative to NW. Representative western blots for (**i**) electron transport system complexes, (**j**) superoxide dismutase isoforms, (**k**) very long chain acyl-CoA dehydrogenase, and (**l**) phosphorylation of pyruvate dehydrogenase; [ab] Superscripts indicate differences at $p < 0.05$. Bars represent mean ± SEM.

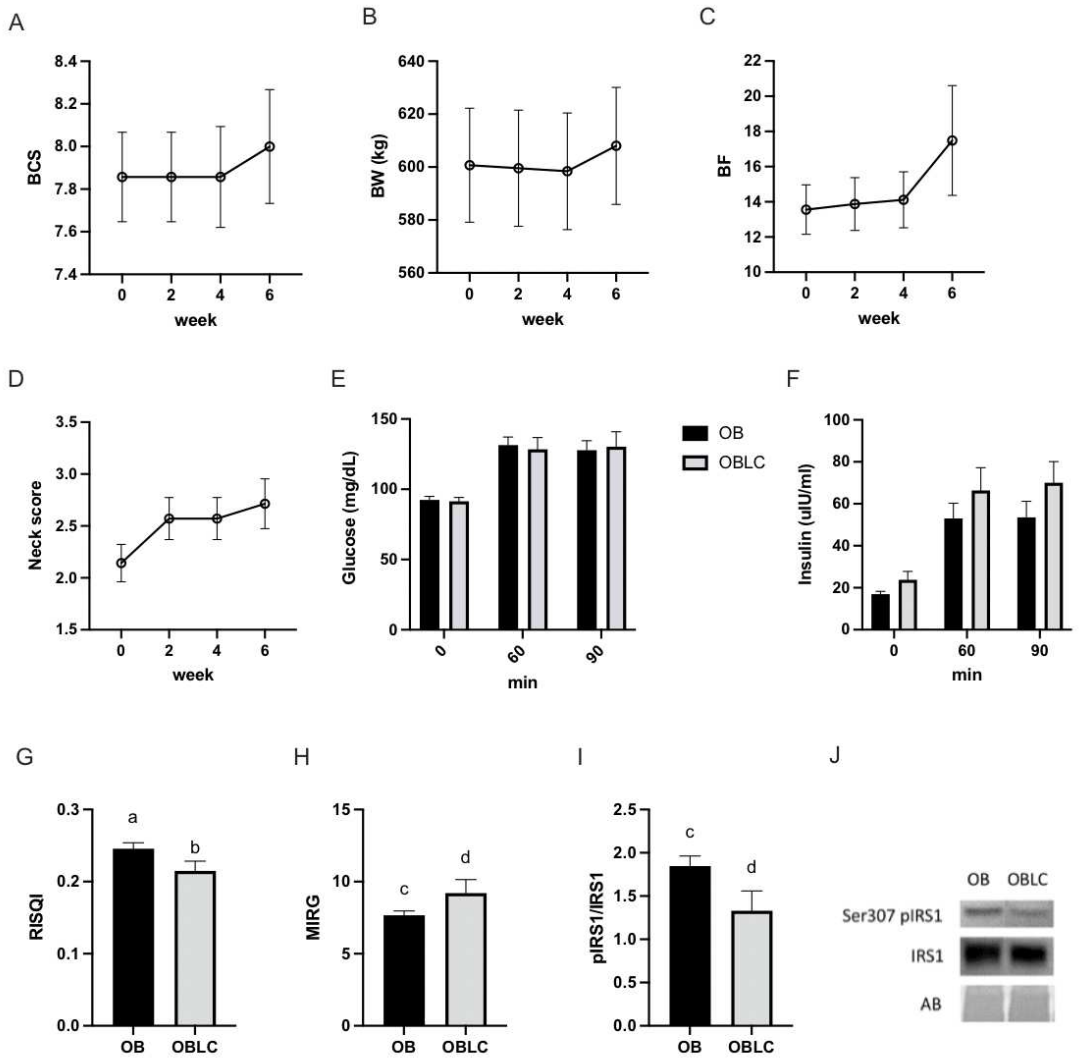

Figure IV-6: Morphometric and metabolic classification of mares during L-carnitine supplementation. Morphometric measurements and assessments of insulin dysfunction were taken at 2-week intervals before and during L-carnitine supplementation to obese mares including (**a**) body condition score (BCS), (**b**) body weight (BW), (**c**) percentage of body fat (BF) calculated using a tailhead fat measurement, (**d**) and cresty neck score (NS). Glucose (**e**) and insulin (**f**) concentrations response within group after oral administration light corn syrup for an oral sugar test at 0 (basal), 60- and 90-min. Proxies, including (**g**) reciprocal of the square root of insulin (RISQI) and (**h**) modified insulin to glucose ratio (MIRG), used to quantify insulin sensitivity and pancreatic response to glucose, respectively; (**i**) Ratio of phosphorylated IRS-1 to total IRS-1 in skeletal muscle; (**j**) Representative western blot for phosphorylation of IRS-1 to total IRS-1; ^{ab} Superscripts indicate differences at $p < 0.05$. ^{cd} Superscripts indicate differences at $p < 0.1$. Graphs represent mean ± SEM.

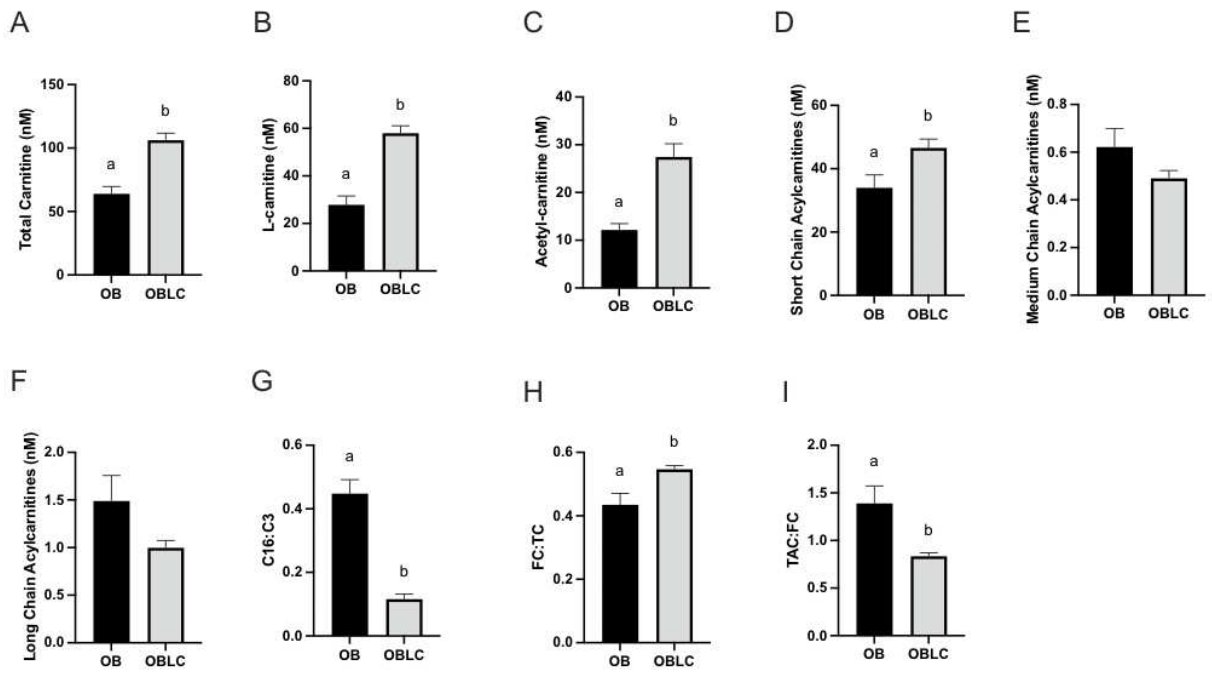

Figure IV-7: Acylcarnitine profile summary following 6 weeks of L-Carnitine. Serum samples were incubated and processed with an internal standard of known concentrations of acylcarnitines and analyzed using liquid chromatography mass spectrometry for obese mares before (OB) and after (OBLC) 6 weeks of L-carnitine supplementation for (**a**) total carnitine, (**b**) L-carnitine, and (**c**) total acetyl carnitines including (**d**) short chain, (**e**) medium chain, and (**f**) long chain. The ratio of (**g**) C16:C3 ratio was used to approximate completeness of β-oxidation as a measure of lipid metabolism efficiency, and ratios of (**h**) free carnitine to total carnitines or (**i**) total acetyl carnitines to free carnitine were used to compare carnitine availability. ^{ab} Superscripts indicate differences at $p < 0.05$. Graphs represent mean ± SEM.

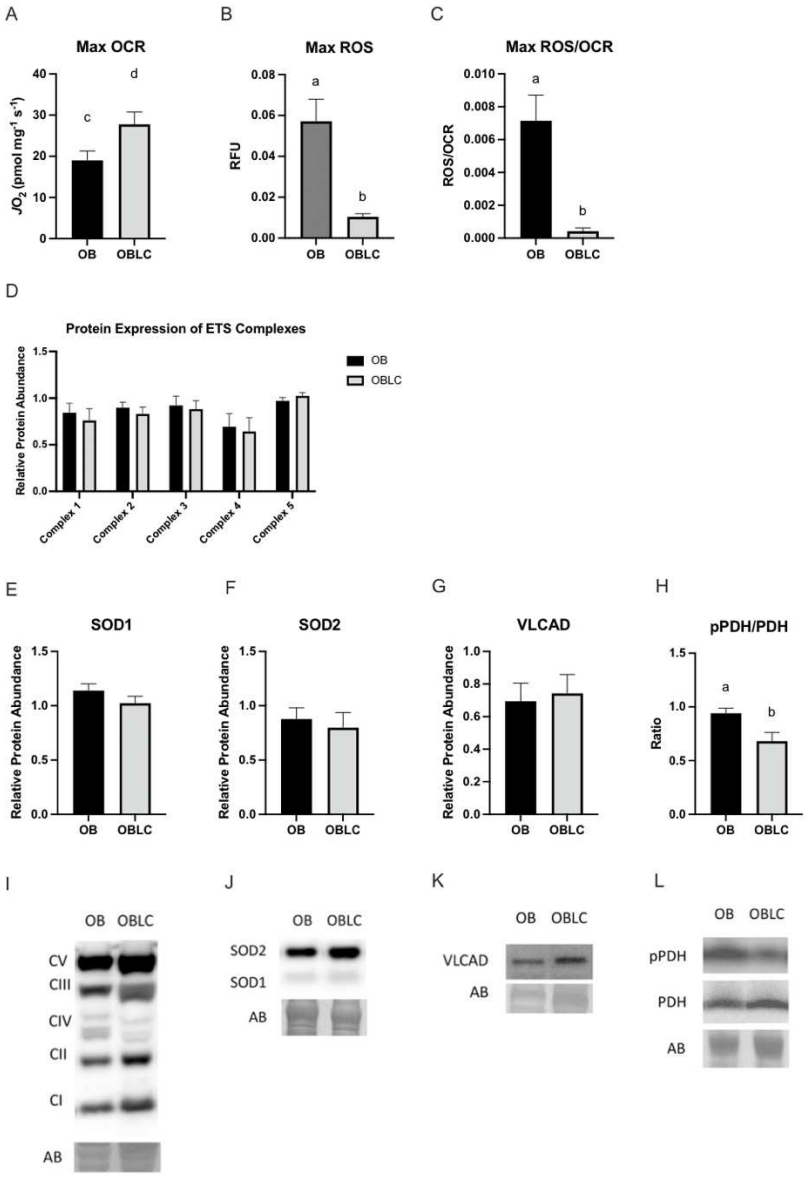

Figure IV-8: Skeletal muscle mitochondrial function. High-resolution respirometry and immunoblotting for selected protein expression was performed in skeletal muscle from obese mares before (OB) and after 6 weeks of dietary L-carnitine (OBLC). Skeletal muscle biopsies were taken from the trapezius muscle and were permeabilized and added to an Oroboros O2K high-resolution respirometer to determine (**a**) mitochondrial oxidative capacity in the presence of metabolic substrates, (**b**) reactive oxygen species production, and (**c**) reactive oxygen species production relative to oxidative capacity. Muscle was used for immunoblotting of (**d**) electron transport system complexes I-V, (**e**, **f**) superoxide dismutase isoforms, (**g**) very long chain acyl-CoA dehydrogenase, and (**h**) phosphorylation of pyruvate dehydrogenase relative to NW. Representative western blots for (**i**) electron transport system complexes, (**j**) superoxide dismutase isoforms, (**k**) very long chain acyl-CoA dehydrogenase, and (**l**) phosphorylation of pyruvate dehydrogenase. ^{ab} Superscripts indicate differences at $p < 0.05$. ^{cd} Superscripts indicate differences at $p < 0.1$. Graphs represent mean ± SEM.

References

1. Giles, S. L., Rands, S. A., Nicol, C. J. & Harris, P. A. Obesity prevalence and associated risk factors in outdoor living domestic horses and ponies. *PeerJ* **2**, e299 (2014).
2. Kosolofski, H. R., Gow, S. P. & Robinson, K. A. Prevalence of obesity in the equine population of Saskatoon and surrounding area. *Canadian Veterinary Journal* **58**,.
3. Ertelt, A., Barton, A.-K., Schmitz, R. R. & Gehlen, H. Metabolic syndrome: is equine disease comparable to what we know in humans? *Endocrine Connections* **3**, R81–R93 (2014).
4. Rendle, D. *et al.* Equine obesity: current perspectives. *UK-Vet Equine* **2**, 1–19 (2018).
5. Johnson, P. J., Wiedmeyer, C. E., LaCarrubba, A., Ganjam, V. K. S. & Messer, N. T. Diabetes, Insulin Resistance, and Metabolic Syndrome in Horses. *J Diabetes Sci Technol* **6**, 534–540 (2012).
6. Morgan, R. A., Keen, J. A., Walker, B. R. & Hadoke, P. W. F. Vascular Dysfunction in Horses with Endocrinopathic Laminitis. *PLoS ONE* **11**, e0163815 (2016).
7. National Health Statistics Reports, Number 158, June 14, 2021. (2021).
8. Rashid, M. N., Fuentes, F., Touchon, R. C. & Wehner, P. S. Obesity and the Risk for Cardiovascular Disease. *Preventive Cardiology* **6**, 42–47 (2003).
9. Wondmkun, Y. T. Obesity, Insulin Resistance, and Type 2 Diabetes: Associations and Therapeutic Implications. *DMSO* **Volume 13**, 3611–3616 (2020).
10. Aronow, W. S. Association of obesity with hypertension. *Ann. Transl. Med.* **5**, 350–350 (2017).
11. Kottaisamy, C. P. D., Raj, D. S., Prasanth Kumar, V. & Sankaran, U. Experimental animal models for diabetes and its related complications—a review. *Lab Anim Res* **37**, 23 (2021).

12. de Mello, A. H., Costa, A. B., Engel, J. D. G. & Rezin, G. T. Mitochondrial dysfunction in obesity. *Life Sciences* **192**, 26–32 (2018).

13. Schrauwen, P., Schrauwen-Hinderling, V., Hoeks, J. & Hesselink, M. K. C. Mitochondrial dysfunction and lipotoxicity. *Biochimica et Biophysica Acta (BBA) - Molecular and Cell Biology of Lipids* **1801**, 266–271 (2010).

14. Siard-Altman, M. H. *et al.* Relationships of inflamm-aging with circulating nutrient levels, body composition, age, and pituitary pars intermedia dysfunction in a senior horse population. *Veterinary Immunology and Immunopathology* **221**, 110013 (2020).

15. Sessions-Bresnahan, D. R., Heuberger, A. L. & Carnevale, E. M. Obesity in mares promotes uterine inflammation and alters embryo lipid fingerprints and homeostasis. *Biology of Reproduction* **99**, 761–772 (2018).

16. Li, M. *et al.* Trends in insulin resistance: insights into mechanisms and therapeutic strategy. *Signal Transduction and Targeted Therapy* **7**, (2022).

17. Stewart-Hunt, L., Pratt-Phillips, S., McCUTCHEON, L. J. & Geor, R. J. Dietary energy source and physical conditioning affect insulin sensitivity and skeletal muscle glucose metabolism in horses: Diet, insulin sensitivity and muscle glucose metabolism in horses. *Equine Veterinary Journal* **42**, 355–360 (2010).

18. Kayar, S. R., Hoppeler, H., Mermod, L. & Weibel, E. R. Mitochondrial size and shape in equine skeletal muscle: A three-dimensional reconstruction study. *Anat. Rec.* **222**, 333–339 (1988).

19. Kearns, C. F., McKeever, K. H. & Abe, T. Overview of Horse Body Composition and Muscle Architecture: Implications for Performance. *The Veterinary Journal* **164**, 224–234 (2002).

20. Tyrovolas, S. *et al.* Factors associated with skeletal muscle mass, sarcopenia, and sarcopenic obesity in older adults: a multi-continent study: Sarcopena and sarcopenic obesity in older adults. *Journal of Cachexia, Sarcopenia and Muscle* **7**, 312–321 (2016).
21. Yaribeygi, H., Farrokhi, F. R., Butler, A. E. & Sahebkar, A. Insulin resistance: Review of the underlying molecular mechanisms. *Journal Cellular Physiology* **234**, 8152–8161 (2019).
22. Waller, A. P., Burns, T. A., Mudge, M. C., Belknap, J. K. & Lacombe, V. A. Insulin Resistance Selectively Alters Cell-Surface Glucose Transporters but not their Total Protein Expression in Equine Skeletal Muscle: Insulin Resistance and Glucose Transport. *Journal of Veterinary Internal Medicine* **25**, 315–321 (2011).
23. Banse, H. E., Frank, N., Kwong, G. P. S. & McFarlane, D. Relationship of oxidative stress in skeletal muscle with obesity and obesity-associated hyperinsulinemia in horses. *Can J Vet Res* **79**, 329–338 (2015).
24. Tangvarasittichai, S. Oxidative stress, insulin resistance, dyslipidemia and type 2 diabetes mellitus. *WJD* **6**, 456 (2015).
25. Morgan, R. A., Keen, J. A. & McGowan, C. M. Treatment of equine metabolic syndrome: A clinical case series. *Equine Vet J* **48**, 422–426 (2016).
26. Argo, C. M. C. G. *et al.* Weight loss resistance: A further consideration for the nutritional management of obese Equidae. *Veterinary Journal* **194**, 179–188 (2012).
27. Noland, R. C. *et al.* Carnitine Insufficiency Caused by Aging and Overnutrition Compromises Mitochondrial Performance and Metabolic Control. *Journal of Biological Chemistry* **284**, 22840–22852 (2009).

28. Muoio, D. M. *et al.* Muscle-Specific Deletion of Carnitine Acetyltransferase Compromises Glucose Tolerance and Metabolic Flexibility. *Cell Metabolism* **15**, 764–777 (2012).

29. Vincent, J. B. New Evidence against Chromium as an Essential Trace Element. *J. Nutr.* **147**, 2212–2219 (2017).

30. Jamilian, M. *et al.* The Influences of Chromium Supplementation on Glycemic Control, Markers of Cardio-Metabolic Risk, and Oxidative Stress in Infertile Polycystic ovary Syndrome Women Candidate for In vitro Fertilization: a Randomized, Double-Blind, Placebo-Controlled Trial. *Biol Trace Elem Res* **185**, 48–55 (2018).

31. Adeva-Andany, M. M., Calvo-Castro, I., Fernández-Fernández, C., Donapetry-García, C. & Pedre-Piñeiro, A. M. Significance of L-Carnitine for Human Health. *IUBMB Life* **69**, 578–594 (2017).

32. Surai, P. F. Antioxidant Action of Carnitine: Molecular Mechanisms and Practical Applications. (2015).

33. Catandi, G. D. *et al.* Oocyte metabolic function, lipid composition, and developmental potential are altered by diet in older mares. *Reproduction* **163**, 183–198 (2022).

34. Jocelyn, N. A., Harris, P. A. & Menzies-Gow, N. J. Effect of varying the dose of corn syrup on the insulin and glucose response to the oral sugar test. *Equine Vet J* **50**, 836–841 (2018).

35. Frank, N. Laboratory Testing for Endocrine and Metabolic Disorders. in *Interpretation of Equine Laboratory Diagnostics* 401–408 (John Wiley & Sons, Inc., 2017). doi:10.1002/9781118922798.ch60.

36. De Laat, M. A., McGree, J. M. & Sillence, M. N. Equine hyperinsulinemia: investigation of the enteroinsular axis during insulin dysregulation. *American Journal of Physiology-Endocrinology and Metabolism* **310**, E61–E72 (2016).

37. Abel, E. D., O'Shea, K. M. & Ramasamy, R. Insulin Resistance: Metabolic Mechanisms and Consequences in the Heart. *Arterioscler Thromb Vasc Biol.* **32**, 2068–2076 (2012).

38. Thomas, D. D., Corkey, B. E., Istfan, N. W. & Apovian, C. M. Hyperinsulinemia: An Early Indicator of Metabolic Dysfunction. *Journal of the Endocrine Society* **3**, 1727–1747 (2019).

39. Merz, K. E. & Thurmond, D. C. Role of Skeletal Muscle in Insulin Resistance and Glucose Uptake. in *Comprehensive Physiology* (ed. Terjung, R.) 785–809 (Wiley, 2020). doi:10.1002/cphy.c190029.

40. Zhao, R., Jiang, S., Zhang, L. & Yu, Z. Mitochondrial electron transport chain, ROS generation and uncoupling (Review). *Int J Mol Med* (2019) doi:10.3892/ijmm.2019.4188.

41. Yu, X. & Long, Y. C. Crosstalk between cystine and glutathione is critical for the regulation of amino acid signaling pathways and ferroptosis. *Scientific Reports* **6**, 30033 (2016).

42. Ribas, V., García-Ruiz, C. & Fernández-Checa, J. C. Glutathione and mitochondria. *Frontiers in Pharmacology* **5**, (2014).

43. Henry, M. L. *et al.* The impact of n-acetyl cysteine and coenzyme q10 supplementation on skeletal muscle antioxidants and proteome in fit thoroughbred horses. *Antioxidants* **10**, (2021).

44. Das, M., Sauceda, C. & Webster, N. J. G. Mitochondrial Dysfunction in Obesity and Reproduction. *Endocrinology* **162**, bqaa158 (2021).

45. Ormazabal, V. *et al.* Association between insulin resistance and the development of cardiovascular disease. *Cardiovasc Diabetol* **17**, 122 (2018).

46. Guerra, I. M. S. *et al.* Mitochondrial Fatty Acid β-Oxidation Disorders: From Disease to Lipidomic Studies—A Critical Review. *International Journal of Molecular Sciences* **23**, (2022).

47. Schlierf, G. & Dorow, E. Diurnal Patterns of Triglycerides, Free Fatty Acids, Blood Sugar, and Insulin during Carbohydrate-Induction in Man and Their Modification by Nocturnal Suppression of Lipolysis. *J. Clin. Invest.* **52**, 732–740 (1973).

48. Tortosa-Caparrós, E., Navas-Carrillo, D., Marín, F. & Orenes-Piñero, E. Anti-inflammatory effects of omega 3 and omega 6 polyunsaturated fatty acids in cardiovascular disease and metabolic syndrome. *Critical Reviews in Food Science and Nutrition* **57**, 3421–3429 (2017).

49. Sinha, S., Haque, M., Lugova, H. & Kumar, S. The Effect of Omega-3 Fatty Acids on Insulin Resistance. *Life* **13**, 1322 (2023).

50. Taouis, M. *et al.* N-3 Polyunsaturated fatty acids prevent the defect of insulin receptor signaling in muscle. *American Journal of Physiology endocrinology and metabolism* **282**, e664–e661 (2002).

51. Bamford, N. J. Clinical insights: Treatment of laminitis. *Equine Vet J* **51**, 145–146 (2019).

52. Respondek, F., Myers, K., Smith, T. L., Wagner, A. & Geor, R. J. Dietary supplementation with short-chain fructo-oligosaccharides improves insulin sensitivity in obese horses. *Journal of Animal Science* **89**, 77–83 (2011).

53. McGowan, C. M., Dugdale, A. H., Pinchbeck, G. L. & Argo, C. M. G. Dietary restriction in combination with a nutraceutical supplement for the management of equine metabolic syndrome in horses. *Veterinary Journal* **196**, 153–159 (2013).

54. Manfredi, J. M., Stapley, E. D., Nadeau, J. A. & Nash, D. Investigation of the Effects of a Dietary Supplement on Insulin and Adipokine Concentrations in Equine Metabolic Syndrome/Insulin Dysregulation. *Journal of Equine Veterinary Science* **88**, (2020).

55. Indiveri, C. *et al.* The mitochondrial carnitine/acylcarnitine carrier: Function, structure and physiopathology. *Molecular Aspects of Medicine* **32**, 223–233 (2011).

56. Virmani, M. A. & Cirulli, M. The Role of L-Carnitine in Mitochondria, Prevention of Metabolic Inflexibility and Disease Initiation. *International Journal of Molecular Sciences* **23**, (2022).

57. Sangouni, A. A. *et al.* The effect of l-carnitine supplementation on insulin resistance, sex hormone-binding globulin and lipid profile in overweight/obese women with polycystic ovary syndrome: a randomized clinical trial. *European Journal of Nutrition* **61**, 1199–1207 (2022).

58. Xu, Y. *et al.* L-carnitine treatment of insulin resistance: A systematic review and meta-analysis. *Advances in Clinical and Experimental Medicine* **26**, 333–338 (2017).

59. Kranenburg, L. C. *et al.* The effect of long-term oral L-carnitine administration on insulin sensitivity, glucose disposal, plasma concentrations of leptin and acylcarnitines, and urinary acylcarnitine excretion in warmblood horses. *Veterinary Quarterly* **34**, 85–91 (2014).

60. Abdali, D., Samson, S. E. & Grover, A. K. How effective are antioxidant supplements in obesity and diabetes? *Medical Principles and Practice* **24**, 201–215 (2015).

61. Formoso, G. *et al.* Inositol and antioxidant supplementation: Safety and efficacy in pregnancy. *Diabetes/Metabolism Research and Reviews* **35**, (2019).

62. Gülçin, I. Antioxidant and antiradical activities of L-carnitine. *Life Sciences* **78**, 803–811 (2006).

63. Ribas, G. S., Vargas, C. R. & Wajner, M. L-carnitine supplementation as a potential antioxidant therapy for inherited neurometabolic disorders. *Gene* **533**, 469–476 (2014).

64. Patel, M. S. & Korotchkina, L. G. *Regulation of Mammalian Pyruvate Dehydrogenase Complex by Phosphorylation: Complexity of Multiple Phosphorylation Sites and Kinases*. *EXPERIMENTAL and MOLECULAR MEDICINE* vol. 33 191–197 (2001).

65. HENNEKE, D. R., POTTER, G. D., KREIDER, J. L. & YEATES, B. F. Relationship between condition score, physical measurements and body fat percentage in mares. *Equine Veterinary Journal* **15**, 371–372 (1983).

66. Carter, R. A., Geor, R. J., Burton Staniar, W., Cubitt, T. A. & Harris, P. A. Apparent adiposity assessed by standardised scoring systems and morphometric measurements in horses and ponies. *The Veterinary Journal* **179**, 204–210 (2009).

67. Gentry, L. R. *et al.* The relationship between body condition score and ultrasonic fat measurements in mares of high versus low body condition. *Journal of Equine Veterinary Science* **24**, 198–203 (2004).

68. Kane RA, Fisher M, Parrett D & Lawrence LM. *[Proceedings of the] 10th Equine Nutrition and Physiology Symposium, June 11-13, 1987, the Fort Collins Marriott, Colorado State University.* (Equine Nutrition and Physiology Society, 1987).

69. Treiber, K. H., Kronfeld, D. S., Hess, T. M., Boston, R. C. & Harris, P. A. Use of proxies and reference quintiles obtained from minimal model analysis for determination of insulin sensitivity and pancreatic beta-cell responsiveness in horses. *American Journal of Veterinary Research* **66**, 2114–2121 (2005).

70. Harris, W. S., Pottala, J. V., Vasan, R. S., Larson, M. G. & Robins, S. J. Changes in Erythrocyte Membrane Trans and Marine Fatty Acids between 1999 and 2006 in Older Americans. *The Journal of Nutrition* **142**, 1297–1303 (2012).

71. *High-Throughput Metabolomics: Methods and Protocols*. vol. 1978 (Springer New York, New York, NY, 2019).

72. Li Puma, L. C. *et al.* Experimental oxygen concentration influences rates of mitochondrial hydrogen peroxide release from cardiac and skeletal muscle preparations. *American Journal of Physiology-Regulatory, Integrative and Comparative Physiology* **318**, R972–R980 (2020).

73. Pesta, D. & Gnaiger, E. High-Resolution Respirometry: OXPHOS Protocols for Human Cells and Permeabilized Fibers from Small Biopsies of Human Muscle. *Methods in molecular biology (Clifton, N.J.)* **810**, 25–58 (2011).

74. Chicco, A. J. *et al.* Adaptive remodeling of skeletal muscle energy metabolism in high-altitude hypoxia: Lessons from AltitudeOmics. *Journal of Biological Chemistry* **293**, 6659–6671 (2018).

75. Dieckmann-Schuppert, A. & Schnittler, H.-J. A simple assay for quantification of protein in tissue sections, cell cultures, and cell homogenates, and of protein immobilized on solid surfaces. *Cell and Tissue Research* **288**, 119–126 (1997).

APPENDIX V

IMPACT OF DIETARY ESSENTIAL FATTY ACIDS ON BLOOD, MUSCLE, AND FOLLICULAR CELL PHOSPHOLIPID COMPOSITION AND MITOCHONDRIAL FUNCTION IN AGED MARES

Abstract

Advancing age is associated with a decline in fertility and functional capacity, which may result in part from suboptimal nutrition and impaired mitochondrial function. Dietary essential polyunsaturated fatty acids (PUFA) are broadly recommended to mitigate weight loss and reduce risk of chronic disease in aged populations, but their effects on mitochondrial function are less clear. The present study investigated the impacts of dietary supplementation with essential omega-3 PUFA (flaxseed oil; N3) or omega-6 PUFA (corn oil, N6) on blood, muscle and follicular cell fatty acid composition and mitochondrial function in aged light-horse mares (23.2 ± 1.1 yr), which are excellent models of human reproductive aging and a focus of dietary interventions in the equine industry. Diets were fed for 6 weeks before adding a supplemental supportive nutrient formulation (DS) designed to optimize equine metabolic health for another 6 weeks. Results demonstrate tissue-specific effects of the dietary oils on mitochondrial function, most notably a decrease in oxidative capacity of platelets and muscle, and greater release of

---

[5]Appendix V has been submitted to *Scientific Reports*. Authors: Kyle J. Fresa, Giovana Catandi, Raul A. Gonzalez-Castro, Asma Omar, Luke Whitcomb, Elaine M. Carnevale, Adam J. Chicco. Funding was provided through the Cecil and Irene Hylton Foundation, American Association of Equine Practitioner Foundation for the Horse research grant (Catandi), and Abney Foundation Scholarship (Catandi, Fresa). Diet nutritional supplement formulas were provided by Platinum Performance, Inc., Buellton, CA.

reactive oxygen species (ROS) from granulosa cells and muscle, with no significant difference in effects between N3 and N6 diets. Addition of the DS improved oxidative phosphorylation efficiency and tended to reduce ROS release across all cell types, and increased basal oocyte oxygen consumption. Taken together, these results provide novel insight to the diverse impacts of dietary PUFA intake on equine mitochondrial function, and suggest that supportive nutrients may be required to prevent negative health effects of dietary oil supplementation in aged mares.

Introduction

Mammalian aging is associated with a gradual decline in body condition that negatively impacts physical capacity, fertility, and quality of life. Malnutrition and weight loss can accelerate these deleterious effects, particularly in species with high physiological demands.[1,2] Equine aging is associated with decrements in skeletal muscle and reproductive function that are similar to those observed in humans, and older horses (>15 years of age) are now estimated to comprise up to one-third of the global equine population.[3–5] Horses may also suffer from sub-optimal nutrition and under-recognized signs of age-related decline, particularly when compounded by poor dental health and gastrointestinal problems.[4] As in humans, dietary supplementation with vegetable oils is commonly recommended for older horses to prevent weight loss, as they are calorie dense and easy to digest.[6,7] The majority of commercially available dietary oils are derived from corn, soybeans, or flax seeds containing predominantly polyunsaturated fatty acids (PUFAs), which are generally recommended over saturated fats for optimal health benefits based largely on human data.[8] However, the biological impacts of dietary PUFA supplementation in horses are less clear, particularly in the setting of advanced age.

Dietary PUFAs are further classified as omega-3 (*n*-3) or omega-6 (*n*-6) fatty acids based on the position of their first double bond counting from the terminal methyl group.[9] Both classes are metabolized by the same desaturase, elongase and oxygenase enzymes to generate distinct long-chain PUFA derivatives with diverse and often opposing biological functions. In the equine industry, dietary oils containing predominantly *n*-6 linoleic acid (LA) extracted from corn and soybeans are most frequently used because they are easily accessible and affordable.[10] This parallels a much greater intake of *n*-6 compared to *n*-3 PUFA in the modern human diet, which is in contrast to the more balanced intake of *n*-6 LA and *n*-3 α-linolenic acid (ALA) in the ancestral diets of humans and equids.[11,12] A greater proportion of dietary *n*-6 PUFA intake has been hypothesized to favor greater inflammatory signaling and increased risk of age-related diseases in humans,[13] prompting recommendations for dietary supplementation with *n*-3 PUFA given their putative anti-inflammatory effects and diverse health benefits.[14] However, the biological impacts of *n*-3 and *n*-6 PUFA are diverse and vary widely across species, physiological systems and disease risk profiles, leading to ongoing debate over their optimal ratio in the diet and its relevance to long-term health outcomes.[15,16]

Age-related decrements in physical performance and fertility have been associated with reduced mitochondrial capacity in skeletal muscle and follicular cells of horses,[17–19] and humans.[20,21] Recently, we found that supplementing the diets of aged mares with *n*-3 PUFA in combination with a proprietary blend of antioxidants, L-carnitine and other supportive nutrients for 8 weeks improved oocyte metabolic capacity, granulosa cell mitochondrial function, and fertility outcomes.[22] However, the independent effects of dietary PUFA (in the absence of supportive supplements) were not investigated, nor whether the impacts of these dietary interventions extended to other tissues and cell types. Consequently, the aim of the present study

was to broadly characterize the effects of dietary *n*-3 and *n*-6 PUFA supplementation on platelet, skeletal muscle and follicular mitochondrial function in aged mares in the presence and absence of supportive dietary nutrients. Impacts on the fatty acid composition of serum, follicular fluid, muscle and granulosa cell phospholipids was also investigated, along with markers of inflammation and skeletal muscle oxidative stress.[23]

Materials and Methods

Animals and experimental design.

All procedures and experimental protocols on live animals were approved by the Institutional Animal Care and Use Committee at Colorado State University and are reported in accordance with ARRIVE guidelines. Cyclic, non-lactating light-horse mares (n=12, 19-27 years of age) were housed in adjacent dry lots with sheds, salt blocks, and water provided *ad libitum*. All animals were fed a base diet of grass/alfalfa mix hay at approximately 2% body weight daily with 57 g of a commercial vitamin and mineral forage balancer (Forage Balancer, Purina® Free Balance® 12:12, Purina Animal Nutrition, Gray Summit, MO, USA). After at least 4 weeks on the base diet, baseline measurements and samples were collected as described below, and mares were divided into two age-matched groups randomly assigned to receive dietary PUFA supplementation as 60 mL of flaxseed oil (N3; 57% ALA, 17% LA; n= 6, 22.5 ± 1.2 yr) or corn oil (N6; 59% LA, <1% ALA; n=6, 23.2 ± 1.1 yr) mixed in 227 g of alfalfa pellets once daily in the morning for the duration of the study. Oils were fortified with antioxidants (d-alpha tocopherol acetate and ascorbyl palmitate) and stored at room temperature and away from direct heat or sunlight to prevent auto-oxidation and preserve shelf life.[24] Following 6 weeks of the N3 or N6 diets, samples were collected to evaluate the independent impacts of dietary PUFA

enrichment on the outcomes described below, and all mares began receiving additional dietary supplementation (DS) designed to support equine metabolic and gastrointestinal health and formulated to support cellular metabolism, including vitamins, trace minerals, amino acids, L-carnitine, antioxidants, prebiotics, and probiotics (187 g daily; Platinum Performance Inc., Buellton, CA). Samples were collected again following 6 weeks on N3 or N6 diets with the additional DS for final measurement of the outcomes described below. Morphometric assessments were performed at 2-week intervals and included BCS (1-9)[25] and cresty neck score (0-5)[26].

Sample Collections.

Blood, ovarian follicle contents, and skeletal muscle biopsies were collected at baseline and following each of the dietary supplementation periods described above. All methods were carried out in accordance with relevant guidelines and regulations. Blood was collected by jugular venipuncture and centrifuged at 3500 x *g* for isolation of serum. Serum was frozen at -80°C for future biochemical analyses. Isolation of platelets was conducted according to Abcam protocol (Abcam, Cambridge, UK).[27] Briefly, blood was collected into 60mL syringes containing 10% citrate-phosphate-dextrose buffer. Samples were transferred into tubes and centrifuged at 200 x *g* for 20 min to obtain platelet-rich plasma (PRP). PRP was removed from the tubes, diluted 1:1 with HEPES-buffered solution containing 1μM prostaglandin I2 (Sigma-Aldrich, St. Louis, MO), and centrifuged at 100 x *g* for 20 min to remove blood cells. The supernatant was removed, centrifuged at 800 x *g* for 10 min, and the resulting platelets were resuspended in Tyrode's buffer containing 5 mM glucose, 3 mg/mL bovine serum albumin, and 1 μM

prostaglandin I2. Platelets were maintained on ice until preparation for respirometry experiments.

Histrelin (0.5 mg IM; Doc Lane, Lexington, KY) was administered to induce follicle and oocyte maturation *in vivo* when the dominant follicle exceeded 35mm and endometrial edema was revealed by ultrasonography. Cumulus oocyte complexes, granulosa cells, and follicular fluid were collected by ultrasound-guided follicular aspirations of preovulatory follicles at 20 ±2 h after induction as previously described.[28] Briefly, the follicular wall was punctured, and follicular fluid (5-10 mL) was collected from the center of the follicular antrum, to avoid blood and cell contamination, into a tube. The follicle was then flushed with Flush Medium (Vigro Complete Flush Solution, Vetoquinol, Fort Worth, TX, USA) with 10 USP units/ml heparin (Sagent, Schaumburg, IL) at 38.5°C, and the aspirate was collected in a sterile bottle. Follicular fluid samples were frozen at -80°C for later biochemical analyses. Sheets of granulosa cells were manually collected from the aspirate, washed in Flush Medium, centrifuged at 800 x *g* for 5 min, treated with red blood cell lysis buffer (Roche, Basel, Switzerland) for 1 min, and then suspended in Flush Medium for later respirometry experiments or frozen for biochemical analyses. Cumulus oocyte complexes were identified using a stereomicroscope with a warming plate to maintain approximate body temperature. Sections of cumulus cells were cut using needle tips from the complex, prior to placing the remaining cumulus oocyte complex in hyaluronidase (80 U/ml) for a few minutes prior to pipetting to separate the remaining cumulus cells from the oocyte. Isolated cumulus cells were frozen at -80°C for future biochemical analyses, and denuded oocytes were preserved in MOPS-buffered medium (G-MOPS™; Vitrolife, Gothenburg, Sweden) and maintained at 4°C until metabolic flux analyses described below.

Punch biopsies of the trapezius muscle were immediately rinsed in BIOPS preservation buffer containing (in mM) 10 Ca-EGTA (0.1 M free calcium), 20 imidazole, 20 taurine, 50 K-MES, 0.5 DTT, 6.56 $MgCl_2$, 5.77 ATP, and 15 phosphocreatine (pH 7.1 with KOH). Approximately 100 mg muscle samples were snap frozen in liquid nitrogen for later analyses, while the remaining sample was transferred to fresh BIOPS buffer on ice until preparation for high-resolution respirometry.

Serum Cytokine Immunoassay.

Serum samples were assayed for various cytokines using a bead-based multiplex assay at an external laboratory (Cornell Animal Health and Diagnostic Center, Ithaca, NY). Samples containing equine cytokines were mixed with anti-cytokine beads and incubated, followed by detection using fluorochrome-conjugated antibodies. Cytokine values were calculated based on five standards included in the assay. Methodology is described in detail elsewhere.[29]

Analysis of phospholipid fatty acid composition.

Total phospholipids were extracted from skeletal muscle biopsies, granulosa cells, follicular fluid, and serum for determination of fatty acid composition by gas chromatography essentially as previously described.[30] Briefly, 10 mg of muscle was homogenized in 800 µL of precooled methanol in a glass homogenizer, while 50 µL of freeze-thawed granulosa cell lysates, follicular fluid, or serum were added directly to 600 µL of precooled methanol in a glass tube. After vortexing samples for 30 seconds, tubes were centrifuged at 900 × *g* for 5 min, the supernatant transferred to a fresh glass tube, and 25 µL of methoxide solution was added to synthesize methyl esters from glycerophospholipids. The reaction was stopped after 3 min by

adding 75 µL of methanolic HCl, and fatty acid methyl esters (FAMEs) were extracted by adding 700 µL of hexane, transferring the upper hexane layer to 2 mL chromatography vials. FAMEs were dried under nitrogen flow and resuspended in hexane for gas chromatography (GC) analysis using an Agilent Technologies DB-225 30m x 0.250mm x 0.25µm column (model 122-2232, J&W Scientific) on an Agilent 6890 Series Gas Chromatograph with a flame ionization detector.[30] A fatty acid standard solution of 1 mg/mL was injected into the GC every 6-7 runs to recalibrate the fatty acid peaks on the chromatograph, enabling relative quantitation of up to 18 fatty acids commonly found in mammalian membranes expressed as a percentage of total phospholipid fatty acids.

High-resolution fluo-respirometry.

Rates of cellular respiration and H_2O_2 release were measured in platelets, granulosa cells and skeletal muscle fibers by high-resolution fluo-respirometry using an Oroboros Oxygraph system with an O2k-Fluo LED2-Module (Oroboros Instruments, Innsbruck, Austria) essentially as previously described.[31] Platelets and granulosa cells were freshly isolated as described above and added directly to the oxygraph chamber containing 2 mL of mitochondrial respiration medium (MiR05) composed of (in mM) 0.5 EGTA, 3 $MgCl_2$ hexahydrate, 60 lactobionic acid, 20 taurine, 10 KH_2PO_4, 20 HEPES, 110 sucrose, and 0.1% fatty acid-free bovine serum albumin (pH 7.1 with KOH) at 37°C with room air-saturated oxygen (~160 µM). Following standardized instrumental and chemical background calibrations, the oxygen consumption rate (OCR) of intact platelets and granulosa cells was measured to determine basal rates of cellular oxidative metabolism supported by endogenous substrates. Cells were then permeabilized with 5 µg/mL digitonin to enable free diffusion of exogenous metabolic substrates to mitochondria without

compromising inner membrane integrity.[32] Muscle biopsies were gently teased in BIOPS on ice and permeabilized with 50 μg/mL saponin before being added to the oxygraph chamber as described above, but with ~400 μM oxygen to overcome diffusion limitations of respirometry in permeabilized muscle fibers.[31]

Following permeabilization, 1 mM malate and 0.05 mM palmitoylcarnitine were added to samples in the oxygraph chamber to assess the capacity for non-coupled "LEAK" respiration supported by fatty acid oxidation (facilitated by proton leak across the inner mitochondrial membrane), followed by the addition of 2.5 mM ADP to generate the oxidative phosphorylation (OXPHOS)-linked OCR. The extent of respiratory control by ADP was expressed as the OXPHOS coupling control factor [1-(LEAK/OXPHOS)] for fatty acid oxidation, where a maximum value of 1.0 represents fully coupled mitochondria (100% control of respiration by ADP), and 0 represents fully uncoupled mitochondria (0% respiratory control by ADP). Finally, the maximal OXPHOS-linked OCR was determined by titrating 5 mM pyruvate and 10 mM succinate to the oxygraph chamber to maximize rates of electron supply from carbohydrate and fatty acid oxidation and a fully reconstituted citric acid cycle.[33]

The net rate of mitochondrial H_2O_2 release (JH_2O_2) was measured during basal and maximal OXPHOS-linked OCR states by monitoring the accumulation of chamber resorufin (Ex/Em 571/585 nm), the stable fluorescent product of 1:1 oxidation of 5 μM Amplex UltraRed by H_2O_2 in the presence of 1 U/mL horseradish peroxidase.[31,34] Sample OCR and JH_2O_2 are expressed relative to mg wet weight of muscle fiber bundles and total protein content of platelet or granulosa cells added to the oxygraph chamber determined by bicinchoninic acid (BCA) assay (Thermo Scientific, #23225).

Oocyte metabolic flux analysis.

Basal (non-stimulated) rates of single oocyte oxygen consumption (OCR; reflecting mitochondrial respiration) and extracellular acidification (ECAR; representing glycolytic flux) were measured using a custom-built metabolic micro-sensor as previously described.[35,36] Briefly, denuded oocytes were gradually warmed to 38.5°C before being transferred to the sensor micro-chamber containing 180 µL of G-MOPS maintained at the same temperature. Oocytes were positioned directly over the working electrodes of a pre-calibrated amperometric oxygen sensor and potentiometric pH sensor to obtain stable measurements of OCR and ECAR, respectively.

Protein Immunoblotting.

Frozen muscle samples (~50 mg) were homogenized in lysis buffer containing (in mM) 150 NaCl, 1 EDTA, 1 EGTA, 5 sodium pyrophosphate, 1 sodium orthovanadate, 20 sodium fluoride added to Mammalian Protein Extraction Reagent (Pierce Cat# 78501) with supplemental Protease Inhibitor Cocktail (Sigma Aldrich Cat# P8340). Protein concentrations of 10,000 × *g* homogenate supernatants were detected by BCA assay. Extracted proteins (30 µg) were electrophoresed on 4-12% Bis-Tris gels and transferred to PVDF membranes, then blocked for 1 h at room temperature with 5% non-fat milk before incubating with the following primary antibodies (1:1000 dilution) overnight at 4C°: Cu/ZN SOD (SOD101, StressGen, Victoria, BC), Mn SOD (SOD111, StressGen, Victoria, BC), NOX4 (PA5-72816, Thermo Scientific, Waltham, MA), 4-Hydroxynonenal (MA527570, Thermo Scientific, Waltham, MA), Malondialdehyde (MA527560, Thermo Scientific, Waltham, MA) Secondary antibodies including Goat anti-Rabbit IgG (AB6721, Abcam, Waltham, MA) and Goat anti-Mouse IgG (AB6789, Abcam, Waltham, MA) were used at a 1:3000 dilution for 1 hour at room temperature. Blotted proteins

were imaged using SuperSignal West Dura Extended Duration Substrate (Lot#VL314742) and a UVP ChemStudio blot imager (Analytik Jena, Germany), normalizing band densities to total protein staining of a 80-100 kDa range of bands near the target protein in each lane using AmidoBlack (Sigma A8181), quantified using ImageJ software (NIH).

Statistical Analysis.

Data from all experiments are presented as group means ± SEM. Following confirmation of normal data distributions using the Shapiro-Wilk test, group comparisons were first performed by one-way ANOVA with repeated measures for each PUFA diet group at baseline, 6 weeks post-diet, and following an additional 6 weeks post-diet +DS. Following a significant ANOVA, individual group comparisons were evaluated by paired t-tests for individual group comparisons. Comparisons between diets were performed by 2-way ANOVA with repeated measure to detect variations due to the PUFA diet, +DS intervention or their interaction. A P value of < 0.05 was considered significant for all statistical analyses.

Results

Animal morphometrics and serum cytokines

Impacts of the dietary interventions on animal condition and serum cytokines are summarized in **Table V-1**. There were no significant effects of PUFA supplementation or addition of the dietary supplement (+DS) on animal body weights or body condition scores, the latter remaining within the normal range of 4-6 for healthy mares across all groups and time points.[25] Similarly, cresty Neck Scores[26] averaged within the normal range of 1.5 - 1.7 across groups and time points, with the exception of a significant decrease following 6 weeks on the N3

diet that increased following the addition of the DS. Serum cytokines levels were highly variable across individuals and groups throughout the study, with significant differences being detected only in tumor necrosis factor-alpha (TNF-α), which increased relative to baseline levels following 6 weeks on the N3 diet (P = 0.043) and following 6 weeks of the N6 diet (P = 0.007).

PUFA diets impact serum, muscle, and follicular phospholipid fatty acid composition

The fatty acid composition of phospholipids extracted from serum (**Table V-2**), skeletal muscle (**Table V-3**), follicular fluid (**Table V-4**), and granulosa cells (**Table V-5**) was investigated at baseline (BL), following 6 weeks of PUFA supplementation (6 weeks), and following 6 additional weeks with the supportive dietary supplements (DS). Overall, both PUFA diets tended to increase the total phospholipid PUFA content and decrease monounsaturated fatty acids (MUFA) across all sample types, with variable and comparatively minor effects on total saturated fatty acids. Impacts of the N6 diet on phospholipid PUFA composition were generally more robust than the N3 diet across samples, and effects of both diets tended to be augmented or unaffected by 6 additional weeks of feeding with the DS. Notable exceptions were a suppression of ALA levels in follicular fluid in N3-fed mares following the DS (**Table V-4**), and a marked suppression of *n*-6 arachidonic acid (ARA) with reciprocal increases in long-chain *n*-3 PUFA in granulosa cells of N3-fed mares following addition of the DS (**Table V-5**). When combining the 6 week and +DS data to improve statistical power for detecting main effects of the PUFA diets, the N6 diet significantly increased proportions of LA (P = 0.0008 – 0.04) and total *n*-6 PUFA (P = 0.0007 – 0.019) in all four sampling sites, with trends for reciprocal decreases in ALA and/or total *n*-3 PUFA that only reached statistical significance in serum (P = 0.015 and 0.002, respectively). Conversely, the N3 diet tended to increase proportions of ALA and/or total *n*-3

PUFA across samples, but this only reached statistical significance for total *n*-3 PUFA in granulosa cells ($P = 0.0005$). Collectively, these trends led to a significantly greater *n*-6/*n*-3 PUFA ratio in the N6 versus N3 diet groups ($P < 0.05$) across all sample types (**Figure V-1**). Taken together, these results demonstrate effects of the N6 and N3 diets on mare phospholipid composition that are generally consistent with their fatty acid composition across multiple biological compartments.

Cell type-specific effects of dietary interventions on mitochondrial bioenergetics

Impacts of the dietary interventions on cellular mitochondrial function varied according to the cell type being studied and outcome examined. In platelets, the N6 and N3 diets both tended to decrease basal OCR and fatty acid-supported LEAK and OXPHOS states (**Figures V-2A-C**), and favored an increase in OXPHOS coupling control in N6 ($P = 0.009$) and N3 after the DS ($P = 0.009$) (**Figure V-2D**). Both diets also tended to decrease in maximal OXPHOS-linked OCR, which only reached statistical significance following addition of the DS ($P < 0.05$; **Figure V-2E**). Trends across timepoint and respiratory states were nearly identical between N6 and N3 diet groups, with no significant differences between diets.

In skeletal muscle fiber bundles, both diets similarly decreased fatty acid-supported LEAK (**Figure V-3A;** $P \leq 0.001$) and OXPHOS states (**Figure V-3B;** $P < 0.01$). However, the DS significantly augmented this decline in the LEAK state ($P \leq 0.001$), leading to marked increases in OXPHOS coupling control in the N6 ($P = 0.006$) and N3 ($P = 0.002$) groups (**Figure V-3C**). Maximal OXPHOS-linked OCR was lower following 6 weeks of the N6 diet ($P = 0.033$) and after DS ($P = 0.021$), but was unaffected in the N3 diet group (**Figure V-3D**).

In granulosa cells, the N6 and N3 diets had no significant effects on OCR or OXPHOS coupling control under any substrate condition after 6 weeks of feeding (**Figure V-4A-E**). However, the additional 6 weeks with DS increased fatty acid-supported OCR in N6 ($P = 0.033$) and N3 ($P = 0.027$) groups (**Figures V-4C**), as well as maximal OXPHOS-linked OCR in N6 ($P = 0.039$) and N3 ($P = 0.007$) groups (**Figures V-4E**). Across all cell types examined, there were no significant differences between the N3 and N6 diets for any of the assayed time points.

PUFA diets with dietary supplement increase oocyte oxygen consumption rate

Oocyte metabolism was evaluated by measuring basal oxygen consumption rate (OCR) and extracellular acidification rate (ECAR; a proxy for glycolytic rate) in single denuded oocytes using a novel micro-sensor within hours of follicular aspiration as previously described.[35] OCR was unaffected by 6 weeks of feeding the N6 or N3 diets, but increased significantly following an additional 6 weeks with the dietary supplement in N6 ($P = 0.012$) and N3 ($P = 0.037$) groups (**Figure V-5A**). Oocyte ECAR was not significantly impacted by either PUFA diet or DS (**Figure V-5B**), suggesting an independent effect of the DS to stimulate basal rates of oocyte oxidative metabolism.

PUFA supplements increase ROS release from granulosa cells, but not platelets

Rates of cellular H_2O_2 release were measured under basal conditions in intact cells and during stimulated OXPHOS-linked respiration in permeabilized cells by fluo-respirometry. In platelets, both N6 and N3 diets tended to decrease H_2O_2 release across the three respiratory states examined, but this only reached statistical significance in the N6 + DS group under basal conditions ($P = 0.007$) due to high variability across samples (**Figures V-6A-C**). Conversely,

both N6 and N3 diets tended to increase H_2O_2 release after 6 weeks of supplementation, with trends for attenuation following addition of the DS that did not reach statistical significance (**Figures V-7A-C**).

PUFAs without supportive DS favors greater ROS release from muscle mitochondria

In permeabilized skeletal muscle fiber bundles, 6 weeks of feeding the N6 or N3 supplements alone significantly increased H_2O_2 release during fatty acid-supported OXPHOS (**Figure V-8A;** $P < 0.001$) and maximal OXPHOS (**Figure V-8B**; $P < 0.05$), which significantly decreased to near baseline levels following the addition of the DS to both diets ($P < 0.0001$). Expression of NADPH oxidase (NOX4), a major physiological source of mitochondrial ROS in skeletal muscle,[37] tended to increase following N6 or N3 feeding and DS periods, reaching statistical significance when diet groups were combined to increase statistical power (**Figure V-8C**; $P < 0.05$). Conversely, expression of the cytosolic (CuZn) and mitochondrial (Mn) isoforms of superoxide dismutase tended to be lower following the N6 and N3 diets and/or DS periods (**Figure V-8D-E**). Levels of lipid peroxidation-derived aldehyde protein adducts malondialdehyde (MDA; **Figure V-8F**) and 4-hydroxynonenal (4-HNE; **Figure V-8G**) were largely unaffected by the dietary interventions, with the exception of lower 4-HNE adducts following 6 weeks of N6 feeding ($P = 0.021$) that was reversed by addition of the DS. Taken together, these results suggest that dietary PUFA supplementation without the supportive DS increases muscle mitochondrial ROS release capacity and reduces antioxidant enzyme expression, but does not increase tissue oxidative stress.

Discussion

The present study is the first to evaluate the biological impacts of dietary essential *n*-6 and *n*-3 PUFA supplementation on serum, blood cells, skeletal muscle and ovarian follicles of older mares. Our results demonstrate that adding PUFA-rich vegetable oils to a standard equine diet increases phospholipid PUFA content across multiple tissues and elicits modest effects the distribution of n-6 and n-3 PUFAs that are generally consistent with their fatty acid composition. Impacts of the N6 diet on phospholipid composition were generally more robust than the N3 diet, while both PUFA diets elicited similar effects on serum cytokines and cellular mitochondrial function. The addition of the dietary supplement tended to improve mitochondrial OXPHOS coupling control and reduce ROS release across all cell types tested, suggesting that these supportive nutrients may be advantageous for obtaining optimal responses to dietary PUFAs in aged mares. Taken together, these results provide novel insight to the biological effects of essential fatty acid supplementation in horses and add to a growing body of evidence that at least some of these effects are largely independent of variations in the *n*-6/*n*-3 PUFA ratio.

Similar to the ancestral human diet, the natural equine diet of grass is rich in *n*-3 ALA compared to *n*-6 LA,[11,12] while modern industrialization has produced diets for both species containing much higher quantities of LA.[10] This has prompted widespread recommendations for dietary supplementation with *n*-3 PUFA to better balance the endogenous distribution of *n*-3 and *n*-6 PUFA and avoid the putative pro-inflammatory effects of excessive dietary *n*-6 PUFA intake.[13] However, few studies have reported health benefits or serum fatty acid composition changes following dietary *n*-3 PUFA supplementation in horses. This may be due in part to a much great abundance of *n*-6 over *n*-3 PUFA in membrane phospholipids. Indeed, we found 3 to 8-fold greater *n*-6 than *n*-3 PUFA levels across the four biological compartments investigated

prior to dietary PUFA supplementation. This was augmented further by the N6 diet, and only modestly attenuated by 2 months on the N3 diet. While the N3 diet tended to increase ALA in all samples, it also increased LA (perhaps due to its presence in flaxseed oil at 17%), which is consistent with previous findings in plasma of young horses.[38] However, the more bioactive longer chain *n*-3 PUFA derivatives of ALA, docosahexaenoic acid (DHA), docosapentaenoic acid (DPA) and eicosapentaenoic acid (EPA), were only readily detected in granulosa cells and muscle tissue, likely reflecting their preferential incorporation to membrane phospholipids. This is in contrast to arachidonic acid (ARA), the long-chain *n*-6 PUFA derivative of LA, which was readily found in all biological samples including serum and follicular fluid. While the efficiency of long-chain PUFA synthesis from ALA and LA *in vivo* has been debated,[39] the greater levels of ARA may result from the much higher levels of LA than ALA present across tissues. Indeed, N3 supplementation tended to decrease ARA and increase long-chain *n*-3 PUFA in granulosa cells and follicular fluid, but not in serum or muscle. More robust displacement of *n*-6 PUFA with reciprocal increases in long-chain *n*-3 PUFA have been reported in multiple biological fluids of horses following long-chain *n*-3 PUFA supplementation,[40,41] but the physiological benefits of these changes are unclear and merit further investigation.

Despite the significantly higher levels of *n*-6 PUFA following the N6 diet in the present study, 5 of 6 cytokines detected in serum were not significantly impacted by either diet. Moreover, TNF-α increased following both N6 and N3 diets, which resolved after addition of the DS in the N6, but not N3 diet. The mechanisms for these effects are unclear, but they highlight a potential pro-inflammatory effect of dietary oil supplements in mares regardless of PUFA composition. Dietary *n*-6 and *n*-3 PUFA have been shown to exacerbate gut inflammation and serum cytokine elevations in patients with Crohn's Disease and murine models,[42] indicating

that the enteric environment can influence systemic effects of dietary PUFA intake. While care was taken to avoid rancidity of oils through proper storage and daily rationing, we cannot rule out the possibility of naturally oxidized oil intake in triggering gut inflammation as described in other species.[43] Resolution of serum TNF-α elevations following addition of the DS to the N6 diet supports the need for supportive nutrients to prevent these potential effects of dietary PUFA supplementation, though this appeared to be insufficient following the N3 diet. Taken together, these results emphasize the importance of considering biological effects of dietary oils beyond those putatively linked to the *n*-6/*n*-3 PUFA ratio and inflammation.

PUFAs have diverse effects on mitochondrial function that vary depending on the cell type, method and duration of administration, and biological context being investigated.[44] This is the first study to evaluate impacts of dietary PUFA supplementation on mitochondrial function in equids, and our results demonstrate cell type-specific effects on respiratory capacity, OXPHOS efficiency and ROS release. In platelets and muscle, both N6 and N3 diets potently decreased mitochondrial respiratory capacity irrespective of substrates used, which tended to decrease further after addition of the DS. These decreases were comparatively greater in the LEAK state, leading to increases in OXPHOS coupling control in both cell types. Lower OCR and OXPHOS efficiency rates have been reported platelet and muscle mitochondria from aged humans,[45,46] suggesting the effects of dietary interventions herein may be advantageous for improving bioenergetic efficiency in aged mares. Indeed, previous studies have demonstrated beneficial effects of dietary PUFA supplementation on indices of OXPHOS efficiency in rat cardiac muscle[47] and human skeletal muscle.[48] Similar effects of the diets on platelet and muscle mitochondrial bioenergetics herein have also been reported in response to aging in humans,[46] suggesting that platelets may serve as a less invasive means of assessing the impacts of aging and

nutritional interventions on muscle mitochondria. However, we caution against making broad generalizations of mitochondrial effects observed in one cell type to another given vastly different metabolic demands and phenotypes.

Impacts of the PUFA supplementation on platelet and muscle mitochondrial ROS release were more variable. The N3 diet tended to decrease platelet ROS release with no additive effect of the DS, which is consistent with previous evidence for an attenuation of ROS production in platelets and neutrophils following 6 weeks of dietary *n*-3 PUFA supplementation in healthy humans.[49] However, both the N3 and N6 diets increased ROS release from muscle mitochondria of mares in the present study, which is consistent with effects of PUFA on multiple cell types,[50,51] but in contrast to effects of *n*-3 PUFA supplementation on skeletal muscle of aged humans[52] and mice fed a high-fat diet.[53] Greater ROS production down-regulates fatty acid oxidation in C2C12 skeletal muscle cells,[54] corroborating the observed link between these two responses herein. This effect was associated with trends for higher NOX4 expression herein, which is known to be upregulated in multiple cell types by inflammatory cytokines,[55] including TNF-α,[56] suggesting potential links to the observed impacts on serum TNF-α herein. Both diets also tended to decrease SOD isozymes in muscle, which may further promote oxidative stress under states of elevated metabolic demand. However, PUFA supplementation tended to either decrease (in N6) or have no effect on indices of lipid peroxidation (in N3), consistent with previous findings in yearling horses.[57] This suggests that endogenous antioxidants or those added to the PUFA-rich oils to preserve shelf life must be sufficient to prevent overt oxidative stress despite a higher ROS release capacity in response to these diets. Indeed, addition of the DS fully reversed these elevations in muscle ROS release capacity, further emphasizing the efficacy and

importance of including supportive antioxidants to PUFA-enriched diets to avoid adverse biological responses.[24]

We employed two different oxygen-sensing technologies to evaluate metabolic responses of granulosa cells and oocytes to the dietary interventions. While these assessments do not represent fertility directly, they provide important insights to the oocyte's environment as it matures within the ovarian follicle. Granulosa cells line the inside of ovarian follicles and are involved in steroidogenesis and provide metabolic support to the oocyte. We found that while short-term PUFA supplementation had minimal effects on granulosa cell and oocyte metabolism, both N6 and N3 diets increased granulosa cell ROS release, which has been linked with reduced oocyte quality in humans[,58]. Addition of the DS attenuated PUFA-induced elevations in granulosa cell ROS release and increased OXPHOS capacity, suggesting a more favorable environment for oocyte development. Indeed, oocyte OCR was markedly increased by addition of the DS, with no significant effects of the PUFA supplements alone. Oocyte mitochondrial function is critical for supporting maturation and early embryo viability[59], and a greater OCR in equine oocytes is associated with improved development into transferable embryos after ICSI.[18,19] Equine oocytes store and utilize fatty acids as a primary source of energy, and oocytes from old mares contain fewer amounts of lipids compared to oocytes from younger mares.[19] Therefore, we postulate that the addition of supportive nutrients present in the DS, specifically L-carnitine and antioxidants, are required to reap the benefits of dietary fatty acids on the follicular environment and support optimal oocyte development in older mares and perhaps other species, as previously demonstrated by our group.[22] In addition, multiple trace minerals have been previously reported to exert beneficial effects on cellular antioxidant status and mitochondrial function in horses.[60,61]

Conclusions

Although the use of dietary oils is an effective method to increase caloric intake in horses, the present study suggests that oil supplementation, regardless of *n*-3 or *n*-6 PUFA content, may induce undesirable effects on mitochondrial oxidative capacity, reactive oxygen species production, and systemic inflammation. However, the addition of dietary support nutrients in combination with either oil type may mitigate these effects, providing a feasible method to optimize equine health following oil feeding. *n*-3 PUFA supplementation did not provide significant benefits to cell function or metabolism compared to *n*-6 PUFA supplementation. Anti-inflammatory effects of omega-3 PUFAs recognized in other species may not play a significant role in horses, as increased TNF-α concentrations as inflammatory marker was observed following both oil treatments. Oil supplementation alone may result in reduced capacity to metabolize lipids and increased ROS production in skeletal muscle, platelets, and granulosa cells. Therefore, long-term health risks in older horses associated with oil feeding should be considered to minimize health consequences. Our study provides evidence that additional supplementation of antioxidants, L-carnitine, and other supportive nutrients is sufficient to reduce the negative effects of oils on cellular health throughout the body and is ideal for the systemic and reproductive health of older horses.

Tables

Table V-1. Animal morphometrics and serum cytokines. Values are mean ± SEM prior to (Baseline), following 6 weeks (Week 6) of flaxseed (N3, n = 6) or corn (N6, n = 6) oil supplementation, and an additional 6 weeks with the dietary supplement (+6 wk DS). Superscripts differ at $P < 0.05$ between weeks within mare's supplementation group by Fisher's LSD test following a significant ANOVA. #$P < 0.05$ vs. other diet for the same time point by 2-way independent samples *t*-test.

	N6 diet			**N3 diet**		
	Baseline	**6 weeks**	**+ 6 wk DS**	**Baseline**	**6 weeks**	**+ 6 wk DS**
Body Weight (kg)	1148 ± 24	1149 ± 23	1175 ± 26	1102 ± 29	1075 ± 31	1135 ± 34
Body Condition Score	5.7 ± 0.5	5.8 ± 0.3	5.7 ± 0.3	5.4 ± 0.6	5.3 ± 0.5	5.6 ± 0.4
Neck Score	1.7 ± 0.4	1.7 ± 0.4	1.5 ± 0.5	**1.5 ± 0.3^{a}**	**0.8 ± 0.3$^{b\#}$**	**1.5 ± 0.4^{a}**
CCL2 (pg/mL)	440 ± 121	1344 ± 860	321 ± 106	2151 ± 1185	1527 ± 702	1332 ± 725
CCL3 (pg/mL)	51213 ± 9039	45323 ± 7664	24607 ± 6255	46066 ± 11191	50891 ± 7648	45703 ± 14394
CCL5 (pg/mL)	566 ± 169	2172 ± 1764	183 ± 44	464 ± 207	330 ± 143	308 ± 76
CCL11 (pg/mL)	2072 ± 349	5380 ± 3364	1408 ± 200	3127 ± 426	2910 ± 634	2907 ± 552
TNFalpha (pg/mL)	**14572 ± 2998^{a}**	**25462 ± 1700^{b}**	**15000 ± 2699^{a}**	**17442 ± 2198^{a}**	**24003 ± 1531^{b}**	**26271 ± 3693^{ab}**

Table V-2. Fatty acid composition of serum phospholipids. Values are mean percentages of total serum phospholipid fatty acids ± SEM prior to (Baseline), following 6 weeks (Week 6) of flaxseed (N3, n = 6) or corn (N6, n = 6) oil supplementation, and an additional 6 weeks with the dietary supplement (+DS). Superscripts differ at $P < 0.05$ between weeks within mare's supplementation group by Fisher's LSD test following a significant ANOVA. #$P < 0.05$ vs. other diet for the same time point by 2-way independent samples *t*-test. Abbreviations not listed above: DHGLA, dihomogammalinolenic acid; EPA, eicosapentaenoic acid; GLA, gamma-linolenic acid; MUFA, monounsaturated fatty acids.

Phospholipid Fatty acids (% total)	**N6 diet**			**N3 diet**		
	Baseline	**6 weeks**	**+ 6 wk DS**	**Baseline**	**6 weeks**	**+ 6 wk DS**
16:0, Palmitic	**17.2 ± 0.7[a]**	**16.6 ± 0.7[a]**	**15.8 ± 0.6[b]**	17.1 ± 0.4	16.6 ± 0.5	15.8 ± 0.6
16:1, Palmitoleic	**1.2 ± 0.1[a]**	**0.7 ± 0.2[b]**	**0.7 ± 0.2[b]**	**1.1 ± 0.1[a]**	**0.9 ± 0.1[b]**	**0.6 ± 0.1[c]**
18:0, Stearic	22.2 ± 0.9	24.0 ± 0.5	21.9 ± 2.2	23.1 ± 0.8	23.8 ± 0.5	23.1 ± 0.7
18:1n9, Oleic	**17.9 ± 1.0[a]**	**11.9 ± 0.4[b]#**	**13.6 ± 1.2[b]**	18.2 ± 2.3	15.7 ± 1.1	14.8 ± 0.8
18:1n7, Vaccenic	**1.3 ± 0.1[a]**	**1.0 ± 0.1[b]**	**0.9 ± 0.2[b]**	1.2 ± 0.1	1.2 ± 0.1	1.0 ± 0.0
18:2n6, Linoleic	**30.8 ± 1.2[a]**	**38.9 ± 0.8[b]#**	**40.8 ± 1.9[b]#**	32.5 ± 1.9	34.3 ± 0.9	35.9 ± 0.7
18:3n3, α-Linolenic	**5.5 ± 0.1[a]**	**4.5 ± 0.3[b]**	**4.1 ± 0.6[b]**	4.2 ± 0.3	4.6 ± 0.5	5.8 ± 1.1
20:0, Arachidic	0.7 ± 0.2	0.5 ± 0.1	0.3 ± 0.1	0.3 ± 0.1	0.3 ± 0.1	0.4 ± 0.1
20:1, Erucic	0.5 ± 0.1	0.1 ± 0.1	0.3 ± 0.1	0.4 ± 0.1	0.4 ± 0.1	0.4 ± 0.1
20:2, Eicosadienoic	0.1 ± 0.1	0.1 ± 0.1	0.1 ± 0.1	0.0 ± 0.0	0.1 ± 0.1	0.1 ± 0.1
20:3n6, DHGLA	0.5 ± 0.1	0.4 ± 0.2	0.4 ± 0.1	0.2 ± 0.1	0.6 ± 0.1	0.6 ± 0.2
20:4n6, Arachidonic	1.3 ± 0.1	1.1 ± 0.1	0.9 ± 0.2	1.3 ± 0.1	1.4 ± 0.1	1.0 ± 0.2
20:3n3, GLA	0.6 ± 0.4	0.0 ± 0.0	0.1 ± 0.1	0.0 ± 0.0	0.1 ± 0.1	0.4 ± 0.2
20:5n3, EPA	0.3 ± 0.2	0.0 ± 0.0	0.0 ± 0.0	0.2 ± 0.1	0.1 ± 0.1	0.1 ± 0.1
Total SFA	40.0 ± 0.8	41.2 ± 0.5	38.1 ± 2.3	40.5 ± 0.9	40.7 ± 0.4	39.3 ± 1.1
Total MUFA	**20.9 ± 1.1[a]**	**13.7 ± 0.5[b]**	**15.5 ± 1.2[b]**	20.9 ± 2.2	18.1 ± 1.1	16.8 ± 0.8
Total PUFA	**39.1 ± 0.9[a]**	**45.1 ± 0.8[b]#**	**46.5 ± 1.5[b]**	**38.5 ± 1.7[a]**	**41.2 ± 1.0[b]**	**43.9 ± 0.4[b]**
Total n-6 PUFA	**32.7 ± 1.2[a]**	**40.6 ± 0.7[b]#**	**42.3 ± 1.9[b]#**	34.1 ± 1.9	36.4 ± 0.9	37.6 ± 0.8
Total n-3 PUFA	**6.3 ± 0.4[a]**	**4.5 ± 0.3[a]**	**4.2 ± 0.6[a]**	4.4 ± 0.3	4.8 ± 0.6	6.3 ± 1.1

Table V-3. Fatty acid composition of follicular fluid phospholipids. Values are mean percentages of total follicular fluid phospholipid fatty acids ± SEM prior to (Baseline), following 6 weeks (Week 6) of flaxseed (N3, n = 6) or corn (N6, n = 6) oil supplementation, and an additional 6 weeks with the dietary supplement (DS). Superscripts differ at $P < 0.05$ between weeks within mare's supplementation group by Fisher's LSD test following a significant ANOVA. #$P < 0.05$ vs. other diet for the same time point by 2-way independent samples *t*-test. Results are presented as mean ± SEM. Abbreviations not listed above: DHGLA, dihomogammalinolenic acid; EPA, eicosapentaenoic acid; GLA, gamma-linolenic acid.

Phospholipid Fatty acids (% total)	**N6 diet**			**N3 diet**		
	Baseline	**6 weeks**	**+ 6 wk DS**	**Baseline**	**6 weeks**	**+ 6 wk DS**
16:0, Palmitic	14.9±0.5	13.8±0.6	14.4±0.6	14.6±0.6	14.6±0.6	14.3±0.4
18:0, Stearic	28.0±1.8	28.3±1.1	27.5±0.7	26.6±1.2	28.4±1.1	27.1±0.6
18:1n9, Oleic	**13.9±0.8^{a}**	**8.8±0.8^{b}#**	**9.2±0.5^{b}#**	15.3±2.9	12.5±0.8	12.4±0.8
18:1n7, Vaccenic	**1.1±0.2^{a}**	**0.5±0.3^{b}**	**0.6±0.3^{a}**	0.5±0.2	0.7±0.3	0.8±0.3
18:2n6, Linoleic	**35.5±1.7^{a}**	**41.3±0.7^{b}**	**43.1±1.2^{b}**	**35.8±2.0^{a}**	**38.1±0.7^{a}**	**40.1±1.2^{b}**
18:3n3, α-Linolenic	**2.7±0.7^{a}**	**2.3±0.3^{a}**	**1.3±0.3^{b}**	**2.1±0.3^{a}**	**3.1±0.3^{b}**	**2.0±0.5^{a}**
20:3n6, DHGLA	1.0±0.5	1.2±0.2	0.7±0.4	0.6±0.3	0.3±0.2	0.3±0.2
20:4n6, Arachidonic	2.5±0.5	2.1±0.3	1.5±0.4	2.0±0.4	1.6±0.3	1.2±0.6
20:3n3, GLA	0.0±0.0	1.5±0.7	1.7±0.7	2.2±1.4	0.8±0.7	1.7±1.1
Total SFA	42.9±1.7	42.2±0.7	41.8±0.7	41.2±0.9	43.0±0.7	41.4±0.6
Total MUFA	**15.4±0.7^{a}**	**9.3±0.7^{b}#**	**9.9±0.6^{b}#**	16.0±2.8	13.2±0.7	13.2±0.8
Total PUFA	**41.7±1.5^{a}**	**48.5±0.9^{b}#**	**48.3±0.7^{b}#**	42.8±2.4	43.8±0.9	45.4±0.8
Total n-6 PUFA	**39.0±1.4^{a}**	**44.6±0.8^{b}#**	**45.3±0.7^{b}#**	38.4±2.4	40.0±0.8	41.6±1.3
Total n-3 PUFA	2.7±0.7	3.9±0.9	3.0±0.8	4.4±1.6	3.9±0.9	3.8±1.5

Table V-4. Fatty acid composition of skeletal muscle phospholipids. Values are mean percentages of total muscle phospholipid fatty acids ± SEM prior to (Baseline), following 6 weeks (Week 6) of flaxseed (N3, n = 6) or corn (N6, n = 6) oil supplementation, and an additional 6 weeks with the dietary supplement (DS). Superscripts differ at $P < 0.05$ between weeks within mare's supplementation group by Fisher's LSD test following a significant ANOVA. #$P < 0.05$ vs. other diet for the same time point by 2-way independent samples *t*-test. Abbreviations not listed above: DHGLA, dihomogammalinolenic acid; EPA, eicosapentaenoic acid; DPA, docosapentaenoic acid; DHA, docosahexaenoic acid.

Phospholipid Fatty acids (% total)	**N6 diet**			**N3 diet**		
	Baseline	**6 weeks**	**+ 6 wk DS**	**Baseline**	**6 weeks**	**+ 6 wk DS**
16:0, Palmitic	**20.8 ± 2.0[a]**	**17.6 ± 1.0[b]**	**17.8 ± 0.5[b]**	20.1 ± 2.1	19.3 ± 1.4	17.4 ± 0.7
16:1, Palmitoleic	1.4 ± 0.9	1.3 ± 0.5	1.3 ± 0.7	2.4 ± 1.1	1.3 ± 0.7	0.9 ± 0.4
18:0, Stearic	13.4 ± 1.0	13.5 ± 0.3	14.2 ± 0.7	12.0 ± 1.0	11.9 ± 0.7	13.2 ± 0.5
18:1n9, Oleic	12.7 ± 2.0	10.6 ± 1.1	11.6 ± 1.4	15.4 ± 2.8	14.5 ± 2.4	11.2 ± 0.5
18:1n7, Vaccenic	3.3 ± 0.5	3.8 ± 0.3	2.1 ± 0.4	3.1 ± 0.1	3.0 ± 0.2	2.7 ± 0.2
18:2n6, Linoleic	**25.9 ± 2.9[a]**	**32.6 ± 2.4[b]**	**30.0 ± 1.5[b]**	25.1 ± 2.7	26.1 ± 2.7	29.9 ± 0.9
18:3n3, α-Linolenic	2.8 ± 0.8	2.6 ± 0.4	2.1 ± 0.2	2.8 ± 0.3	3.3 ± 0.5	3.1 ± 0.4
20:1, Erucic	0.0 ± 0.0	0.2 ± 0.2	0.2 ± 0.2	0.0 ± 0.0	0.4 ± 0.4	0.0 ± 0.0
20:2, Eicosadienoic	0.0 ± 0.0	0.2 ± 0.2	0.2 ± 0.2	0.2 ± 0.2	0.2 ± 0.2	0.0 ± 0.0
20:3n6, DHGLA	0.9 ± 0.4	0.4 ± 0.3	1.0 ± 0.4	1.3 ± 0.4	0.5 ± 0.3	0.4 ± 0.3
20:4n6, Arachidonic	4.6 ± 1.0	6.9 ± 0.6	7.9 ± 0.7	7.5 ± 1.1	7.0 ± 0.9	8.6 ± 0.3
20:3n3, GLA	0.9 ± 0.8	0.1 ± 0.1	0.0 ± 0.0	0.0 ± 0.0	0.3 ± 0.3	0.2 ± 0.2
20:5n3, EPA	5.1 ± 1.9	1.5 ± 0.6	2.9 ± 1.0	4.1 ± 2.5	3.9 ± 1.3	2.5 ± 0.5
22:5n3, DPA	4.6 ± 1.3	5.7 ± 0.8	4.7 ± 0.7	3.9 ± 0.9	5.1 ± 1.3	5.2 ± 0.8
22:6n3, DHA	3.7 ± 1.2	3.0 ± 0.7	4.0 ± 1.0	2.2 ± 0.5	3.1 ± 1.0	4.6 ± 1.1
Total SFA	34.2 ± 2.3	31.1 ± 1.0	32.0 ± 0.7	32.0 ± 1.8	31.2 ± 1.0	30.7 ± 0.8
Total MUFA	17.3 ± 2.8	15.8 ± 1.5	15.2 ± 2.3	20.9 ± 3.9	19.2 ± 3.3	14.7 ± 0.9
Total PUFA	48.5 ± 5.0	53.1 ± 2.4	52.8 ± 2.1	47.1 ± 5.4	49.5 ± 3.9	54.6 ± 1.1
Total n-6 PUFA	**31.4 ± 3.6[a]**	**40.1 ± 2.9[b]**	**39.1 ± 1.5[b]**	34.1 ± 4.1	33.8 ± 3.6	39.0 ± 1.0
Total n-3 PUFA	17.1 ± 2.2	12.9 ± 1.3	13.7 ± 1.9	13.0 ± 3.1	15.7 ± 1.5	15.6 ± 1.4

Table V-5. Fatty acid composition of granulosa cell phospholipids. Values are mean percentages of total granulosa cell phospholipid fatty acids ± SEM prior to (Baseline), following 6 weeks (Week 6) of flaxseed (N3, n = 6) or corn (N6, n = 6) oil supplementation, and an additional 6 weeks with the dietary supplement (DS). Superscripts differ at $P < 0.05$ between weeks within mare's supplementation group by Fisher's LSD test following a significant ANOVA. #$P < 0.05$ vs. other diet for the same time point by 2-sided independent samples *t*-test. Abbreviations not listed above: DHGLA, dihomogammalinolenic acid; EPA, eicosapentaenoic acid; ETA, Eicosatrienoic acid; DPA, docosapentaenoic acid; DHA, docosahexaenoic acid.

Phospholipid Fatty acids (% total)	**N6 diet**			**N3 diet**		
	Baseline	**6 weeks**	**+ 6 wk DS**	**Baseline**	**6 weeks**	**+ 6 wk DS**
16:0, Palmitic	21.2 ± 1.2	19.1 ± 1.0	18.1 ± 0.6	20.7 ± 1.0	18.9 ± 1.0	18.2 ± 0.7
16:1, Palmitoleic	**2.3 ± 0.4^{a}**	**1.1 ± 0.2^{b}**	**1.1 ± 0.2^{b}#**	**1.0 ± 0.3^{a}**	**1.5 ± 0.2^{a}**	**0.4 ± 0.1^{b}**
18:0, Stearic	**16.4 ± 0.7^{a}**	**19.1 ± 1.4^{b}**	**21.8 ± 1.1^{b}#**	**19.2 ± 1.2^{a}**	**17.2 ± 1.4^{a}**	**25.0 ± 0.4^{b}**
18:1n9, Oleic	**23.1 ± 1.0^{a}**	**19.0 ± 0.2^{b}#**	**17.3 ± 0.7^{c}**	**22.4 ± 1.2^{a}**	**20.6 ± 0.2^{a}**	**17.9 ± 0.6^{b}**
18:1n7, Vaccenic	2.1 ± 0.4	2.3 ± 0.1	2.1 ± 0.1	2.3 ± 0.5	2.0 ± 0.1	2.1 ± 0.0
18:2n6, Linoleic	**17.8 ± 1.0^{a}**	**21.5 ± 0.6^{b}**	**22.3 ± 0.6^{b}#**	**17.9 ± 1.1^{a}**	**20.3 ± 0.6^{b}**	**20.2 ± 0.7^{b}**
18:3n6, GLA	0.3 ± 0.2	0.5 ± 0.1	0.1 ± 0.1	0.3 ± 0.2	0.6 ± 0.1	0.0 ± 0.0
18:3n3, α-Linolenic	0.3 ± 0.2	0.1 ± 0.1	1.3 ± 0.4	**0.6 ± 0.3^{a}**	**0.7 ± 0.1^{a}**	**1.6 ± 0.3^{b}**
20:0, Arachidic	0.0 ± 0.0	0.1 ± 0.1	0.0 ± 0.0	0.0 ± 0.0	0.1 ± 0.1	0.1 ± 0.1
20:1, Erucic	0.1 ± 0.0	0.2 ± 0.2	0.7 ± 0.3	0.6 ± 0.4	0.5 ± 0.2	0.6 ± 0.2
20:2, Eicosadienoic	0.4 ± 0.2	0.9 ± 0.1	1.0 ± 0.2	0.1 ± 0.1	0.7 ± 0.1	0.5 ± 0.2
20:3n6, DHGLA	1.4 ± 0.3	1.4 ± 0.2	1.5 ± 0.3	1.9 ± 0.5	1.7 ± 0.2	1.4 ± 0.2
20:4n6, Arachidonic	10.6 ± 1.1	12.0 ± 0.7	10.8 ± 1.3	**11.3 ± 0.8^{a}**	**10.5 ± 0.7^{a}**	**7.8 ± 0.4^{b}#**
20:3n3, ETA	0.0 ± 0.0	0.1 ± 0.2	0.1 ± 0.1	**0.0 ± 0.0^{a}**	**0.2 ± 0.2^{a}**	**1.0 ± 0.2^{b}#**
20:5n3, EPA	1.0 ± 0.4	0.6 ± 0.2	0.7 ± 0.3	**0.9 ± 0.3^{a}**	**1.2 ± 0.2^{a}**	**1.5 ± 0.2^{a}#**
22:4n6, Adrenic	1.1 ± 0.4	0.6 ± 0.2	0.2 ± 0.2	0.3 ± 0.2	0.6 ± 0.2	0.1 ± 0.1
22:5n3, DPA	1.3 ± 0.4	0.9 ± 0.1	0.8 ± 0.4	**0.4 ± 0.2^{a}#**	**1.7 ± 0.1^{b}#**	**0.9 ± 0.5^{a}**
22:6n3, DHA	0.5 ± 0.2	0.7 ± 0.1	0.0 ± 0.0	0.2 ± 0.1	0.9 ± 0.1	0.6 ± 0.5
Total SFA	37.6 ± 1.4	38.3 ± 0.6	39.9 ± 0.8	**39.9 ± 0.8^{a}**	**36.2 ± 0.6^{a}#**	**43.2 ± 1.1^{b}#**
Total MUFA	**27.7 ± 1.1^{a}**	**22.6 ± 0.4^{b}**	**21.2 ± 0.8^{b}**	**26.3 ± 1.4^{a}**	**24.6 ± 0.4^{a}#**	**21.0 ± 0.8^{b}**
Total PUFA	**34.7 ± 2.4^{a}**	**39.2 ± 0.4^{b}**	**38.9 ± 1.0 ^{a}**	**33.8 ± 1.5^{a}**	**39.2 ± 0.4^{b}**	**35.7 ± 1.1^{a}**
Total n-6 PUFA	**31.6 ± 1.6^{a}**	**36.9 ± 0.7^{b}#**	**36.0 ± 1.1^{b}#**	31.8 ± 1.5	34.4 ± 0.7	30.0 ± 1.1
Total n-3 PUFA	3.1 ± 0.9	2.3 ± 0.5	2.9 ± 0.7	**2.0 ± 0.6^{a}**	**4.8 ± 0.5^{b}#**	**5.7 ± 0.7^{b}#**

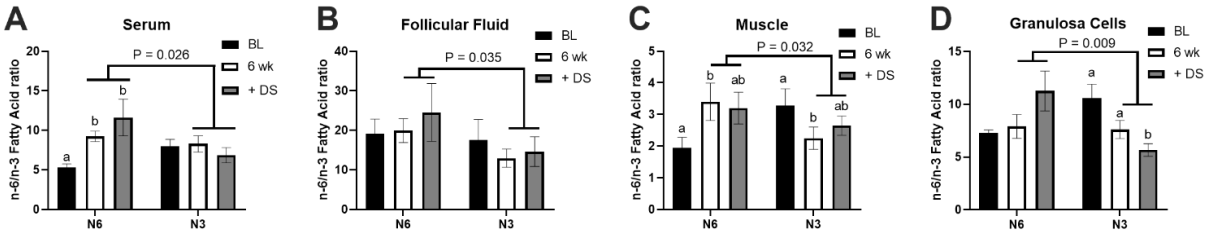

Figure V-1. Polyunsaturated fatty acid (PUFA) composition in various tissues following dietary oil feeding. The ratio of omega-3 to omega-6 PUFA was determined in serum (**A**), follicular fluid (**B**), skeletal (trapezius) muscle tissue (**C**), and granulosa cells (**D**) prior to (BL) and following 6 weeks of corn (N6) or flaxseed (N3) diets, and following 6 additional weeks with the added dietary supplement (+DS). Follicular fluid and granulosa cells were collected from preovulatory dominant follicles 24±2 h after maturation induction and skeletal muscle biopsies were obtained from the trapezius muscle. Graphs represent mean ± SEM of $N = 6$ mares per group. Superscripts differ at $P < 0.05$ between weeks within mare's supplementation group by Fisher's LSD test following a significant ANOVA. Noted P values indicate significant differences in the combined 6 wk and +DS time points between N6 and N3 cohorts by 1-sided independent sample t-tests at $P < 0.05$.

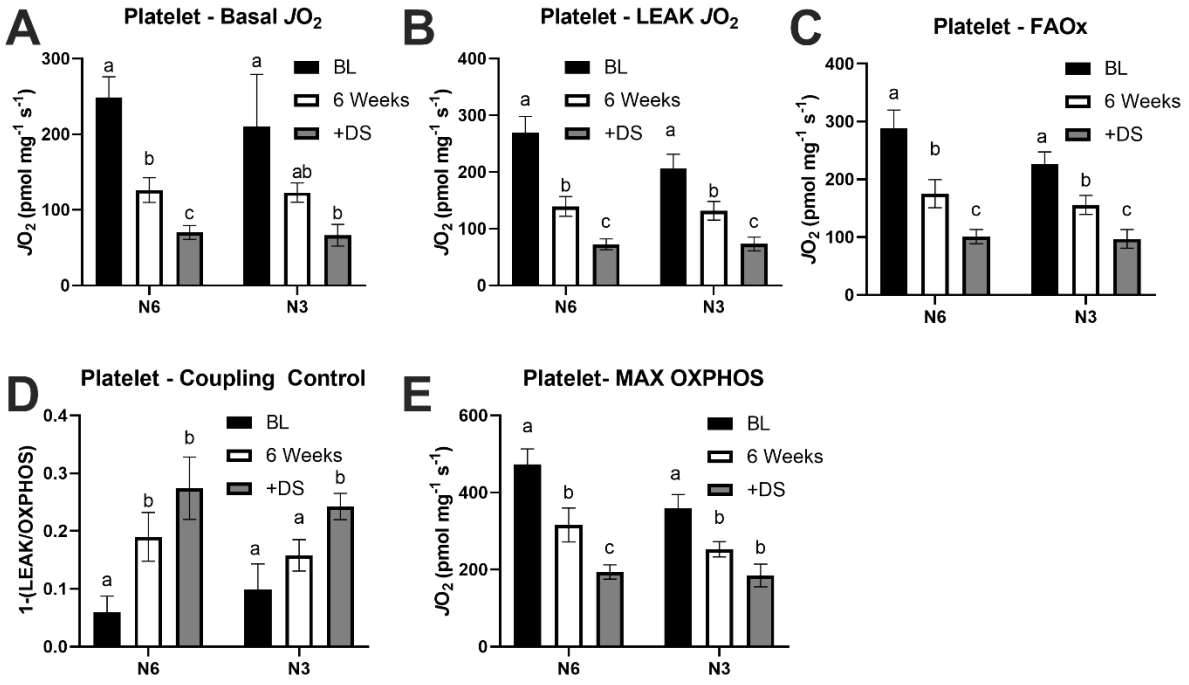

Figure V-2. Platelet oxidative metabolism. High resolution respirometry was performed on platelets isolated from mares at baseline (BL), following 6 weeks of feeding the flaxseed (N3) or corn oil (N6) supplements, and following an additional 6 weeks with dietary supplement (+DS). Rates of oxygen consumption (JO_2) were measured in intact cells under basal condition supported by endogenous substrates **(A)**, followed by permeabilization with digitonin and the addition of malate and palmitoylcarnitine to generate the LEAK JO_2 **(B)**. ADP was then added to generate the OXPHOS supported by fatty acid oxidation (FAOx; **C**) and enable calculation of FAOx-linked coupling control (**D**), followed by the addition of pyruvate, glutamate and succinate to support maximal OXPHOS-linked JO_2 (**E**). Graphs represent mean ± SEM of $N = 6$ mares per group. Superscripts differ at $P < 0.05$ between weeks within mare's supplementation group by Fisher's LSD test following a significant ANOVA.

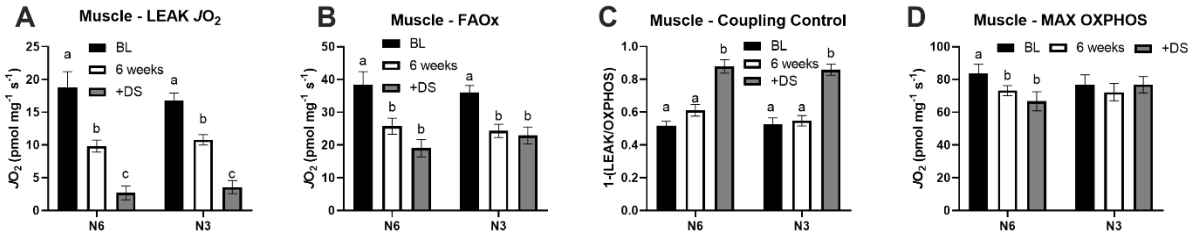

Figure V-3. Skeletal muscle oxidative metabolism. High resolution respirometry was performed on skeletal muscle fiber bundles (3-4 mg) isolated from trapezius biopsies obtained at baseline (BL), following 6 weeks of feeding the flaxseed (N3) or corn oil (N6) supplements, and following an additional 6 weeks with dietary supplement (+DS). Rates of oxygen consumption (JO_2) were measured following by permeabilization with saponin and the addition of malate and palmitoylcarnitine to generate the LEAK JO_2 **(A)**. ADP was then added to generate the OXPHOS supported by fatty acid oxidation (FAOx; **B**) and enable calculation of FAOx-linked coupling control (**C**), followed by the addition of pyruvate, glutamate and succinate to support maximal OXPHOS-linked JO_2 (**D**). Graphs represent mean ± SEM of $N = 6$ mares per group. Superscripts differ at $P < 0.05$ between weeks within mare's supplementation group by Fisher's LSD test following a significant ANOVA.

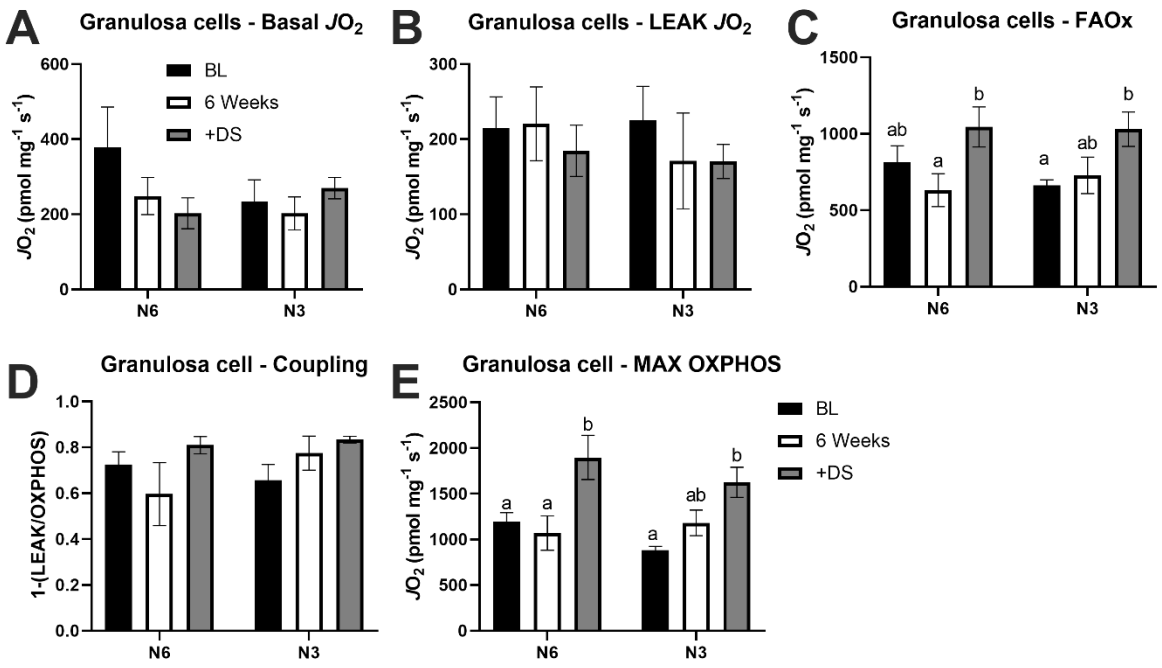

Figure V-4. Granulosa cell oxidative metabolism. High resolution respirometry was performed on granulosa cells obtained during aspiration of preovulatory follicles at baseline (BL), following 6 weeks of feeding the flaxseed (N3) or corn oil (N6) supplements, and following an additional 6 weeks with the dietary supplement (+DS). Rates of oxygen consumption (JO_2) were measured in intact cells under basal condition supported by endogenous substrates **(A)**, followed by permeabilization with digitonin and the addition of malate and palmitoylcarnitine to generate the LEAK JO_2 **(B)**. ADP was then added to generate the OXPHOS supported by fatty acid oxidation (FAOx; **C**) and enable calculation of FAOx-linked coupling control (**D**), followed by the addition of pyruvate, glutamate and succinate to support maximal OXPHOS-linked JO_2 (**E**). Graphs represent mean ± SEM of $N = 6$ mares per group. Superscripts differ at $P < 0.05$ between weeks within mare's supplementation group by Fisher's LSD test following a significant ANOVA.

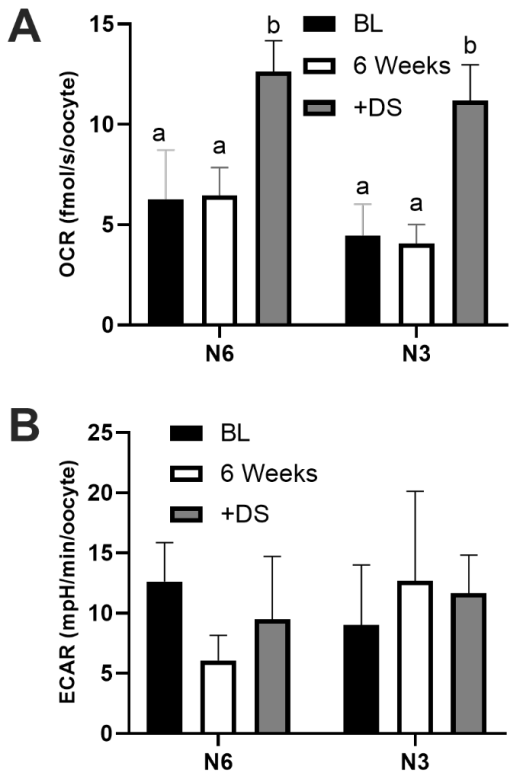

Figure V-5. Oocyte metabolism. Oocytes obtained from preovulatory follicles of mares prior to (BL), following 6 weeks of N6 or N3 supplementation (6 weeks), and after an additional 6 weeks of diets with the dietary supplement (+DS). A custom-built metabolic micro-sensor was used to measure **(A)** basal rates of oxygen consumption (OCR) as a measure of oxidative metabolism and (**B**) extracellular acidification rate (ECAR) as a measure of anaerobic glycolysis. Graphs represent mean ± SEM. Superscripts differ at $P < 0.05$ between weeks within mare's supplementation group by Fisher's LSD test following a significant ANOVA.

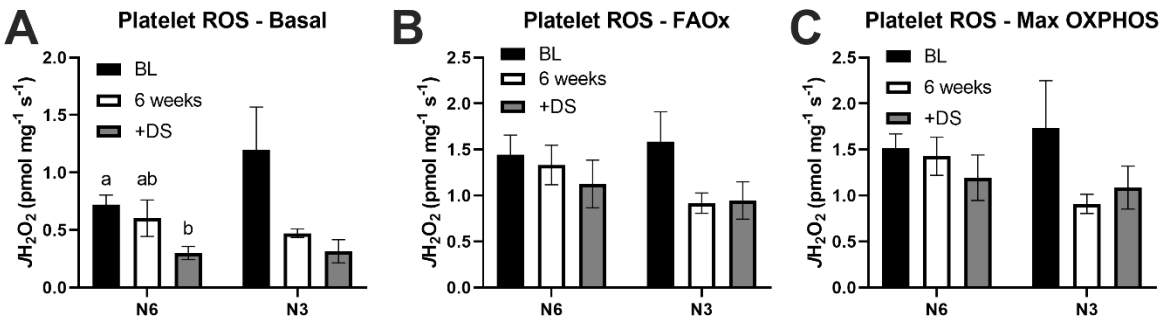

Figure V-6. Platelet ROS release. Rates of cellular reactive oxygen species (ROS) release rates were measured in platelets isolated from mares at baseline (BL), following 6 weeks of feeding the flaxseed (N3) or corn oil (N6) supplements, and following an additional 6 weeks with dietary supplement (+DS). Rates of hydrogen peroxide release (JH_2O_2) were measured as the accumulation of resorufin fluorescence in respirometry chambers containing intact cells under basal conditions supported by endogenous substrates **(A)**, following permeabilization with digitonin and the addition of malate, palmitoylcarnitine and ADP to generate fatty acid-supported OXPHOS (FAOx; **B**), and following the addition of pyruvate, glutamate and succinate to support maximal OXPHOS-linked JO_2 (**C**). Graphs represent mean ± SEM of $N = 6$ mares per group. Superscripts differ at $P < 0.05$ between weeks within mare's supplementation group by Fisher's LSD test following a significant ANOVA.

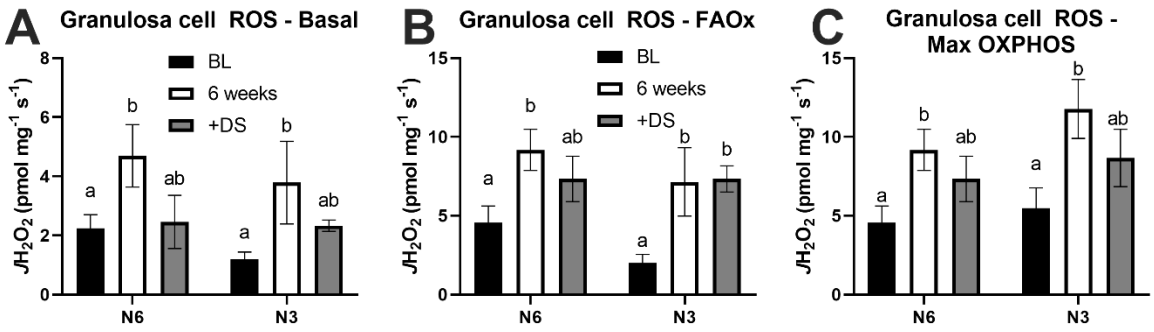

Figure V-7. Granulosa cell ROS release. Rates of cellular reactive oxygen species (ROS) release rates were measured in granulosa cells obtained during aspiration of preovulatory follicles at baseline (BL), following 6 weeks of feeding the flaxseed (N3) or corn oil (N6) supplements, and following an additional 6 weeks with dietary supplement (+DS). Rates of hydrogen peroxide release (JH_2O_2) were measured as the accumulation of resorufin fluorescence in respirometry chambers containing intact cells under basal conditions supported by endogenous substrates **(A)**, following permeabilization with digitonin and the addition of malate, palmitoylcarnitine and ADP to generate fatty acid-supported OXPHOS (FAOx; **B**), and following the addition of pyruvate, glutamate and succinate to support maximal OXPHOS (**C**). Graphs represent mean ± SEM of $N = 6$ mares per group. Superscripts differ at $P < 0.05$ between weeks within mare's supplementation group by Fisher's LSD test following a significant ANOVA.

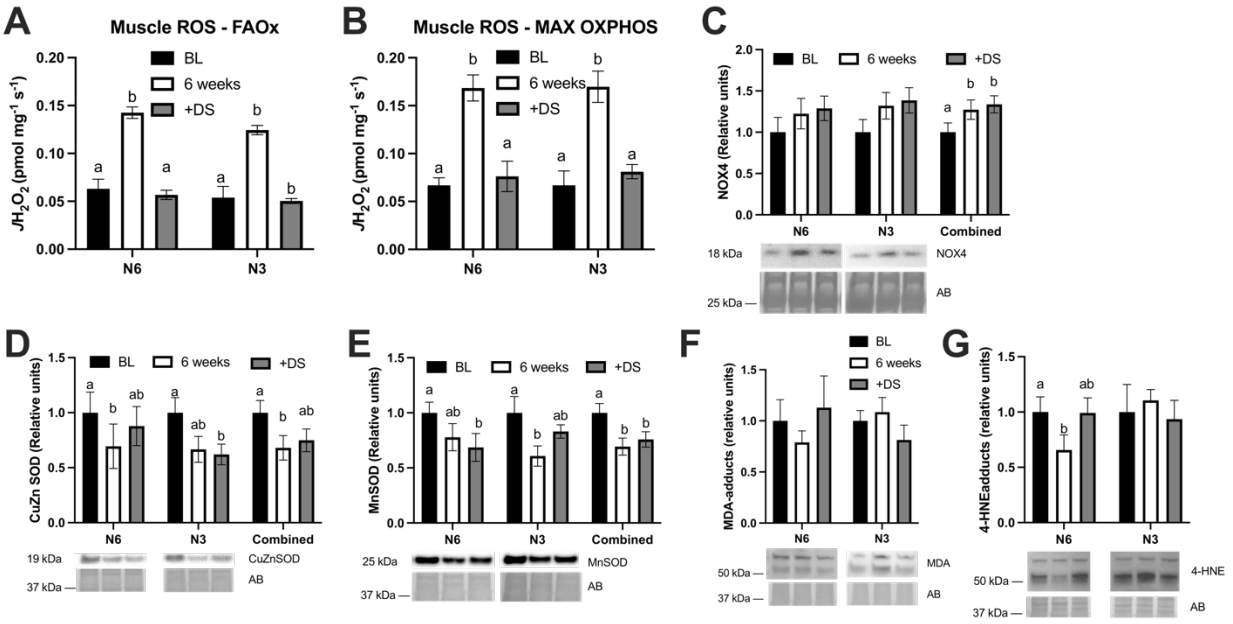

Figure V-8. Skeletal muscle ROS release and related parameters. Skeletal muscle (trapezius) biopsies were processed for assessment of reactive oxygen species (ROS) release or protein immunoblotting at baseline (BL), following 6 weeks of feeding the flaxseed (N3) or corn oil (N6) supplements, and following an additional 6 weeks with dietary supplement (+DS). Rates of hydrogen peroxide release (JH_2O_2) were measured as the accumulation of resorufin fluorescence in respirometry chambers containing saponin-permeabilized fiber bundles following the addition of malate, palmitoylcarnitine and ADP to generate fatty acid-supported OXPHOS (FAOx; **A**), and following the addition of pyruvate, glutamate, and succinate to support maximal OXPHOS (**B**). Muscle protein homogenates were immunoblotted for NADPH oxidase 4 (NOX4; **C**), mitochondrial superoxide dismutase (MnSOD; **D**), cytosolic superoxide dismutase (CuZnSOD**, E**), and protein adducts of the lipid peroxidation aldehydes malondialdehyde (MDA; **F**) and 4-hydroxynonenal (4-HNE, **G**)-protein adducts. Graphs represent mean ± SEM of N = 6 mares per group. Superscripts differ at $P < 0.05$ between weeks within mare's supplementation group by Fisher's LSD test following a significant ANOVA.

References

(1) Larsson, L.; Degens, H.; Li, M.; Salviati, L.; Lee, Y. I.; Thompson, W.; Kirkland, J. L.; Sandri, M. Sarcopenia: Aging-Related Loss of Muscle Mass and Function. *Physiol. Rev.* **2019**, *99* (1), 427–511. https://doi.org/10.1152/physrev.00061.2017.

(2) Dent, E.; Wright, O. R. L.; Woo, J.; Hoogendijk, E. O. Malnutrition in Older Adults. *The Lancet* **2023**, *401* (10380), 951–966. https://doi.org/10.1016/S0140-6736(22)02612-5.

(3) Kim, J.; Hinchcliff, K. W.; Yamaguchi, M.; Beard, L. A.; Markert, C. D.; Devor, S. T. Age-Related Changes in Metabolic Properties of Equine Skeletal Muscle Associated with Muscle Plasticity. *Vet. J.* **2005**, *169* (3), 397–403. https://doi.org/10.1016/j.tvjl.2004.03.016.

(4) Ireland, J. L. Demographics, Management, Preventive Health Care and Disease in Aged Horses. *Vet. Clin. North Am. Equine Pract.* **2016**, *32* (2), 195–214. https://doi.org/10.1016/j.cveq.2016.04.001.

(5) Rizzo, M.; Du Preez, N.; Ducheyne, K. D.; Deelen, C.; Beitsma, M. M.; Stout, T. A. E.; De Ruijter-Villani, M. The Horse as a Natural Model to Study Reproductive Aging-Induced Aneuploidy and Weakened Centromeric Cohesion in Oocytes. *Aging* **2020**, *12* (21), 22220–22232. https://doi.org/10.18632/aging.104159.

(6) Jarvis, N. G. Nutrition of the Aged Horse. *Vet. Clin. North Am. Equine Pract.* **2009**, *25* (1), 155–166. https://doi.org/10.1016/j.cveq.2009.01.003.

(7) Siciliano, P. D. Nutrition and Feeding of the Geriatric Horse. *Vet. Clin. North Am. Equine Pract.* **2002**, *18* (3), 491–508. https://doi.org/10.1016/S0749-0739(02)00028-7.

(8) Mozaffarian, D.; Micha, R.; Wallace, S. Effects on Coronary Heart Disease of Increasing Polyunsaturated Fat in Place of Saturated Fat: A Systematic Review and Meta-Analysis of

Randomized Controlled Trials. *PLoS Med.* **2010**, *7* (3), e1000252. https://doi.org/10.1371/journal.pmed.1000252.

(9) Tortosa-Caparrós, E.; Navas-Carrillo, D.; Marín, F.; Orenes-Piñero, E. Anti-Inflammatory Effects of Omega 3 and Omega 6 Polyunsaturated Fatty Acids in Cardiovascular Disease and Metabolic Syndrome. *Crit. Rev. Food Sci. Nutr.* **2017**, *57* (16), 3421–3429. https://doi.org/10.1080/10408398.2015.1126549.

(10) O'Connor, C. I.; Lawrence, L. M.; St. Lawrence, A. C.; Janicki, K. M.; Warren, L. K.; Hayes, S. The Effect of Dietary Fish Oil Supplementation on Exercising Horses. *J. Anim. Sci.* **2004**, *82* (10), 2978–2984. https://doi.org/10.2527/2004.82102978x.

(11) Simopoulos, A. P. Human Requirement for N-3 Polyunsaturated Fatty Acids. *Poult. Sci.* **2000**, *79* (7), 961–970. https://doi.org/10.1093/ps/79.7.961.

(12) Clauss, M.; Codron, D.; Hummel, J. Equid Nutritional Physiology and Behavior: An Evolutionary Perspective. *J. Equine Vet. Sci.* **2023**, *124*, 104265. https://doi.org/10.1016/j.jevs.2023.104265.

(13) Chilton, F.; Murphy, R.; Wilson, B.; Sergeant, S.; Ainsworth, H.; Seeds, M.; Mathias, R. Diet-Gene Interactions and PUFA Metabolism: A Potential Contributor to Health Disparities and Human Diseases. *Nutrients* **2014**, *6* (5), 1993–2022. https://doi.org/10.3390/nu6051993.

(14) Ishihara, T.; Yoshida, M.; Arita, M. Omega-3 Fatty Acid-Derived Mediators That Control Inflammation and Tissue Homeostasis. *Int. Immunol.* **2019**, *31* (9), 559–567. https://doi.org/10.1093/intimm/dxz001.

(15) Kris-Etherton, P.; Fleming, J.; Harris, W. S. The Debate about N-6 Polyunsaturated Fatty Acid Recommendations for Cardiovascular Health. *J. Am. Diet. Assoc.* **2010**, *110* (2), 201–204. https://doi.org/10.1016/j.jada.2009.12.006.

(16) Sherratt, S. C. R.; Libby, P.; Budoff, M. J.; Bhatt, D. L.; Mason, R. P. Role of Omega-3 Fatty Acids in Cardiovascular Disease: The Debate Continues. *Curr. Atheroscler. Rep.* **2023**, *25* (1), 1–17. https://doi.org/10.1007/s11883-022-01075-x.

(17) Li, C.; White, S. H.; Warren, L. K.; Wohlgemuth, S. E. Effects of Aging on Mitochondrial Function in Skeletal Muscle of American American Quarter Horses. *J. Appl. Physiol.* **2016**, *121* (1), 299–311. https://doi.org/10.1152/japplphysiol.01077.2015.

(18) Catandi, G.; Obeidat, Y.; Stokes, J.; Chicco, A.; Chen, T.; Carnevale, E. Effects of Maternal Age on Oxygen Consumption of Oocytes and in Vitro-Produced Equine Embryos. *Reprod. Fertil. Dev.* **2020**, *32* (2), 175–175.

(19) Catandi, G. D.; Obeidat, Y. M.; Broeckling, C. D.; Chen, T. W.; Chicco, A. J.; Carnevale, E. M. Equine Maternal Aging Affects Oocyte Lipid Content, Metabolic Function and Developmental Potential. *Reproduction* **2021**, *161* (4), 399–409. https://doi.org/10.1530/REP-20-0494.

(20) Pasquariello, R.; Ermisch, A. F.; Silva, E.; McCormick, S.; Logsdon, D.; Barfield, J. P.; Schoolcraft, W. B.; Krisher, R. L. Alterations in Oocyte Mitochondrial Number and Function Are Related to Spindle Defects and Occur with Maternal Aging in Mice and Humans†. *Biol. Reprod.* **2019**, *100* (4), 971–981. https://doi.org/10.1093/biolre/ioy248.

(21) Grevendonk, L.; Connell, N. J.; McCrum, C.; Fealy, C. E.; Bilet, L.; Bruls, Y. M. H.; Mevenkamp, J.; Schrauwen-Hinderling, V. B.; Jörgensen, J. A.; Moonen-Kornips, E.; Schaart, G.; Havekes, B.; De Vogel-van Den Bosch, J.; Bragt, M. C. E.; Meijer, K.;

Schrauwen, P.; Hoeks, J. Impact of Aging and Exercise on Skeletal Muscle Mitochondrial Capacity, Energy Metabolism, and Physical Function. *Nat. Commun.* **2021**, *12* (1), 4773. https://doi.org/10.1038/s41467-021-24956-2.

(22) Catandi, G. D.; LiPuma, L.; Obeidat, Y. M.; Maclellan, L. J.; Broeckling, C. D.; Chen, T.; Chicco, A. J.; Carnevale, E. M. Oocyte Metabolic Function, Lipid Composition, and Developmental Potential Are Altered by Diet in Older Mares. *Reproduction* **2022**, *163* (4), 183–198. https://doi.org/10.1530/REP-21-0351.

(23) Aleksandrova, K.; Koelman, L.; Rodrigues, C. E. Dietary Patterns and Biomarkers of Oxidative Stress and Inflammation: A Systematic Review of Observational and Intervention Studies. *Redox Biol.* **2021**, *42*, 101869. https://doi.org/10.1016/j.redox.2021.101869.

(24) Fritsche, K. L.; Johnston, P. V. Rapid Autoxidation of Fish Oil in Diets without Added Antioxidants. *J. Nutr.* **1988**, *118* (4), 425–426. https://doi.org/10.1093/jn/118.4.425.

(25) HENNEKE, D. R.; POTTER, G. D.; KREIDER, J. L.; YEATES, B. F. Relationship between Condition Score, Physical Measurements and Body Fat Percentage in Mares. *Equine Vet. J.* **1983**, *15* (4), 371–372. https://doi.org/10.1111/j.2042-3306.1983.tb01826.x.

(26) Carter, R. A.; Geor, R. J.; Burton Staniar, W.; Cubitt, T. A.; Harris, P. A. Apparent Adiposity Assessed by Standardised Scoring Systems and Morphometric Measurements in Horses and Ponies. *Vet. J.* **2009**, *179* (2), 204–210. https://doi.org/10.1016/j.tvjl.2008.02.029.

(27) Abcam. Isolation of Human Platelets from Whole Blood. https://www.abcam.com/protocols/isolation-of-human-platelets-from-whole-blood.

(28) Carnevale, E. M. Advances in Collection, Transport and Maturation of Equine Oocytes for Assisted Reproductive Techniques. *Vet. Clin. North Am. Equine Pract.* **2016**, *32* (3), 379–399. https://doi.org/10.1016/j.cveq.2016.07.002.

(29) Wagner, B.; Freer, H. Development of a Bead-Based Multiplex Assay for Simultaneous Quantification of Cytokines in Horses. *Vet. Immunol. Immunopathol.* **2009**, *127* (3–4), 242–248. https://doi.org/10.1016/j.vetimm.2008.10.313.

(30) Mulligan, C. M.; Le, C. H.; deMooy, A. B.; Nelson, C. B.; Chicco, A. J. Inhibition of Delta-6 Desaturase Reverses Cardiolipin Remodeling and Prevents Contractile Dysfunction in the Aged Mouse Heart Without Altering Mitochondrial Respiratory Function. *J. Gerontol. Ser. A* **2014**, *69* (7), 799–809. https://doi.org/10.1093/gerona/glt209.

(31) Li Puma, L. C.; Hedges, M.; Heckman, J. M.; Mathias, A. B.; Engstrom, M. R.; Brown, A. B.; Chicco, A. J. Experimental Oxygen Concentration Influences Rates of Mitochondrial Hydrogen Peroxide Release from Cardiac and Skeletal Muscle Preparations. *Am. J. Physiol.-Regul. Integr. Comp. Physiol.* **2020**, *318* (5), R972–R980. https://doi.org/10.1152/ajpregu.00227.2019.

(32) Doerrier, C.; Garcia-Souza, L. F.; Krumschnabel, G.; Wohlfarter, Y.; Mészáros, A. T.; Gnaiger, E. High-Resolution FluoRespirometry and OXPHOS Protocols for Human Cells, Permeabilized Fibers from Small Biopsies of Muscle, and Isolated Mitochondria. In *Mitochondrial Bioenergetics: Methods and Protocols*; Palmeira, C. M., Moreno, A. J., Eds.; Springer New York: New York, NY, 2018; pp 31–70. https://doi.org/10.1007/978-1-4939-7831-1_3.

(33) Pesta, D.; Gnaiger, E. High-Resolution Respirometry: OXPHOS Protocols for Human Cells and Permeabilized Fibers from Small Biopsies of Human Muscle. *Methods Mol. Biol. Clifton NJ* **2011**, *810*, 25–58. https://doi.org/10.1007/978-1-61779-382-0_3.

(34) Starkov, A. A. Measurement of Mitochondrial ROS Production. In *Protein Misfolding and Cellular Stress in Disease and Aging*; Bross, P., Gregersen, N., Eds.; Methods in Molecular Biology; Humana Press: Totowa, NJ, 2010; Vol. 648, pp 245–255. https://doi.org/10.1007/978-1-60761-756-3_16.

(35) Obeidat, Y. M.; Cheng, M.-H.; Catandi, G.; Carnevale, E.; Chicco, A. J.; Chen, T. W. Design of a Multi-Sensor Platform for Integrating Extracellular Acidification Rate with Multi-Metabolite Flux Measurement for Small Biological Samples. *Biosens. Bioelectron.* **2019**, *133*, 39–47. https://doi.org/10.1016/j.bios.2019.02.069.

(36) Cheng, M.-H.; Chicco, A. J.; Ball, D.; Chen, T. W. Analysis of Mitochondrial Oxygen Consumption and Hydrogen Peroxide Release from Cardiac Mitochondria Using Electrochemical Multi-Sensors. *Sens. Actuators B Chem.* **2022**, *360*, 131641. https://doi.org/10.1016/j.snb.2022.131641.

(37) Bedard, K.; Krause, K.-H. The NOX Family of ROS-Generating NADPH Oxidases: Physiology and Pathophysiology. *Physiol. Rev.* **2007**, *87* (1), 245–313. https://doi.org/10.1152/physrev.00044.2005.

(38) Mowry, K. C.; Thomson-Parker, T. L.; Morales, C.; Fikes, K. K.; Stutts, K. J.; Leatherwood, J. L.; Anderson, M. J.; Smith, R. X.; Suagee-Bedore, J. K. Effects of Crude Rice Bran Oil and a Flaxseed Oil Blend in Young Horses Engaged in a Training Program. *Animals* **2022**, *12* (21). https://doi.org/10.3390/ani12213006.

(39) Williams, C. M.; Burdge, G. Long-Chain *n* −3 PUFA: Plant *v* . Marine Sources. *Proc. Nutr. Soc.* **2006**, *65* (1), 42–50. https://doi.org/10.1079/PNS2005473.

(40) Pearson, G.; Goodale, M.; Wakshlag, J.; Fortier, L. Dose-Dependent Increase in Whole Blood Omega-3 Fatty Acid Concentration in Horses Receiving a Marine-Based Fatty-Acid Supplement. *J. Equine Vet. Sci.* **2022**, *108*. https://doi.org/10.1016/j.jevs.2021.103781.

(41) Christmann, U.; Hancock, C. L.; Poole, C. M.; Emery, A. L.; Poovey, J. R.; Hagg, C.; Mattson, E. A.; Scarborough, J. J.; Christopher, J. S.; Dixon, A. T.; Craney, D. J.; Wood, P. L. Dynamics of DHA and EPA Supplementation: Incorporation into Equine Plasma, Synovial Fluid, and Surfactant Glycerophosphocholines. *Metabolomics* **2021**, *17* (5). https://doi.org/10.1007/s11306-021-01792-5.

(42) Schwärzler, J.; Mayr, L.; Vich Vila, A.; Grabherr, F.; Niederreiter, L.; Philipp, M.; Grander, C.; Meyer, M.; Jukic, A.; Tröger, S.; Enrich, B.; Przysiecki, N.; Tschurtschenthaler, M.; Sommer, F.; Kronberger, I.; Koch, J.; Hilbe, R.; Hess, M. W.; Oberhuber, G.; Sprung, S.; Ran, Q.; Koch, R.; Effenberger, M.; Kaneider, N. C.; Wieser, V.; Keller, M. A.; Weersma, R. K.; Aden, K.; Rosenstiel, P.; Blumberg, R. S.; Kaser, A.; Tilg, H.; Adolph, T. E. PUFA-Induced Metabolic Enteritis as a Fuel for Crohn's Disease. *Gastroenterology* **2022**, *162* (6), 1690–1704. https://doi.org/10.1053/j.gastro.2022.01.004.

(43) Zhang, Y.; Mahmood, T.; Tang, Z.; Wu, Y.; Yuan, J. Effects of Naturally Oxidized Corn Oil on Inflammatory Reaction and Intestinal Health of Broilers. *Poult. Sci.* **2022**, *101* (1), 101541. https://doi.org/10.1016/j.psj.2021.101541.

(44) Rohrbach, S. Effects of Dietary Polyunsaturated Fatty Acids on Mitochondria. *Curr. Pharm. Des.* **2009**, *15* (36), 4103–4116. https://doi.org/10.2174/138161209789909692.

(45) Jedlička, J.; Kunc, R.; Kuncová, J. Mitochondrial Respiration of Human Platelets in Young Adult and Advanced Age – Seahorse or O2k? *Physiol. Res.* **2021**, S369–S379. https://doi.org/10.33549/physiolres.934812.

(46) Braganza, A.; Corey, C. G.; Santanasto, A. J.; Distefano, G.; Coen, P. M.; Glynn, N. W.; Nouraie, S.-M.; Goodpaster, B. H.; Newman, A. B.; Shiva, S. Platelet Bioenergetics Correlate with Muscle Energetics and Are Altered in Older Adults. *JCI Insight* **2019**, *4* (13), e128248. https://doi.org/10.1172/jci.insight.128248.

(47) Mulligan, C. M.; Sparagna, G. C.; Le, C. H.; De Mooy, A. B.; Routh, M. A.; Holmes, M. G.; Hickson-Bick, D. L.; Zarini, S.; Murphy, R. C.; Xu, F. Y.; Hatch, G. M.; McCune, S. A.; Moore, R. L.; Chicco, A. J. Dietary Linoleate Preserves Cardiolipin and Attenuates Mitochondrial Dysfunction in the Failing Rat Heart. *Cardiovasc. Res.* **2012**, *94* (3), 460–468. https://doi.org/10.1093/cvr/cvs118.

(48) Herbst, E. A. F.; Paglialunga, S.; Gerling, C.; Whitfield, J.; Mukai, K.; Chabowski, A.; Heigenhauser, G. J. F.; Spriet, L. L.; Holloway, G. P. Omega-3 Supplementation Alters Mitochondrial Membrane Composition and Respiration Kinetics in Human Skeletal Muscle. *J. Physiol.* **2014**, *592* (6), 1341–1352. https://doi.org/10.1113/jphysiol.2013.267336.

(49) Varming, K.; Schmidt, E. B.; Svaneborg, N.; Møller, J. M.; Lervang, H.-H.; Grunnet, N.; Jersild, C.; Dyerberg, J. The Effect of N-3 Fatty Acids on Neutrophil Chemiluminescence. *Scand. J. Clin. Lab. Invest.* **1995**, *55* (1), 47–52. https://doi.org/10.3109/00365519509075377.

(50) Schönfeld, P.; Schlüter, T.; Fischer, K.-D.; Reiser, G. Non-Esterified Polyunsaturated Fatty Acids Distinctly Modulate the Mitochondrial and Cellular ROS Production in Normoxia

and Hypoxia. *J. Neurochem.* **2011**, *118* (1), 69–78. https://doi.org/10.1111/j.1471-4159.2011.07286.x.

(51) Suzuki, N.; Sawada, K.; Takahashi, I.; Matsuda, M.; Fukui, S.; Tokuyasu, H.; Shimizu, H.; Yokoyama, J.; Akaike, A.; Nakaji, S. Association between Polyunsaturated Fatty Acid and Reactive Oxygen Species Production of Neutrophils in the General Population. *Nutrients* **2020**, *12* (11), 3222. https://doi.org/10.3390/nu12113222.

(52) Lalia, A. Z.; Dasari, S.; Robinson, M. M.; Abid, H.; Morse, D. M.; Klaus, K. A.; Lanza, I. R. Influence of Omega-3 Fatty Acids on Skeletal Muscle Protein Metabolism and Mitochondrial Bioenergetics in Older Adults. *Aging* **2017**, *9* (4), 1096–1129. https://doi.org/10.18632/aging.101210.

(53) Martins, A. R.; Crisma, A. R.; Masi, L. N.; Amaral, C. L.; Marzuca-Nassr, G. N.; Bomfim, L. H. M.; Teodoro, B. G.; Queiroz, A. L.; Serdan, T. D. A.; Torres, R. P.; Mancini-Filho, J.; Rodrigues, A. C.; Alba-Loureiro, T. C.; Pithon-Curi, T. C.; Gorjao, R.; Silveira, L. R.; Curi, R.; Newsholme, P.; Hirabara, S. M. Attenuation of Obesity and Insulin Resistance by Fish Oil Supplementation Is Associated with Improved Skeletal Muscle Mitochondrial Function in Mice Fed a High-Fat Diet. *J. Nutr. Biochem.* **2018**, *55*, 76–88. https://doi.org/10.1016/j.jnutbio.2017.11.012.

(54) Cabrero, À.; Alegret, M.; Sánchez, R. M.; Adzet, T.; Laguna, J. C.; Carrera, M. V. Increased Reactive Oxygen Species Production Down-Regulates Peroxisome Proliferator-Activated α Pathway in C2C12 Skeletal Muscle Cells. *J. Biol. Chem.* **2002**, *277* (12), 10100–10107. https://doi.org/10.1074/jbc.M110321200.

(55) Ferreira, L. F.; Laitano, O. Regulation of NADPH Oxidases in Skeletal Muscle. *Free Radic. Biol. Med.* **2016**, *98*, 18–28. https://doi.org/10.1016/j.freeradbiomed.2016.05.011.

(56) Basuroy, S.; Bhattacharya, S.; Leffler, C. W.; Parfenova, H. Nox4 NADPH Oxidase Mediates Oxidative Stress and Apoptosis Caused by TNF-α in Cerebral Vascular Endothelial Cells. *Am. J. Physiol.-Cell Physiol.* **2009**, *296* (3), C422–C432. https://doi.org/10.1152/ajpcell.00381.2008.

(57) White-Springer, S. H.; Vineyard, K. R.; Kivipelto, J.; Warren, L. K. Dietary Omega-3 Fatty Acid Supplementation Does Not Impair Vitamin E Status or Promote Lipid Peroxidation in Growing Horses. *J. Anim. Sci.* **2021**, *99* (7), skab177. https://doi.org/10.1093/jas/skab177.

(58) Karuputhula, N. B.; Chattopadhyay, R.; Chakravarty, B.; Chaudhury, K. Oxidative Status in Granulosa Cells of Infertile Women Undergoing IVF. *Syst. Biol. Reprod. Med.* **2013**, *59* (2), 91–98. https://doi.org/10.3109/19396368.2012.743197.

(59) Gu, L.; Liu, H.; Gu, X.; Boots, C.; Moley, K. H.; Wang, Q. Metabolic Control of Oocyte Development: Linking Maternal Nutrition and Reproductive Outcomes. *Cell. Mol. Life Sci.* **2015**, *72* (2), 251–271. https://doi.org/10.1007/s00018-014-1739-4.

(60) Latham, C. M.; Dickson, E. C.; Owen, R. N.; Larson, C. K.; White-Springer, S. H. Complexed Trace Mineral Supplementation Alters Antioxidant Activities and Expression in Response to Trailer Stress in Yearling Horses in Training. *Sci. Rep.* **2021**, *11* (1), 7352. https://doi.org/10.1038/s41598-021-86478-7.

(61) Owen, R. N.; Semanchik, P. L.; Latham, C. M.; Brennan, K. M.; White-Springer, S. H. Elevated Dietary Selenium Rescues Mitochondrial Capacity Impairment Induced by Decreased Vitamin E Intake in Young Exercising Horses. *J. Anim. Sci.* **2022**, *100* (8), skac172. https://doi.org/10.1093/jas/skac172.